SAN FRANCISCO WATERFRONT COASTAL FLOOD STUDY, CA

DRAFT APPENDIX B.1.1 – COASTAL EXTREME WATER LEVELS AND HIGH TIDE FLOODING

JANUARY 2024

USACE TULSA DISTRICT | THE PORT OF SAN FRANCISCO

THIS PAGE IS INTENTIONALLY BLANK.

Executive Summary

The U.S. Army Corps of Engineers (USACE) in partnership with the Port of San Francisco (POSF), are leading the San Francisco Waterfront Coastal Flood Study (SFWCFS) to evaluate existing and future coastal flood hazards along the City and County of San Francisco (CCSF) shoreline on the bayside of the city. To support this study, USACE selected the Generation II Coastal Risk Model (G2CRM) for evaluating potential damages associated with existing and future coastal flood hazards, and their respective economic costs. This report presents the technical work to develop the coastal storm inputs for G2CRM, with a focus on characterizing the complex San Francisco Bay (Bay) coastal hazards along the CCSF bayside shoreline and to develop coastal storm databases that appropriately represent these hazards.

San Francisco Bay is the largest estuary in the western U.S., with a contributing watershed that includes nearly 40% of California with substantial freshwater flows entering through the Sacramento River. The 300-foot-deep Golden Gate inlet connects the Bay with the Pacific Ocean, and the tides, ocean-driven swells, and extreme ocean water levels all enter the Bay through this single inlet. The large expanse of the Bay and the complex topography surrounding the Bay can transform storm-driven winds in a multitude of directions depending on the primary driver of the onshore or offshore winds or the track of the large storm system descending on the Bay Area. The water levels and wave heights of the Bay exhibit a high degree of variability driven by many factors, including the bathymetry, astronomical and oceanic cycles, windspeeds and direction, and atmospheric events. In the Bay, no single storm event produces the highest water level and highest wave hazard along the entire shoreline.

Two primary storm categories influence coastal hazards and flooding throughout the Bay Area and along the San Francisco shoreline: extratropical cyclones, which develop offshore and bring low barometric pressure, high winds, and heavy rain, and atmospheric rivers, which originate in the tropics and can bring heavy rain and high winds. These storm systems also occur concurrently, and a single atmospheric river event can be associated with a series of back-to-back extratropical cyclones. The most damaging storms that have occurred between 1980 and today have resulted from the concurrence of a large and rapidly intensifying extratropical cyclone, or bomb cyclone, and an atmospheric river off the California coastline. This combination is projected to become even more damaging in the future.

Model output from the FEMA San Francisco Bay Area Coastal Study Bay-wide numerical modeling effort was used to develop coastal storm databases that consider both high tide and extreme water levels. The study area was divided into four model areas, and each model area is associated with its own coastal storm database to best approximate tidal amplification and variations in the wave climate along San Francisco's Bay shoreline. The tidal amplification could not be reproduced using astronomical tides pulled from multiple tide gages within G2CRM, as this dynamic is dependent on Bay bathymetry, shoreline orientation, and tidal reflections that produce a combination of standing and progressive tidal waves within the Bay. Only a well-calibrated Bay-wide hydrodynamic model can adequately reproduce this dynamic.

The FEMA model output helped define water levels that represent high tide water levels (from the monthly to six-month recurrence intervals) and extreme water levels (from the annual to the 1% annual chance recurrence intervals). The difference between mean higher high water and the 1% annual chance extreme water level is about 3.5 feet, and the difference between the 10% and 1% annual chance extreme water level is about 12 inches. Therefore, with only 12 inches of sea level rise, a water level with a 1% annual chance of occurring each year today will have a 10% annual chance of occurring. According to the 2022 Federal Sea Level Rise Report: *Global and Regional Sea Level Rise Scenarios for the United States*, 12 inches of sea level rise is likely to occur by 2050. With 24 inches of sea level rise, today's 1% annual chance extreme water level could occur annually. For San Francisco's low-lying and highly urbanized communities adjacent to the Bay shoreline, even relatively

small amounts of sea level rise can result in extensive inland flooding the likes of which San Francisco has never seen.

This report is accompanied by the coastal storm databases and data files required for the G2CRM storm inputs. Full documentation of the formulation and evaluation of Future Without Project conditions will be presented in the Integrated Feasibility Report, which will undergo USACE Agency Technical Review and Policy Review when the Draft and Final Report are submitted.

Table of Contents

Appendices

Appendix A Threshold Selection Plots

Appendix B Storm Event Hydrographs

Tables

Figures

THIS PAGE IS INTENTIONALLY BLANK.

Acronyms and Abbreviations

AEP	annual exceedance probability
Bay	San Francisco Bay
Bay Area	San Francisco Bay Area
CCSF	City and County of San Francisco
CSD	coastal storm database
ENSO	El Niño Southern Oscillation
FEMA	Federal Emergency Management Agency
FIRM	Flood Insurance Rate Map
G2CRM	Generation II Coastal Risk Model
GIS	geographic information systems
GPD	generalized pareto distribution
MA	model area
MHHW	mean higher high water
mph	miles per hour
MSL	mean sea level
NAVD88	North American Vertical Datum of 1988
NOAA	National Oceanic and Atmospheric Administration
OPC	Ocean Protection Council
PDO	Pacific Decadal Oscillation
POT	peak over threshold
POSF	Port of San Francisco
Q-Q	quantile-quantile
SFO	San Francisco International Airport
SFPUC	San Francisco Public Utilities Commission
SFWCFS	San Francisco Waterfront Coastal Flood Study
SWEL	stillwater elevation
TWL	total water level
USACE	U.S. Army Corps of Engineers
USGS	U.S. Geological Survey
WCE	wave crest elevation

Glossary

extreme water level(s)	Coastal water level elevation(s) in the absence of waves occurring with an average event frequency between 0.01 events/year (often referred to as the 1% annual chance event) and 1 event/year (the annual high water level) (Sweet et al. 2022b).
high tide flooding	Flooding that is associated with a frequent water level and/or total water level, often used to describe flooding that occurs in the absence of a storm event (i.e., minor or nuisance high tide flooding).
high tide water level(s)	Coastal water level elevation(s) in the absence of waves occurring with an average event frequency between 1 event/year (annual water level) and 10 to 12 events/year (monthly water level).
major flooding	Major flooding is severe, resulting in extensive inundation of numerous roads and buildings with a significant threat to property and life.
minor flooding	Minor flooding is disruptive, shallow flooding with a low threat of property damage.
moderate flooding	Moderate flooding is widespread with an elevated threat of property damage.
total water level(s)	Coastal water level elevation(s) calculated offshore (i.e., not directly along the shoreline or at a structure) that include the combined water level and wave height elevation with an average event frequency between 0.01 events/year and 10 to 12 events/year. Future condition total water levels also include sea level rise.
wave runup elevation	The elevation of the coastal water level at the shoreline that includes consideration of wave setup and swash and is a function of wave height and shoreline slope.

1   Introduction

The U.S. Army Corps of Engineers (USACE) in partnership with the Port of San Francisco (POSF), are leading the San Francisco Waterfront Coastal Flood Study (SFWCFS) to evaluate existing and future coastal flood hazards along the City and County of San Francisco (CCSF) shoreline on the bayside of the city. To support this study, USACE selected the Generation II Coastal Risk Model (G2CRM) for evaluating potential damages associated with existing and future coastal flood hazards, and their respective economic costs.

This report presents the technical work to develop the storm inputs for G2CRM; however, the data set and coastal analysis presented within this report will support a wide range of analyses outside of G2CRM, including providing downstream boundary conditions for the San Francisco Public Utilities Commission model of the combined sewer system; providing water level and wave information along the 7.5 miles shoreline to inform alternatives development, overtopping analysis, and risk communication; informing conceptual engineering analyses; and analyzing wave runup and the wave energy dissipation potential provided by different flood risk reduction and adaptation measures. These additional analyses will be documented separately as the SFWCFS progresses.

This report focuses on characterizing the complex San Francisco Bay (Bay) coastal hazards along the CCSF bayside shoreline, and the analysis required to develop coastal storm databases (CSDs) that appropriately represent these hazards within G2CRM. The development of the CSDs included extensive testing within G2CRM, relying on supporting data files developed by USACE in support of the SFWCFS G2CRM analysis.

The report is organized as follows:

- Section 3: Generation II Coastal Risk Model: an overview of G2CRM and model assumptions
- Section 2: Study Area: definition of the G2CRM Model Areas
- Section 4: San Francisco Bay Area (Bay Area) Storm Climatology: overview of Bay Area storms and storm identification criteria
- Section 5: San Francisco Coastal Dynamics: review of Bay hydrodynamics, wave dynamics, and non-tidal residual
- Section 6: FEMA San Francisco Bay Area Coastal Study: summary of the large-scale numerical modeling study completed by FEMA to support updates to the coastal flood hazard mapping
- Section 7: Coastal Storm Database Development
- Section 8: References: all data sources and references cited within this report

This report is accompanied by the coastal storm databases and data files required for the G2CRM storm inputs. Full documentation of the formulation and evaluation of Future Without Project conditions will be presented in the Integrated Feasibility Report, which will undergo USACE Agency Technical Review and Policy Review when the Draft and Final Report are submitted.

THIS PAGE IS INTENTIONALLY BLANK.

2 Generation II Coastal Risk Model

The USACE Institute for Water Resources, in cooperation with USACE Engineer Research and Development Center, developed G2CRM as a planning level tool to support flood risk reduction studies by estimating storm-driven damages and costs using a probabilistic life cycle. Key features of G2CRM include the ability to use readily available data from existing numerical hydrodynamic and wave modeling studies and sources and its integration with GIS. G2CRM can generate a wide variety of outputs for estimating damages and costs, and characterizing and communicating risk, to help assess future without project conditions and to inform project plan formulation over time.

G2CRM requires three primary input data sets:

- System: the bounding study area; discretization of the region of interest in upland model areas (MAs), where each MA defines a region that experiences similar coastal hazards, or a discrete area of interest for quantifying potential damages; and information describing existing (or planned) flood protection structures.
- Assets: both spatial and non-spatial information characterizing all structures of interest within the study area (for example, first floor elevation, number of stories, present value, foundation type, construction type, and occupancy) and parameters defining the number of times each structure can be rebuilt or the maximum sustained damage threshold for each structure.
- Storm Inputs: coastal water levels and wave parameters offshore of the shoreline representative of either actual storm events across a range of recurrence probabilities, or synthetic storm events characteristic of actual storm recurrence probabilities.

The System and Assets input files were developed and documented separately by USACE and are not documented within this report. This report documents the development of the Storm Inputs.

2.1 G2CRM Limitations and Assumptions

Important G2CRM limitations and assumptions that are relevant to the coastal storm inputs include:

- G2CRM is a planning level tool for estimating damages and costs associated with storm events over a defined planning horizon.
- G2CRM is not a numerical hydrodynamic or wave dynamic model and relies on coastal storm input files to define the coastal water level and wave inputs.
- G2CRM does not address precipitation-related flooding.
- G2CRM specific sea level rise projections are applied, and the relative sea level rise increase is added to the input peak water level + wave height combination for each storm event. No additional trends can be added within G2CRM, for example, approximations of large-scale climatic phenomenon such as the El Niño Southern Oscillation (ENSO) and Pacific Decadal Oscillation (PDO) cannot be added to the water levels over the duration of the simulation.
- G2CRM does not capture the effect of storm duration outside of the time to fill in a modeled area with the weir flow assumptions inside the model. Duration of flooding must be addressed externally to G2CRM.
- G2CRM supports events of any duration, but unless a stage volume curve is used only the peak (water level + wave height combination) of the event is applied to a given modeled area.
- G2CRM calculates the damages for the peak water level + wave height combination in a modeled area using a bathtub approach.
- G2CRM assumes all events are independent of each other and prohibits overlapping of events.
- G2CRM requires that the storm events occur at the same overall distribution across a simulation; therefore, increases in storm frequency over time cannot be assessed within G2CRM. Although the number of storm

events will not increase, the addition of sea level rise will result in an increase of damages. Individual assets will be flooded with increasing frequency over the 100-year simulation.

• G2CRM requires relative storm recurrence probabilities, calculated using the defined storm input suite.

2.2 Pacific Coast versus Atlantic/Gulf Coast Application

The use of G2CRM for the SFWCFS represents the first application of the model along the west coast of the U.S. The dominant extreme Pacific coast storm systems and coastal hazards are different than those that occur along the Atlantic and Gulf coasts. Therefore, the application of G2CRM for this study differs from previous Atlantic and Gulf coast applications.

The magnitude of storm surge from any storm system is influenced by the depth of the ocean as the system approaches the coast. Coastlines with a broad shallow continental shelf, as found on the Atlantic and Gulf coasts, can support the development of large storm surges. In contract, the Pacific coast is characterized by a narrow, steep shelf with deep ocean water relatively close to the shoreline, which inhibits the development of large storm surges (Serafin et al. 2019).

Hurricanes and cyclones create a complex combinations of storm surge and wave hazards along both coasts. G2CRM was originally developed for hurricanes, which are rotating low-pressure weather systems that originate over tropical or subtropical waters. Tropical cyclones are classified based on their maximum sustained windspeeds, with hurricanes having maximum sustained windspeeds exceeding 74 miles per hour (mph), and major hurricanes (i.e., category 3, 4 or 5 on the Saffir-Simpson Hurricane Wind Scale) having maximum sustained windspeeds exceeding 111mph. The low pressure in the center of a hurricane drives about 5% of the storm surge (for every millibar drop in atmospheric pressure within a storm system, the ocean water level rises about 0.4 inch), while most of the storm surge is driven by the high-speed rotating winds that push ocean water toward the coast. The combination of the low-pressure zone and high-speed rotating winds create a mound of water that moves with the hurricane storm track; although this could be considered a combination of storm surge and wave hazards, the height of the mound of water when the storm makes landfall is generally referred to as the storm surge. Landfalling hurricanes are generally considered rare events; however, hurricane intensity and frequency are increasing as ocean sea surface temperatures increase with the warming climate (Hosseini et al. 2018, Patricola and Wehner 2018, Chan et al. 2021, Vecchi et al. 2021).

Within the Earth's middle latitudes, between 30- and 60-degrees latitude, cyclones are called mid-latitude cyclones or extratropical cyclones that impact the Pacific and Atlantic coasts (Colle et al. 2015, Booth et al. 2017, Dacre 2020). Extratropical cyclones are frequent winter weather systems that generally travel from west to east, vary in size and strength, with a low-pressure core and high rotating windspeeds that can resemble a hurricane when viewed via satellite imagery (Catto 2016). However, hurricanes and extratropical cyclones have many differentiating features, including their frequency of occurrence, duration, vertical wind and temperature profile, and their direction of movement.

Extratropical cyclones can produce cloudy skies and mild rain and they can produce a myriad of extreme weather conditions including coastal storm surge, high winds, heavy precipitation, thunderstorms, and tornadoes. These cyclones form along weather fronts, producing rapid changes in temperature and dew point. Multiple extratropical cyclones may pass over the same area in sequence within a short period of time (days to weeks) (Dacre and Pinto 2020). In October 2021, the third extratropical cyclone in a cyclone cluster or "family" occurred alongside an atmospheric river and brought extreme rainfall and high winds to the western U.S. and Canada as it experienced explosive cyclogenesis. Explosive cyclones, or "bomb" cyclones are associated with extreme and rapid pressure drops, and bomb cyclones can cause significant flooding and damage due to heavy precipitation, large storm surge, and strong winds (Catto 2016).

Because extratropical cyclones over the Pacific Ocean remain in deep ocean water until they are very near the shoreline due to the narrow continental shelf along the Pacific coast, the rotating winds within extratropical

cyclones cannot create a mound of water comparable to hurricanes. Instead, the storm surge is limited to the increase in water level driven by the decrease in barometric pressure within the storm system. Similar to hurricanes, the frequency and intensity of extreme extratropical cycles are increasing with climate change (Danard et al. 2004). And the combination of extratropical cyclones and atmospheric rivers are projected to have the largest increase in intensity under the warming climate (Patricola et al. 2022).

Most large, historic extratropical cycles that have impacted the Bay Area and the San Francisco shoreline have had barometric pressure drops on the order of 20 to 30 millibars, corresponding to a storm surge height of 8 to 12 inches (May et al. 2019). When coupled with El Nino effects and other ocean and atmospheric process that influence water levels, a large rise in ocean water level on the Pacific coast is generally in the range of 3 to 3.5 feet. This increase is small when compared with the Bay tide range (6 to 8 feet); therefore, the timing of the tides and the peak storm surge can influence whether Bay water levels rise high enough to cause localized flooding of low-lying areas. However, the largest rises in ocean water levels observed at the NOAA Presidio tide gage near San Francisco have never occurred at high tide in over 100 years of observations. The complex combination of oceanic cycles and atmospheric processes that elevate Bay water levels is therefore challenging to untangle from the daily rise and fall and ebb and flow of the tide.

The differences between the Pacific coast hazards (small storm surge, frequent, sequential, and long duration events) and Atlantic/Gulf coast hazards (large storm surge, rare, distinct, and limited duration events), along with the challenges associated with adequately representing the Bay's tidal variations (see Section 6) require adjustment in how the CSDs are developed and used within G2CRM. Additional details on CSD development are presented in Section 7.

2.3   San Francisco Bay Tidal Datums

The water levels in this report are all reported relative to NAVD88. At the Presidio tide gage, 0 feet NAVD88 is only 0.06 feet below the mean lower low water (MLLW) tidal datum associated with the 1983 – 2001 tidal epoch (Figure 2-1). The relationship between the tidal datums and NAVD88 varies throughout the Bay, with MLLW decreasing and mean higher high water (MHHW) increasing to the south, as shown relative to the Alameda tide gage.
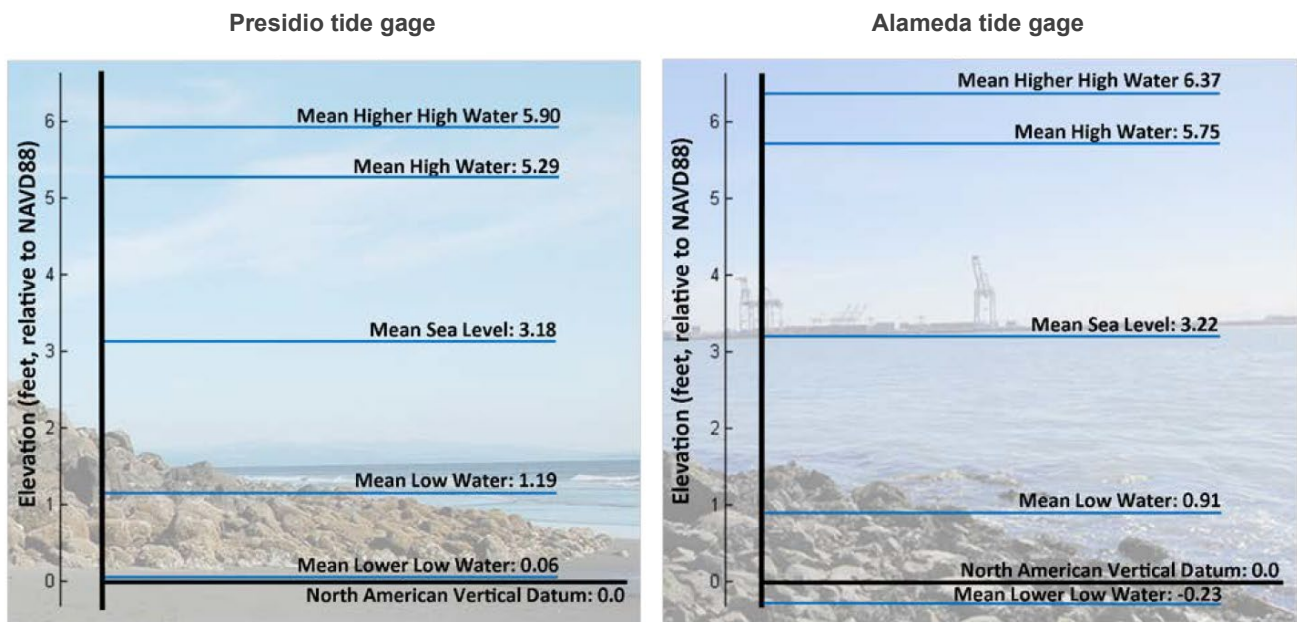
Figure 2-1. Comparison of San Francisco Bay Tidal Datums and NAVD88

3   Study Area

The CCSF is located on the Central California coastline, on the northern tip of peninsula, just south of the Golden Gate – the connection between the Pacific Ocean and the Bay (Figure 3-1). The Bay Area has a variable climate that is dominated by many large-scale atmospheric and oceanic processes. Although generally characterized by a mild Mediterranean climate with dry summers and cool, wet winters, the Bay Area is also a region that experiences volatile storms that can cause widespread flooding in low-lying coastal areas.

The POSF manages 7.5 miles of shoreline along the San Francisco waterfront from Aquatic Park near the Golden Gate to Heron's Head Park (Figure 3-2). Much of the northern shoreline (that is, north of the San Francisco Giants ballpark) is engineered with bulkhead wharves and finger piers, while the southern shoreline includes two inlets (Mission Creek and Islais Creek), working piers (Piers 80 – 96), and areas with sensitive habitat such as the Pier 94 wetlands and Heron's Head Park. Much of the areas inland from the shoreline are built on reclaimed land (bay fill) that was filled over time to support the construction of the historic Embarcadero seawall in the late 1800s, and the ship building industries that supported the World Wars in the early 1900s (Figure 3-3). This man-made shoreline is relatively flat, with a mean elevation of approximately 11.8 feet North American Vertical Datum of 1988 (NAVD88) (Figure 3-4). Therefore, when Bay waters overtop the shoreline, the entire shoreline can quickly be overtopped.

Figure 3-5 presents the existing FEMA floodplain, which was analyzed and mapped relative to 2008 ocean and Bay water levels. The POSF shoreline area is currently mapped as Zone D, which indicates an existing but unquantified flood risk. The areas inland of the shoreline are high-density urban and industrial areas. Businesses and residents are located within the existing FEMA floodplain along Islais Creek, and substantially more structures and infrastructure are located within areas that could be flooded if sea level rise trends along the higher projections. The CCSF requires that all capital projects within the Sea Level Rise Vulnerability Zone (Figure 3-6), an area that could be flooded by a 1% annual chance coastal flood coupled with 66 inches of sea level rise (relative to the year 2000 water levels), consider sea level rise adaptation as part of the project planning and design process (CPC 2020). The CCSF also completed a comprehensive Sea Level Rise and Consequence Assessment which includes exposure, vulnerability, and consequence information for transportation, wastewater and stormwater, water, energy, parks and open space, and POSF assets within the Sea Level Rise Vulnerability Zone (CCSF 2020).

Source: (May et al. 2016b)

Figure 3-1. San Francisco Bay Coastal and Estuarine System
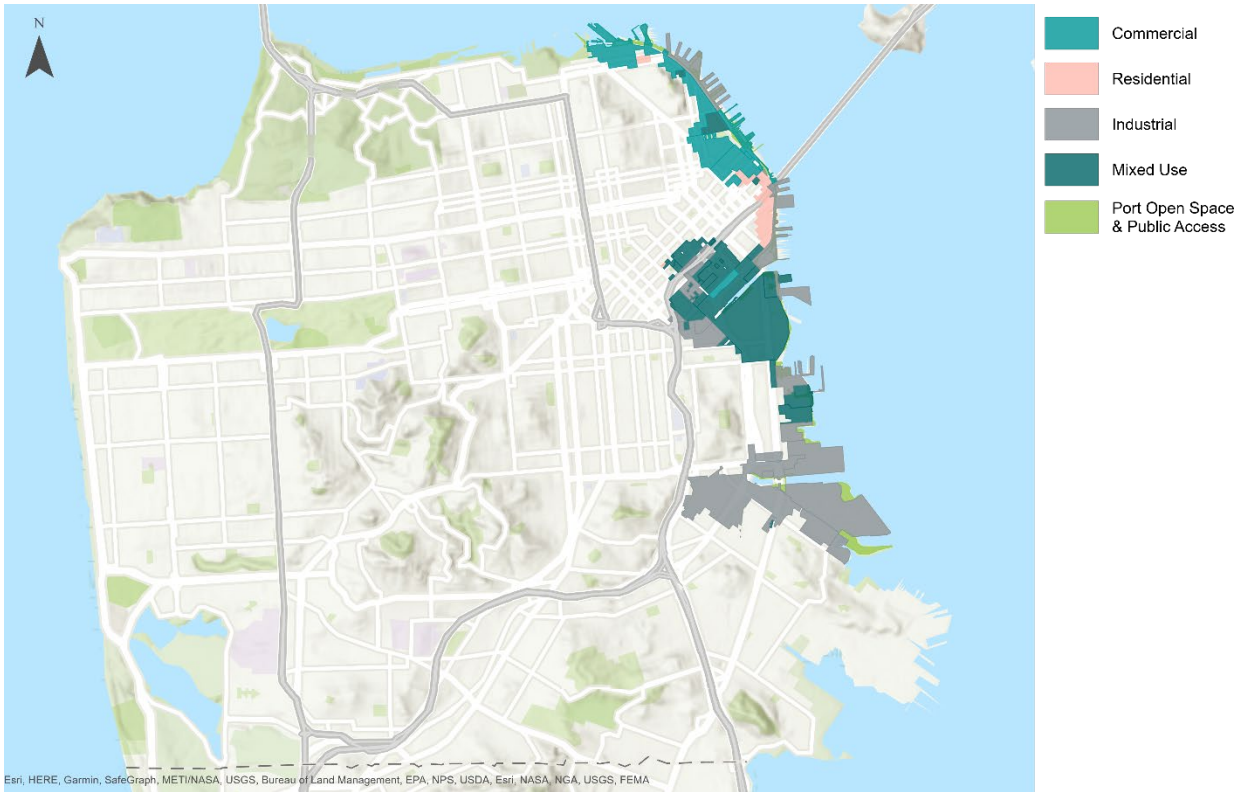
Source: (SF Planning 2019)

Figure 3-2. POSF of San Francisco Land Use
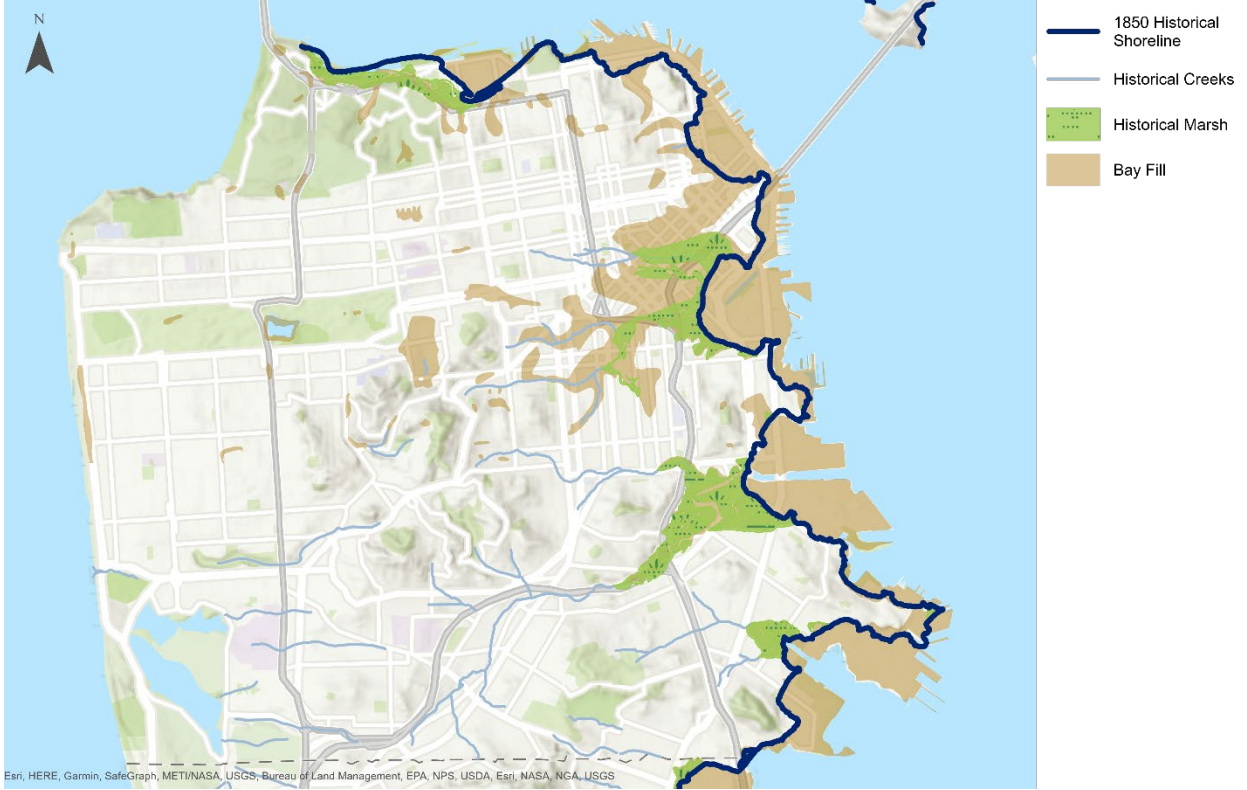
Source: (SFEI 1998)

Figure 3-3. Historic Shoreline and Area of Reclaimed Land Built on Bay Fill

Distribution of Shoreline Elevation
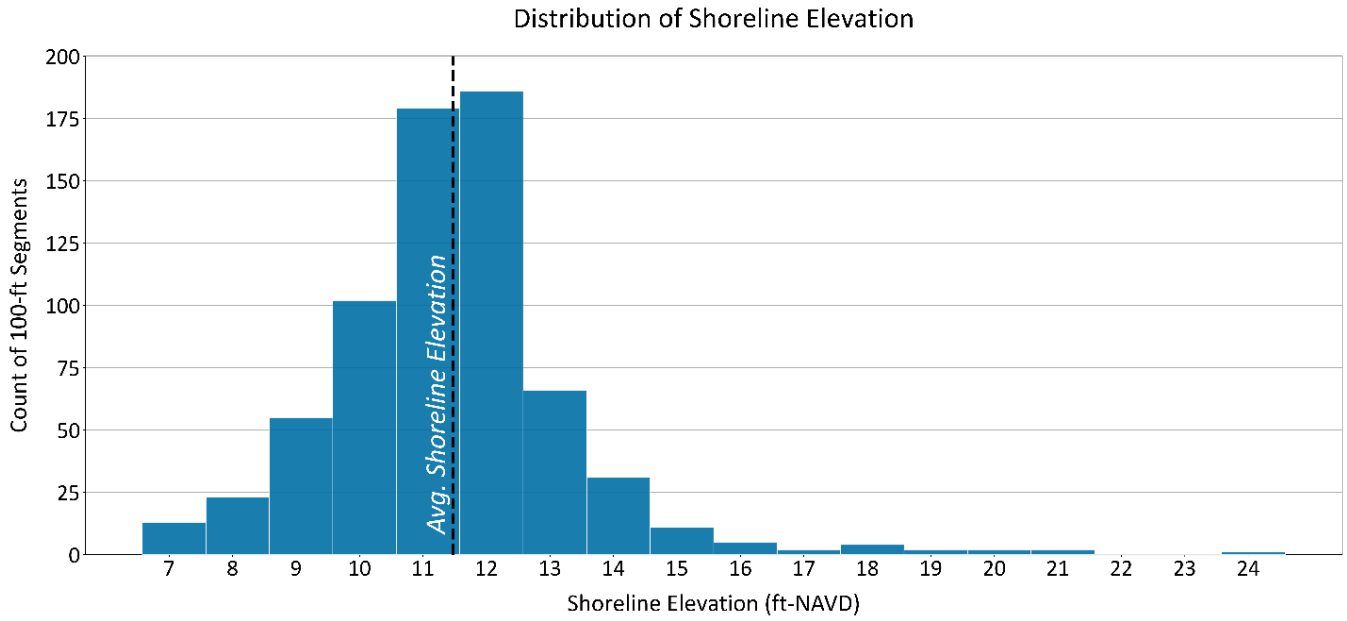
Source: (Port of San Francisco 2021a)

Figure 3-4. Elevation of the POSF Shoreline
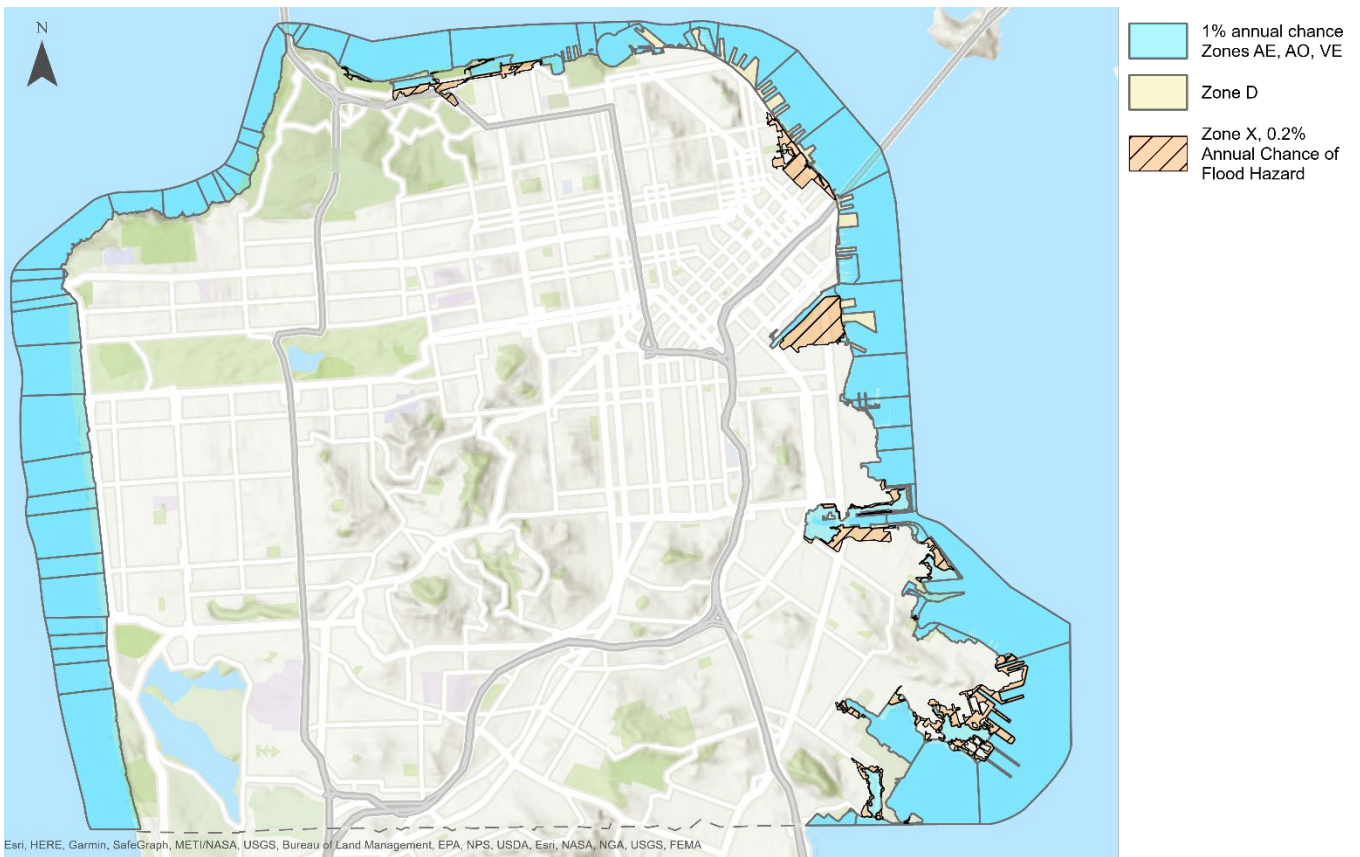
Source: (FEMA 2021)

Figure 3-5. FEMA 1% Annual Chance Coastal Floodplain (relative to 2008)

Source: (CPC 2020)

Figure 3-6. San Francisco Sea Level Rise Vulnerability Zone (relative to 2000)
The Sea Level Rise Vulnerability Zone encompasses the area that could be flooded by a 1% annual chance coastal flood coupled with 66 inches of sea level rise (relative to the year 2000 water levels).

3.1 Model Areas and Reaches

Although the San Francisco shoreline is relatively flat (that is, uniform in elevation), the hydrodynamics and wave dynamics of the Bay vary greatly along the shoreline. To support capturing the most representative hydrodynamic and wave conditions within the G2CRM modeling effort, the study area was divided into four reaches with seven MAs (Figure 3-7). The MA boundaries were selected to represent different hydrodynamic (bayside) and hydrologic (inland) conditions, which also correlate with the historic areas of bay fill. MA1 represents the northern most reach and is the area with the least historic bay fill. MA2 includes San Francisco's downtown financial district, constructed on bay fill over the former Yerba Buena Cove. MA3 includes Mission Creek and its surrounding area, constructed on bay fill over the former Mission Bay cove, as well as the marshlands and floodplains of Mission Creek. Mission Creek was placed underground in culverts. MA4 includes Islais Creek and its surrounding areas, constructed on bay fill over the former 2-mile wide Islais Creek estuary and the creek's former marshlands and floodplain. The Islais Creek watershed is the largest watershed in San Francisco; however, most of the creek was placed underground in culverts.

Four MAs (MA1 thru MA4) are capture the developed areas inland from the shoreline, and three MAs (MA5 thru MA7) capture the unprotected overwater structures in front of MA1 thru MA3. MA4 does not have an associated unprotected overwater MAs because the pier structures in this area are primarily built on bay fill, although marginal wharfs are present along the Bay edge to provide deep water berths. The inland extent of MA1 thru MA4 were defined to extend beyond the potential inland flooding associated with the State of California's 2100

Plausible, High Impact sea level rise scenario[1] coupled with the 1% AEP coastal event. This inland extent was selected to capture all potential assets that could be impacted by coastal storm events through the end of the 2090 planning horizon. The study planning horizon has been extended to 2140, and the inland extend of the MAs as well as the well as the corresponding assets within the MAs are in the process of being updated by the USACE economic team. Please refer to the Economic Appendix for the updated representation of the inland MA boundaries.

To support the G2CRM economic analysis, four CSDs were created, with each CSD capturing the offshore water level and wave dynamics that are most representative of its corresponding reach. MA1 and MA5 are associated with CSD1, MA2 and MA6 are associated with CSD2, MA3 and MA7 area associated with CSD3, and MA4 is associated with CSD4. The CSDs are the primary coastal inputs for G2CRM. The following subsections detail the data sources, and the analysis completed, to develop the four CSDs.

---

[1] The State of California 2100 Plausible, High Impact sea level rise scenario is 7 feet, which is 1.5 feet higher than the USACE High sea level rise projection of 5.5 feet (USACE 2019; OPC and CNRA 2018).
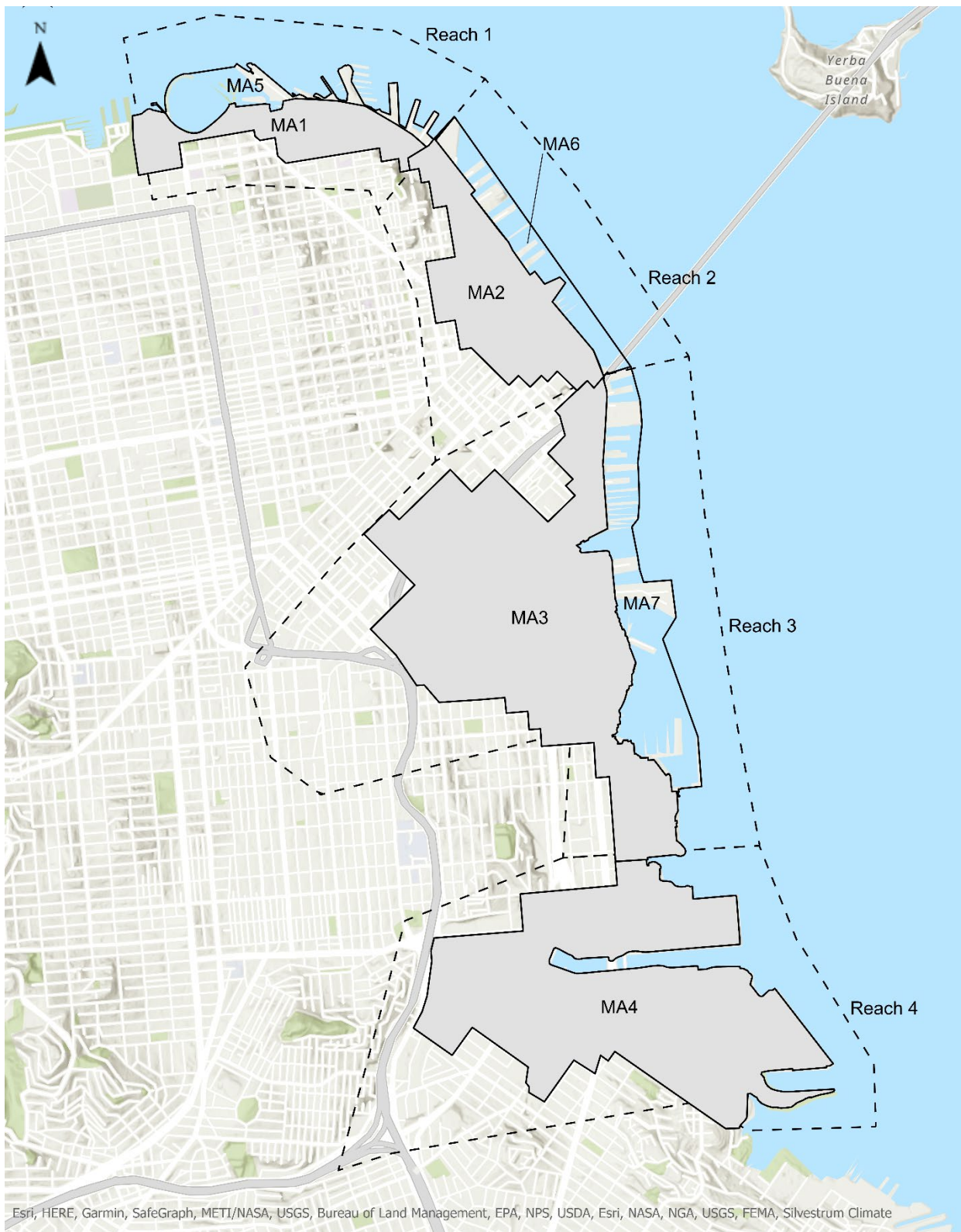
Figure 3-7. Model Areas and Reaches

The major POSF and CCSF assets within each reach are described below. Additional information on each reach is available on the [Port Waterfront Resilience Program website](#). The economic analysis, documented separately, contains more details on the assets within each reach and the associated damage related assumptions.

3.1.1   Reach 1: Northern Waterfront

This reach includes Aquatic Park, Fisherman's Wharf, Pier 31 to Pier 35, and the North Beach neighborhood. This area contains unique open space, recreational opportunities, historic resources, and tourism attractions that are recognized as global icons and are one of the most popular tourist areas within the State of California. This area also hosts San Francisco's commercial fishing fleet and fish processing centers, and a diverse array of water-dependent maritime functions.

This reach is subdivided into three subareas to support the development of neighborhood-scale geographic adaptation strategies: Aquatic Park, Fisherman's Wharf, and Piers 31-35. Additional information on each subarea is available in the Subarea Profiles, Problems, Opportunities, Objectives, Consideration, and Constraints (POOCCs), and the Flood Risks Profiles. Links to these documents are provided below.

- Aquatic Park: [Subarea Profile](#), [POOCC](#), [Flood Risk Profile](#)
- Fisherman's Wharf: [Subarea Profile](#), [POOCC](#), [Flood Risk Profile](#)
- Pers 31-35: [Subarea Profile](#), [POOCC](#), [Flood Risk Profile](#)

3.1.2   Reach 2: Embarcadero

This reach spans from the international cruise terminal at Pier 27 to the west to the San Francisco-Oakland Bay Bridge to the east. This area comprises a significant portion of the Embarcadero Historic District and includes popular sites such as the Exploratorium, Embarcadero promenade, and the Ferry Building. This neighborhood represents the Bay Area's largest and densest job center, and in addition to the ferry terminals includes key transportation nodes, such as BART, Muni, and regional bus lines. The many transportation hubs and businesses in the Financial District make this area central to the San Francisco economy.

This reach is subdivided into two subareas to support the development of neighborhood-scale geographic adaptation strategies: Northwest Waterfront and the Ferry Building. Additional information on each subarea is available in the Subarea Profiles, Problems, Opportunities, Objectives, Consideration, and Constraints (POOCCs), and the Flood Risks Profiles. Links to these documents are provided below.

- Northeast Waterfront: [Subarea Profile](#), [POOCC](#), [Flood Risk Profile](#)
- Ferry Building: [Subarea Profile](#), [POOCC](#), [Flood Risk Profile](#)

3.1.3   Reach 3: Mission Bay / Mission Creek

This reach spans from the Bay Bridge to the north and the former Potrero Power Plant in the south. The area includes the South Beach neighborhood, Mission Creek, the surrounding shoreline, and some of its watershed. It includes regional destinations such as, the Chase Center, and the University of California San Francisco (UCSF) Mission Bay Campus and Medical Center, as well as extensive housing and commercial buildings, some of which are in the development phase. (The San Francisco Giants ballpark (Oracle Park) and the Bay waterfront of the South Beach subarea are being included in the Northern Waterfront work).

The area includes the Mission Creek tidal inlet, which has a houseboat community and is crossed by two drawbridges and transportation assets. This area also includes important CCSF and regional infrastructure, including the San Francisco 4th and King Street Caltrain Depot, Bay Bridge touchdown, PG&E substation, San Francisco Public Utilities Commission (SFPUC) Channel Force Main, POSF maintenance facility, T-Third Muni Line, and the planned Mission Bay Ferry Terminal and future California high speed rail alignment.

To capture these unique differences in support of the development of neighborhood-scale geographic adaptation strategies, the Mission Bay/Bayview geography is subdivided into five subareas: South Beach, Mission Creek, Mission Rock, Mission Bay, and Pier 70. Additional information on each subarea is available in the Subarea Profiles, Problems, Opportunities, Objectives, Consideration, and Constraints (POOCCs), and the Flood Risks Profiles. Links to these documents are provided below.

- South Beach: Subarea Profile, POOCC, Flood Risk Profile
- Mission Creek: Subarea Profile, POOCC, Flood Risk Profile
- Mission Rock: Subarea Profile, POOCC, Flood Risk Profile
- Mission Bay: Subarea Profile, POOCC, Flood Risk Profile
- Pier 70: Subarea Profile, POOCC, Flood Risk Profile

3.1.4 Reach 4: Islais Creek / Bayview

This geography covers the southeastern edge of San Francisco, from Pier 80 in the Potrero Hill neighborhood in the north, to Heron's Head Park in the south. In between, it spans a large portion of the Bayview North Islais Creek neighborhood and watershed, the industrial zone surrounding Islais Creek, and the industrially used piers along the waterfront.

The area also includes vital connections between the southern and northern parts of the city, such as the Illinois Street and Third Street drawbridges that cross Islais Creek and Third Street, including the Muni T-Third Light Rail Line (Muni T-Line), and is traversed by many critical regional transportation assets, including the California Department of Transportation (Caltrans) freeways, Caltrain, and a planned future high-speed rail alignment.

The Bayview Islais Creek neighborhood is ethnically diverse with large Black, Asian, and Latino populations, and has a strong African American cultural legacy, with most of this area included within the recently created African American Arts and Cultural Heritage District. The Islais Creek watershed has environmental challenges due to the long-standing presence of industrial uses and freight transportation, and residents of this neighborhood have experienced significant historical and environmental injustices. San Francisco's shoreline is incredibly complex in terms of its engineering and design, as well as its character, culture, businesses, and residents (City and County of San Francisco 2020).

To capture these unique differences in support of the development of neighborhood-scale geographic adaptation strategies, the Islais Creek/Bayview geography is subdivided into five subareas: Pier 80, Islais Creek, Cargo Way, Piers 94 and 96, and Heron's Head Park. Additional information on each subarea is available in the Subarea Profiles, Problems, Opportunities, Objectives, Consideration, and Constraints (POOCCs), and the Flood Risks Profiles. Links to these documents are provided below.

- Pier 80: Subarea Profile, POOCC, and Flood Risk Profile
- Islais Creek: Subarea Profiles, POOCC, and Flood Risk Profile
- Cargo Way: Subarea Profiles, POOCC, and Flood Risk Profile
- Pier 94 and 96: Subarea Profiles, POOCC, and Flood Risk Profile
- Heron's Head: Subarea Profiles, POOCC, and Flood Risk Profile

4 San Francisco Bay Area Storm Climatology

Two primary storm categories can produce coastal hazards and flooding throughout the Bay Area and along the San Francisco shoreline: extratropical cyclones, which develop offshore and bring low barometric pressure, high winds, and heavy rain, and atmospheric rivers, which originate in the tropics can bring heavy precipitation and high winds. These storm systems also occur concurrently, and a single atmospheric event can be associated with a series of extratropical cyclones (Zhang et al. 2019, Dacre and Pinto 2020). Table 4-1 notes which storm drivers increase each respective coastal hazard. Both storm types can bring high winds, the winds are often transformed (i.e., changed in direction) as they flow over the Bay Area's complex topography, creating wind-driven wave patterns that cannot be directly correlated to the storms primary wind direction and may vary by MA due to differences in shoreline orientation. Both storm types can also bring heavy rainfall, which can exacerbate coastal flooding in low-lying areas along the shoreline. Even if Bay waters do not overtop the shoreline, high Bay water levels can prohibit stormwater conveyance to the Bay and cause inland flooding. This dynamic is not considered within G2CRM and will be considered separately through a collaboration with the SFPUC.

Table 4-1. Storm Drivers that Increase San Francisco Bay Coastal Hazards

Driver of Change	Bay Coastal Hazard		
	Water Levels	Ocean Swell	Wind-driven Waves
Barometric Pressure Drop	✓		
High Winds		✓	✓
Heavy Rain			

Both storm systems generally impact San Francisco for between one and five days, although storm conditions can last much longer when multiple systems develop back-to-back (May et al. 2019). The most damaging storms that have occurred between 1980 and today have resulted from the concurrence of a large and rapidly intensifying extratropical cyclone, or bomb cyclone, and an atmospheric river off the California coastline. This combination is projected to become even more damaging in the future (Patricola et al. 2022). However, for the purposes of the G2CRM coastal inputs, no increase in storm intensity or frequency is considered over time. Instead, the timeseries of historic storm events is assumed to be stationary, due to the limitations and underlying assumptions inherent in the G2CRM planning tool (see Section 2.1).

Large-scale climate cycles (for example, ENSO and PDO) also contribute to elevated water levels and coastal flooding (Barnard et al. 2015, May et al. 2016a). These climate cycles can increase the strength of extratropical cyclones and atmospheric rivers (storms that occur during El Niño winters often carry more precipitation and can bring higher windspeeds than those that occur during La Niña winters) (Patricola et al. 2019). Although the influence of ENSO and PDO are captured within the timeseries of historic observations and numerical model output analyzed for this study, no changes to these large-scale climatic phenomena in the future are considered within the coastal input to G2CRM. This is due to the limitations inherent in the G2CRM planning tool (see Section 2.1), and the uncertainties related to projecting climate change related changes to the large-scale climate cycles.

Although recent research studies generally agree that the number and duration of strong La Niña events are likely to increase under a warming climate (Cai et al. 2015, Marjani et al. 2019), there is less agreement on strong El Nino events, with projections ranging from a slight decrease to nearly doubling the number of strong El Nino events under a warming climate (Cai et al. 2014a, Kim et al. 2014, Marjani et al. 2019). Although climate change will influence ENSO and the devastating impacts associated with extreme El Niño events, El Niño is never the

only factor impacting the probability of climate extremes, and several processes are still to poorly understood to develop long-term projections (Goddard and Gershunov 2020). ENSO is arguably the most dramatic year-to-year variation of the Earth's climate system, and how climate change will affect ENSO is the subject of increased scientific focus (McPhaden et al. 2020). In the absence of considering future increases in storm intensity and frequency over time, and future changes to ENSO which could have substantial impacts on number and magnitude of future San Francisco flood events, the resultant economic damages calculated by G2CRM should be considered a lower bound, particularly when lower rates of sea level rise are evaluated.

The following sections describe typical extratropical cyclone and atmospheric river conditions that impact the study area, how ENSO and PDO influence local climate and water level conditions, and a characterization of large storms that impacted the study area.

4.1   Extratropical Storms (low-pressure systems)

Extratropical storms that impact the central California coast are governed by the North Pacific High; a persistent zone of high pressure located over the northeastern Pacific Ocean near the Aleutian Islands. The strength and location of this system varies annually and seasonally. During the summer months, the high-pressure zone migrates northward and diverts most storm tracks to the north. During the winter months, the high-pressure system shifts to the south, allowing intense extratropical storms to impact central and southern California. These large and energetic storms can generate offshore waves of 20 to 30 feet and wind speeds of over 40 mph (Griggs et al. 2005). The area of low-pressure within the storm allows ocean waters to expand, temporarily increasing the water surface elevation. For every millibar drop in atmospheric pressure within a storm system, the ocean water level rises about 0.4 inch (USGS 1999). Figure 4-1 shows the size of the low-pressure system associated with an extratropical storm off the Pacific coast of the U.S.
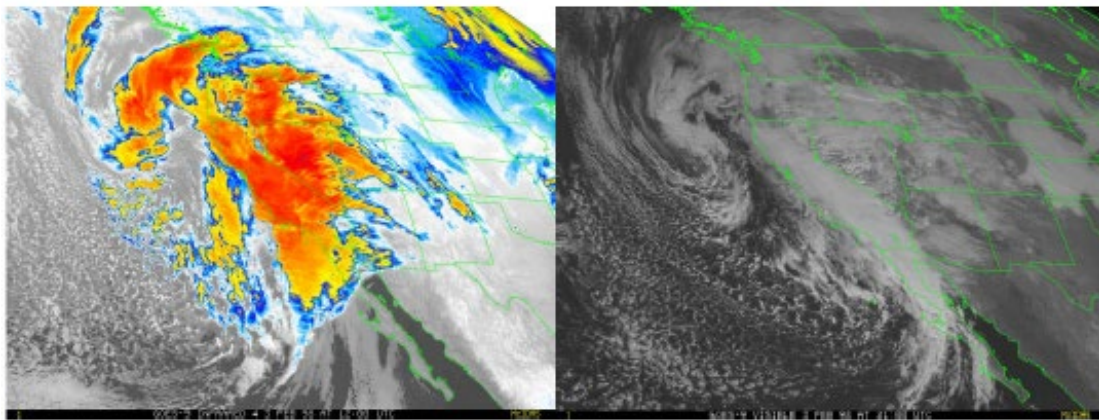
Source: (NCDC 1998)

Figure 4-1. Visible Satellite (right panel) and Infrared Image of the Low-pressure System on February 3, 1998

4.2   Atmospheric Rivers

Atmospheric rivers are narrow, ribbon-like bands of moisture that originate from the tropics and result in substantial rainfall (May et al. 2016a). The most familiar atmospheric river along the Pacific coast is the "Pineapple Express," which brings warm, moist water vapor from the tropics near Hawaii to central California and other areas along the Pacific coast. The impacts of atmospheric rivers are most pronounced during the winter months. Figure 4-2 shows an image of the atmospheric river that dropped significant rainfall on central and northern California on December 11, 2014, and resulted in widespread flooding, street closures, and power outages across the Bay Area.
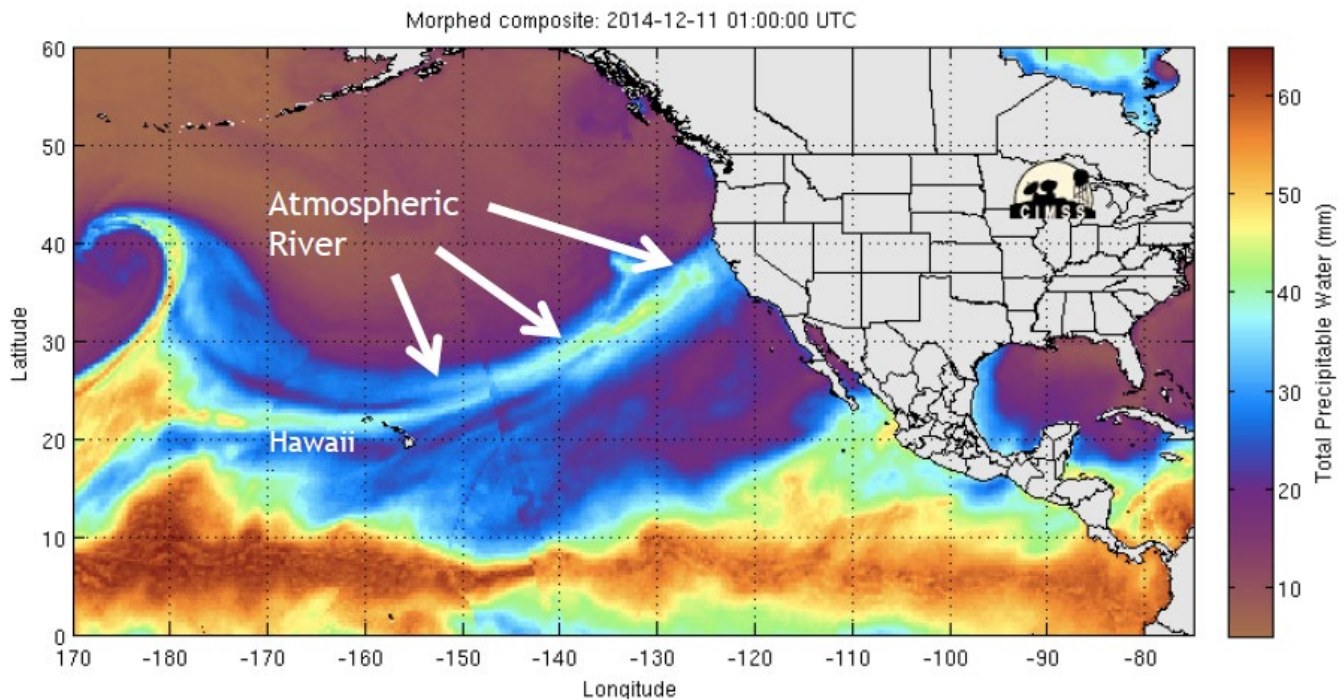
Source: Cooperative Institute for Meteorological Satellite Studies

Figure 4-2. Atmospheric River Resulting in Heavy Rains Across the Bay Area on December 11, 2014

4.3   El Niño Southern Oscillation

Water levels in the Bay are strongly influenced by the ENSO cycle. Under La Niña conditions, global trade winds blow from east to west across the Pacific Ocean, moving warm surface water away from the Americas and toward the western Equatorial Pacific (May et al. 2016a). The warm waters then move up to Japan and down to Australia. Figure 4-3 (right) highlights the cooler expanse of water along the equatorial Pacific associated with La Nina conditions. Every 2 to 7 years, the global trade winds weaken and can reverse, causing warm, equatorial waters to flow east toward the Americas (Figure 4-3, left). During strong El Niños, unusually warm waters migrate northward along the California coast. The warm, less dense, coastal waters can result elevated water levels for prolonged periods (that is, weeks to months).

During El Niño, atmospheric and oceanographic conditions in the Pacific Ocean produce severe winter storms that can result in Bay Area flooding. Tides within the Bay are often elevated 0.3 to 1.0 foot above astronomical predictions, and wind waves and ocean-driven swells can elevate local water levels further.
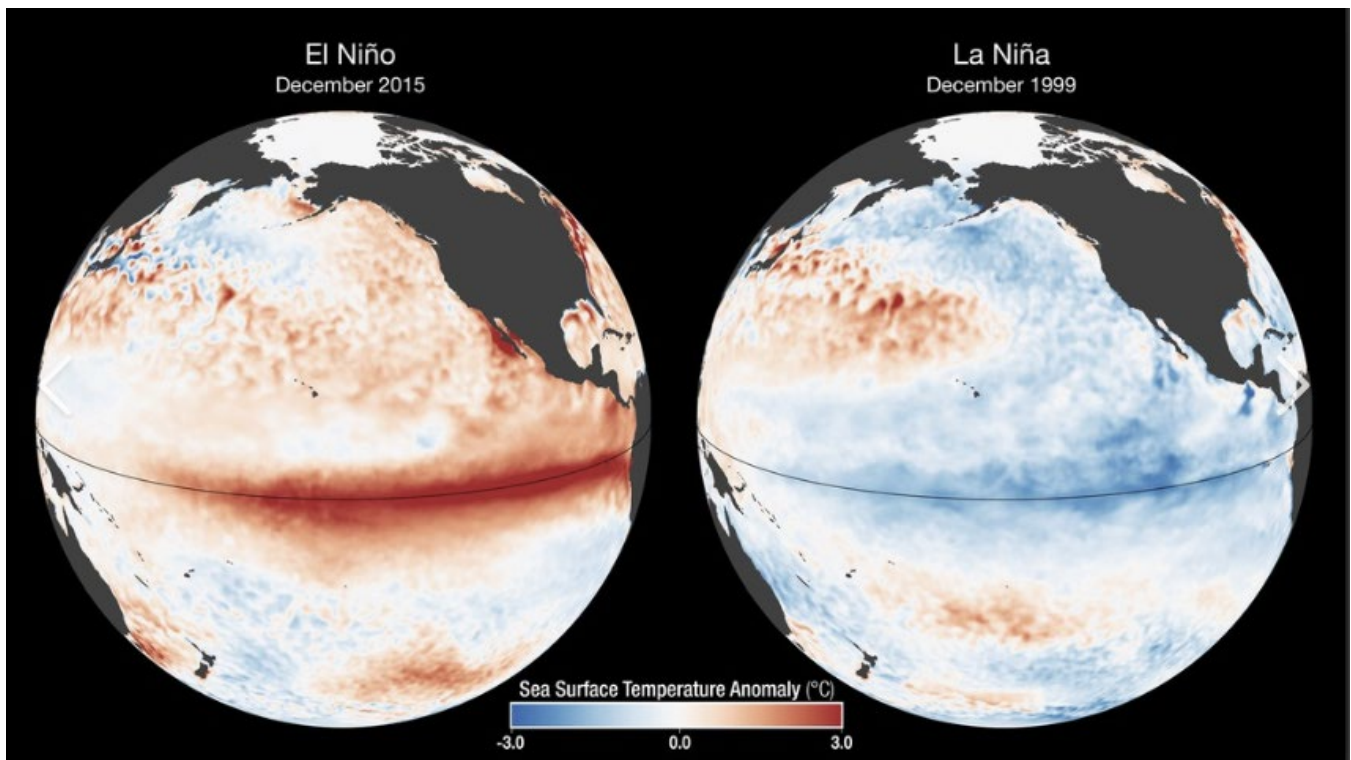
Figure 4-3. Sea Surface Temperatures associated with El Niño and La Niño Conditions

4.4 Pacific Decadal Oscillation

The PDO produces an atmospheric shift similar to ENSO, but it varies over a time scale of decades rather than years. The PDO can remain in the same phase for 20 to 30 years. The extreme phases of the PDO are classified as warm or cool based on observed ocean temperature anomalies and sea surface elevations in the eastern equatorial Pacific Ocean. Shifts in the PDO can intensify or diminish the impacts of ENSO-related events. For example, if both ENSO and PDO are in a warm phase, El Niño impacts may be magnified; alternatively, if ENSO is in a warm phase and the PDO is in a cool phase, El Niño-related impacts may be dampened or prevented from occurring (Zervas 2009, Teegavarapu and Schmidt 2019).

The PDO was primarily in a cool phase from 1998 to 2013, suppressing El Niño conditions and water elevations along the Pacific coast and California (May et al. 2016a). Evidence suggests that the last PDO shift occurred in 2014 and is currently strongly warm, which may enhance local water levels and future El Niño events. Figure 4-4 shows the sea surface temperature variation from the long-term average in the Pacific Ocean, attributed to PDO and El Niño, during a positive or warm phase. When the PDO is in its warm phase, warmer than average waters are located along the Pacific coast of the US and Canada, with warmer water also located along the equatorial Pacific (positive values on Figure 4-4, left). Cooler than average waters are observed in the western Pacific (negative values on Figure 4-4, left). When the PDO is in its cool phase, these temperature anomalies are reversed, and cooler waters are found along the Pacific coast of the US and Canada and the along the equatorial Pacific, and warmer than average waters are observed in the western Pacific. The temperature deviations from the long-term average associated with El Niño can be more pronounced, with warmer than average waters observed along the equatorial Pacific in El Niño years (Figure 4-4, right), and cooler than long-term average waters observed during La Niña years.
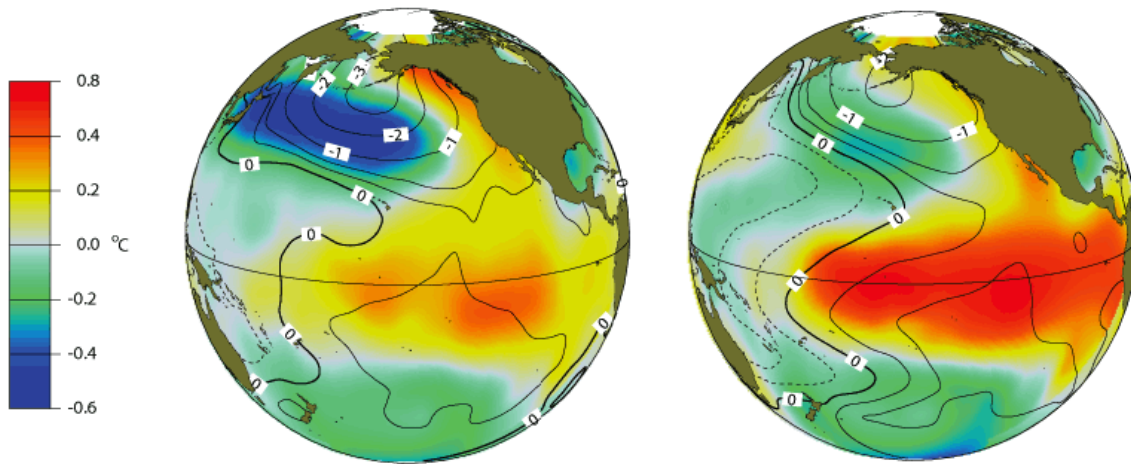
Source: (Climate Impacts Group 2009)

Figure 4-4. Typical PDO (left) and ENSO (right) Sea Surface Temperature Departures from Long-term Average (during positive years)

4.5   Storm Characterization

Local storm identification criteria were developed for the Extreme Precipitation Study to support the San Francisco Public Utilities Commission (SFPUC), the POSF, and the San Francisco International Airport (SFO) (May et al. 2019). Past storm events that occurred between 1980 and the present were reviewed and compared with local newspaper stories of damage to Bay Area communities to identify a suite of relevant storm characteristics related to large and damaging storm events. Although large storm events occurred prior to 1980, satellite imagery and other data are only available for storms that have occurred within approximately the past four decades.

Using the overall characteristics of the storms identified by the agencies as a guide, the full climatological record of historic large storms that have occurred since 1980 were reviewed with respect to the following parameters at the National Oceanic and Atmospheric Administration (NOAA) San Francisco Downtown Weather Station[2] and the NOAA SFO Weather Station.[3] Parameters such as storm track and landfall location, which are important for Atlantic and Gulf coast hurricanes, are less relevant for Pacific coast storm systems. Two storm types impact northern California and the west coast, extratropical cyclones and atmospheric rivers. Both can provide mild showers to torrential rainfall, high winds, wave hazards, and elevated Bay water levels. Extratropical cyclones and atmospheric rivers can occur on their own, or they can co-occur. Extratropical cyclones can impact an extremely large area (that is, the entire west coast of the U.S., as shown in Figure 4-1); therefore, the extract center of the storm, and landfall location of the center of the storm, is not a significant contributor to the magnitude of the impacts. Similarly, atmospheric rivers can have a long, wide, and meandering path that make storm track and landfall location less relevant for characterizing Bay Area impacts, particularly when they are accompanied by multiple extratropical cyclones occurring in series.

The following characteristics were considered to have the most relevance for San Francisco, particularly when combined with local agency knowledge of impacts and newspaper articles related to flooding and damages. Although the precipitation related characteristics are not relevant for the G2CRM coastal storm inputs, they are

---

[2] COOP: 047772 – San Francisco Downtown CA US (1980 – 2011); SFPUC RG31 Station – Mission Street (2011 – 2018)

[3] WBAN:23234 San Francisco International Airport, CA US (1980 – 2013), https://www.ncdc.noaa.gov

nevertheless helpful in communicating the importance of considering precipitation-related flooding and impacts outside of G2CRM.

- Storm duration (that is, storm start and end dates)
- Maximum hourly wind speed and direction
- Minimum barometric pressure
- Maximum wind gust
- Strength of El Niño/La Niña using the Oceanic Niño Index
- Storm type (for example, atmospheric river, extratropical cyclone, atmospheric river combined with an extratropical)
- Storm total precipitation
- 1-hour, 3-hour, 12-hour, and 24-hour maximum precipitation

The following parameters were analyzed at the Presidio tide gage:[4]

- Predicted astronomical tide levels
- Observed water levels
- Non-tidal residual (predicted – observed water levels)

The review of the available data, coupled with desktop research related to storm impacts around the region, identified 15 large storms events that appeared to represent the range of climatic conditions (for example, precipitation, windspeed, and storm surge conditions) that are most relevant for the CCSF. The parameters were cataloged to compare the storm characteristics across the 15 storms (Table 4-2). The selected storms include a range of storm types and a range of El Niño conditions, and the order of the storms presented is not intended to represent any ranking related to the storm characteristics or storm-related damages. The 15 storms presented in Table 4-2 are also not intended to represent the storm catalog used to develop the CSDs for G2CRM; instead, the table informs relevant west coast storm characteristics, storm duration, and storm season to support CSD development.

The large storms in Table 4-2 have durations ranging from one day to eleven days, with an average duration of about 4.5 days. However, the long storm durations of 9 and 11 days associated with the storm events in 1998 and 1986 respectively are associated with atmospheric rivers coupled with a series of extratropical cyclones and are therefore not representative of a single storm duration. Removing these two storms results in an average storm duration of 3.4 days.

A storm duration of 3 days was selected for identifying and selecting storm events for the coastal storm inputs to G2CRM. G2CRM does not support the selection of varying storm durations. In addition, in the absence of applying a stage volume curve within G2CRM, only the peak water level + wave height combination from the 3-day event is selected for assessing damages. The peak water level + wave height combination is extended inland using the bathtub method to support the damage calculations. Therefore, for the purposes of the coastal storm inputs, adequately capturing the peak water level and wave height combination is more important than capturing the correct storm duration. This approach is a simplifying assumption that means inland areas behind coastal defenses will flood with the slightest amount of overtopping. Although this assumption may seem an overestimate of inland flooding, comparisons of the bathtub approach with more sophisticated numerical models that simulate the physical processes of coastal overtopping, wave hazards, and groundwater flooding due to sea level rise can result in an increase in the total land area impacted by sea level rise by up to 50 percent (Anderson et al. 2018). In the absence of two- or three-dimensional numerical modeling that incorporates all of the relevant physical

---

[4] 9414290 – NOAA San Francisco Presidio Tide Station (1898 – 2019)

processes of interest, the bathtub approach represents a reasonable assumption that may over or underestimate future inland flooding as the shoreline is overtopped.

Table 4-2. Key Observed Historical Storm Events and Storm Characteristics

Storm Year	Storm Duration (days)	Storm Dates NOAA SF Downtown Station[a] Storm Start	Storm End	Storm Type	ONI [b]	Precipitation Totals SF Downtown Station[c] Storm Total (in)	1-hr MAX (in)	3-hr MAX (in)	12-hr MAX (in)	24-hr MAX (in)	Wind Speed (max hourly) SFO (mph)	Wind Gust (instantaneous) SFO (deg)	SFO (mph)	Min Barometric Pressure SFO (mb)	Max Non-tidal Residual Presidio (feet)	Maximum Observed Water Level Presidio (feet-NAVD)	Residual (Storm Surge) at Max Observed Water Level Presidio (feet)
2014	5	12/2/2014	12/6/2014	cyclone	+0.7	3.4	0.8	1.2	1.6	2.3	31	180	39	1005.1	1.4	7.8	1.3
2014	2	12/11/2014	12/12/2014	AR + cyclone	+0.7	3.7	0.6	1.0	2.5	3.5	29	150	45	999.3	1.9	6.3	1.5
1982	3	1/3/1982	1/5/1982	AR + weak cyclone	0.0	4.7	0.5	1.1	2.7	4.2	30	140	35	1003.3	1.4	7.0	1.1
1994	4	11/4/1994	11/7/1994	AR	+1.0	6.9	0.7	1.9	5.0	6.2	23	360	32	1011.3	0.5	7.2	0.3
1998	9	1/31/1998	2/8/1998	AR + cyclone	+1.9	9.2	0.4	0.9	2.4	3.6	30	110	41	989.0	3.1	8.5	2.5
1995	4	12/10/1995	12/13/1995	AR + cyclone	-1.0	5.5	0.5	1.0	2.5	3.7	54	220	55	999.0	2.1	6.4	1.5
1986	11	2/11/1986	2/21/1986	AR + cyclone	-0.5	7.8	0.8	1.2	1.7	1.9	48	190	56	998.0	1.8	6.6	1.2
1983	4	1/21/1983	1/24/1983	AR + cyclone	+2.2	2.4	0.4	0.7	1.2	1.2	29	210	52	1007.1	1.6	7.6	1.4
2009	1	10/13/2009	10/13/2009	AR + cyclone	+1.0	2.5	0.5	1.1	2.4	-	41	180	56	995.2	1.6	6.6	1.1
2018	2	1/8/2018	1/9/2018	AR from south + weak cyclone	-0.9	2.6	0.1	0.4	1.3	2.4	32	280	46	1015.6	1.0	6.7	0.9
2008	6	1/22/2008	1/28/2008	cyclone from high-latitudes	-1.6	4.5	0.4	1.1	2.7	3.2	24	180	38	999.2	1.1	6.8	0.1
1990	3	2/15/1990	2/17/1990	cyclone from high-latitudes	+0.2	1.8	0.3	0.7	1.4	1.5	55	220	62	1006.1	0.9	5.7	0.2

Storm Year	Storm Duration (days)	Storm Dates NOAA SF Downtown Station[a]		Storm Type	ONI [b]	Precipitation Totals SF Downtown Station[c]					Wind Speed (max hourly)	Wind Gust (instantaneous)	Min Barometric Pressure	Max Non-tidal Residual	Maximum Observed Water Level	Residual (Storm Surge) at Max Observed Water Level
		Storm Start	Storm End			Storm Total (in)	1-hr MAX (in)	3-hr MAX (in)	12-hr MAX (in)	24-hr MAX (in)	SFO (mph)	SFO (deg)	SFO (mph)	SFO (mb)	Presidio (feet)	Presidio (feet-NAVD)	Presidio (feet)
2004	4	2/24/2004	2/27/2004	AR + cyclone	+0.3	2.3	0.7	1.4	1.9	2.0	31	130	45	1002.2	1.9	6.2	0.8
2005	3	12/29/2005	12/31/2005	AR	-0.8	3.0	0.6	1.1	2.4	2.8	38	190	55	998.9	1.3	8.0	1.2
2017	6	1/7/2017	1/12/2017	AR + cyclone	-0.3	3.9	0.3	0.4	1.1	1.4	44	170	61	1005.8	1.4	7.7	0.7

[a] Storm start/end dates and precipitation characteristics using NOAA San Francisco Downtown Station (COOP: 047772; 1980 – 2011); SFPUC Mission Street Station (ID: RG31; 2011 – 2018).

[b] ONI is a 3-month running mean of sea surface temperature anomalies in the Niño 3.4 region (of the Pacific Ocean). This is a measure used to define El Niño or La Niña events. ONI between 1.0 and 1.5 is classified as moderate; between 1.5 and 2.0 as strong; and above 2.0 as very strong.

[c] Precipitation related characteristics are not relevant for the G2CRM coastal storm inputs; however, they are nevertheless helpful in communicating the importance of considering precipitation-related flooding and impacts outside of G2CRM.

AR = atmospheric river
deg = degree(s)
in = inch(es)
mb = millibars
ONI = Oceanic Niño Index

5   FEMA San Francisco Bay Area Coastal Study

FEMA conducted detailed coastal engineering analyses of the shoreline and coastal areas within the nine Bay Area counties – Alameda, Contra Costa, Marin, Napa, San Francisco, San Mateo, Santa Clara, Solano, and Sonoma counties. The coastal hazard analysis was used to update the coastal Flood Insurance Rate Maps (FIRMs) for San Francisco that became effective on March 23, 2021.

The previous Bay coastal flood hazard mapping was based on the 1984 USACE study San Francisco Bay Tidal Stage vs. Frequency Study (USACE 1984), and did not include any wave hazard analysis. In 2004, FEMA initiated the San Francisco Bay Area Coastal Study, and its companion Open Pacific Coast Study, which represented the first comprehensive California statewide assessment of coastal hazards (including wave hazards) ever completed. The FEMA modeling relied on the MIKE21 suite of models (DHI 2011, 2013) to complete a comprehensive assessment of historical storm events and coastal hazards with a long-term hindcast, and each phase of the FEMA study underwent independent technical review. The high-fidelity numerical modeling output that provides the foundation for the updated FEMA FIRMs is well suited for providing the coastal storm inputs required for G2CRM.

The FEMA FIRMs present the 1%-annual-chance and 0.2%-annual chance coastal flood hazard based on a long-term modeling hindcast, using a statistical approach that analyzes multiple processes across the historic storm events (FEMA 2016). The FEMA modeling captures the full range of water levels and wave dynamics along the Bay shoreline, and the model was well calibrated to both daily tidal conditions and large storm events.

FEMA evaluates many combinations of the physical processes that can occur simultaneously during storm events (for example, ocean swell, locally generated wind-driven waves, tidal variations, and elevated water levels during El Niño conditions) using guidelines developed for the Pacific coast (FEMA 2005) and sheltered waters (FEMA 2008). In the Bay, no single storm event produces the highest water level and highest wave hazard along the entire shoreline (May et al. 2016a). In fact, no single storm event produces either the highest water levels or the highest wave hazards along the shoreline due to the size and complexity of the Bay and the storm events that occur in the Bay Area (Conner et al. 2011). Developing a statistical estimate of the 1%-annual chance coastal flood hazards by analyzing discrete events (i.e., event-based analysis) is therefore challenging in the Bay Area, and FEMA selected a response-based analysis approach which required a long history of observations or model output of Bay water levels and wave dynamics, and a probabilistic analysis to estimate extreme water levels and wave heights (Gumbel 2004, FEMA 2005, 2016, Drobyshevski et al. 2014, Koohi Kheili et al. 2021).

FEMA relied on a regional MIKE21 Flow (HD) and Spectral Wave (SW) hydrodynamic and wave dynamic numerical model of the Bay to develop a 31-year continuous timeseries of water levels and waves to represent the long history needed to support a response-based approach (DHI 2011, 2013). The modeling was conducted in two stages.[5] The first stage focused on the north and central Bay (north of the San Mateo-Hayward Bridge) and the second stage focused on the south Bay. The numerical modeling effort underwent independent peer review by USACE staff and BakerAECOM (a FEMA subcontractor). All model output used to inform the G2CRM CSDs was derived directly from the FEMA numerical modeling effort, the foundational data that underlies the FEMA coastal hazard analysis.

---

[5] The FEMA San Francisco Bay regional hydrodynamic modeling studies were completed in two stages due to the nature in which the FEMA studies were originally contracted. The first stage covered the entire San Francisco Bay, with an emphasis on accurately modeling tide and wave processes in the North and Central Bays, north of the San Mateo-Hayward Bridge. The regional model was later refined to better characterize the more complex South Bay bathymetry and hydrodynamics.

The following subsections provide a brief summary of the numerical modeling effort. Additional details are available in Regional Coastal Hazard Modeling Study for North and Central San Francisco Bay and Regional Coastal Hazard Modeling Study for South San Francisco Bay (DHI 2011, 2013).

5.1 MIKE21 HD Model

Figure 5-1 presents the model domain and the location of the Open Pacific Coast and Sacramento River boundary conditions. The grid resolution of the model is 100 meters, and the model output includes a continuous 31-year simulation from January 1, 1973 to January 1, 2004. The offshore wave data to drive the MIKE21 SW model was the primary limiting data set for the length of the MIKE21 HD and SW simulations (Section 5.2.2). Data used to drive the model include:

- Bathymetric and topographic data compiled from best available data sources as of 2010
- Measured 1-hourly time variation of the Pacific Ocean offshore tide level (baselined to 2008 water levels to remove the sea level rise trend)
- Two-dimensional, 1-hourly wind fields covering the Bay, using multiple wind stations.
- Daily mean discharge of the Sacramento River, which has a contributing watershed of roughly 40% of the state of California (Figure 5-1)
- Daily mean discharge of the other main tributaries entering the Bay (Figure 5-1)

The detailed two-dimensional wind fields were created using three wind stations: San Francisco Airport, Oakland Airport, and Travis Air Force Base. A more sophisticated meteorological model was tested, but it was over-smoothing the peak windspeeds and was deemed less appropriate than the wind field derived from the three wind stations. Wind data was collected and reviewed at 72 wind stations throughout the Bay Area from the National Climatic Data Center, NOAA's Center for Operational Oceanographic Products and Services, California Irrigation Management Information System, and the Bay Area Air Quality Management District. Most stations, except for the three stations selected as the primary data sources for the wind fields, only had partial coverage during the period of interest (DHI 2011).

The MIKE21 model was calibrated and validated using 21 available tide gages in the Bay. Although the Presidio tide gage provides a consistent long-term record of Bay tides, the remaining stations include partial records. Some stations include multi-year records, whereas others may have recorded data for less than 10 years with stops and starts in data collection. Each model calibration and validation period included elevated Bay water levels (that is, coastal storm events), and measurements from at least two tide gages. The Presidio tide gage was used for all model calibration and validations. The model was calibrated to two storm periods and validated with 11 additional storm periods. The model is well calibrated to Bay water levels with details presented in *Regional Coastal Hazard Modeling Study for North and Central San* Francisco Bay (DHI 2011).

5.2 MIKE21 SW Model

Two MIKE21 SW computations domains were developed to model wind-driven waves within the Bay (Figure 5-2), and longer-period ocean swell entering through the Golden Gate.

5.2.1 Wind-driven Waves

The MIKE21 SW computational mesh uses an unstructured triangular element mesh (Figure 5-2). Element sizes vary from 400 to 500 meters away from the shoreline to 150 to 200 meters near the shoreline. There are no open boundary conditions, as the purpose of this model is to capture the generation of wind-driven drives within the Bay. Two boundary conditions are applied:

- Two-dimensional hourly wind fields (same as noted in Section 5.1)
- Two-dimensional water levels interpolated onto the computational mesh from MIKE21 HD

Limited wave data was available for calibration of the wave model, although all available wave data were collected and reviewed at the time the modeling was completed. The data included academic research data collected by Stanford University graduate students, wave data collected by SFO in 1999-2000 to inform a separate numerical modeling effort, and wave data collected in 2005 by Sea Engineering.

The final model was run for the full 31-year simulation period from January 1, 1973 to January 1, 2004.

5.2.2 Ocean Swell

The MIKE21 SW model was also used to simulate the offshore swell propagation and penetration through the Golden Gate and into the Bay. The computational mesh uses a triangular element mesh (Figure 5-3). The resolution of the model is coarser in the north and south Bay based on exploratory simulations that showed that swell wave energy reaching these areas is negligible, and swell heights were generally on the order of 1 to 2 centimeters. Two boundary conditions are applied:

- Ocean wave parameters from two GROW hindcast simulations provided by Oceanwater, Inc.[6]
- Two-dimensional water levels interpolated onto the computational mesh from MIKE21 HD

Calibration and validation of the swell model was limited to use of measurements at two locations outside the Bay offshore of Stinson Beach and Pacifica, and one location inside the Bay near Fisherman's Wharf. The confidence of the swell model results could have increased had more reliable and longer-term wave measurements been available inside the Bay.

The final model was run for the full 31-year simulation period from January 1, 1973 to January 1, 2004.

---

[6] The availability of this data limited the length of the simulation to 31 years. After the completion of this study, Oceanweather, Inc. produced additional hindcast data to support the FEMA Open Pacific Coast Study. However, the San Francisco Bay regional numerical modeling was already complete.
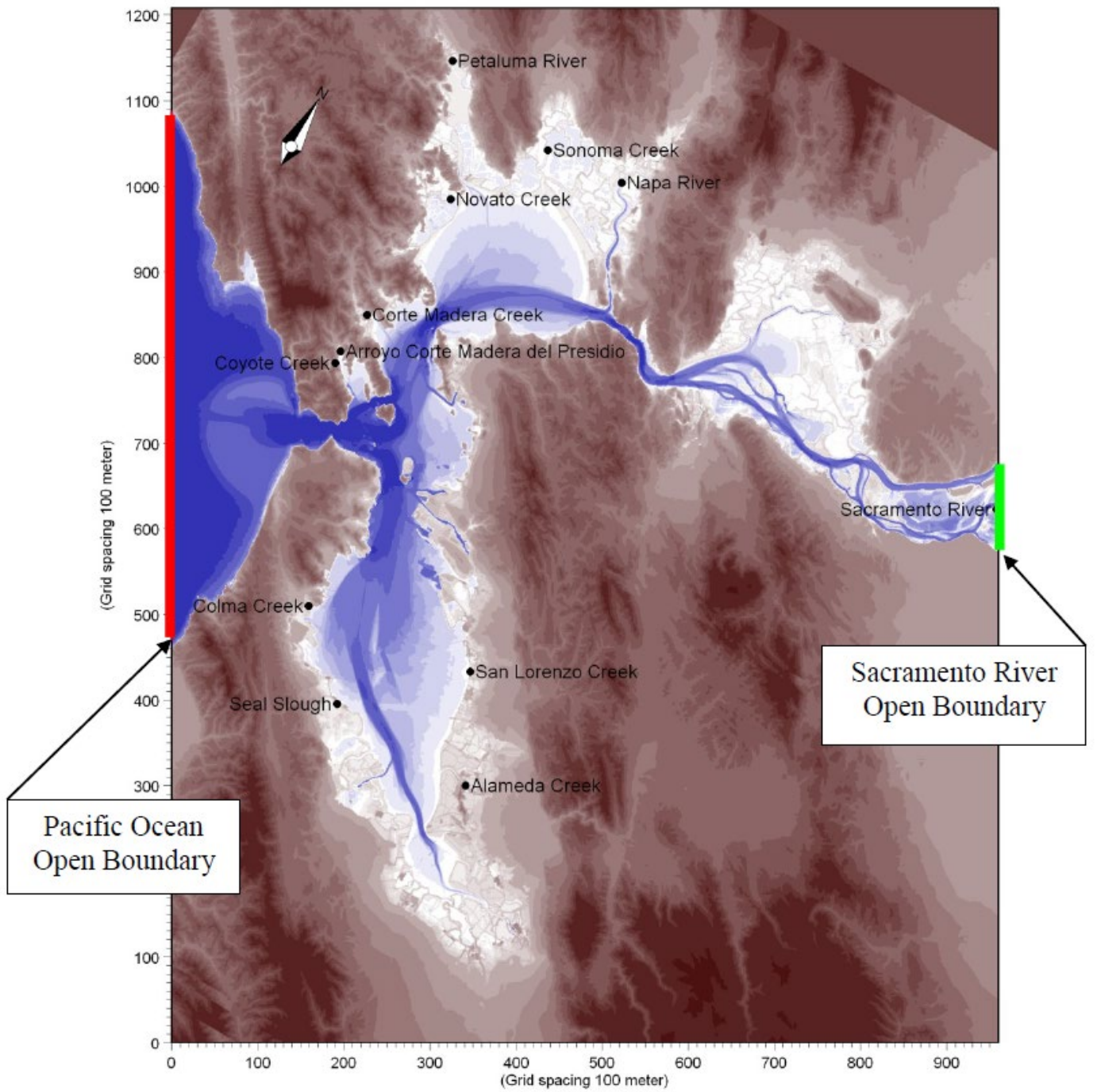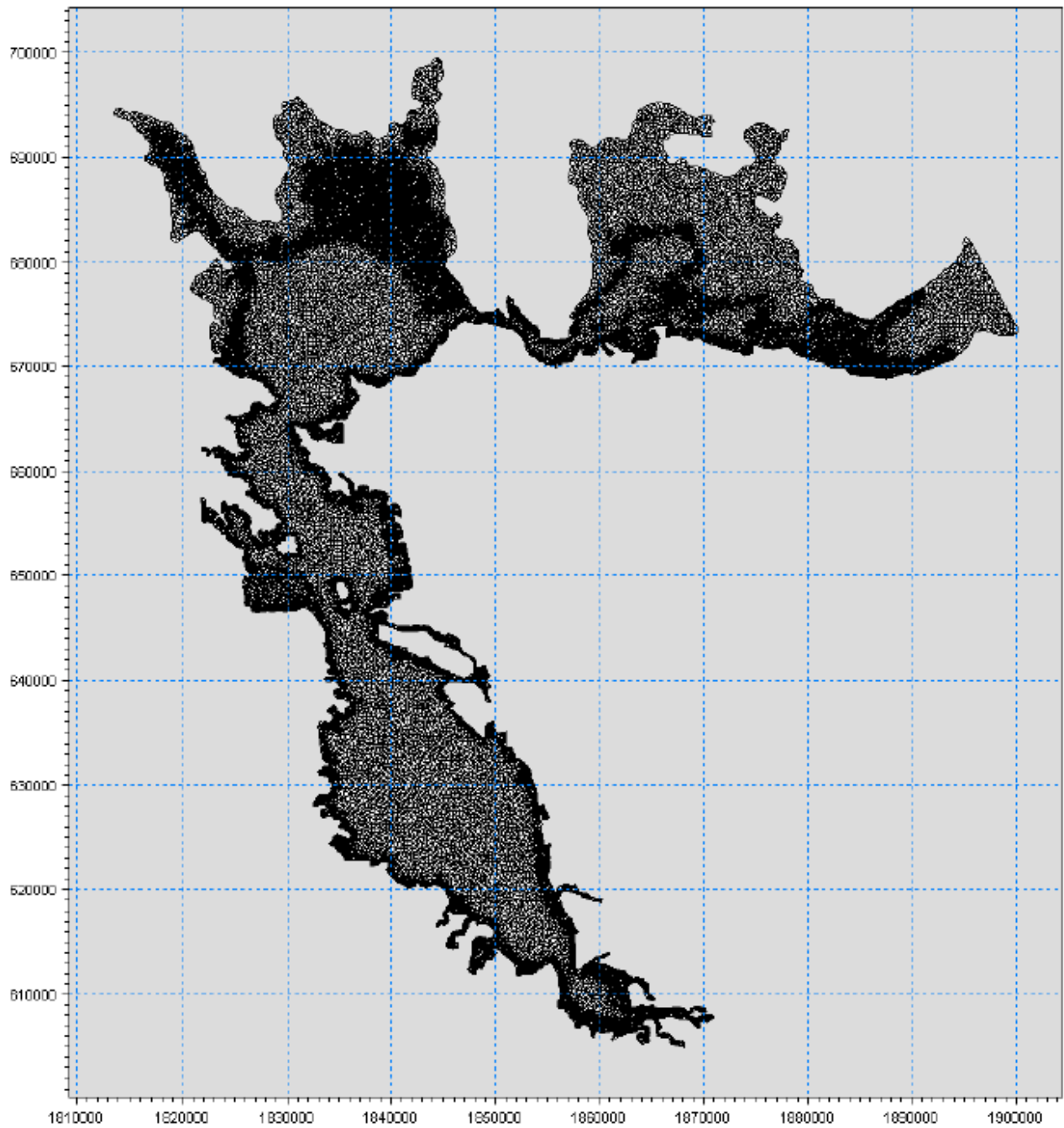
Source: (DHI 2011)

Figure 5-1. FEMA MIKE21 HD Model Domain and Boundary Condition Locations

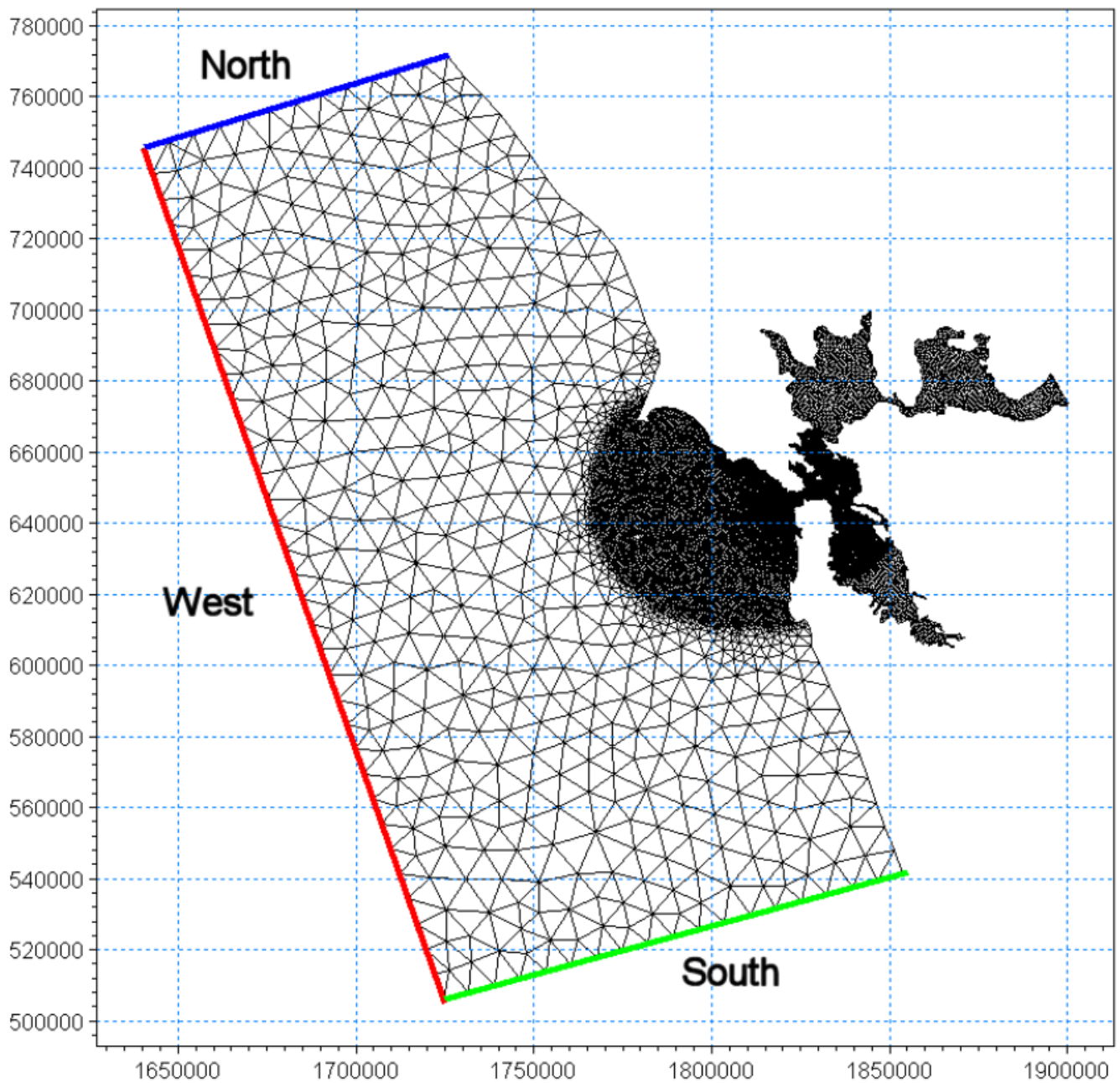Note: The black dots represent the freshwater inflow source locations.

Source: (DHI 2011)

Figure 5-2. MIKE21 SW Computational Mesh for Wind-driven Waves

Note: Coordinates are in California State Plane III, North American Datum 1983, meters.

Figure 5-3. MIKE21 SW Model Computational Mesh for Ocean Swell

Note: Colored lines indicate the positions of the open boundaries. Coordinates are in California State Plane III, North American Datum 1983, meters.

5.3   Production Simulations

The regional modeling occurred in three steps:

1. Bay water levels were simulated with MIKE21 HD using an ocean tidal boundary condition wind fields and river discharges.

2. Wind-driven waves were modeled in MIKE21 SW using two-dimensional wind fields and the Bay water levels from Step 1.

3. Ocean swell were modeled in MIKE21 SW using an offshore boundary condition from Oceanweather, Inc. GROW hindcast database and the Bay water levels from Step 1.

The final production simulations created 31-year time series of model output (for example, water levels, wind-driven wave characteristics, and ocean swell characteristics) at over 8,000 points along the complex Bay shoreline to support the response-based analysis. Water level information was saved at 15-minute increments, and wave characteristics were saved at 1-hour increments, which are commensurate with the tidal boundary conditions and wind-field inputs to the model, respectively. Model output points were located along the shoreline at the zero-foot NAVD 88 contour and 300 feet offshore of the zero-foot contour. Due to the shallow depths along the Bay shoreline, some locations only have data for 300 feet offshore. These time series files of model output along the shoreline were used to inform the development of the CSDs, as presented in Section 7.

Figure 6-2 and Figure 6-19 present the variation in MHHW and the 1% AEP water levels at a subset of model output points along the San Francisco shoreline. Figure 5-4 presents the 1% AEP for the wind-generated significant wave heights. Figure 5-5 presents the 1% AEP for the wave crest elevations. Figure 5-6 presents the 1% AEP for the long-period ocean swell that entered through the Golden Gate. All 1% AEPs were derived from the full time series at each model output from the 1973 to 2004 simulations using the MIKE21 HD and SW calibrated and validated models.
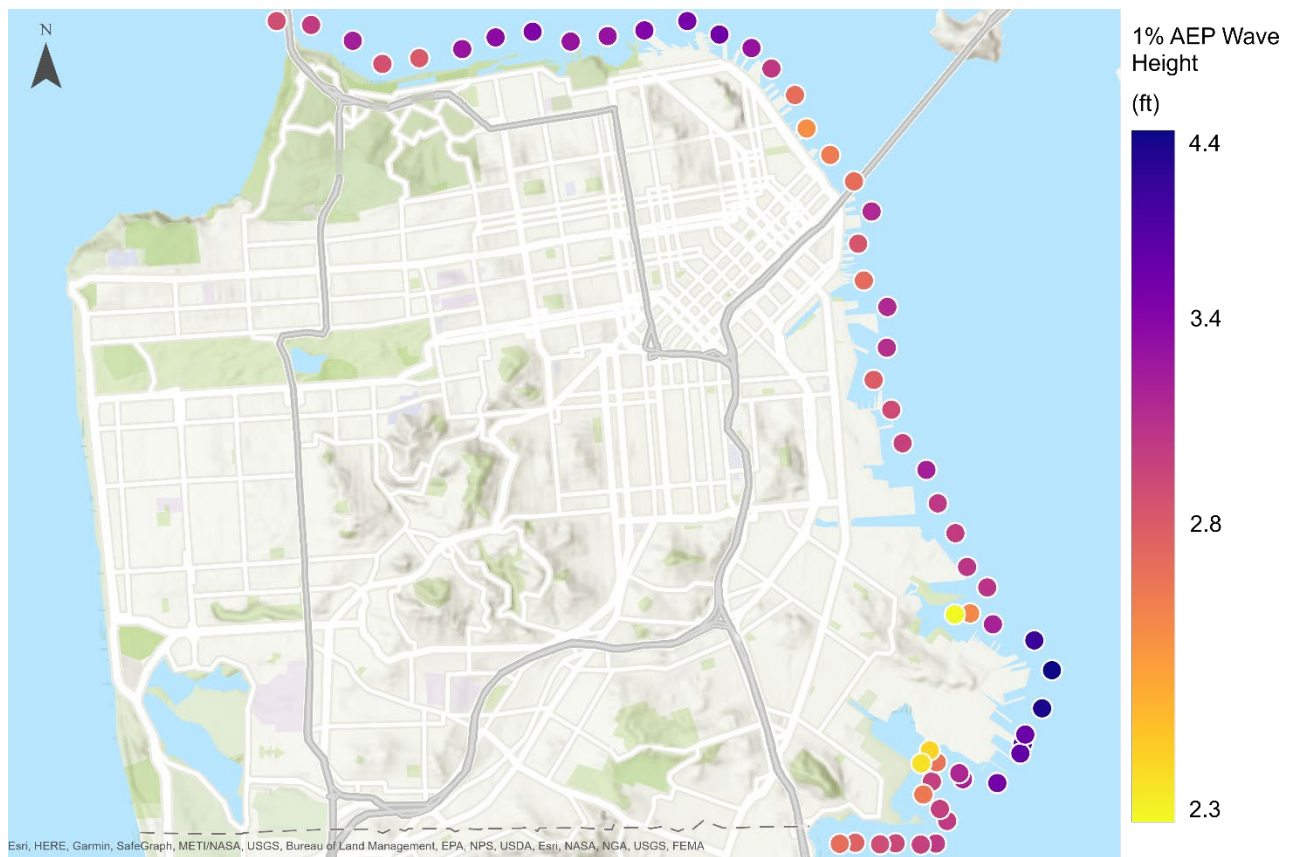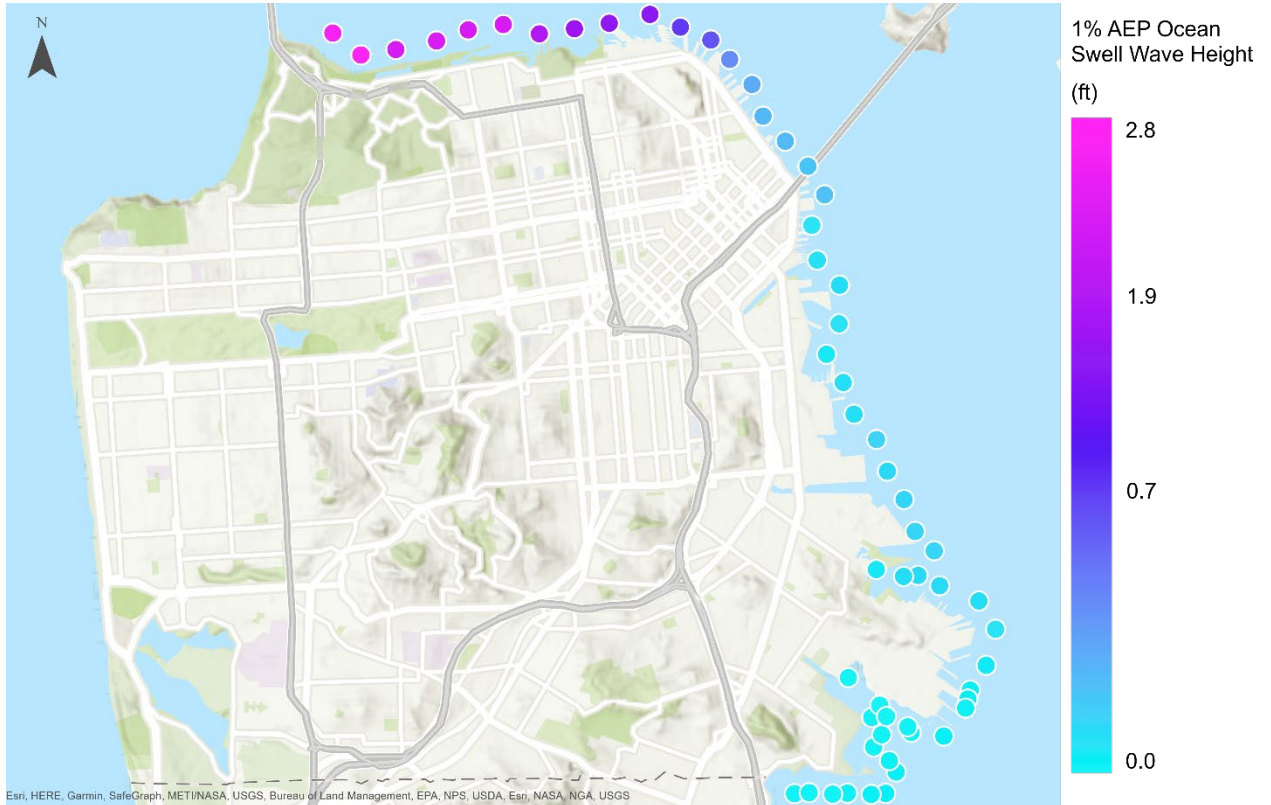

Source: (DHI 2011)

Figure 5-4. Variations in 1% AEP Wave Height (relative to 2008)
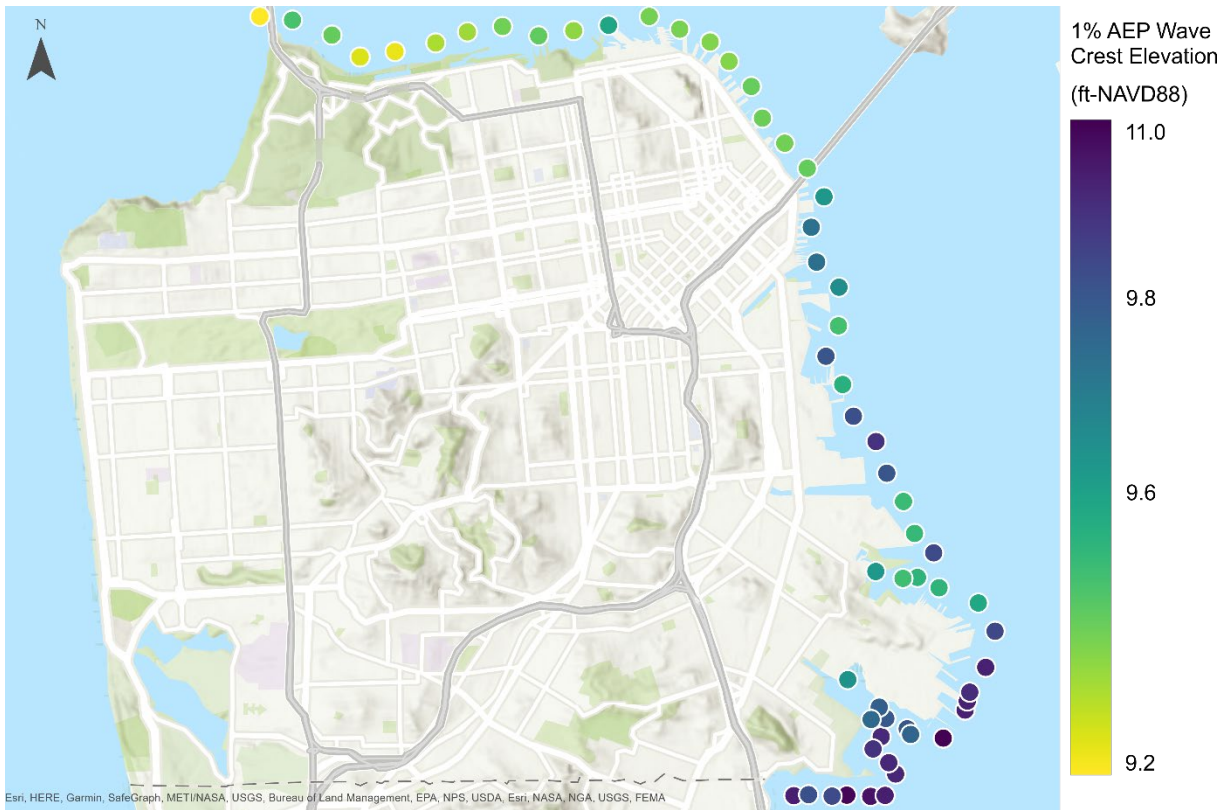
Source: (DHI 2011)

Figure 5-5. Variations in 1% AEP Wave Crest Elevation (relative to 2008)

Source: (DHI 2011)

Figure 5-6. Variations in 1% AEP Ocean Swell Wave Height (relative to 2008)

5.4   Simulation Period Uncertainty

The FEMA modeling relied on the period from 1973 to 2004, a 31-year length of record, to perform response-based analysis and develop reasonable estimated of the 1% and 0.2% annual chance coastal flood hazards. The period of record was selected based on the availability of boundary condition data, and the requirement of having a minimum of 30 years of record to estimate the 1% annual chance coastal water level. Additional periods of record are analyzed, using observed water levels from the Presidio tide gage, to assess if the 1973 to 2004 period of record is a reasonable approximation of post 2004 water levels.

Mean sea level has risen over the past century, as shown on Figure 5-7. The rise in sea level has not been constant but has varied over time in response to natural climate variability. This variability can also be observed in Table 5-1 and Figure 5-8, which present frequent and extreme water levels calculated from four different periods of record, with all water levels baselined to the year 2000 for consistent comparison. All four periods of record produce similar results, however, the period of record from 1973 – 2004 produces the highest water levels for the 25-year, 50-year, and 100-year recurrence intervals. All more recent periods of record produce lower more frequent water levels than the full period of record from 1900 – 2020. The Federal Sea Level Rise Task Force relied on the period of record from 1970 – 2020 for its nationwide assessment of frequent and extreme coastal water levels and the response of coastal water levels to climate change (Sweet et al. 2022b).

The use of FEMA's 1973 to 2004 period of record, which includes the two highest water levels on record at the Presidio tide gage recorded in 1983 and 1998, may include higher than warranted low frequency events, in particular the 50-year and 100-year recurrence intervals. However, most statistical techniques require that data is stationary, while most oceanic and atmospheric processes are noticeably nonstationary, calling into question the appropriate period of record for such analysis. In addition, the statistical analysis will specify the water levels to be used across the 100-year analysis period, from 2040 to 2140. Although sea level rise will be added across the analysis period, all other variations that could occur in response to climate change are not considered within G2CRM. Although the 1973 to 2004 period may be biased high for the low return frequencies, the more accurate representation of tidal amplification from north to south for the MAs, and the addition of variable wave dynamics along the shoreline for each MA, justify the use of the FEMA model output as the preferred coastal storm inputs for G2CRM.
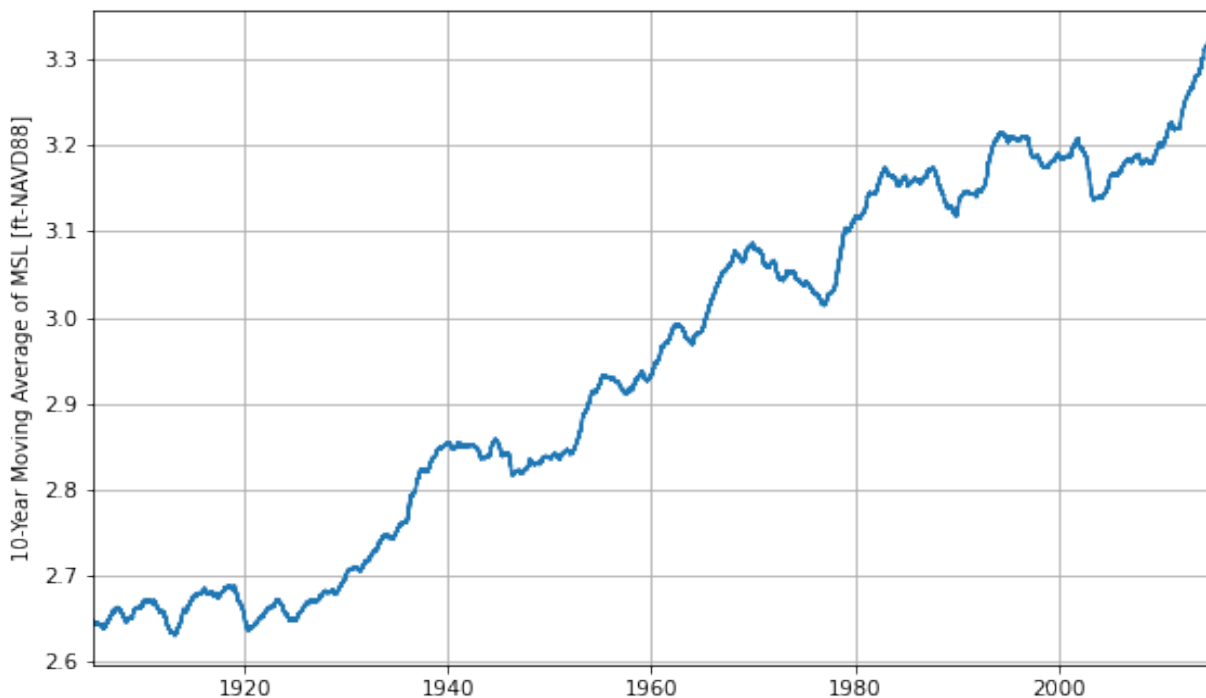

Figure 5-7. Ten-year Moving Average of Mean Sea Level

Table 5-1. Frequent and Extreme Water Levels for Various Periods of Record (relative to 2000)

Frequency	EY	AEP	Recurrence	Water Levels at the Presidio Tide Gage (feet NAVD88)			
				1900 - 2020	1973 - 2004	1973 - 2020	1970 - 2020
Very Frequent	12	99.999386%	1-month	7.05	6.89	6.86	6.93
	6	99.75%	2-month	7.24	7.01	6.96	7.05
	4	98.17%	3-month	7.36	7.07	7.04	7.10
	3	95.17%	4-month	7.44	7.14	7.12	7.14
	2	86.47%	6-month	7.55	7.24	7.22	7.23
Frequent	1	63.21%	1-year	7.75	7.44	7.41	7.40
	0.5	39.35%	2-year	7.94	7.65	7.62	7.59
	0.2	18.13%	5-year	8.19	7.99	7.90	7.88
	0.1	9.52%	10-year	8.38	8.28	8.12	8.13
Rare	0.04	3.92%	25-year	8.63	8.72	8.44	8.50
	0.02	1.98%	50-year	8.81	9.11	8.70	8.83
	0.01	1.00%	100-year	8.99	9.55	8.97	9.19

Note: Water levels in this table are calculated based on the observed water levels at the Presidio Tide Gauge. The FEMA San Francisco Bay Area Coastal Study modeled Bay water levels between 1973 and 2004; therefore, the values presented for 1973 – 2004 most closely represent the values used to inform the coastal storm databases developed as inputs to G2CRM.
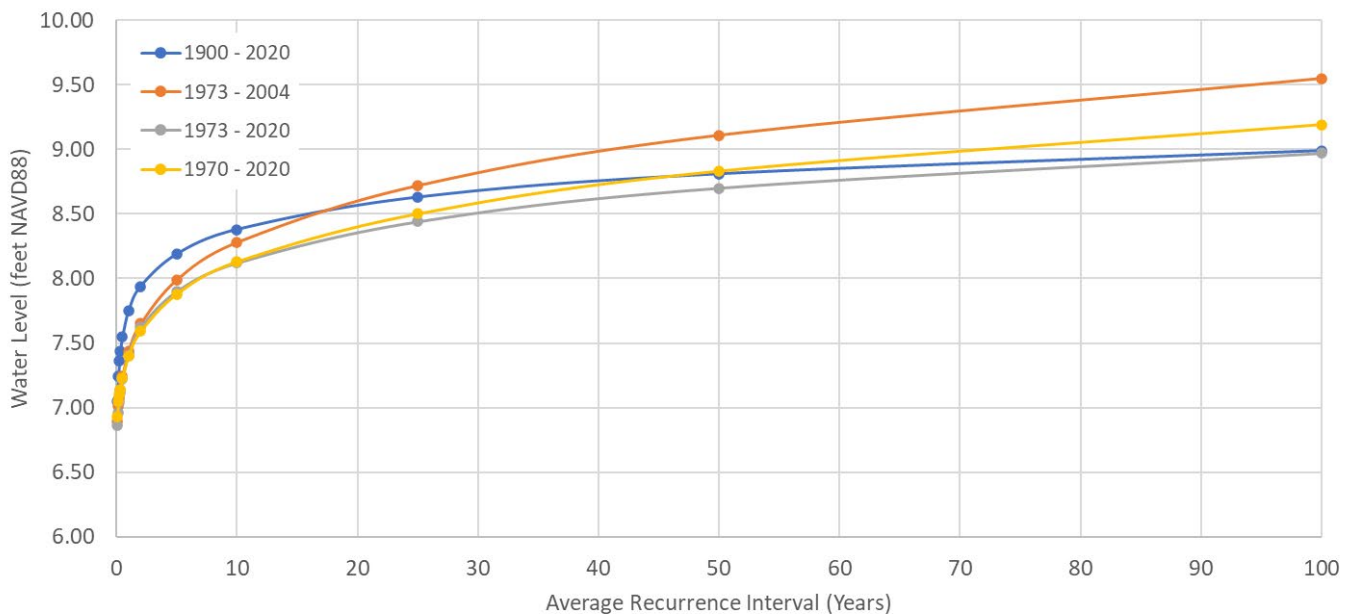
Note: Water levels in this figure are calculated based on the observed water levels at the Presidio Tide Gauge. The FEMA San Francisco Bay Area Coastal Study modeled Bay water levels between 1973 and 2004; therefore, the values presented for 1973 – 2004 most closely represent the values used to inform the coastal storm databases developed as inputs to G2CRM.

Figure 5-8. Water Level Elevations versus Average Recurrence Interval for Various Periods of Record (relative to 2000)

6   San Francisco Bay Coastal Dynamics

San Francisco Bay is the largest estuary in the western U.S., with a contributing watershed that includes nearly 40% of California (May et al. 2016b). The 300-foot-deep Golden Gate inlet connects the Bay with the Pacific Ocean (Figure 3-1), and the tides, ocean-driven swells, and extreme water levels all enter the Bay through this single inlet. The large expanse of the Bay allows for the generation of wind-driven waves that are independent from oceanic processes, and the complex topography surrounding the Bay can transform the winds in a multitude of directions depending on the primary driver of the onshore or offshore winds or the track of the large storm system descending on the Bay Area. The water levels and wave heights of the Bay exhibit a high degree of variability driven by many factors, including the bathymetry, astronomical and oceanic cycles, windspeeds and direction, and atmospheric events (Section 4).

Table 6-1 presents the physical processes that affect Bay coastal water levels near San Francisco. Extreme water levels, as measured by the Presidio tide gage, generally exclude high-frequency wave effects, and include processes between tsunami and ocean-basin variability, and low-frequency trends such as land ice melt/discharge and thermal expansion. The FEMA hydrodynamic water level input therefore includes these processes. The FEMA wave model output captures the wind-wave effects. Small tsunamis, as they occurred between 1973 and 2004, are captured in the Presidio tide gage and FEMA hydrodynamic model output. Although there is risk that larger tsunamis could occur in the Bay Area (James Barnts et al. 2014), this risk is not included in the coastal storm inputs for G2CRM. Vertical land motion, including land subsidence and settlement in areas of Bay fill, is not captured by the Presidio tide gage or FEMA San Francisco Bay modeling, but should be considered during the design of coastal flood defense structures.

Table 6-1. Physical Processes affecting Bay Coastal Water levels and their Temporal and Spatial Scales

Physical Process	Spatial Scale			Temporal Scale	Potential Magnitude (yearly)
	Global	Regional	Local		
Wind Wave Effects			✓	seconds to minutes	<5 feet
Tsunami		✓	✓	minutes to hours	<60 feet
Wind Setup		✓	✓	minutes to days	<0.5 feet
Storm Surge		✓	✓	minutes to days	<1.5 feet
Ocean Swell		✓	✓	minutes to days	<4 feet
Tides		✓	✓	hours to years	<8 feet
Ocean/Atmospheric Variability (e.g., ENSO response)		✓	✓	days to years	<1.5 feet
Ocean Gyre and Over-turning Variability		✓	✓	years to decades	<1.5 feet
Land Ice Melt/Discharge	✓	✓	✓	years to centuries	inches
Thermal Expansion	✓	✓	✓	years to centuries	inches
Vertical Land Motion		✓	✓	minutes to centuries	<inches to feet

Source: (Sweet et al. 2022, CPC 2020)

6.1   Tidal Water Levels

The water levels of the Bay are highly dynamic, with an average daily tide range of approximately 6 feet near the Golden Gate.[7] Due to the complex bathymetry and geographical configuration of the Bay, the tide range and elevation vary spatially. Interactions among tidal processes (for example, reflection of tidal waves), bathymetric variations, and shoreline orientation amplify the tides with increasing distance from the Golden Gate inlet (Conomos 1979). Figure 6-1 presents the variation in mean higher high water (MHHW) along the Bay shoreline. The tide range also varies along the same gradient, with a 6-foot tide range near the Presidio tide gage and an 8-foot tide range in the far south bay. Even on a smaller scale along the San Francisco shoreline, the elevation of MHHW varies by approximately 0.5 foot between Aquatic Park and Heron's Head Park along the 7.5-mile study area shoreline (Figure 6-2).

The water levels of the Bay vary based on several tidal and oceanic cycles that range in scale from hours to millennia (see Table 6-1), as well as short- to medium-term increases due to atmospheric conditions (for example, the weather). The following five tidal and oceanic cycles are the primary drivers of regular (non-climate change related) water level variations, presented in order of increasing timescale from shortest to longest:

- A mixed semidiurnal tidal cycle, with two high tides and two low tides occurring each day, with each of the four tides reaching different elevations (Conomos 1979). These astronomical tides are driven by the gravitational attraction between the rotating earth, moon, and sun (Figure 6-3).

- A 14-day spring-neap cycle, with the highest energy (and largest tide range) occurring during spring tides during the new and full moon, and the lowest energy (and smallest tide range) occurring during neap tides when the sun and moon are at right angles to each other (Figure 6-4).

- An annual cycle in which water levels are generally lower in the spring and early summer and higher in the early fall through winter. The spring drop in sea level along the California coast, and observed at the San Francisco Presidio tide gage, results from the onset of strong winds blowing toward the Equator (USGS 1999). These winds, plus the Coriolis effect,[8] push surface waters away from the coast. The higher sea level in the fall and winter are caused by the relaxation of these alongshore winds, coupled with the expansion of water caused by summer and fall warming trends. Since 2013, the water level drop in the spring has been less pronounced and water levels have remained high throughout the summer due to the presence of a large, unusually warm patch of water off the coast commonly referred to as "the Blob" (Stanley 2016). The Blob has affected water levels and west coast weather from Alaska to California (Hayhoe et al. 2018). It is currently unknown if this phenomenon will continue to persist.

[7] Tide range is the difference between the elevation of the mean highest high tide and mean lowest low tide.

[8] The Coriolis effect is the tendency of winds and currents to veer to the right in the Northern Hemisphere and to the left in the Southern Hemisphere.

MHHW
(ft-NAVD88)

7.5

7.1

6.7

6.3

5.9
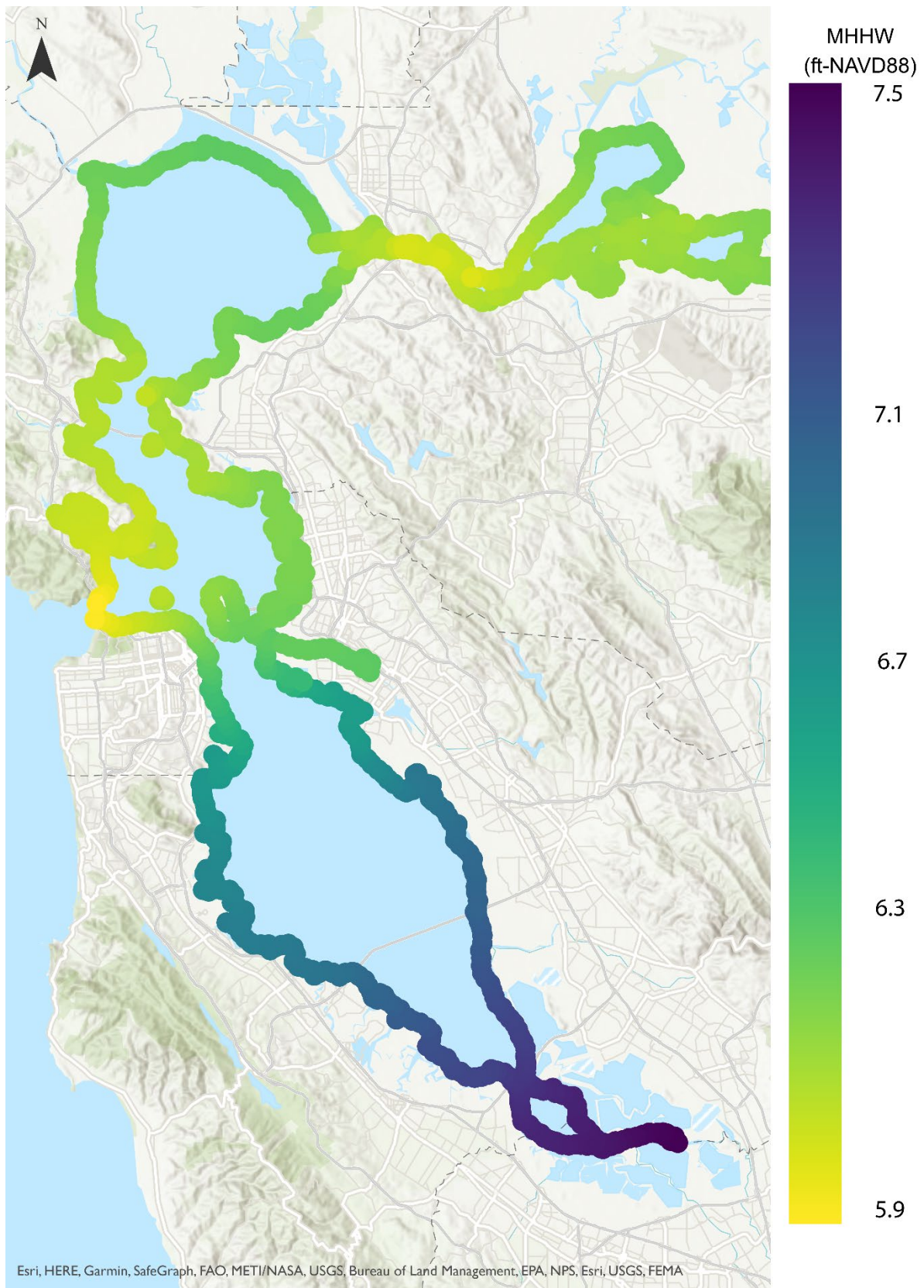
Source: (DHI 2011, 2013, May et al. 2016b)

Figure 6-1. Baywide Variation in Mean Higher High Water (relative to 2008)
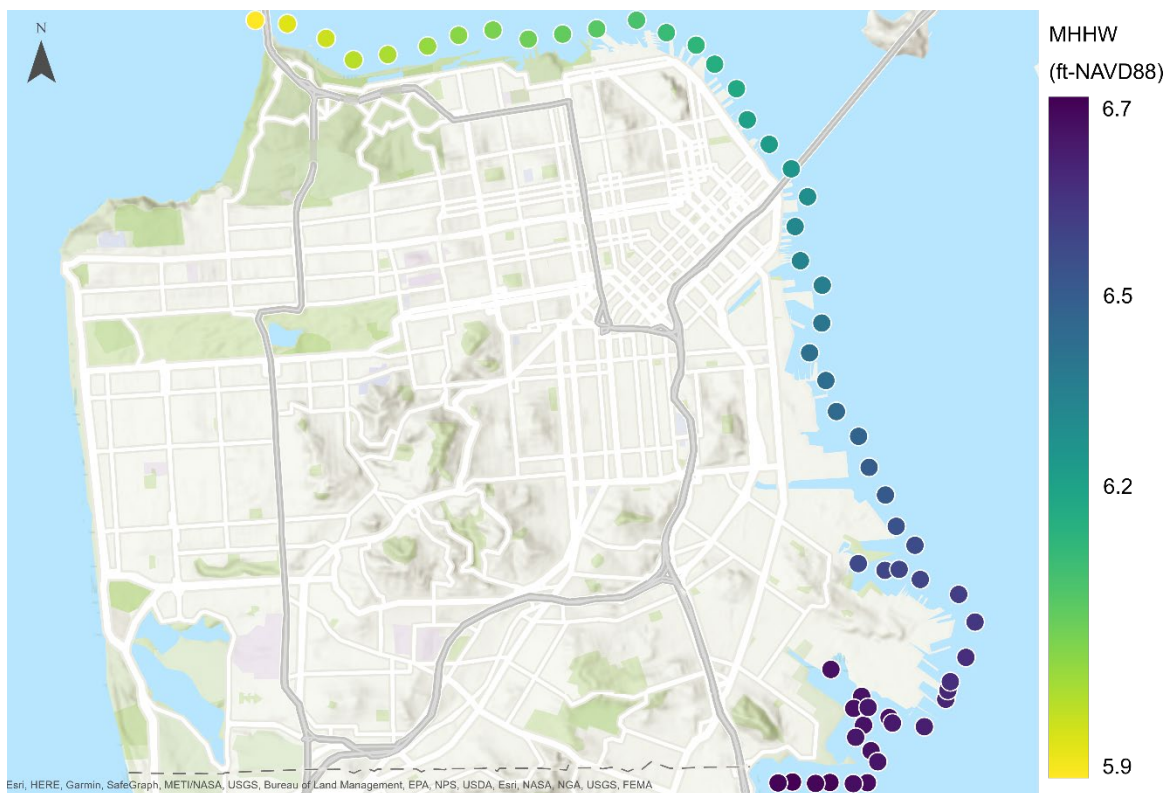
Source: (DHI 2011, May et al. 2016b)

Figure 6-2. San Francisco Shoreline Variation in Mean Higher High Water (relative to 2008)

- The El Niño/La Niña cycle (ENSO) where every 2 to 7 years the equatorial trade winds relax, or even reverse, and warm surface water moves back along the Equator toward South America (USGS 1999, Park et al. 2012). During El Niño conditions, unusually long, low waves are generated in the Pacific Ocean called "Kelvin waves." These waves appear to be about 6,000 miles long, traveling at speeds of more than 5 mph, with heights of up to 12 inches (USGS 1999). As a Kelvin wave moves along the west coast, the higher water levels are propagated into the Bay. During the 1997/1998 El Niño season, Kelvin waves began raising sea levels by 6 inches in early May, and by late fall of 1997, water temperatures were well above normal, causing an additional rise of about 8 inches due to thermal expansion that lasted into spring 1998 (USGS 1999). El Niño's impact on water levels, temperature, and precipitation appears to be increasing under a warming climate (Cayan et al. 2007, Gratiot et al. 2008, Cai et al. 2014b, Fasullo et al. 2018).

- PDO is a long-term (for example, 20 – 30 years) ocean fluctuation of sea surface temperatures in the Pacific Ocean. PDO includes both warm and cool phases which alter upper level atmospheric winds, affecting ocean water levels, hurricane activity, droughts, and floods (DeFlorio et al. 2013). It is believed that if both ENSO and PDO are in the same phases, the El Niño/La Niña impacts are magnified, and if they are out of phase, they may offset one another (Zervas 2009, Teegavarapu and Schmidt 2019). The phase of the PDO can also affect the relative local rate of sea level rise. The cool phase of the PDO pushes warm water away from the U.S. Pacific coast, suppressing local sea level rise. This dynamic led to a slower than anticipated rate of sea level rise measured at the Presidio tide gage from the mid-1990s until about 2011. The PDO is currently in a warm phase, and NASA scientists are observing faster-than-average sea level rise along the west coast (NASA 2021).
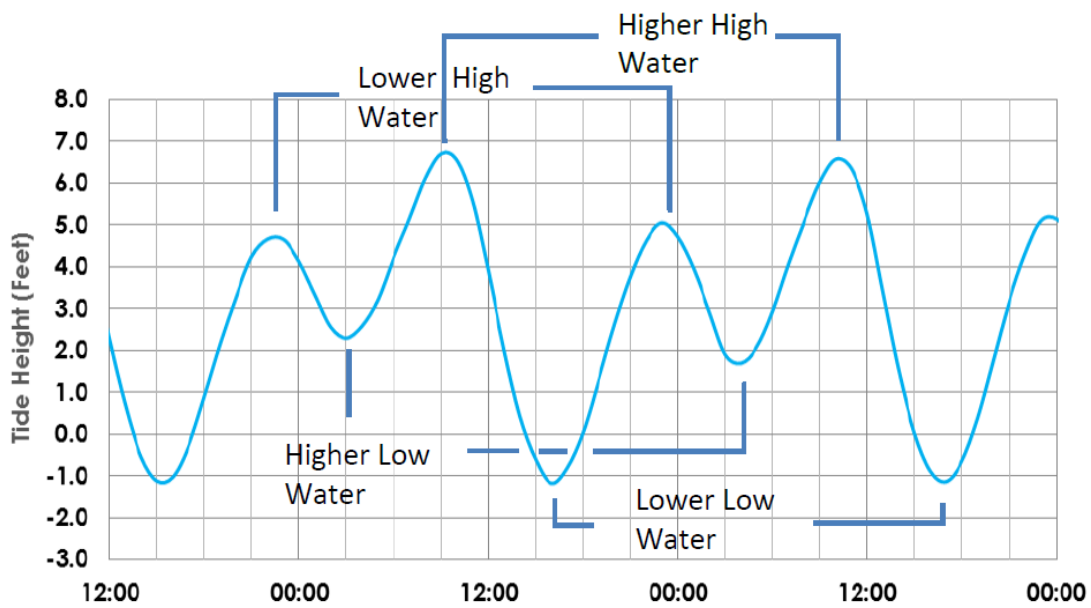
Source: *(May et al. 2016b), retrieved from NOAA Presidio tide gage*

Figure 6-3. Daily High Tide and Low Tide Patterns in a Mixed Semidiurnal Tide
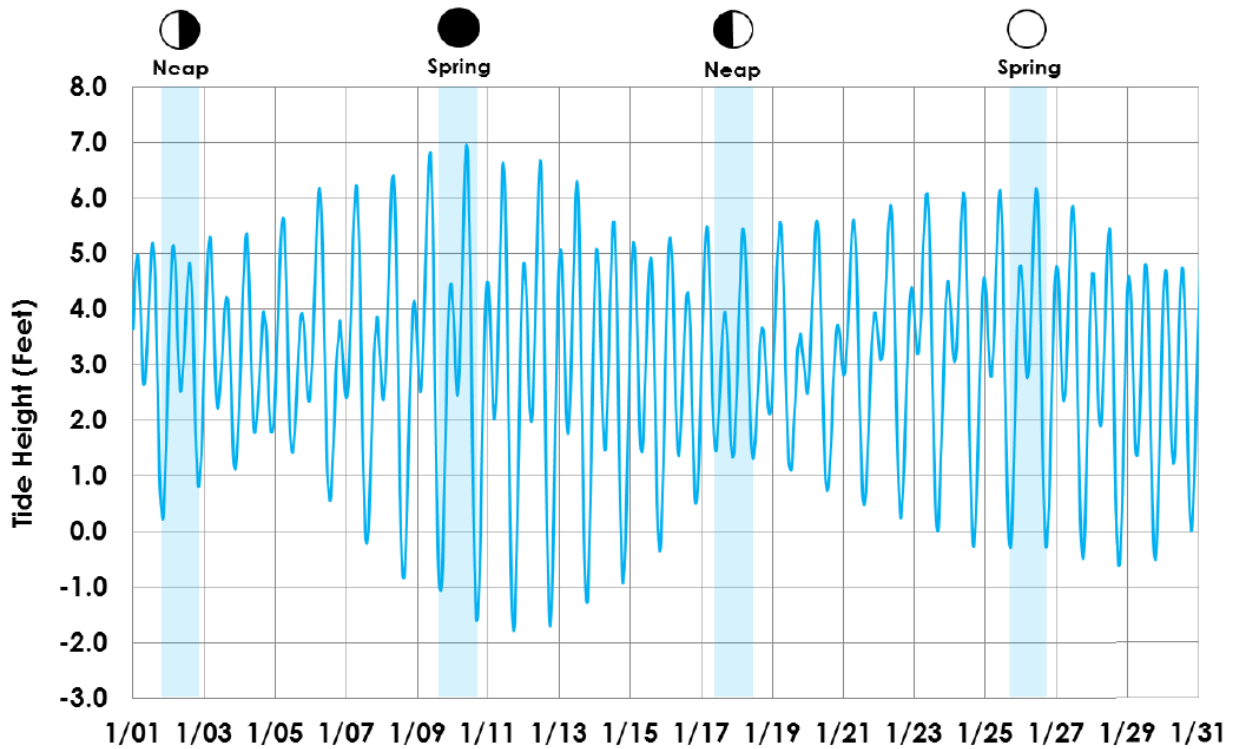
Source: *(May et al. 2016b), retrieved from NOAA Presidio tide gage*

Figure 6-4. Monthly Spring and Neap Tide Pattern

6.2   Wind Waves

The wind climate above the Bay and the larger Bay Area is highly variable, and the steep topography, hills, and valleys throughout the Bay Area drive complex local wind patterns. Due to the large size of the Bay, the winds have sufficient fetch to generate wind-driven waves that are 3 to 5 feet in height along the most exposed sections of the Bay shoreline when windspeeds are high and the wind is blowing toward the shoreline. Strong windspeeds in almost any direction will impact a section of the Bay shoreline. However, due to the orientation of the San Francisco shoreline, the most impactful winds are (1) easterly (that is, offshore) winds that can impact the shoreline from the Ferry Building and southward, (2) north and northeasterly winds that can impact the northern waterfront, and (3) southeasterly winds that can impact the southern waterfront (Figure 6-5). Strong winds blowing over the Pacific Ocean can also drive longer-period ocean swell that enter through the Golden Gate. The dynamics of the ocean swell are discussed in Section 6.3.

The strongest winds of the year occur during spring (that is, March, April, and May). The large storm systems that occur in winter often continue into March. However, by April, the storm tracks shift farther north and large storms in April and May are infrequent. West to northwest winds blow along the California coast in the spring, driven by the higher pressure over the ocean and the lower pressure over land as the land warms. Stronger springtime wind events can exceed 30 mph over the ocean, with strong winds funneling through the Golden Gate and generating wind-waves across the central bay. Figure 6-6 shows the wind rose summarizing the spring wind speed and direction recorded at SFO and Oakland International Airport.

Summer (that is, June, July, and August) winds are generally lighter with a persistent northwest direction, referred to as onshore flow or a sea breeze that is driven by the daytime heating over land. As the land warms, the winds pick up, reaching a maximum in the late afternoon and early evening hours, and then gradually subsiding by late evening. The winds move through the Golden Gate, and then fan out in a northerly direction toward the north bay and a southerly direction toward the south bay. The wind-driven waves are primarily generated from local winds over the Bay, and the longer-period ocean swells contribute much less to the overall wave heights in spring and summer than they do in late fall to early spring.

Occasionally, summer winds can reverse for 2 to 3 days at time when the usual pattern of high pressure over the ocean and low pressure over land is disrupted. A higher-pressure zone over the Pacific Northwest can shift the low-pressure zone over interior California to the west and over the ocean. These offshore winds are strongest at night and in the early morning hours, and strong winds can form a funnel over the open water from the Carquinez Straight toward San Francisco and out through the Golden Gate. These 20 to 35 mph winds can create large wind-driven waves capable of impacting the San Francisco shoreline. Figure 6-7 presents the wind rose summarizing the summer wind speed and direction recorded at SFO and the Oakland International Airport.

In fall (that is, September, October, and November), the pressure gradients lose their strength and windspeeds are reduced over the ocean and the Bay. However, when warm temperatures persist over the Bay Area into fall, the temperature differences across the larger Bay Area region can generate local winds. However, these local winds generally produce wind-driven waves that can impact the San Mateo and Marin coastlines, and wind-driven waves throughout the rest of the Bay are usually at their lowest heights of the year in the fall. Figure 6-8 presents the wind rose summarizing fall wind speed and direction recorded at SFO and the Oakland International Airport.

**Figure 6-5. Ocean Swell and Wind-driven Waves Illustration**

Wind directions are most variable in the winter months, and wind-driven waves can impact shorelines across the Bay. Windspeeds greater than 58 mph have been recorded at the Oakland International Airport, and windspeeds over 100 mph have been recorded on highly exposed ridge areas. Figure 6-9 presents the wind rose summarizing the winter season wind speed and direction recorded at SFO and the Oakland International Airport.

Figure 6-10 presents wind roses from multiple weather stations across the Bay Area. The differences evident across the Bay Area are driven by differences in the local topography that can funnel and re-direct local winds from larger systems and pressure gradients, as well as locally generated winds driven by temperature gradients across the Bay Area. Figure 6-11 presents the variations in the 1% AEP significant wave heights offshore of the Bay shoreline (not including wave runup). The 1% AEP wave heights vary from about 2 to 4.5 feet along the San Francisco shoreline, which is consistent with most exposed (that is, non-sheltered) areas. The largest 1% AEP significant wave heights are found across the Bay along the SFO shoreline. It should be noted that no single event results in these 1% AEP significant wave heights along the entire shoreline. Figure 6-11 presents a compilation of over 9000 model output points along the Bay shoreline, and the 1% AEP values were calculated individually at each point.
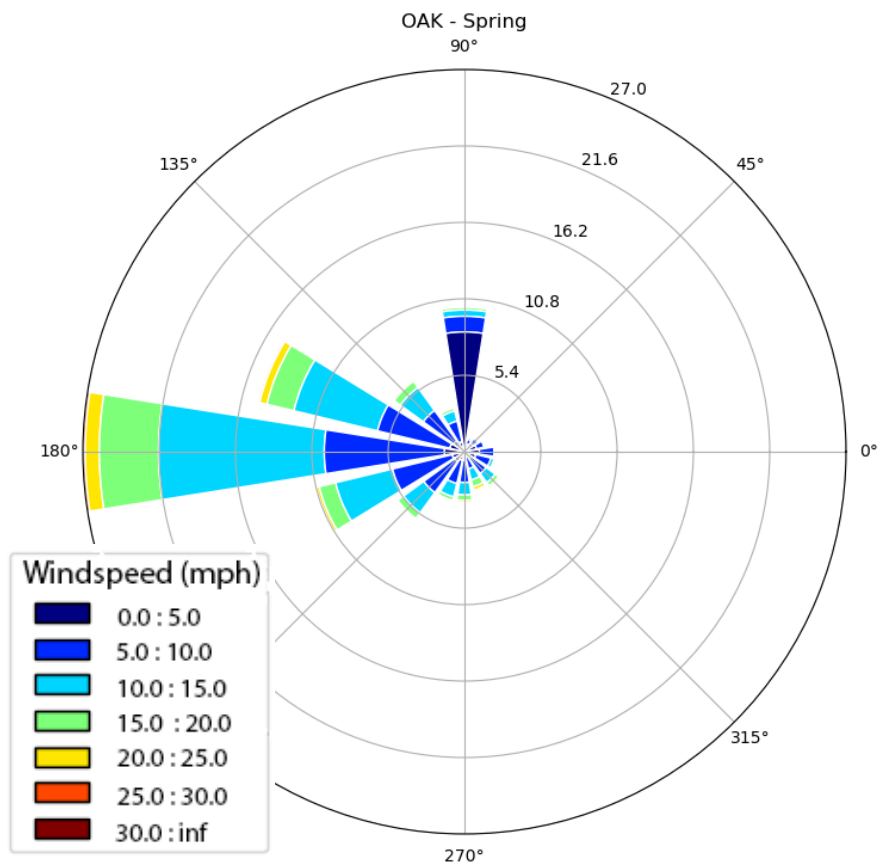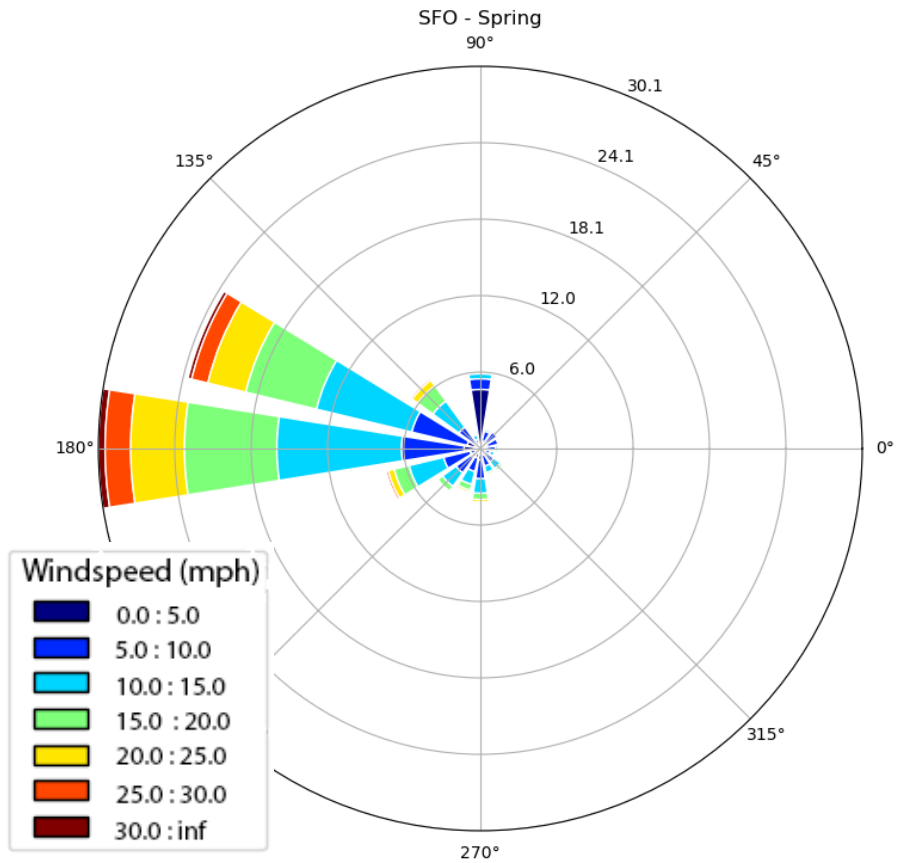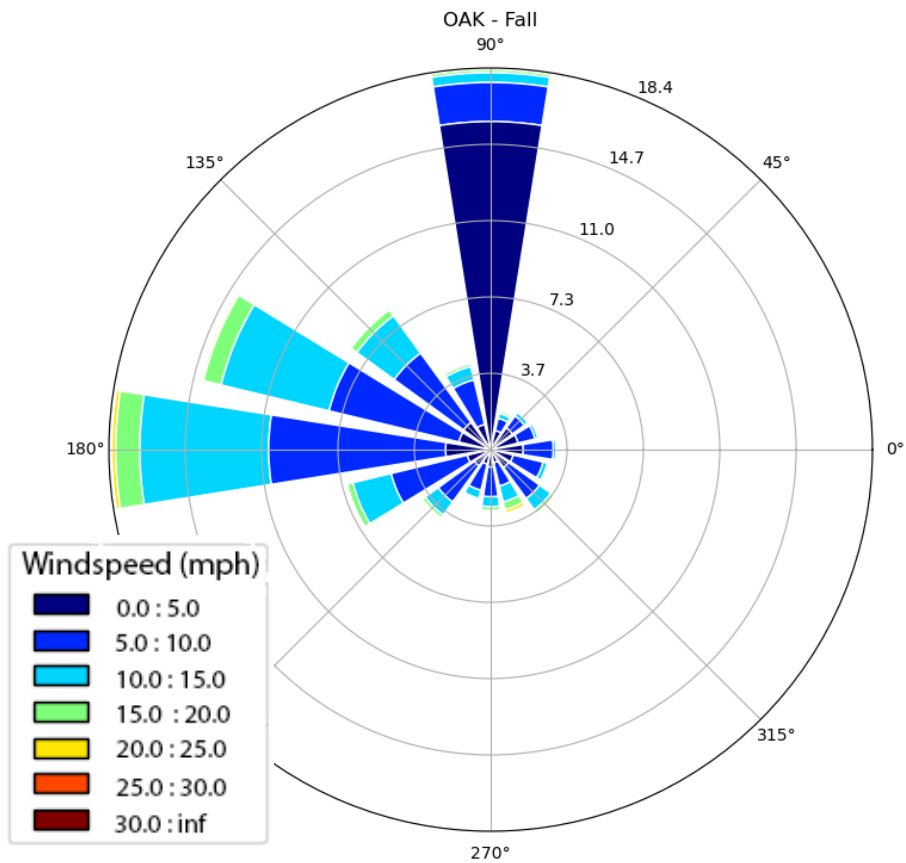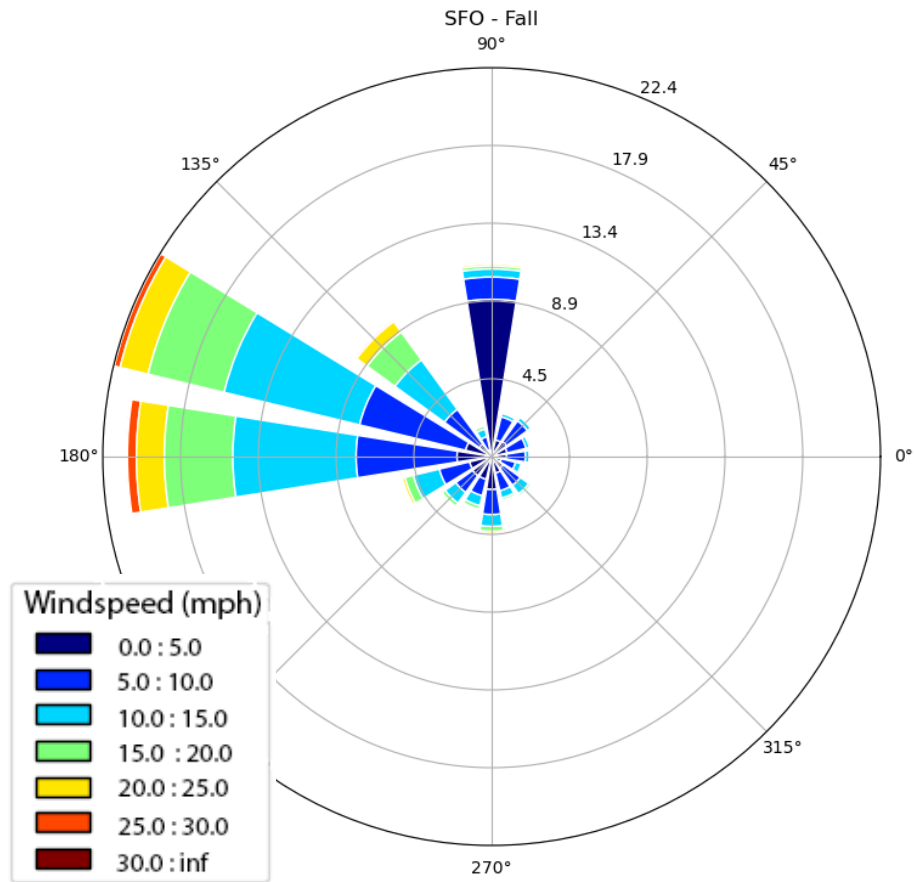
Source: SFO and OAK NCDC wind stations

Figure 6-6. Spring Sustained Hourly Windspeeds at San Francisco (top) and Oakland International (bottom) Airports
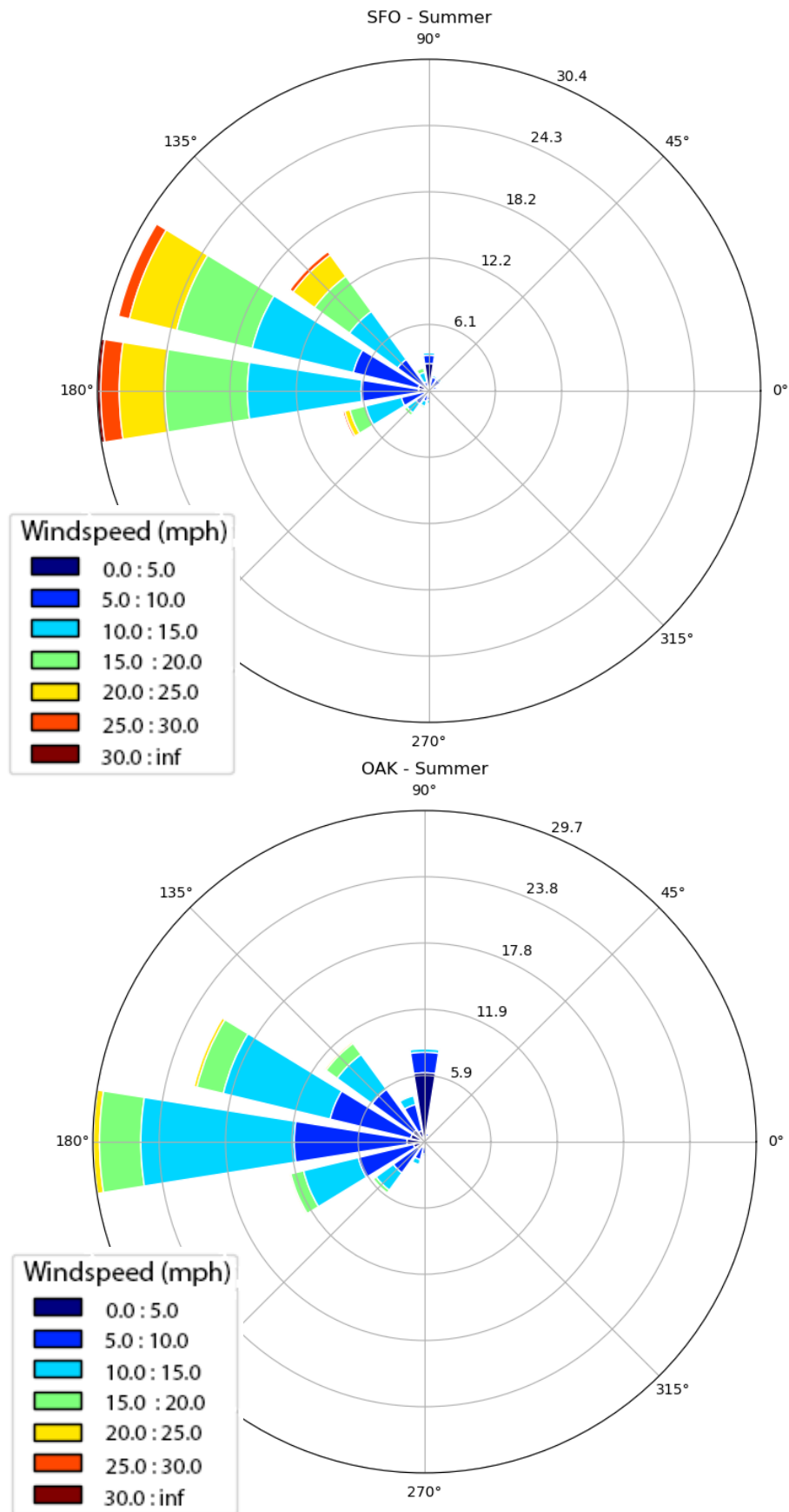
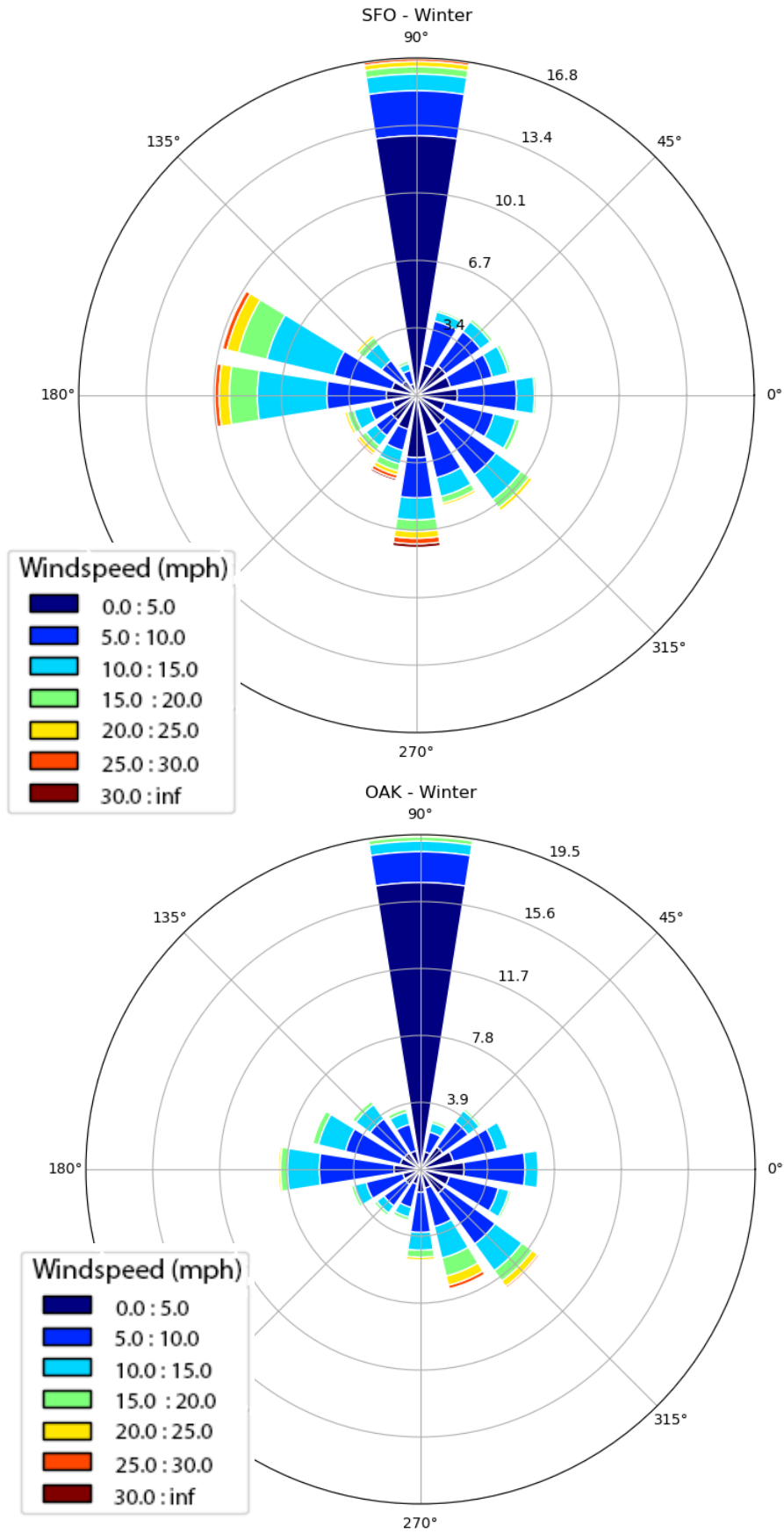*Source: SFO and OAK NCDC wind stations*

Figure 6-7. Summer Sustained Hourly Windspeeds at San Francisco (top) and Oakland International (bottom) Airports

Source: SFO and OAK NCDC wind stations

Figure 6-8. Fall Sustained Hourly Windspeeds at San Francisco (left) and Oakland International (right) Airports

SFO - Winter

OAK - Winter

Windspeed (mph)
- 0.0 : 5.0
- 5.0 : 10.0
- 10.0 : 15.0
- 15.0 : 20.0
- 20.0 : 25.0
- 25.0 : 30.0
- 30.0 : inf

Source: SFO and OAK NCDC wind stations

Figure 6-9. Winter Sustained Hourly Windspeeds at San Francisco (left) and Oakland International (right) Airports
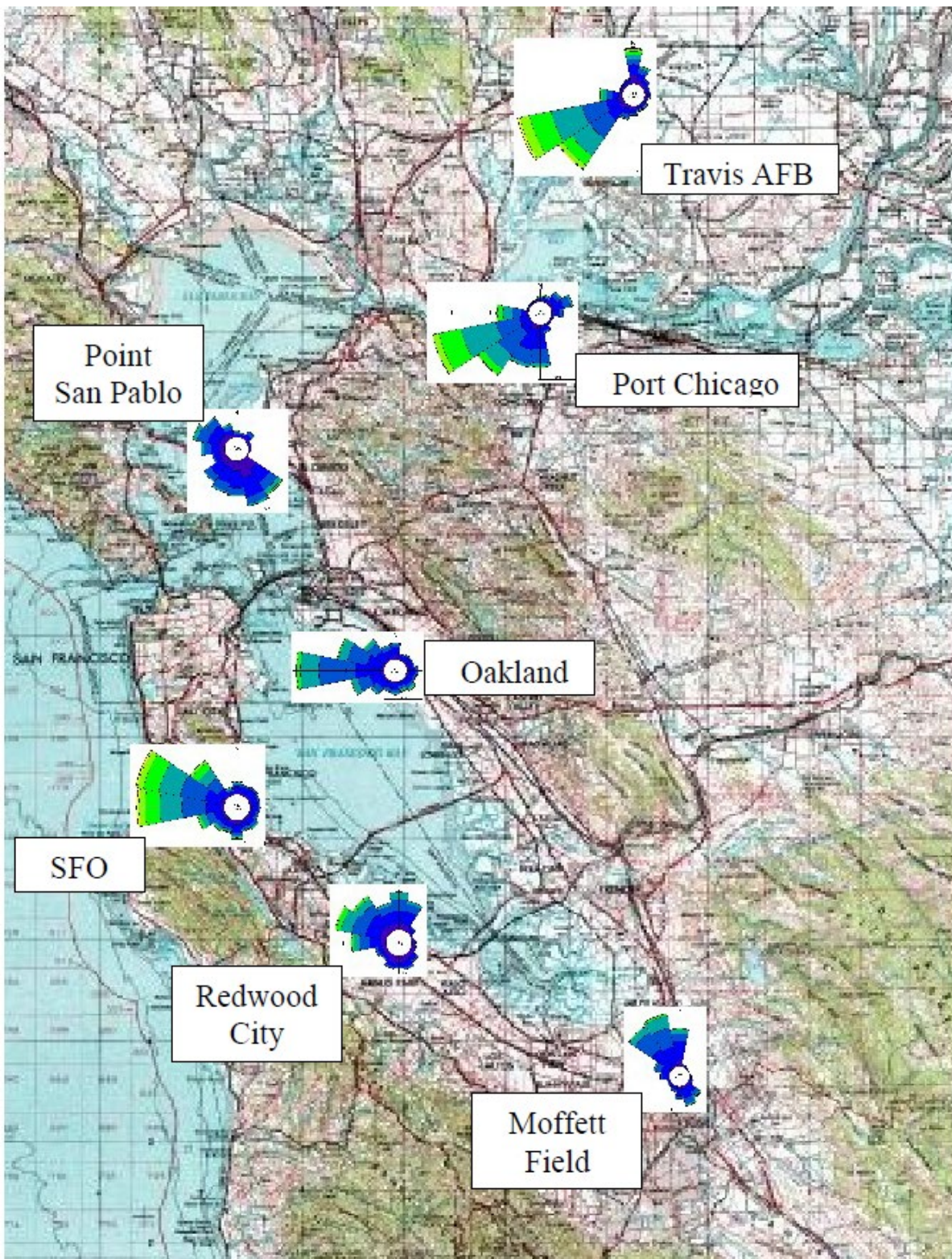
Source: (DHI 2011)

Figure 6-10. Wind Roses around the San Francisco Bay Area

Note: Although seven wind stations are noted above, DHI (2011) evaluated 32 wind stations in the north Bay, 23 wind stations in the central Bay, and 17 wind stations in the south Bay. The wind stations noted above had the longest, most contiguous, and verified hourly data available at the time of the DHI (2011) study.

1% AEP Wave Height (ft)

4.6

3.6

2.7

1.9

0.7
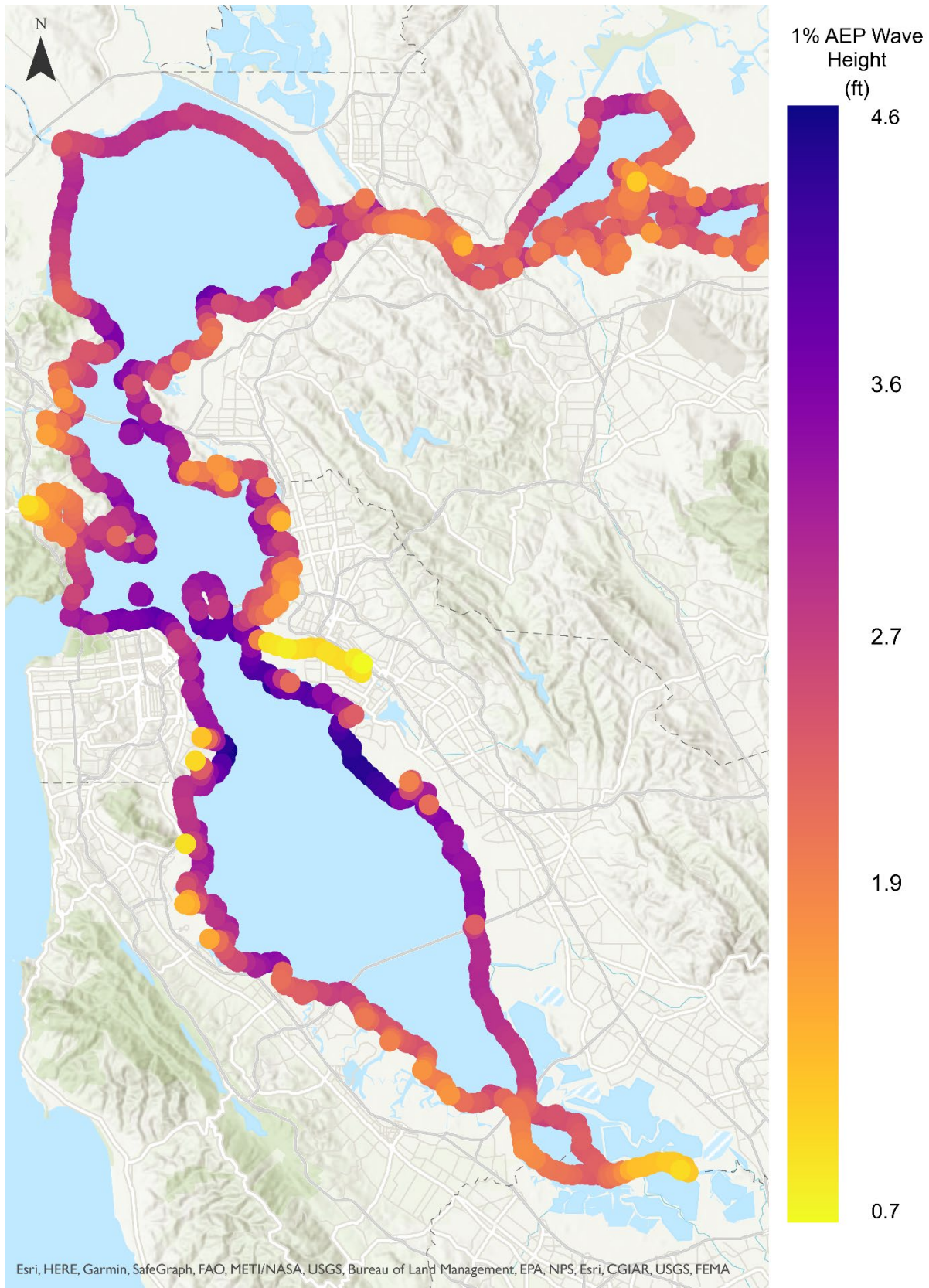
Source: (DHI 2011, 2013)

Figure 6-11. Baywide Variation in 1% AEP Wave Heights (relative to 2008)

6.3   Ocean Swell

The San Francisco shoreline is also impacted by ocean-driven swell (that is, the longer-period waves that develop in the Pacific Ocean where the onshore fetch can span thousands of miles), creating damaging waves along the energetic open coast. As the storms over the Pacific Ocean begin to become stronger and more frequent by late October and into November, longer-period ocean swells begin to penetrate through the Golden Gate. The storm tracks across the Pacific and toward the west coast becomes increasingly active in November, and extratropical cyclones and atmospheric rivers begin to roll through the Bay Area. As the ocean-driven swell propagates through the narrow and deep Golden Gate channel, the swell waves continue to travel generally in the same direction, as illustrated on Figure 6-5. The waves quickly dissipate energy and decrease in height as they enter the Bay. The 1% AEP swell wave height is approximately 8 feet at the Golden Gate Bridge, and this wave height decreases to about 2.5 feet offshore of Aquatic Park, and to about 0.5 feet at the San Francisco-Oakland Bay Bridge (Figure 6-12).

The ocean swell waves are not strongly correlated with wind measurements recorded in the Bay, as the Bay's complex topography can re-direct the winds and create a within-Bay wind field that is quite different from the winds that can blow for hundreds of miles over the Pacific Ocean. However, ocean swell waves are likely correlated with offshore winds and the extreme storms that impact the Bay Area. Figure 6-12 shows the variation in the 1% AEP swell wave heights along the Bay shoreline. The influence of the swell waves is largely limited to the central Bay, along the San Francisco and Marin County shorelines between the Golden Gate Bridge and the San Francisco-Oakland Bay Bridge and the San Rafael-Richmond Bridge, respectively. The swell waves can also impact Alameda County on the eastern Bay shoreline, directly across the Bay from the connection with the Pacific Ocean. The swell waves are generally not observed to turn and propagate into the north or south Bay.

Along the San Francisco shoreline, the ocean swell waves can elevate the offshore Bay water levels, making them an important consideration when evaluating coastal hazards. However, these waves travel parallel to the shoreline, and do not travel directly toward the shoreline contributing to wave-driven runup and overtopping. The ocean swell waves could more directly impact the overwater piers along the northern waterfront. Pier specific analysis related to the wave hazards was not completed by FEMA and is not included within G2CRM.
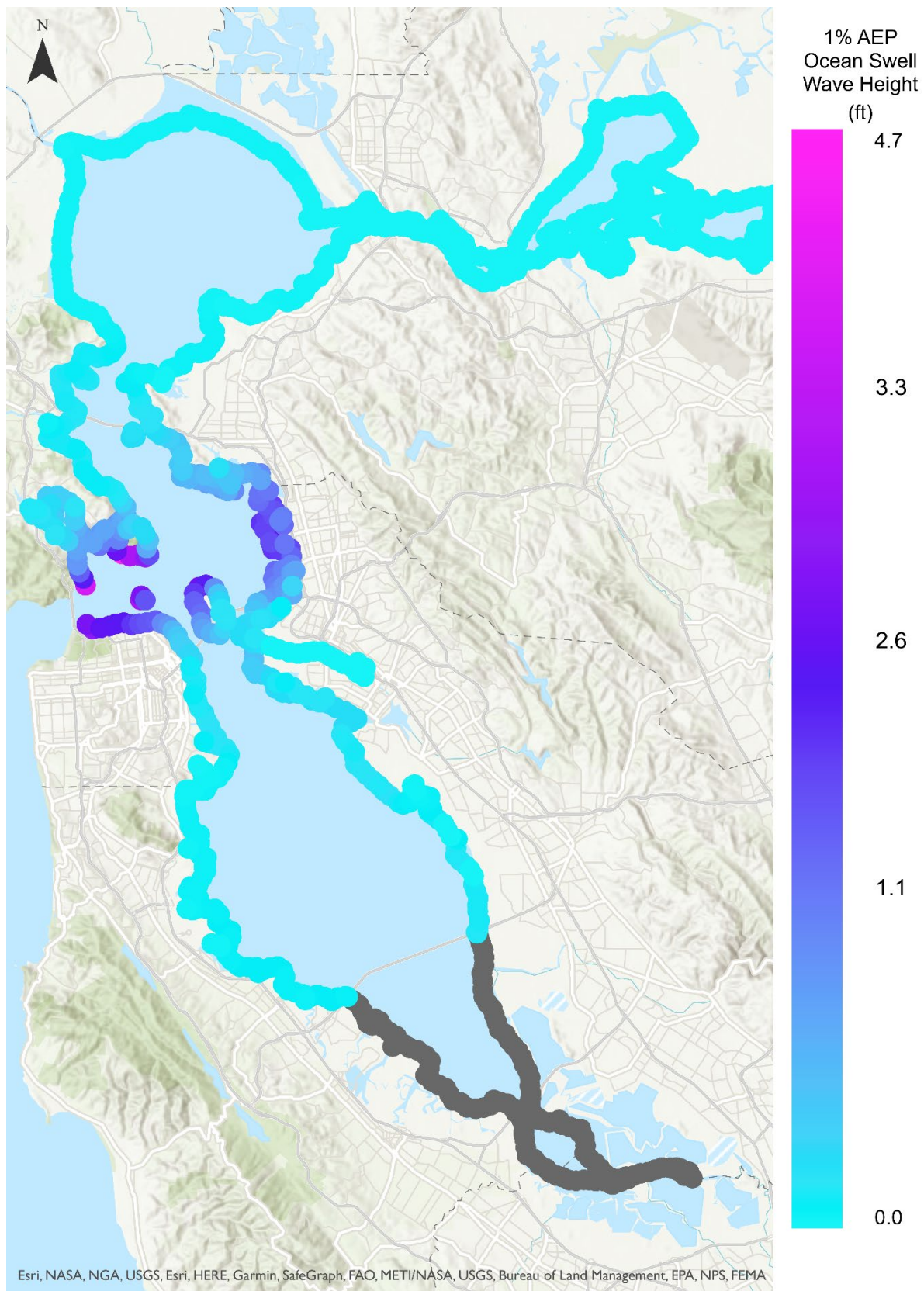
Source: (DHI 2011; 2013)

Figure 6-12. Baywide Variations in 1% AEP Ocean Swell Wave Height (relative to 2008)

Note: The gray dots represent a "null" value. The DHI (2013) modeling study did not include the open ocean wave boundary condition since the DHI (2011) study showed that swell waves do not penetrate into the south Bay.

6.4   Water Levels

Most analyses of flooding and flood-related damage and loss focus on extreme events with relatively rare occurrence frequencies, such as the 1-percent-annual-chance flood event (that is, an event with a 1-percent annual exceedance probability [AEP], or 1% AEP). The coastal storm inputs developed for G2CRM include coastal events that range from the monthly water level (99.9994% AEP) to the annual (1-year) water level events (63.2% AEP) to the 100-year extreme water level (1% AEP). These events are considered very frequent to frequent to rare based on their recurrence interval (Table 6-2). Events with a larger recurrence interval (lower return frequency), such as the 200-year (0.5% AEP) or 500-year (0.2% AEP) event are considered very rare. In the Bay, these very rare events are associated with water levels only slightly above the 100-year (1% AEP) event as the lower frequency event water levels asymptote toward a maximum potential value (Figure 6-13). Figure 6-14 presents high tide (monthly) versus extreme tide (1% AEP) floodextents under the USACE intermediate and USACE high sea level rise projections.

Table 6-2. Frequency of Water Levels or Events (relative to 2000)

| Frequency	EY	AEP	Recurrence	Presidio Water Level (feet NAVD88)[a]	
				1900 - 2020	1970 - 2020
Very Frequent	12	99.999386%	1-month	6.87	6.91
	6	99.75%	2-month	6.98	7.01
	4	98.17%	3-month	7.04	7.09
	3	95.17%	4-month	7.12	7.17
	2	86.47%	6-month	7.23	7.28
Frequent	1	63.21%	1-year	7.42	7.47
	0.5	39.35%	2-year	7.62	7.67
	0.2	18.13%	5-year	7.88	7.95
	0.1	9.52%	10-year	8.09	8.18
Rare	0.04	3.92%	25-year	8.36	8.48
	0.02	1.98%	50-year	8.57	8.73
	0.01	1.00%	100-year	8.78	8.98

[a] Water Levels (feet NAVD88) are calculated for the Presidio tide gage, baselined to 2000
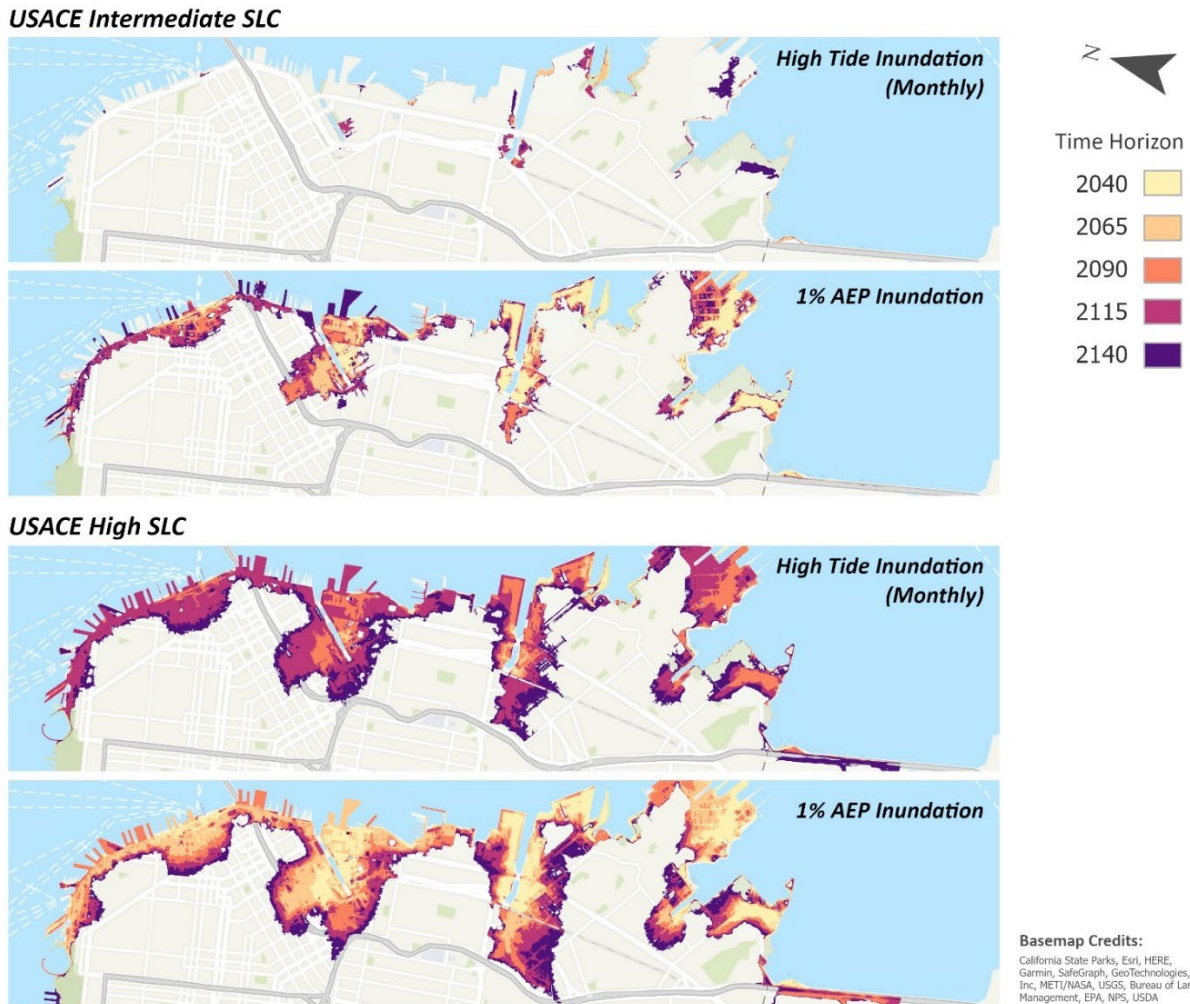Notes:
AEP = Annual exceedance probability
EY = Average number of exceedances per year
NAVD88 = North American Vertical Datum of 1988
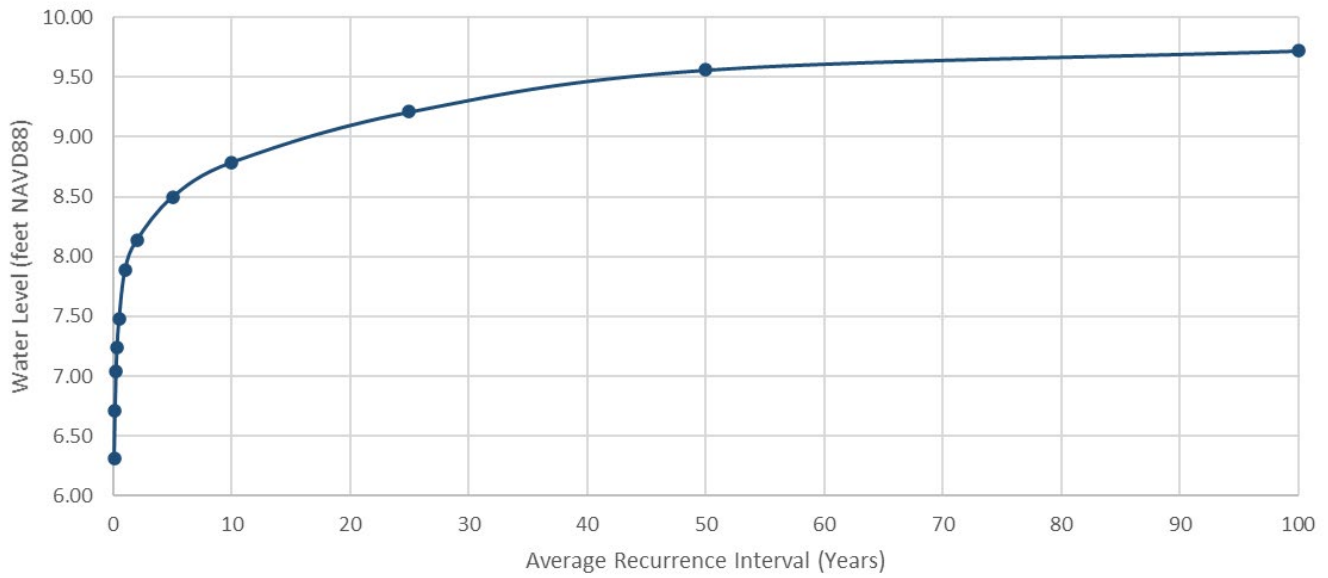
Figure 6-13. Water Level Elevations versus Average Recurrence Interval for Model Area 1 (relative to 2000)


Figure 6-14. High Tide (monthly) and Extreme (1% AEP) Water Level Flood Extents with USACE Intermediate and USACE High SLC

6.4.1 High Tide Water Levels

In the Bay, the difference between mean higher high water (MHHW) and the 1% AEP coastal water level is on the same order of magnitude as future sea level rise by the year 2100.[9] Future flooding by high frequency events could result in more damage and disruption to shoreline communities and infrastructure than lower frequency events (Sweet et al. 2016, 2018, Ghanbari et al. 2019, Taherkhani et al. 2020). High frequency events include very frequent events (such as the 6-month to 1-month water level), and near daily events or high tide flooding (Table 6-2).

For example, if sea level rises by 6 inches, a 1% AEP water level (100-year water level) will become an about 4% AEP water level (about 25-year water level) in the Bay (Vandever et al. 2017, CCSF 2020). If sea levels rise by 24 inches, Bay Area coastal communities could experience multiple flood events, in addition to 90 to 150 days of high tide flooding, each year (Ghanbari et al. 2019, Sidder 2019). Figure 6-15 provides a schematic example of this dynamic. Before sea level rise, a hypothetical flooding threshold could be overtopped a few times each year, primarily in the winter season (Figure 6-15, left). However, with sea level rise, the same flooding thresholds could be overtopped frequently throughout the entire year (Figure 6-15, right). This more frequent, yet less severe flooding will cause chronic and cumulative damages (FEMA 2015, Sievanen et al. 2018, Sidder 2019). Therefore, developing an appropriate strategy to adequately account for high tide flooding along the POSF shoreline is important for the POSF and CCSF.

Figure 6-16 and Figure 6-17 are adapted from the University of Hawaii Sea Level Center Flooding Days Projection Tool, configured for San Francisco and using the USACE Intermediate (NOAA Intermediate Low), USACE High (NOAA Intermediate High), and approximately the CA OPC Likely (NOAA Intermediate) sea level rise projections (OPC and CNRA 2018, USACE 2019a, University of Hawaii 2021, Sweet et al. 2022b). This tool provides an estimate of the number of days a given flood threshold could be overtopped, based on the NOAA sea level rise projections and their median and likely ranges.
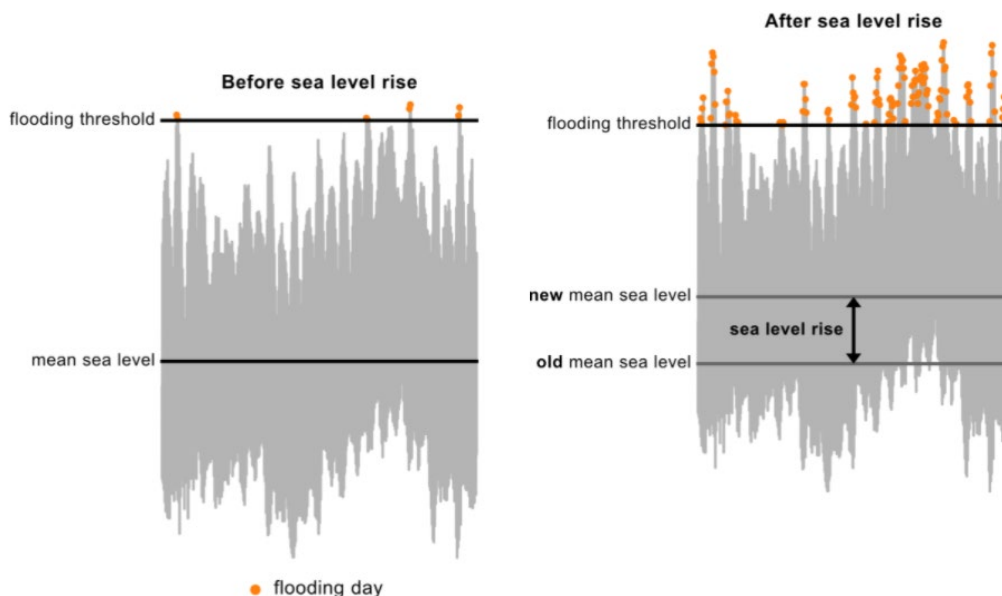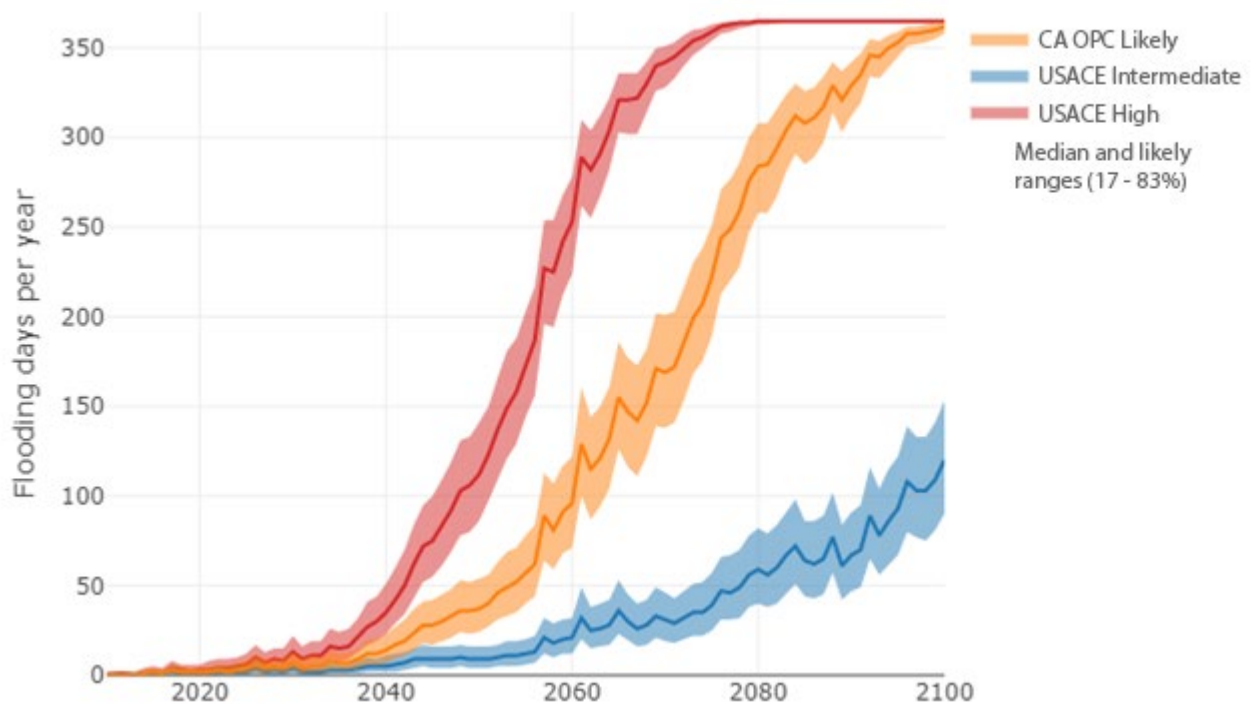

Source: (University of Hawaii 2021)

Figure 6-15. Schematic of the Effect of Sea Level Rise on Flooding Events

---

[9] The 1% AEP water level at the Presidio tide gauge is approximately 37 to 41 inches above mean higher high water (MHHW). This is comparable in magnitude to projected sea level rise amount on the USACE High and the State of California Likely sea level rise projections by the year 2100 (USACE 2019; OPC and CNRA 2018).

Table 6-3. Comparing NOAA, USACE, and California Sea Level Rise Projections

NOAA (Sweet et al. 2017a)	USACE / California OPC
Low	USACE Low (NRC 2012)
Intermediate Low	USACE Intermediate (NRC 2012)
Intermediate	~ California OPC Likely (OPC and CNRA 2018)
Intermediate-High	USACE High (NRC 2012)
High	~ CA OPC Plausible, High Impact (1:200) (OPC and CNRA 2018)

Source: (University of Hawaii 2021)

Figure 6-16. High Tide Flooding Days per Year with a Flooding Threshold of about 8.4 feet NAVD88 in San Francisco
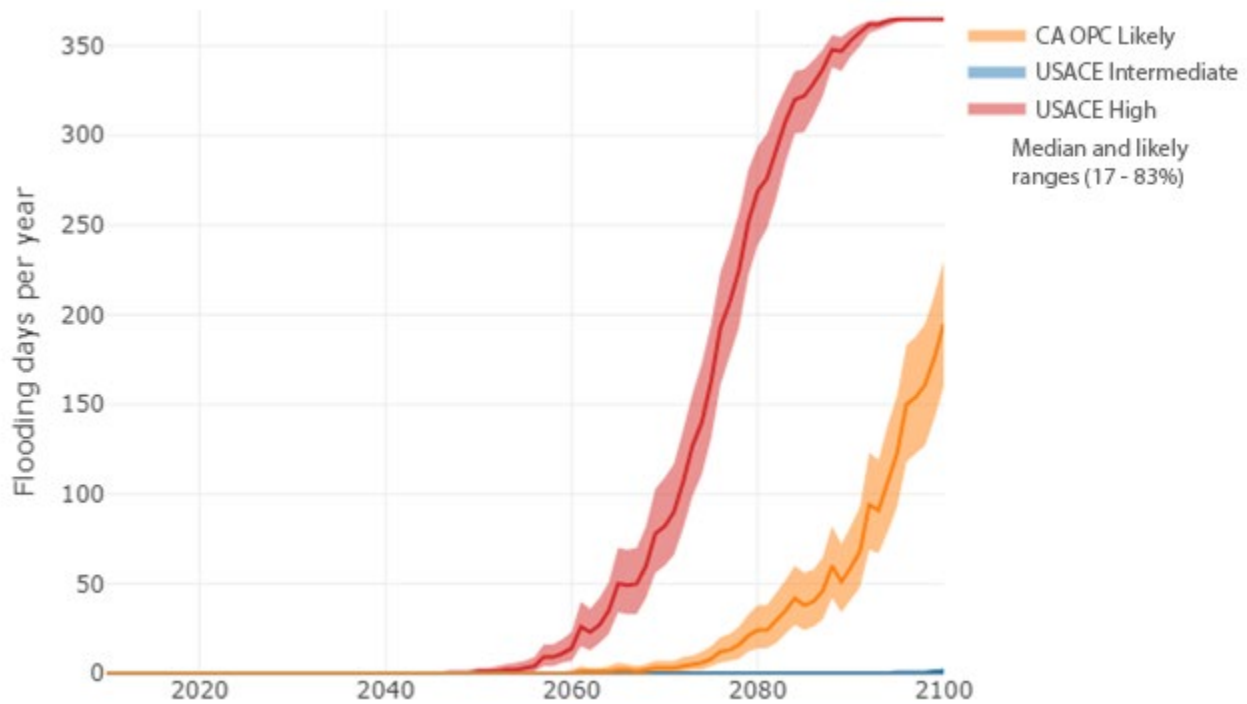
Source: (University of Hawaii 2021)

Figure 6-17. High Tide Flooding Days per Year with a Flooding Threshold of about 11.8 feet NAVD88 in San Francisco

As sea levels rise, high tide flooding will become more frequent along the POSF's waterfront shoreline. Some areas of the shoreline, such as the near the Ferry Building along the Embarcadero waterfront, experience minor high tide flooding today during the highest annual tides (such as a King Tide[10]) that occur each year in the winter months, particularly when high winds push additional water over the shoreline. This area has a flooding threshold of about 18 to 22 inches above MHHW, or approximately 8.4 feet North American Vertical Datum of 1988 (NAVD88). Figure 6-16 presents the number of days each year that high tides would overtop this flood threshold over time. Today, this threshold would be overtopped between 1 and 6 times each year. By 2030, this threshold could be overtopped between 1 and 22 times depending on the rate of sea level rise. By 2050, this threshold could be overtopped between 4 and 150 times. By 2070, this threshold could be exceeded every day of the year under the highest sea level rise projections – in the absence of high winds and coastal storm events.

The mean shoreline elevation along the POSF's waterfront is about 11.8 feet NAVD88 (Port of San Francisco 2021b). Using this elevation as a flooding threshold, high tide shoreline overtopping is not anticipated until closer to 2050 (Figure 6-17). By 2050, high tides could overtop this flooding threshold 0 to 3 times per year. By 2060, high tides could overtop this flooding threshold by 0 to 23 times per year, depending on the rate of sea level rise. Under the highest sea level rise projections, high tides could overtop the shoreline every day by 2090 in the absence of high winds and coastal storm events.

Although Figure 6-16 and Figure 6-17 help highlight the potential timing and importance of high tide flooding for San Francisco, they do not highlight the scale of the problem, the locations most at risk, or the potential inland

---

[10] A King Tide is a non-scientific term often used to describe exceptionally high tides that are naturally occurring, predictable events that can occur a few times per year when there is alignment between the gravitational pull of the sun and the moon on the tides.

extent of high tide flooding. To better characterize this dynamic, water level and wave inputs that represent high tide flooding were developed for G2CRM.

High tide water levels that represent the 6-month, 4-month, 3-month, 2-month, and 1-month return frequencies were analyzed for incorporation within G2CRM. The monthly recurrence interval was selected as the highest frequency threshold for consistency with Sweet et al (2022). Analysis of events more frequent than monthly poses a challenge for G2CRM as events can become overlapping (for example, if a weekly event is used, it is likely that more extreme events may happen concurrently within the model, resulting in model simulation failure). The use of monthly events did not cause model failure. Additional evaluation of repetitive high tide flooding and its implications to the G2CRM economic damage assumptions is documented separately within the Economic Appendix.

6.4.2 Extreme Water Levels

California winter storms typically bring high rainfall, low atmospheric pressure, and strong winds (Section 4 and Table 4-2). These conditions can combine with the oceanic cycles (that is, El Niño and the PDO), and other factors, to produce Bay water levels that are significantly higher than normal (that is, extreme water levels). When higher high tide is elevated above normal, this is often referred to along the California coast as an extreme tide. For the purposes of this report, the term extreme water level is used for consistency with Sweet et al. (2022). Although this elevated water level is a combination of the astronomical tide and many other factors (that is, the non-tidal residual at higher high tide), this elevated "extreme" water level is not necessarily storm driven. It is a product of multiple factors and may or may not have a storm-driven component. For example, a King Tide during an El Niño winter and the warm PDO phase could be 18 inches or more above the MHHW elevation, in the absence of a storm.

Except for King Tides, which are predictable astronomical tides, extreme water levels represent a temporary, short-term (hours to months) increase in sea level above the predicted astronomical tide level (Table 6-1). This difference in water elevation between the predicted and observed tides may include storm surge, El Niño and/or PDO cycles, local wind setup, freshwater inflows, or a combination of these factors. Observations of extreme water level at tide stations typically do not include short-term wave effects, although wave effects can also influence water levels at the shoreline. Because of the absence of wave effects, the extreme water level elevation is also referred to as the stillwater elevation (SWEL). An extreme water level with a 1% annual chance of occurring may be referred to as the 100-year extreme water level elevation, the 100-year SWEL, the 1%-annual-chance SWEL, or the 1%- annual exceedance probability (AEP) (1% AEP). For consistency in terminology, this report uses the term AEP when referring to water levels that exceed average annual maximum values. Extreme water levels used in this assessment range from the 50% (2-year) AEP to the 1% (100-year) AEP.

Figure 6-18 presents the variation in the 1% AEP water levels along the entire Bay shoreline. As observed on Figure 6-1 for MHHW, tidal amplification results in an increase in the 1% AEP water levels to the north and the south of the Golden Gate. Figure 6-19 presents the local variation in the 1% AEP water levels along the San Francisco shoreline, with a similar 0.5-foot difference observed between Aquatic Park and Heron's Head Park.

Another useful metric for evaluating coastal hazards is the total water level (TWL) elevation, which includes a combination of water levels and wave hazards (ocean swell and wind-driven waves). The 1% AEP TWL typically consists of a Bay water level below the 1% AEP water level coupled with a companion wave height that is smaller than the 1% AEP wave height. In other words, the peaks are not coincident as they are driven by separate forcings – the 1% AEP TWL does not equal the 1% AEP water level plus 1% AEP wave height. Offshore, the 1% AEP TWL is better characterized as the 1% AEP wave crest elevation (WCE), so as not to confuse it with the TWL calculated directly at the shoreline that includes the additional component of wave runup. In most cases, the 1% AEP TWL directly at the shoreline (with wave runup) is greater than the offshore 1% AEP WCE.
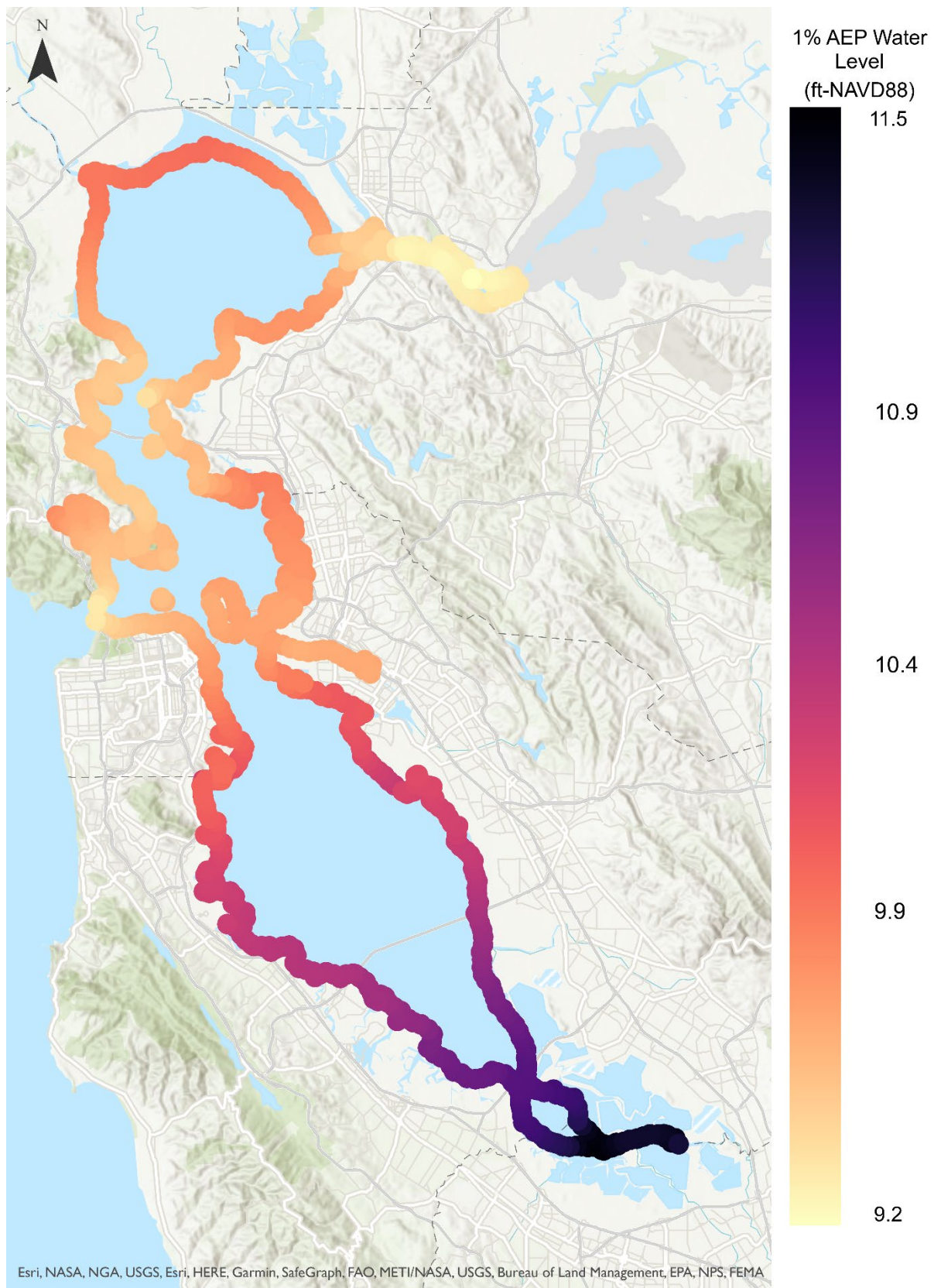
Source: (DHI 2011, 2013, May et al. 2016b)

Figure 6-18. Baywide Variation in 1% AEP Water Level (relative to 2008)
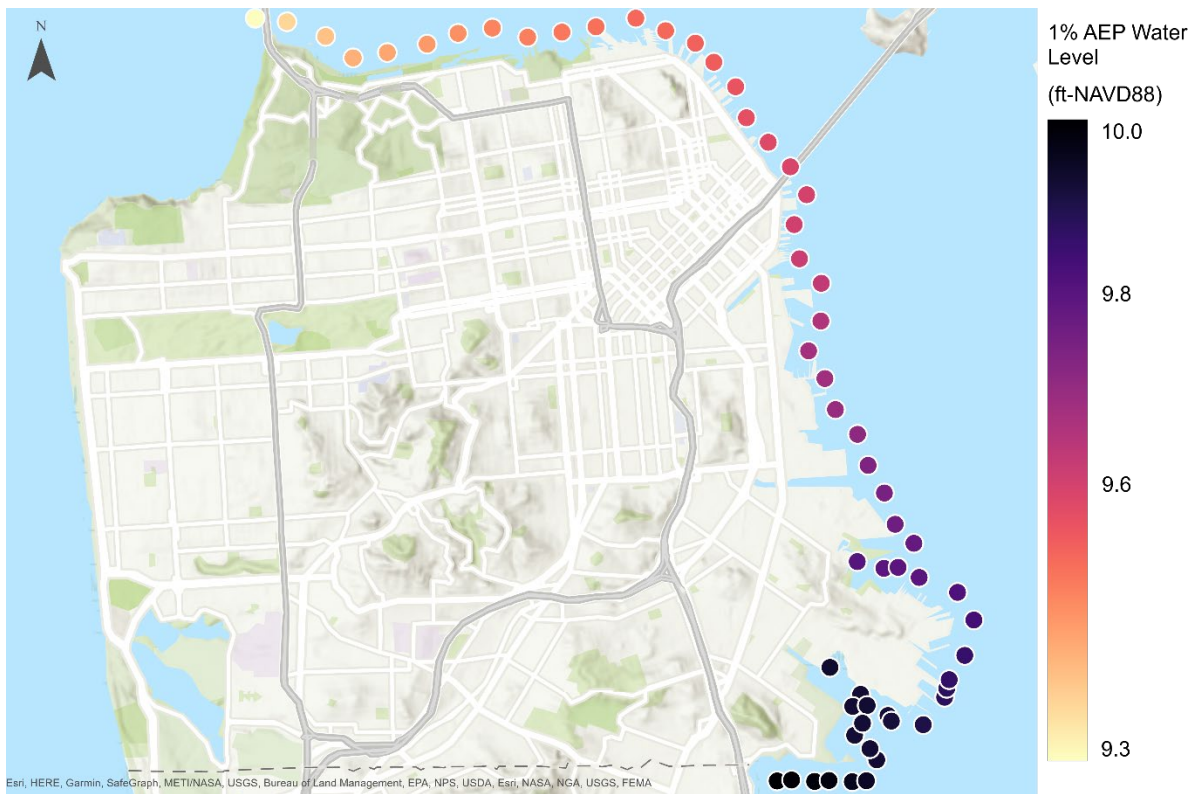
Source: (DHI 2011, 2013, May et al. 2016b)

Figure 6-19. San Francisco Variation in 1% AEP Water Level (relative to 2008)

Extreme water levels that represent the 100-year, 50-year, 25-year, 10-year, 5, year, 2-year, and 1-year return frequencies were analyzed for incorporation within G2CRM. The 100-year, or 1% AEP, extreme water level was selected as the lowest return frequency due to the nature of extratropical storm systems which tend to have small differences between 100-year, 200-year, and lower return frequencies (Figure 6-13). For San Francisco, the difference between the 10-year and the 100-year return frequency is less than twelve inches (Table 6-2). The difference between the 100-year and 200-year is likely on the order of inches, and the difference between the 100-year and 500-year is likely less than 6 inches. The maximum extreme water level elevations asymptote to about 10 feet NAVD88, as shown on Figure 6-13. Although the use of the 31-year continuous timeseries of water levels allows for a robust estimate of 100-year and more frequent water levels, a 31-year period of record is insufficient for estimating the lower frequency water levels elevations. Given the infrequency of these events, the low likelihood of one occurring over the 100-year period of analysis, and the small difference between the 100-year, 200-year, and 500-year event, reliance on high tide and extreme water level elevations from the monthly event to the 100-year event is considered sufficient for estimating future flooding and the associated damages within G2CRM.

THIS PAGE IS INTENTIONALLY BLANK.

7   Coastal Storm Database Development

The economic outputs from G2CRM are only reliable for assessing coastal hazard related damage if the coastal storm inputs accurately represent the local coastal hazards.

With an understanding of Bay water levels and wave hazards firmly in hand, the coastal storm inputs and the respective CSDs can be developed using the FEMA San Francisco Bay Area Coastal Study model output as an appropriate historical long-term water level and wave data set of sufficient record length. USACE usually relies on coastal storm hazard data, including numerical and probabilistic modeling results, available through the Engineer Research and Development Center (ERDC) Coastal and Hydraulics Laboratory (CGL) Coastal Hazards System (CHS)[11]. However, at present, sufficient high-resolution numerical modeling of coastal storms along the California coast and the San Francisco Bay is not available through CHS. The FEMA model output provides the most reasonable and comprehensive alternate data set, and the model output is widely used by local and state agencies and communities in the Bay Area.

The primary steps used to develop the CSDs are as follows:

1. Baseline all water levels to a consistent year to remove historical sea level rise trends.

2. Complete extreme value analysis to define high frequency (high tide) and low frequency (extreme) water level elevations for a range of exceedance probabilities.

3. Identify relevant hydrographs from the model output based on the range of target exceedance probabilities.

4. Pair the high tide and extreme water level elevation timeseries for each hydrograph with the corresponding wave height timeseries (filtered in the direction perpendicular to the shoreline, so only waves traveling towards the shoreline are included in the overland G2CRM analysis).

As described in Section 3.1, the San Francisco G2CRM model is divided into seven MAs (MA1 thru MA7) that correspond to the four CSDs. MA1 and MA5 are associated with CSD1, MA2 and MA6 are associated with CSD2, MA3 and MA7 area associated with CSD3, and MA4 is associated with CSD4. Four FEMA model output locations were selected offshore of the San Francisco shoreline, in approximately the middle of each MA (or set of MAs if an onshore and offshore MA is present), to provide the historical long-term water level elevations and wave heights for database development (Figure 7-1).

---

[11] https://chs.erdc.dren.mil/
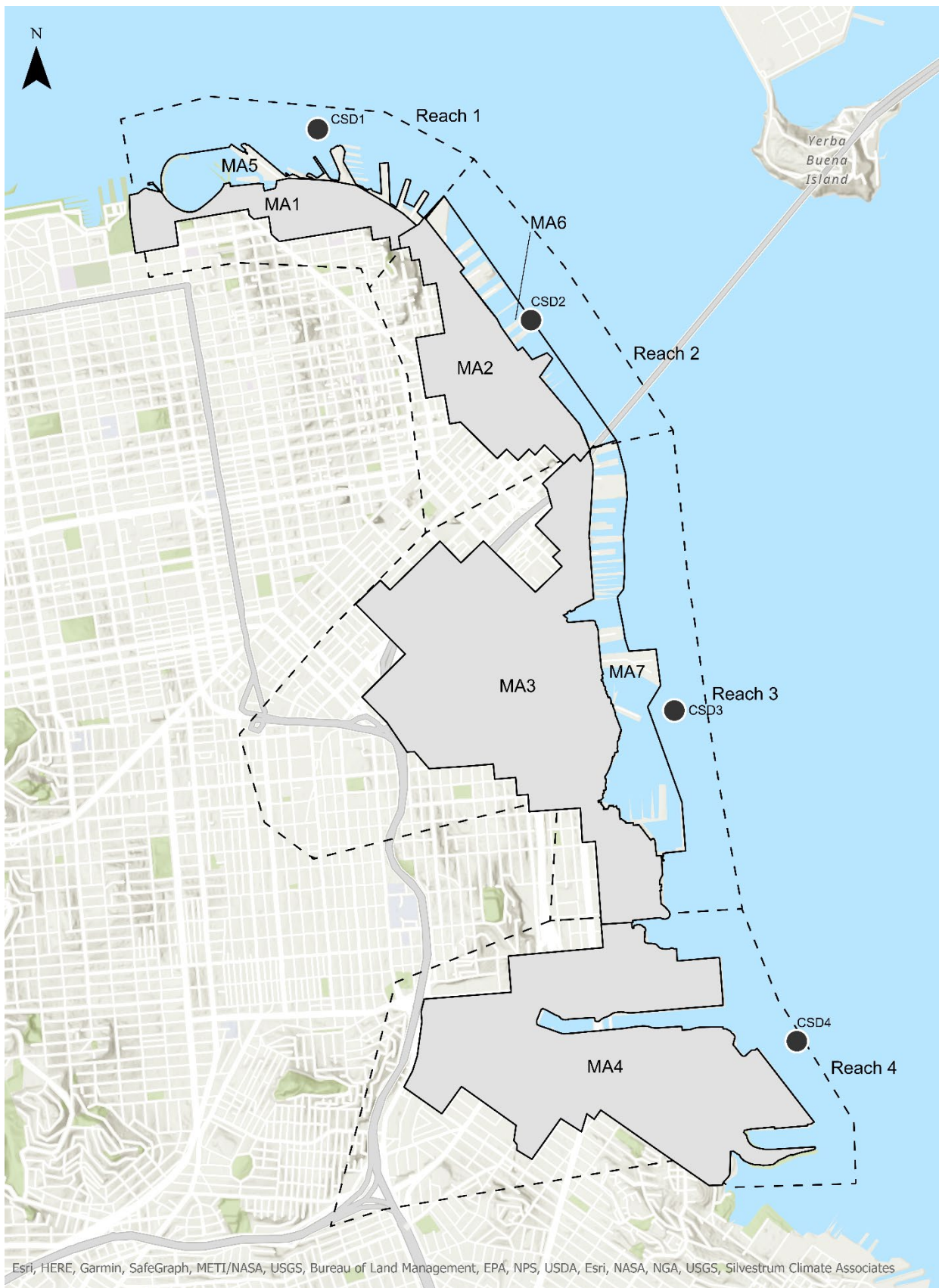
Figure 7-1. G2CRM Model Areas and Coastal Storm Database Input Locations

7.1 Sea Level Re-baselining

The extreme value analysis requires removing the historical sea level trends to create a stationary data set, which is a requirement of the extreme event statistical analysis.[12] Since mean sea level (MSL) recorded at the Presidio tide gage has risen continuously since tide gage measurements began in 1854, this requires selecting a reference year so that all water levels are baselined to one consistent vertical elevation. USACE relies on three primary sea level rise projections - Low, Intermediate, and High - that are baselined relative to 1992 water level elevations (USACE 2019b, 2019a, 2020). The CCSF and the State of California rely on the OPC sea level rise projections – Likely, and 1:200 (Plausible, High Impact) - that are baseline relative to 2000 water level elevations (OPC and CNRA 2018, CPC 2020). The five 2022 sea level rise projections from Sweet et al. (2022) are shown on Figure 7-2, representing best available climate science (IPCC 2021). The OPC and USACE sea level rise projections that are similar but are based on older science. The California OPC curves are based on OPC and CNRA (2018) and IPCC (2014); the USACE curves are based on NRC (2012) and IPCC (2007) (Table 6-3). G2CRM can simulate all five sea level rise projections – independent from the CSDs – to evaluate future coastal hazards. The sea level rise projections used in G2CRM rely on OPC and CNRA (2018) and NRC (2012) and have not been updated to reflect the latest science reflected in Figure 7-2.
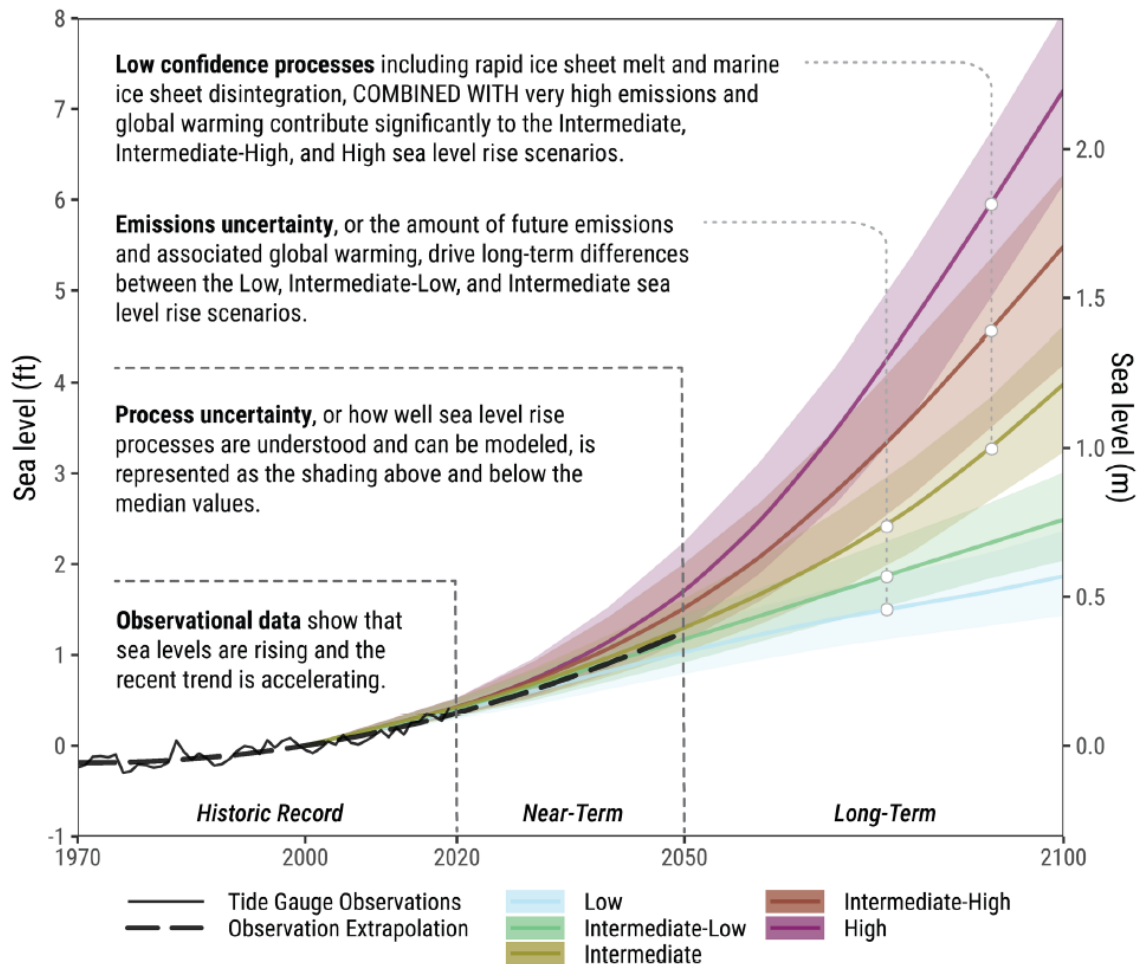
Source: Collini et al. (2022); Sweet et al. (2022); IPPC (2021)

Figure 7-2. Sea Level Rise Projections based on Best Available Science

---

[12] Re-baselining the data in this manner removes the non-stationarity relative to sea level rise. However, additional non-stationarity in the data may be present relative to other climate change factors, such as increasing storm intensity and frequency.

Figure 5-7 presents the 10-year moving average of mean sea level at the Presidio tide gage, and Table 7-1 presents annual mean sea level calculated at the Presidio tide gage for four years of interest. Mean sea level in 1992 was about 3 inches (0.25 feet) higher than in 2000, and mean sea level in 2020 remains about 0.6 inches below mean 1992 water level elevations. However, there is significant variability in mean sea level due to seasonal trends, storm activity, natural processes (Table 6-1), and sea level rise. Although coastal storm events greater than the 25-year (0.04% AEP) have not occurred in the past decade, the 10-year moving average of mean sea level has increased steadily (Figure 5-7). This trend is not evident when assessing annual mean sea level, as shown in Table 7-1.

As shown on Figure 7-3, regional mean sea level rise for California and southern Oregon is trending with the NOAA Intermediate sea level rise projections (Collini et al. 2022, Sweet et al. 2022b), which most closely correlates with the CA OPC Likely sea level rise projection (Table 6-3). The observation-based extrapolation provides a likely trajectory of current sea level rise, based on greenhouse gas emissions that have already occurred, with an emphasis on regional tide gage observations between 1970 and 2020 that include water levels elevated by storms and El Niño conditions (Hamlington et al. 2021, Sweet et al. 2022b) This trend is not extended past 2050 because of uncertainties related to future global greenhouse gas emissions and changes in physical processes that could occur under a warming climate (such as rapid ice sheet melt and marine ice disintegration).

Table 7-1. Annual Mean Sea Level (MSL) at the Presidio Tide Gage

Year	Annual MSL (feet NAVD88)
1992	3.34
2000	3.09
2008	3.11
2020	3.29
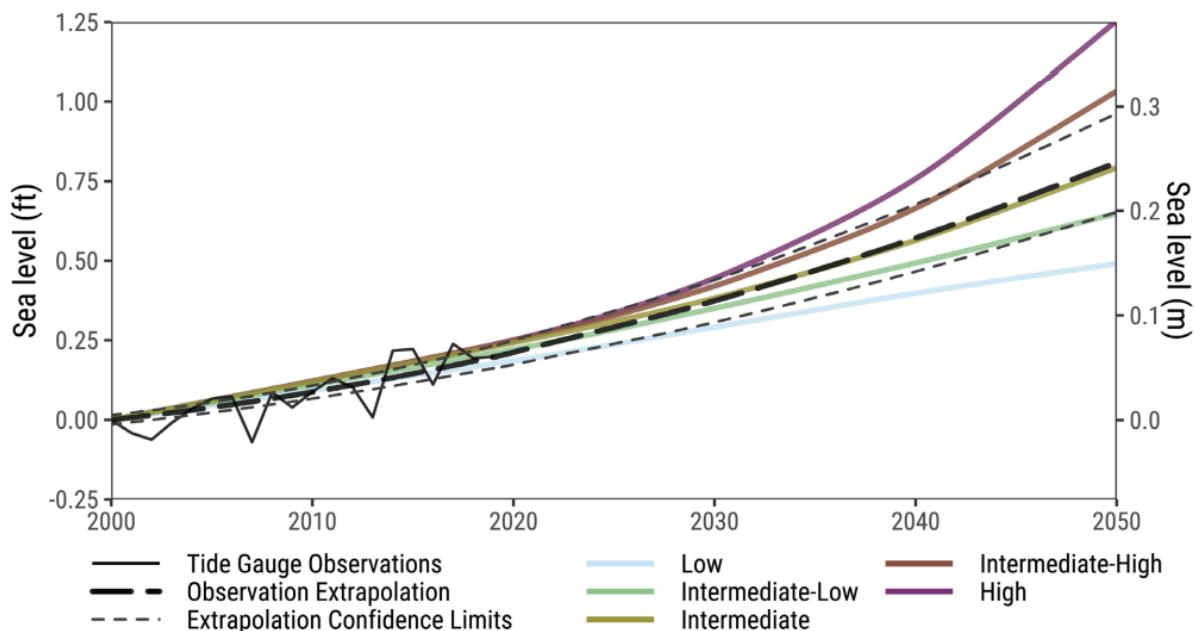
Source: Collini et al. (2022); Sweet et al. (2022)

Figure 7-3. Regional Sea Level Rise Scenarios and Observations for California and southern Oregon

The FEMA model output is baselined to the year 2008 (DHI 2011). The use of the FEMA model output within G2CRM required re-baselining the water levels to 1992 when applying the USACE sea level rise projections, and re-baselining to 2000 when applying the OPC sea level rise projections. Therefore, two complete sets of four CSDs were developed to inform the USACE and POSF analysis of future sea level rise. The 1992 CSDs are used when evaluating economic damages relative to the USACE sea level rise projections, and the 2000 CSDs are used when evaluating the OPC sea level rise projections. Although there are only small differences between the 1992 and 2000 water level elevations, this re-baselining correction preserves the integrity of the model output and prevents underestimating or overestimating economic damages based on an incorrect baseline.

7.2 Extreme Value Analysis

The CSDs were populated with historical storm hydrographs meeting the target exceedance probabilities for each model output point. Exceedance probability curves were calculated for each model output point, for each re-baselined water level timeseries (1992 and 2000), resulting in a total of eight exceedance probability curves for extracting the individual historic storm hydrographs.

Methods from extreme value theory were used to analyze the statistical distributions describing the extreme values (1-year recurrence interval and greater) of the Bay water levels, with focus on the tail of the distributions. There are two well-known approaches to derive extreme event values from a probability distribution - the block maxima approach, and the threshold exceedance approach (also known as peak over threshold [POT]).

The block maxima approach is the most common. This requires fitting a continuous probability distribution (for example, generalized extreme value) to block maxima (for example, annual water level maxima) to estimate a return level for a given interval of time and quantile. The elevation expected to be exceeded once every annual period, for the 0.99 quantile, is commonly known as the 1% AEP. Return levels can be calculated for a range of target AEPs once the probability distribution is appropriately fitted to the maxima values. The probability distribution is fitted using a set of governing parameters (for example, shape, scale, and location) commonly estimated using maximum likelihood methods. However, although this approach performs well on record lengths that extend for several decades, for shorter record lengths it can fail to account for the total range of high tide heights (Goring et al. 2011). Where storm surge magnitudes exceed the range of high tide heights, this shortcoming is not significant. However, in coastal environments where the range of high tide heights is larger than the range of storm surge heights, this shortcoming can be significant (Goring et al. 2011). In San Francisco Bay, where the range in high tide heights is large relative to the range in storm surge heights, the use of the classical general extreme value analysis using maximum likelihood with the 31-year timeseries of FEMA model output is therefore not recommended.

The alternative POT approach uses more maxima in a data set by reducing the time-block dimension and considering any maxima above a defined threshold (therefore using the data more efficiently). Given that the length of hindcast available for the modeled water levels (31 years) approaches the minimum number of years required to derive the bookend 1% AEP threshold (FEMA 2016), the POT approach was selected to construct the exceedance probability curves and return levels for development of the CSDs. The maxima series determined from the POT method is described by the generalized pareto distribution (GPD), as suggested by extreme value theory (Zervas 2013, FEMA 2016). Once a threshold is defined, the distribution is fit to the maxima to infer the return levels. Goodness of fit is evaluated using both the cumulative distribution function and a quantile-quantile (Q-Q) analysis.

7.2.1 Threshold Selection and Return Levels

The choice of threshold for the maxima series is sensitive to the characteristics of the maxima and extreme value theory principles. An optimal threshold should balance bias and variance in the parameter estimators for GPD (Bommier 2014, Choi et al. 2019). For example, an increasingly higher threshold will reduce bias to stabilize the parameter (for example, shape, scale, and location) estimates, but will also consequently increase the variance

and error when less maxima are considered. An optimal approach seeks to lower the threshold (that is, to increase the size of the maxima series) with a goal of reducing the variance until bias is compromised.

The POT approach to selecting maxima first requires that single events be defined, ensuring multiple maxima from the same storm system are not drawn into the maxima series, so that each storm system is evaluated independently. Unique events were defined by requiring a minimum inter-event time of 2 days within the modeled water levels. Any water level maxima below the highest peak of a single storm event were dropped from the analysis.

Once the unique event maxima pool was created for each MA, the maxima thresholds were selected. The threshold selection employed a sensitivity framework that calculated the resultant water level for the 1% AEP using a GPD fit, repeated for a range of maxima thresholds that are defined by a range of quantiles (for example, 90th percentile to 99th percentile of all water level maxima). The 1% AEP was selected as the metric for the sensitivity analysis because it is the lowest exceedance probability relevant to the study, and the scarcity of maxima exceeding this return level during the 31-year hindcast is likely to contribute to the largest error and instability in the parameter estimations for the GPD fitting.

The maxima threshold methodology is summarized as follows:

- For each set of modeled water level maxima (one for each MA and sea level rise baseline), a subset of water level maxima was identified when exceeding the elevations for a range of quantile bins from 0.99 to 0.9 (99th to 90th percentile), using a step of 0.01. This generally corresponds to between 1 and 64 water level maxima events per year, over the entire length of record.

- The GPD distribution was fit to the maxima corresponding to each quantile bin, returning the water level value with a 1% AEP. The GPD parameters were estimated using the method of L-moments (Hosking and Wallis 1997), which is known to be more effective and less sensitive to outliers than ordinary moments (for example, maximum likelihood) (Gubareva and Gartsman 2010).

- Using the 1% AEP return for each quantile bin, a set of stable candidate thresholds were identified through comparison to the 1% AEP value and the results of the neighboring quantile bins. The goal of this comparison was to identify a region of stability within the 1% AEP results while increasing the maxima selection threshold and using the median result from all quantile bins as an upper and lower bound for the search window. A region of stability concludes there is a stability in the parameter estimation (for example, shape, scale, and location) for the GPD distribution, especially the tail. Figure 7-4 thru Figure 7-9 (top plots) illustrate a sample plot of the 1% AEP values calculated for the range of quantiles evaluated at one location with modeled output.

- The final selection is made through quantifying goodness of fit of the GPD model, by evaluating the root mean square error from Q-Q plots between the empirical quantiles and expected quantiles from the reference GPD model (Figure 7-4 thru Figure 7-9, bottom plots).

The GPD model was then used to generate exceedance probability curves for each MA and sea level rise baseline. The AEPs of interest for extreme water levels are 63.21% (1-year), 39.3% (2-year), 18.1% (5-year), 9.5% (10-year), 3.9% (25-year), 2% (50-year), and 1% (100-year). The AEPs of interest of high tide water levels are 99.9994% (1-month), 99.75% (2-month), 98.17% (3-month), 95.17% (4-month), and the 86.47% (6-month).

An automated approach to select the most appropriate threshold based on the observed and modeled data was developed to evaluate and obtain the most reasonable goodness of fit for threshold selection, using both the observed Presidio water levels and the modeled FEMA water levels. The recommended threshold occurs where the root mean square error is at its minimum (see solid vertical line on Figure 7-4 thru Figure 7-9). At higher thresholds, the model sacrifices the fit of the lesser extremes to obtain a better fit of the most extreme events

(Figure 7-4). At lower thresholds, the fit of the extremes is sacrificed (Figure 7-6). Appendix A provides threshold selection plots by MA.

For the 120-year record of Presidio water levels, a high threshold of 0.997 remains within the stable area of the GPD model (the green band), converging towards an annual maximum approach with the selection of just over one peak event per year (Figure 7-4). This threshold is above the recommended threshold, and the fit is biased towards the extreme end of the distribution; however, the fit remains similar to that of a lower threshold (0.98) that is closer to that recommended (Figure 7-5). The long period of record has relatively few extreme water levels, with only 5 observed water levels above 8.25 feet NAVD88, and two observed water levels above 8.5 feet NAVD88. Fitting the bulk of the observations to these 5 extreme water levels is not recommended. If the threshold us lowered to 0.965, the threshold is located outside of the stable area, reducing the goodness of fit in the extreme water levels (Figure 7-6). The 120-year period of record has a relatively long stability band; however, the goodness of fit in the extreme upper end (that is, the lowest return frequency events) still oscillates along the one-to-one fit line. This is most likely related to the low number of very extreme (rare) events, even with the 120-year period of record.

The same comparison is provided for the 31-year timeseries of FEMA model output. The threshold of 0.997 is above the stability area, likely due to the shorter period of record when compared with the Presidio observations (Figure 7-7). The lower threshold of 0.98 is closer to the recommended threshold and within the stabile area, providing an improved fit to both the lessor extremes and higher extreme events (Figure 7-8). Similar to the Presidio analysis, the lowest threshold of 0.965 is below the stability band, resulting in a poor fit to the higher extremes and reduced extreme water level elevations (Figure 7-9).

The two highest water levels on record occur in the early 1980s, and therefore captured in both the 120-year and 31-year periods of record. For the 120-year record, the two highest water levels on record have a return period of roughly 50-years, depending on the approach used. For the 31-year of record, the GPD model used estimated that these two events are too high compared to the rest of the record to be a 30-year event. This lends confidence to the overall approach for estimating return periods for the low frequency extreme water levels using the 31-year FEMA period of record.
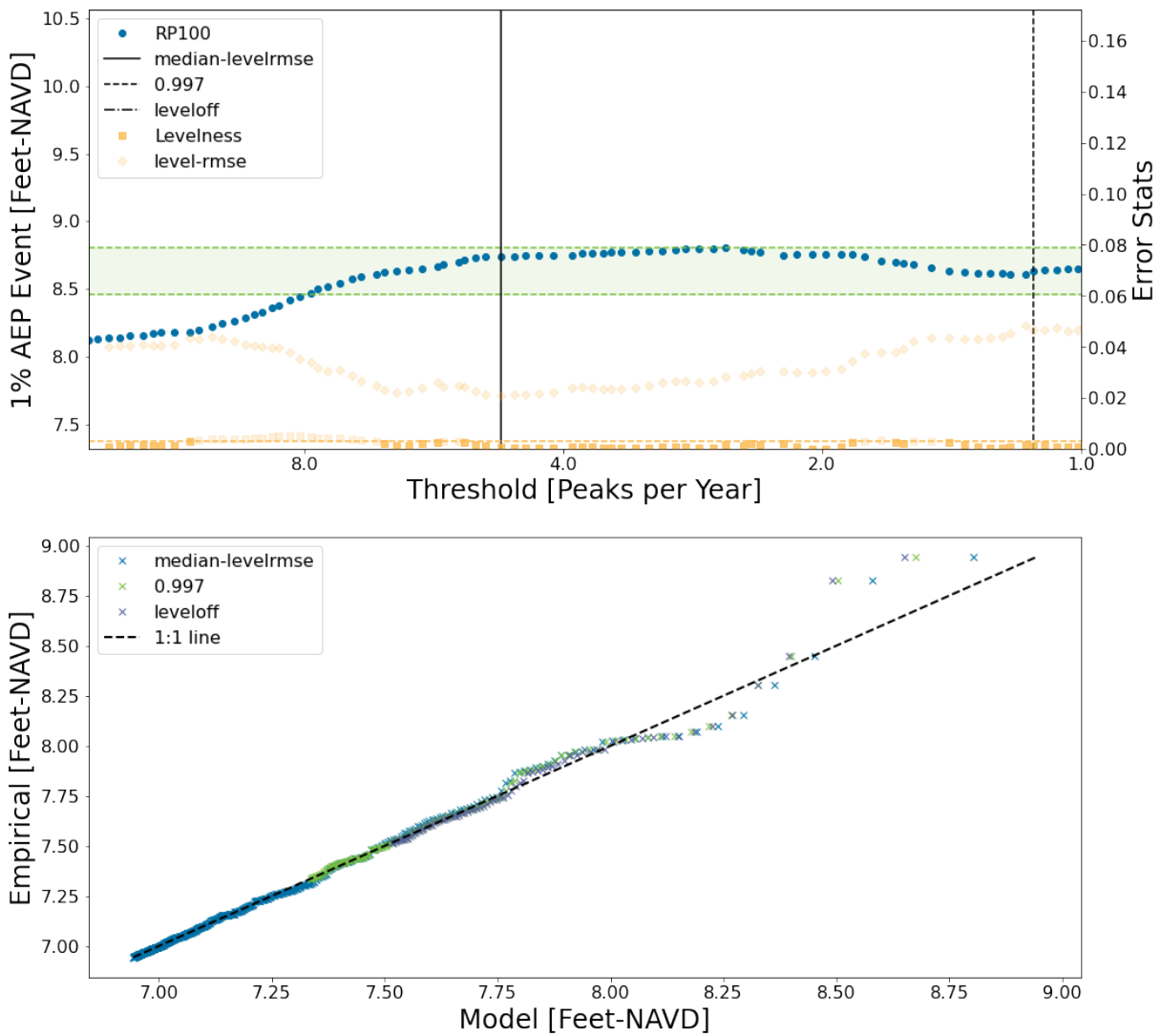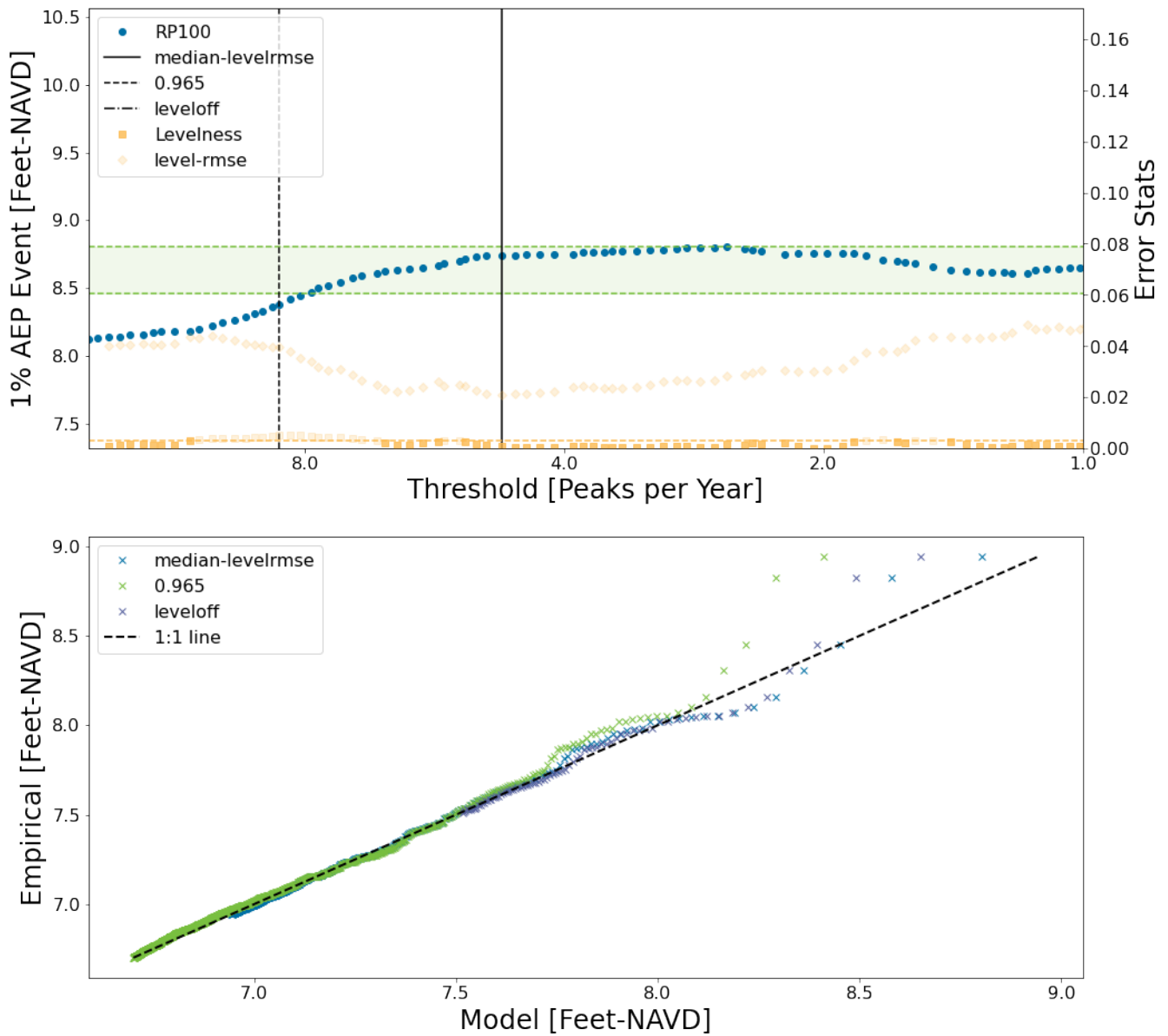
Figure 7-4. Observed Presidio water levels (1900 to 2020) GPD Threshold = 0.997
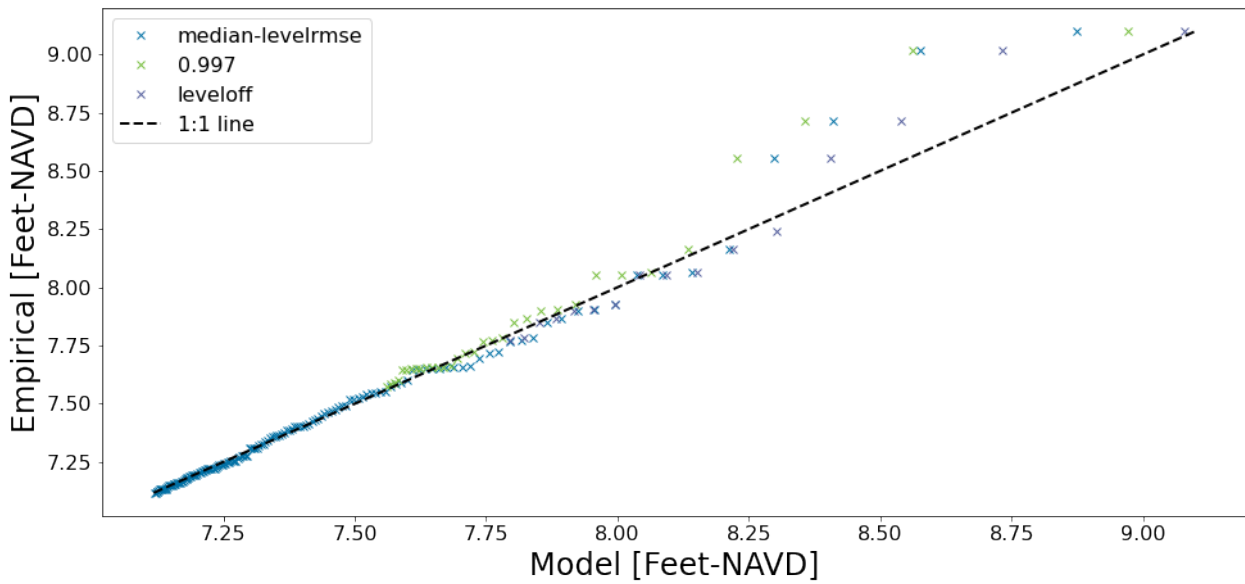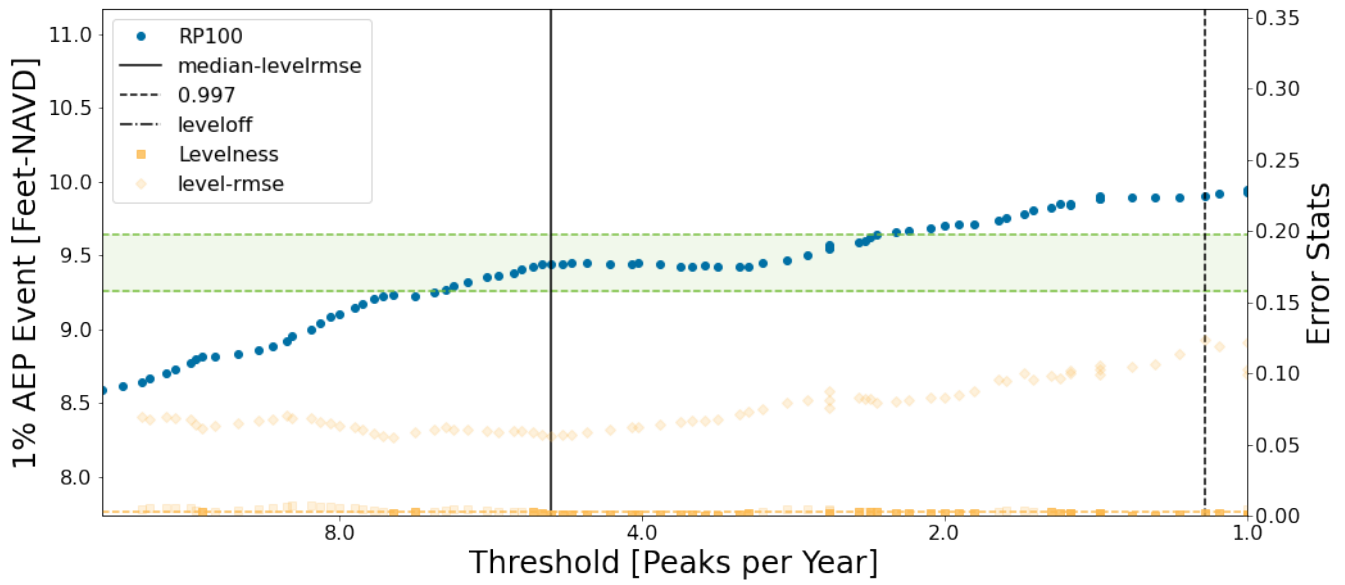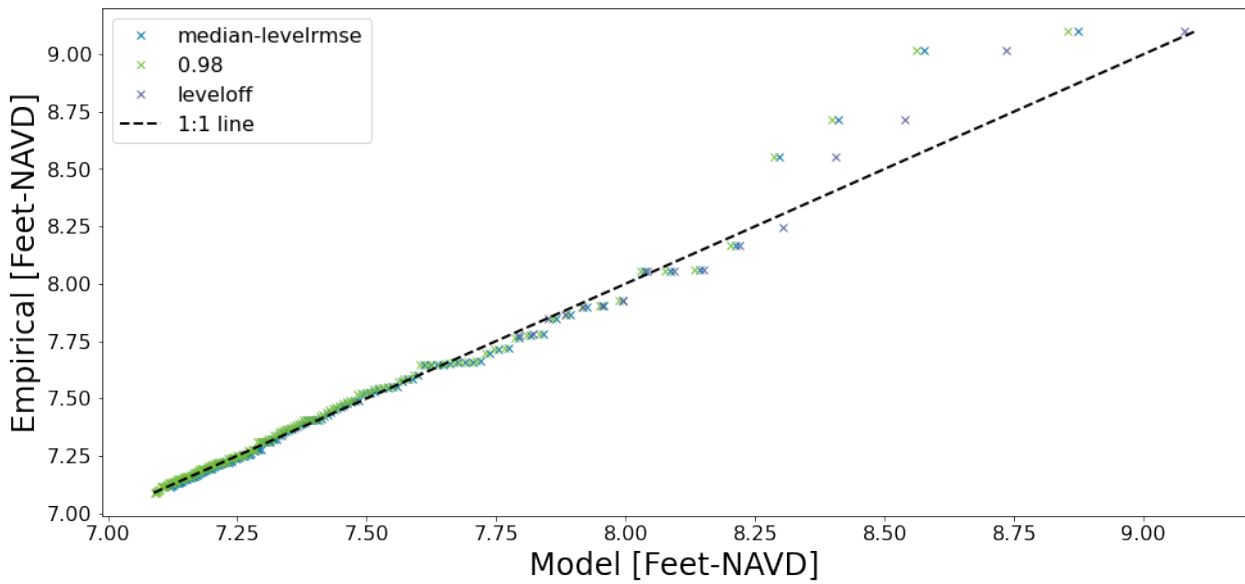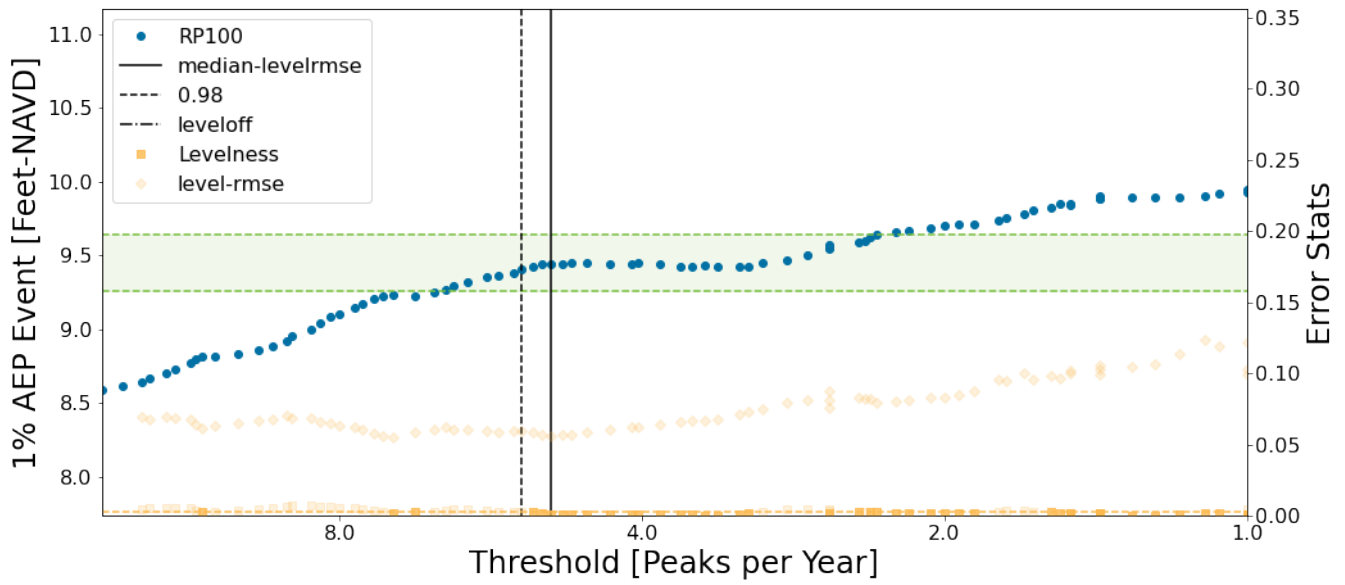
Notes:

1. Horizontal band (in green) denotes the stability area from which the final quantile threshold can be selected, based on the median of all 1% AEP water levels corresponding to all quantiles from 0.90 to 0.99th percentile of all water level maxima.

2. Vertical line (in black) denotes the recommended quantile for the water level maxima threshold. This selection is based on where the root mean square error is at a minimum (and within the green stability band).

3. Vertical line (dotted) denoted the threshold tested.
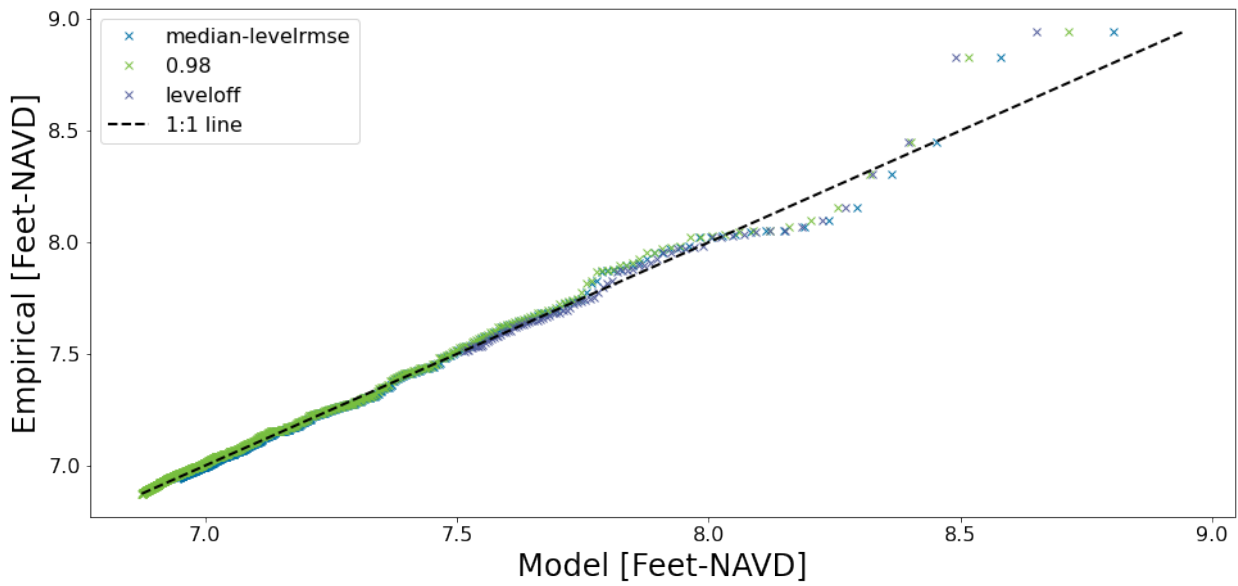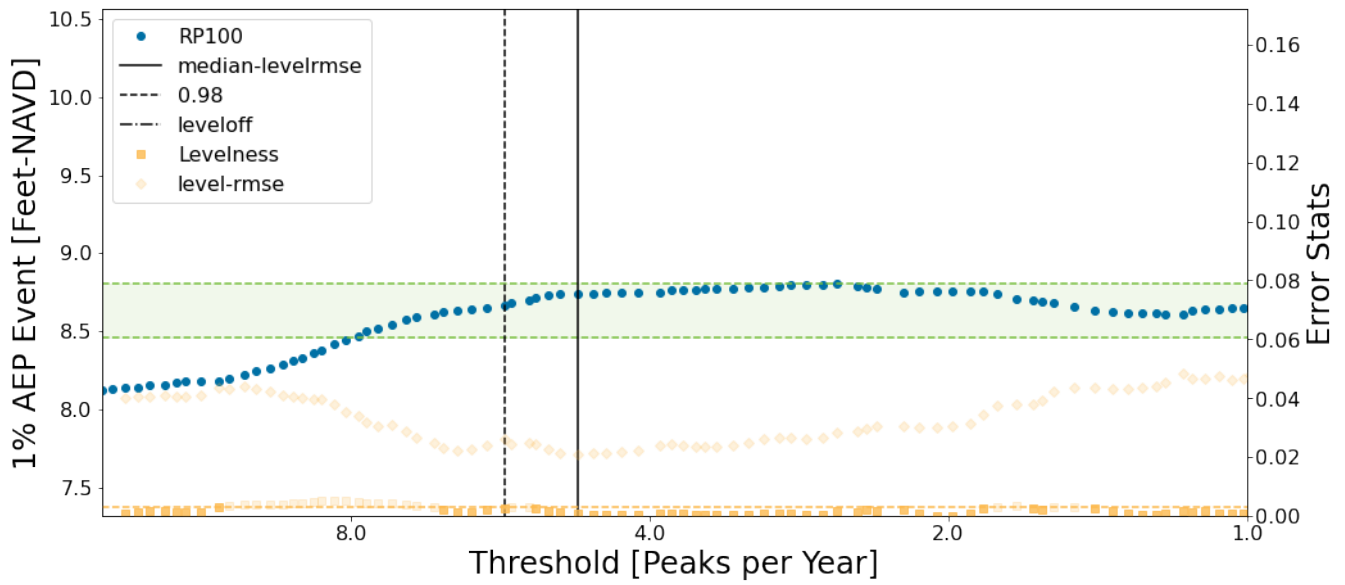
Figure 7-5. Observed Presidio water levels (1900 to 2020) GPD Threshold = 0.98

Notes:

1. Horizontal band (in green) denotes the stability area from which the final quantile threshold can be selected, based on the median of all 1% AEP water levels corresponding to all quantiles from 0.90 to 0.99th percentile of all water level maxima.

2. Vertical line (in black) denotes the recommended quantile for the water level maxima threshold. This selection is based on where the root mean square error is at a minimum (and within the green stability band).

3. Vertical line (dotted) denoted the threshold tested.

Figure 7-6. Observed Presidio water levels (1900 to 2020) GPD Threshold = 0.965

Notes:

1. Horizontal band (in green) denotes the stability area from which the final quantile threshold can be selected, based on the median of all 1% AEP water levels corresponding to all quantiles from 0.90 to 0.99th percentile of all water level maxima.

2. Vertical line (in black) denotes the recommended quantile for the water level maxima threshold. This selection is based on where the root mean square error is at a minimum (and within the green stability band).

3. Vertical line (dotted) denoted the threshold tested.

Figure 7-7. Modeled FEMA water levels (1973 to 2004) GPD Threshold = 0.997

Notes:

1. Modeled data from MA1 was selected as it is closest to the Presidio tide gage

2. Horizontal band (in green) denotes the stability area from which the final quantile threshold can be selected, based on the median of all 1% AEP water levels corresponding to all quantiles from 0.90 to 0.99th percentile of all water level maxima.

3. Vertical line (in black) denotes the recommended quantile for the water level maxima threshold. This selection is based on where the root mean square error is at a minimum (and within the green stability band).

4. Vertical line (dotted) denoted the threshold tested.

Figure 7-8. Modeled FEMA water levels (1973 to 2004) GPD Threshold = 0.98

Notes:

1. Modeled data from MA1 was selected as it is closest to the Presidio tide gage

2. Horizontal band (in green) denotes the stability area from which the final quantile threshold can be selected, based on the median of all 1% AEP water levels corresponding to all quantiles from 0.90 to 0.99th percentile of all water level maxima.

3. Vertical line (in black) denotes the recommended quantile for the water level maxima threshold. This selection is based on where the root mean square error is at a minimum (and within the green stability band).

4. Vertical line (dotted) denoted the threshold tested.
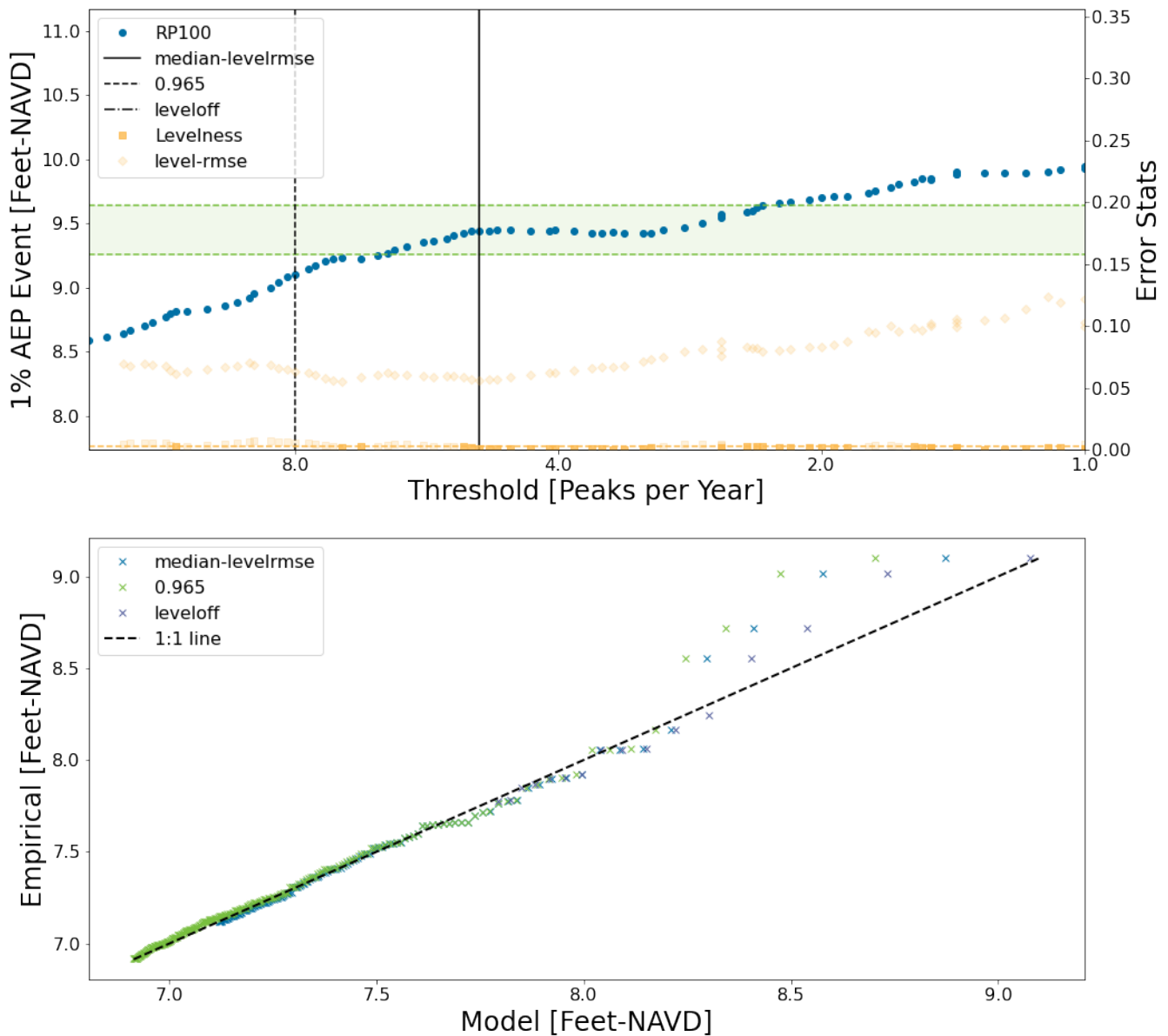
Figure 7-9. Modeled FEMA water levels (1973 to 2004) GPD Threshold = 0.965

Notes:

1. Modeled data from MA1 was selected as it is closest to the Presidio tide gage

2. Horizontal band (in green) denotes the stability area from which the final quantile threshold can be selected, based on the median of all 1% AEP water levels corresponding to all quantiles from 0.90 to 0.99th percentile of all water level maxima.

3. Vertical line (in black) denotes the recommended quantile for the water level maxima threshold. This selection is based on where the root mean square error is at a minimum (and within the green stability band).

4. Vertical line (dotted) denoted the threshold tested.

7.2.2   Event Strength Classification

The peak water level elevations corresponding to the target event exceedance probabilities (event strength) were used to catalog matching storm maxima, that is, classify all historical storm events matching the high frequency water levels: 99.9994% (1-month), 99.75% (2-month), 98.17% (3-month), 95.17% (4-month), and the 86.47% (6-month), as well as the low frequency water levels 63.21% (1-year), 39.3% (2-year), 18.1% (5-year), 9.5% (10-year), 3.9% (25-year), 2% (50-year), and 1% (100-year) AEP. Historical maxima were clustered into their

respective event strength using the mid points between each respective AEP water level. For the lowest AEP (99.9994%), events were clustered using plus or minus half of the distance between the AEP water levels for 99.9994% and 99.75%. For each storm event matching the event strength criteria, the hourly water level data from the modeled hindcast was extracted for a duration of 3 days (using the criteria in Section 4.5) and saved in 1-hour intervals centered on the peak. This approach is consistent with that presented in (Sanderson et al. 2019) for developing representative storm surge hydrographs from a large-scale numerical model for G2CRM CSDs.

Using this methodology, no storms with peaks matching the 1% AEP were identified, as the highest water levels on record were considered more representative of a 2% AEP. Synthetic storm hydrographs with peaks matching the 1% AEPs were generated by scaling the largest event from the non-synthetic storm pool and amplifying its magnitude such that it matches the theoretical strength of a 1% AEP water level. This was repeated for all data sets for each MA and each sea level rise baseline.

Table 7-2 presents the number of peak water levels matching each return frequency using the event strength selection method for the low frequency events, and Table 7-3 presents the same for the high frequency events. An interevent filter applied during the POT analysis removes any consecutive events that occur, thus removing many smaller events that occur the day before or after a higher strength event. Although larger storm systems and climatic and oceanic events that result in 10-year to 100-year extreme water levels may elevate Bay water levels for three days or longer, many of the high frequency water levels may last for a much shorter duration. However, to support the development of the G2CRM CSDs, all hydrographs regardless of return frequency were set equal to three days.

While AEP corresponds to a frequency that all events that exceed that value could occur, the storm catalog presented in Table 7-2 only captures events close to the AEP event strength. Table 7-4 and Table 7-6 present the water level elevations for each associated AEP, baselined to 1992 and 2000 water levels, respectively. Both tables show the tidal amplification that occurs between MA1 and MA4, and the slight elevation in water levels between the 1992 and 2000 baseline. The hydrographs selected from the full model time series for all storm events in the coastal storm catalog are presented in Appendix B.

Table 7-2. Coastal Storm Catalog: Number of Storms per Model Area per Low Frequency AEP

Model Area	1-year (63.2%)	2-year (39.3%)	5-year (18.1%)	10-year (9.5%)	25-year (3.9%)	50-year (2%)	100-year (1%)[a]
1	27	10	4	1	2	2	1
2	26	11	4	1	1	2	1
3	24	11	5	1	1	2	1
4	22	10	5	1	1	2	1
Total	99	42	18	4	5	8	4

[a] 1% AEP were developed using a scaled synthetic hydrograph

Table 7-3. Coastal Storm Catalog: Number of Storms per Model Area per High Frequency AEP

Model Area	1-month (99.9994%)	2-month (99.75%)	3-month (98.17%)	4-month (95.17%)	6-month (86.47%)
1	179	104	42	39	29
2	167	99	38	36	29
3	142	91	49	31	31
4	151	95	46	26	40
Total	639	389	175	132	129

Table 7-4. Low Frequency AEP Values per Model Area (relative to 1992)

Model Area	1-year (63.2%)	2-year (39.3%)	5-year (18.1%)	10-year (9.5%)	25-year (3.9%)	50-year (2%)	100-year (1%)[a]
1	7.58[b]	7.81	8.13	8.38	8.72	8.99	9.27
2	7.70	7.93	8.25	8.52	8.89	9.19	9.51
3	7.86	8.09	8.41	8.67	9.03	9.32	9.63
4	7.98	8.21	8.52	8.76	9.09	9.34	9.59

[a] 1% AEP were developed using a scaled synthetic hydrograph.
[b] Values are presented to two significant digits for comparison purposes, although the accuracy of the model output and analysis results do not include this level of precision.
[c] Values presented do not include the contribution of wind driven waves.

Table 7-5. High Frequency AEP Values per Model Area (relative to 1992)

Model Area	1-month (99.9994%)	2-month (99.75%)	3-month (98.17%)	4-month (95.17%)	6-month (86.47%)
1	6.76[a]	6.90	7.06	7.18	7.29
2	6.96	7.05	7.22	7.32	7.48
3	7.09	7.18	7.37	7.46	7.58
4	7.18	7.29	7.48	7.57	7.69

[a] Values are presented to two significant digits for comparison purposes, although the accuracy of the model output and analysis results do not include this level of precision.
[b] Values presented do not include the contribution of wind driven waves.

Table 7-6. Low Frequency AEP Values per Model Area (relative to 2000)

Model Area	1-year (63.2%)	2-year (39.3%)	5-year (18.1%)	10-year (9.5%)	25-year (3.9%)	50-year (2%)	100-year (1%)[a]
1	7.63[b]	7.86	8.18	8.43	8.80	9.09	9.40
2	7.75	7.98	8.30	8.56	8.94	9.25	9.58
3	7.91	8.14	8.46	8.72	9.09	9.39	9.71
4	8.02	8.25	8.56	8.81	9.14	9.40	9.66

[a] 1% AEP were developed using a scaled synthetic hydrograph.
[b] Values are presented to two significant digits for comparison purposes, although the accuracy of the model output and analysis results do not include this level of precision.
[c] Values presented do not include the contribution of wind driven waves.

Table 7-7. High Frequency AEP Values per Model Area (relative to 2000)

Model Area	1-month (99.9994%)	2-month (99.75%)	3-month (98.17%)	4-month (95.17%)	6-month (86.47%)
1	6.82[a]	6.94	7.11	7.23	7.34
2	6.93	7.08	7.24	7.35	7.44
3	7.09	7.24	7.39	7.51	7.64
4	7.24	7.35	7.53	7.62	7.74

[a] Values are presented to two significant digits for comparison purposes, although the accuracy of the model output and analysis results do not include this level of precision.
[b] Values presented do not include the contribution of wind driven waves.

7.2.3 High Frequency Monthly Water Levels

As shown on Table 7-3, there are 639 unique monthly water level hydrographs within the storm catalog. To better represent the seasonality of the high frequency water levels – higher monthly water levels occur in the winter months and lower monthly water levels occur in the spring months – the extreme value analysis and event selection was completed for each month across the 31-year of record. Table 7-8 presents the monthly high frequency water level elevations for MA1, and Table 7-9 thru Table 7-11 present the same information for MA2 thru MA3, respectively. This analysis was also completed relative to the 2000 water level baseline to support CSD development for use with the OPC sea level rise projections.

Table 7-8. High Frequency Monthly AEP Values Model Area 1 (relative to 1992)

Model Area 1	1-month (99.9994%)	2-month (99.75%)	3-month (98.17%)	4-month (95.17%)	6-month (86.47%)
Jan	6.75[a]	6.99	7.30	7.49	7.63
Feb	6.59	6.90	7.13	7.30	7.43
Mar	6.29	6.54	6.76	6.87	6.95
Apr	5.99	6.34	6.62	6.73	6.80
May	6.14	6.48	6.75	6.87	6.94
Jun	6.38	6.77	7.06	7.18	7.24
Jul	6.64	6.88	7.07	7.16	7.22
Aug	6.44	6.64	6.83	6.94	7.01
Sep	6.33	6.50	6.65	6.74	6.80
Oct	6.38	6.78	6.89	6.95	7.02
Nov	6.58	6.90	7.15	7.29	7.39
Dec	6.84	7.20	7.43	7.56	7.66

[a] Values are presented to two significant digits for comparison purposes, although the accuracy of the model output and analysis results do not include this level of precision.
[b] Values presented do not include the contribution of wind driven waves.

Table 7-9. High Frequency Monthly AEP Values Model Area 2 (relative to 1992)

Model Area 2	1-month (99.9994%)	2-month (99.75%)	3-month (98.17%)	4-month (95.17%)	6-month (86.47%)
Jan	7.05[a]	7.48	7.59	7.64	7.71
Feb	6.57	6.90	7.21	7.39	7.52
Mar	6.40	6.65	6.87	6.99	7.07
Apr	6.12	6.47	6.75	6.86	6.92
May	6.25	6.61	6.90	7.03	7.11
Jun	6.51	6.88	7.17	7.29	7.35
Jul	6.81	7.05	7.20	7.28	7.34
Aug	6.67	6.91	6.98	7.07	7.14
Sep	6.46	6.63	6.78	6.87	6.93
Oct	6.50	6.91	7.02	7.09	7.15
Nov	6.67	7.01	7.28	7.43	7.53
Dec	6.96	7.32	7.55	7.69	7.79

[a] Values are presented to two significant digits for comparison purposes, although the accuracy of the model output and analysis results do not include this level of precision.
[b] Values presented do not include the contribution of wind driven waves.

Table 7-10. High Frequency Monthly AEP Values Model Area 3 (relative to 1992)

Model Area 3	1-month (99.9994%)	2-month (99.75%)	3-month (98.17%)	4-month (95.17%)	6-month (86.47%)
Jan	7.09[a]	7.41	7.62	7.78	7.90
Feb	6.85	7.15	7.36	7.54	7.66
Mar	6.53	6.77	7.01	7.13	7.21
Apr	6.28	6.64	6.90	7.01	7.07
May	6.71	7.08	7.18	7.22	7.24
Jun	6.66	7.04	7.34	7.45	7.52
Jul	6.91	7.16	7.37	7.46	7.52
Aug	6.81	7.05	7.14	7.23	7.30
Sep	6.59	6.77	6.91	7.00	7.06
Oct	6.66	7.07	7.18	7.25	7.31
Nov	6.87	7.21	7.45	7.58	7.68
Dec	7.09	7.46	7.72	7.86	7.96

[a] Values are presented to two significant digits for comparison purposes, although the accuracy of the model output and analysis results do not include this level of precision.[b] Values presented do not include the contribution of wind driven waves.

Table 7-11. High Frequency Monthly AEP Values Model Area 4 (relative to 1992)

Model Area 4	1-month (99.9994%)	2-month (99.75%)	3-month (98.17%)	4-month (95.17%)	6-month (86.47%)
Jan	7.18[a]	7.50	7.72	7.89	8.01
Feb	6.87	7.12	7.43	7.62	7.75
Mar	6.62	6.87	7.11	7.22	7.30
Apr	6.41	6.75	7.00	7.11	7.17
May	6.80	7.17	7.27	7.31	7.34
Jun	6.79	7.14	7.44	7.56	7.63
Jul	7.03	7.27	7.47	7.57	7.62
Aug	6.88	7.11	7.23	7.33	7.40
Sep	6.69	6.87	7.01	7.10	7.16
Oct	6.76	7.18	7.29	7.36	7.41
Nov	6.97	7.31	7.55	7.69	7.78
Dec	7.25	7.58	7.81	7.94	8.04

[a] Values are presented to two significant digits for comparison purposes, although the accuracy of the model output and analysis results do not include this level of precision.
[b] Values presented do not include the contribution of wind driven waves.

7.2.4   Coupled Wind-driven Waves

To complement the hourly water level hydrographs matching the event strength criteria, the corresponding spectral significant wave height output was extracted from the modeled hindcast. The wave data was filtered to select only those waves traveling toward the shoreline. Waves that travel parallel to shoreline or away from the shoreline do not represent a wave hazard for the corresponding MA. For each storm event presented in Appendix B, there is an hourly time series of modeled water levels and wave heights for the duration of the 72-hour storm. For the synthetic events (1% AEP) created for the CSDs, the wave heights for the two 2% AEP (50-year) events were compared, and the timeseries of larger wave heights was selected to pair with the 1% AEP synthetic events. The wave data used without any modifications.

7.3   Database Compilation

The coastal inputs to G2CRM require an excel file with full timeseries of hourly water levels and wave heights for each hydrograph with an associated storm name; a storm input file that identified the relative probability of each storm name and the season in which it could occur; and a storm season input file that defines a number for each season.

7.3.1   Water Level and Wave Height Hydrographs

To compile the full CSD for each MA required assembling the full suite of water level and wave data for each storm event identified in Table 7-2 and Table 7-3. For example, the CSD for MA1 (CSD1) includes the water levels and wave heights for the storms identified offshore of MA1, as well as the water levels and wave heights that occurred offshore of MA1 at the time of the storms identified for MA2, MA3, and MA4, resulting in a total of 180 storm events within CSD1. Similarly, the CSD for MA2 (CSD2) includes the water levels and wave heights for the storms identified offshore of MA2, as well as the water levels and wave heights that occurred offshore of MA2 at the time of the storms identified for MA1, MA3, and MA4, resulting in total of 180 storm events within CSD2.

7.3.2   Relative Probabilities

The water level selection approach provides 99 unique 63.2% AEP (1-year) storm events within G2CRM, each with varying water levels and wave heights representing conditions that have occurred concurrently across the shoreline. Similarly, there are 42 50% AEP (2-year) storm events, eighteen 20% AEP (5-year) storm events, and so on. Rather than using the recurrence intervals within the G2CRM storm input file, G2CRM requires the relative probabilities. This requires dividing the recurrence intervals by the total number of storms for each recurrence interval and multiplying this number by the total number of storms in the catalog.

7.3.3   Storm Seasons

G2CRM requires the definition of seasons so that storms are pulled from the CSDs during the time period of the year when they are most likely to occur. Fourteen seasons were defined to support the G2CRM simulation of San Francisco Bay dynamics. Table 7-12 presents the seasons. Each month is defined as a season, and only high frequency hydrographs that occurred historically during that month can be selected. The highest frequency event is monthly, therefore the average number of storms that can be pulled each month across multiple iterations was to set to one to represent observed conditions.

The low frequency events generally occurred between October and March, most often occurring in December and January. However, G2CRM does not allow a storm season to span the end of the calendar year (that is, the storm season cannot be defined to start on 10/1 and end on 3/31). Therefore, the storm season was split into two seasons, with one occurring from 10/1 to 12/31, and one occurring from 1/1 to 3/31. The most frequent low-frequency event is yearly; therefore, on average one storm should occur. Since each season is 3 months long, the number of storms that could occur each season was set equal to 0.5. However, when completing G2CRM simulations and extracting the stage verses frequency curve from the model output, an insufficient number of storms was being pulled to match the input stage verses frequency curve. When the average number of storms per season was increased to 0.52, the input stage verses frequency curves were a better match for the output stage verses frequency curves.

The maximum number of storms per season was set equal to 2. However, the G2CRM simulations were less sensitive to this input parameter compared to the average number of storms per season.

Table 7-12. G2CRM Storm Seasons

Season	Start Day	End Day	Average Storms in Season	Maximum Storms in Season
1	1/1	1/31	1	2
2	2/1	2/28	1	2
3	3/1	3/31	1	2
4	4/1	4/30	1	2
5	5/1	5/31	1	2
6	6/1	6/30	1	2
7	7/1	7/31	1	2
8	8/1	8/31	1	2
9	9/1	9/30	1	2
10	10/1	10/31	1	2
11	11/1	11/20	1	2
12	12/1	12/31	1	2
13	10/1	12/31	0.52	2
14	1/1	3/31	0.52	2

7.4   G2CRM Input Files

Additional documents provided along with this report include the supporting data files for the inputs to G2CRM, and the direct input files to G2CRM, relative to both 1992 and 2000 water levels. CSD and G2CRM input files were developed for the low-frequency extreme water levels, as well as the combination of high-frequency and low-frequency water levels (high tide and extreme water levels).

Each suite of G2CRM input files includes:

- Four Excel files with the water levels and wave heights associated with the hydrographs; 1 Excel file per MA. The Excel files are set up for conversion to .h5 G2CRM input files
- Four .h5 files for direct input to G2CRM
- One .h5 metadate file
- One Excel file defining the full catalog of storms for input to G2CRM
- One Excel file defining the storm seasons for input to G2CRM

An excel file defining the OPC Likely and Plausible, High Impact (1:200) sea level rise curves is also provided for use with the storm inputs relative to 2000.

7.5   G2CRM Output

A G2CRM simulation generally includes running multiple iterations over the project's planning horizon, such as present day to 2140. Each iteration includes a different suite of extreme water levels and high tide water levels pulled from the CSDs using a Monte Carlo approach, based on the storms' relative probabilities and the seasons in which they occur. A series of simulations were completed to verify that the suite of water levels associated with

the storms selected within G2CRM across 100 model iterations produce a water level verses return frequency curve that matches the G2CRM inputs (that is, the model is performing as expected with respect to the suite of storms selected across multiple iterations), and that the total water levels (water levels + wave heights + sea level rise) are reflective of the expected behavior.

7.5.1 Water Level verses Return Frequencies

The water levels versus return frequencies using the G2CRM output were evaluated using two approaches: the summation method and extreme value analysis. The summation method includes summing the peak water levels selected for each return frequency, divided by the total number events selected for each return frequency, to estimate the average peak water level for each return frequency. Figure 7-10 presents this comparison using 100 G2CRM iterations with extreme storms water levels; and Figure 7-11 presents this comparison using 100 G2CRM iterations with high tide and extreme water levels. In both cases, the input curves compare well with both the summation method and the extreme value analysis. This comparison provides confidence that the CSDs are adequately representing San Francisco Bay water levels.
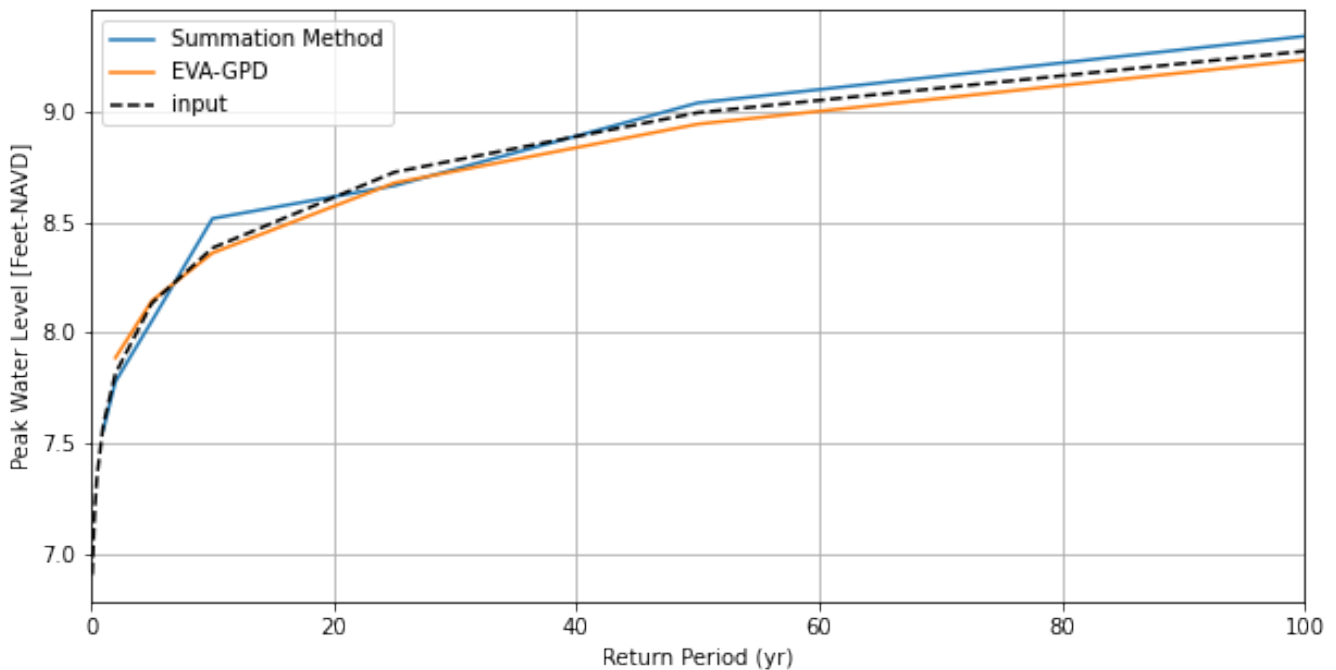
Figure 7-10 Peak Water Level Verses Return Period for Extreme Water Levels (relative to 1992)

Based on 100 G2CRM iterations using the CSDs with extreme storms only (that is, the 1-year to 100-year return periods). Peak water levels do not include the contribution from wind-driven waves.
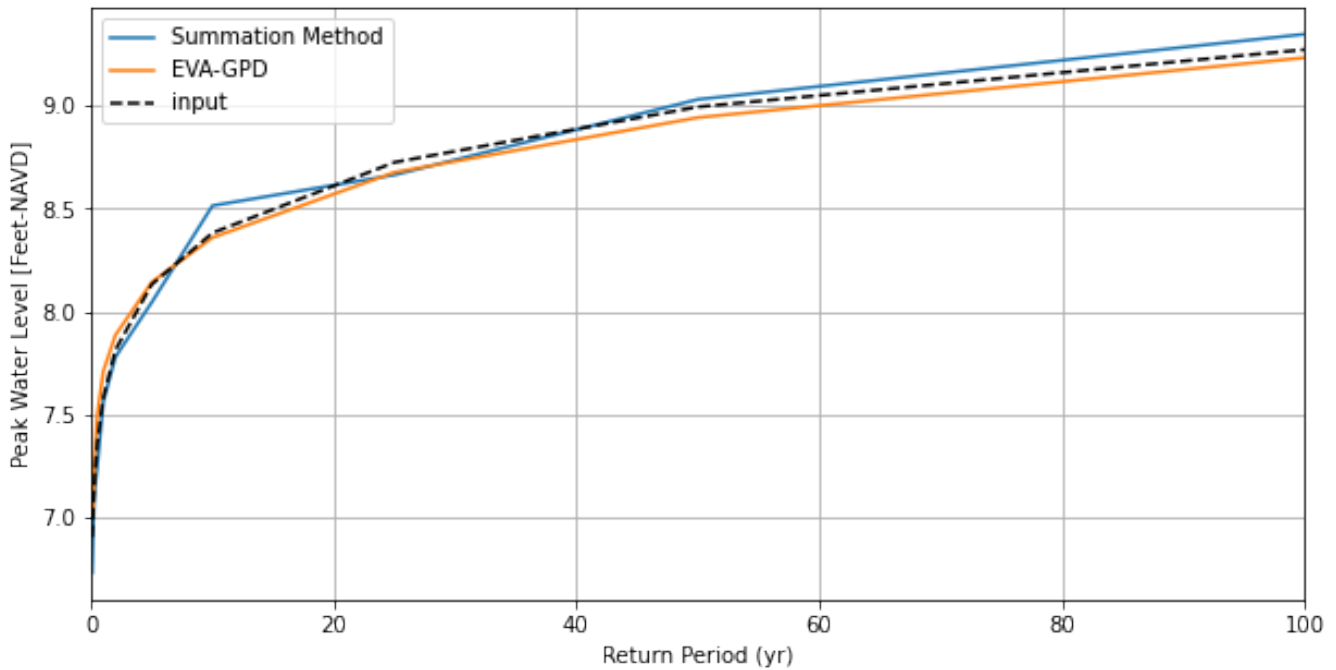
Figure 7-11 Peak Water Level Verses Return Period for High Tide and Extreme Water Levels (relative to 1992)

Based on 100 G2CRM iterations using the CSDs with extreme storms only (that is, the 1-year to 100-year return periods). Peak water levels do not include the contribution from wind-driven waves.

7.5.2 Total Water Levels Verses Threshold Elevations

Figure 7-12 presents the extreme water levels selected for one iteration (high tide water levels were not included), broken down into the extreme water level, wave height, sea level rise, and the total water level which is the sum of the three components. All water level elevations are baselined to 1992 and using the USACE high sea level rise projection. For a shoreline elevation of 10 feet NAVD88, the suite of storms selected in this iteration would result in shoreline overtopping around 2037. After about 2055, all storms selected would overtop the shoreline. However, another iteration with a different suite of storms could result in earlier or later overtopping depending on the suite of storms selected and the timing of when they occur.

Figure 7-13 presents one iteration with both high tide and extreme water levels. For a shoreline elevation of 10 feet NAVD88, the shoreline is first overtopped by an extreme water level around 2038. The shoreline is overtopped by all extreme and high tide water levels by about 2076, meaning the shoreline would be overtopped on at least a monthly basis (the highest frequency event included in the CSDs). It should be noted that some total (high tide) water levels may exceed total (extreme) water levels based on the associated paired wave heights. In general, the wave heights paired with the water level hydrographs are less than one foot in height; however, the San Francisco shoreline is sensitive to small differences in water level, sea level rise, and wave heights.

The comparisons shown in Figure 7-12 and Figure 7-13 provide confidence that G2CRM is representing the correct behavior within the simulations, increasing the total water levels over time, resulting in increased overtopping along the low-lying topographic thresholds along the San Francisco shoreline.
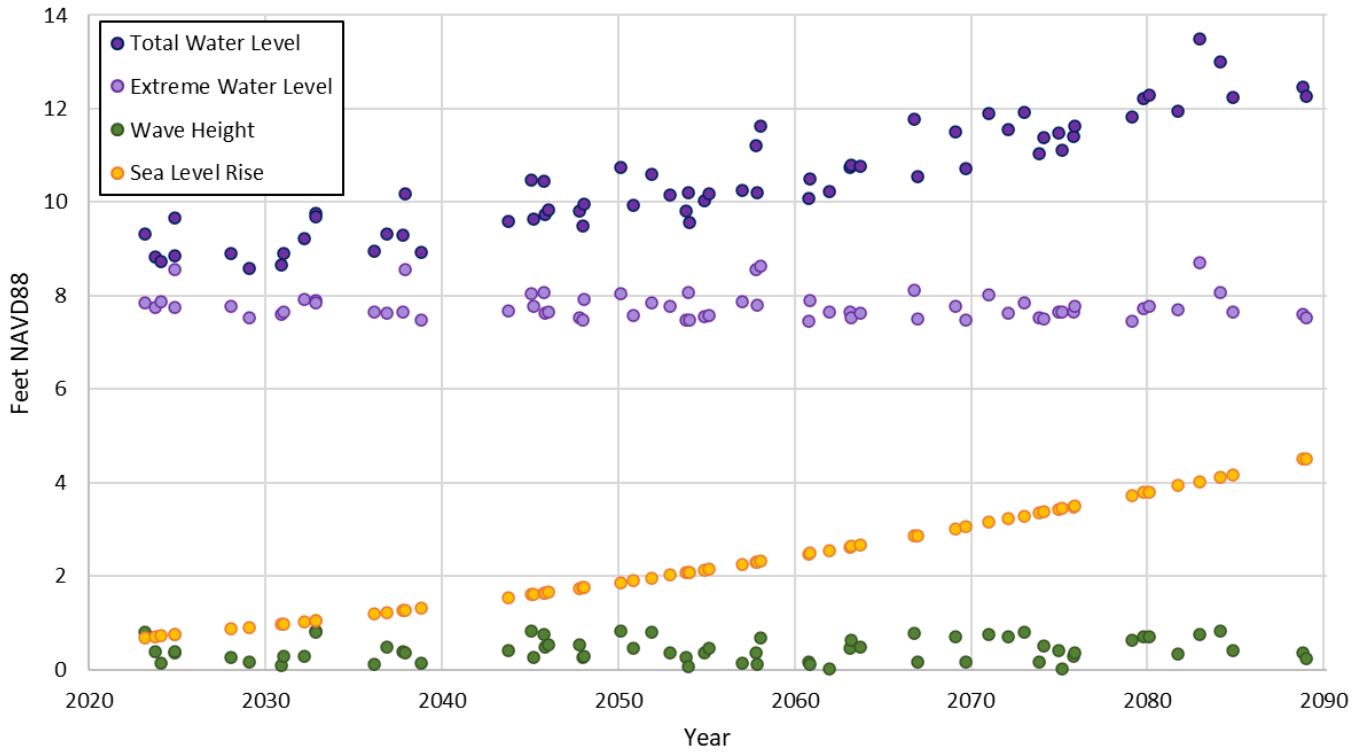
Figure 7-12 G2CRM Extreme Water Levels Selected for Model Area 1

USACE High Sea Level Rise (relative to 1992)
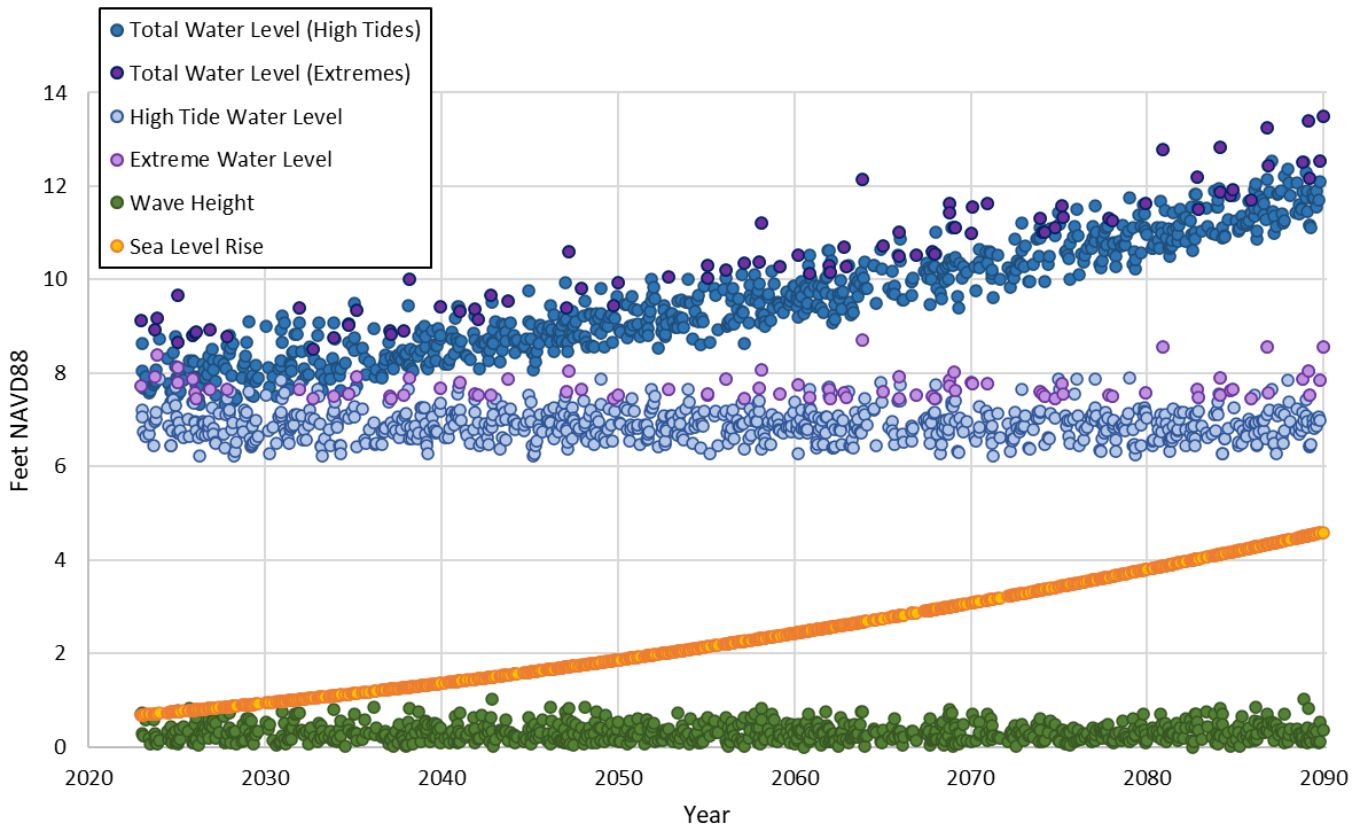
Figure 7-13 G2CRM Extreme and High Tide Water Levels Selected for Model Area 1

USACE High Sea Level Rise (relative to 1992)

THIS PAGE IS INTENTIONALLY BLANK

8   References

Anderson, T. R., C. H. Fletcher, M. M. Barbee, B. M. Romine, S. Lemmo, and J. M. S. Delevaux. 2018. Modeling multiple sea level rise stresses reveals up to twice the land at risk compared to strictly passive flooding methods. Scientific Reports 8:14484. DOI:10.1038/s41598-018-32658-x

Barnard, P. L., A. D. Short, M. D. Harley, K. D. Splinter, S. Vitousek, I. L. Turner, J. Allan, M. Banno, K. R. Bryan, A. Doria, J. E. Hansen, S. Kato, Y. Kuriyama, E. Randall-Goodwin, P. Ruggiero, I. J. Walker, and D. K. Heathfield. 2015. Coastal vulnerability across the Pacific dominated by El Niño/Southern Oscillation. Nature Geoscience 8:801–807

Bommier, E. 2014. Peaks-over-threshold Modeling of Environmental Data. Project Report. Department of Mathematics, Uppsala University, Uppsala University

Booth, J. F., E. Dunn-Sigouin, and S. Pfahl. 2017. The Relationship Between Extratropical Cyclone Steering and Blocking Along the North American East Coast. Geophysical Research Letters 44:11,976-11,984. DOI:10.1002/2017GL075941 Date Accessed: September 4, 2022

Cai, W., S. Borlace, M. Lengaigne, P. van Rensch, M. Collins, G. Vecchi, A. Timmermann, A. Santoso, M. J. Mcphaden, L. Wu, M. H. England, G. Wang, E. Guilyardi, and F. F. Jin. 2014a. Increasing frequency of extreme El Niño events due to greenhouse warming. Nat Clim Change 4:111–116. DOI:10.1038/nclimate2100 Date Accessed: September 4, 2022

Cai, W., S. Borlace, M. Lengaigne, P. Van Rensch, M. Collins, G. Vecchi, A. Timmermann, A. Santoso, M. J. Mcphaden, L. Wu, M. H. England, G. Wang, E. Guilyardi, and F. F. Jin. 2014b. Increasing frequency of extreme El Niño events due to greenhouse warming. Nature Climate Change 4:111–116. DOI:10.1038/nclimate2100

Cai, W., G. Wang, A. Santoso, M. J. Mcphaden, L. Wu, F. F. Jin, A. Timmermann, M. Collins, G. Vecchi, M. Lengaigne, M. H. England, D. Dommenget, K. Takahashi, and E. Guilyardi. 2015. Increased frequency of extreme La Niña events under greenhouse warming. Nat Clim Change 5:132–137. DOI:10.1038/nclimate2492 Date Accessed: September 4, 2022

Catto, J. L. 2016, June 1. Extratropical cyclone classification and its use in climate studies. Blackwell Publishing Ltd. DOI:10.1002/2016RG000519

Cayan, D. R., P. D. Bromirski, K. Hayhoe, M. Tyree, M. D. Dettinger, and R. E. Flick. 2007. Climate change projections of sea level extremes along the California coast. Climatic Change 87:57–73. DOI:10.1007/s10584-007-9376-7

CCSF. 2020. Sea Level Rise Vulnerability and Consequence Assessment. City and County of San Francisco, San Francisco Planning and the Office of Resilience and Capital Planning, San Francisco, CA. https://sfplanning.org/sea-level-rise-action-plan

Chan, D., G. A. Vecchi, W. Yang, and P. Huybers. 2021. Improved simulation of 19th-and 20th-century North Atlantic hurricane frequency after correcting historical sea surface temperatures. Page Sci. Adv. http://advances.sciencemag.org/

Choi, Y., S. M. Yeon, H. Kim, and D. Lee. 2019. Extreme Value Analysis of Statistically Independent Stochastic Variables. Journal of Ocean Engineering and Technology 33:222–228. DOI:10.26748/ksoe.2018.093

City and County of San Francisco. 2020. Sea Level Rise Vulnerability and Consequences Assessment. San Francisco, CA

Climate Impacts Group. 2009. The Washington State Climate Change Impacts Assessment. June 2009

Colle, B. A., J. F. Booth, and E. K. M. Chang. 2015. EXTREME EVENTS (A SOBEL AND SJ CAMARGO, SECTION EDITORS) A Review of Historical and Future Changes of Extratropical Cyclones and Associated Impacts Along the US East Coast. Extreme Events. DOI:10.1007/s40641-015-0013-7

Collini, R., J. Carter, L. Auermuller, L. Engeman, K. Hintzen, J. Gambill, R. Johnson, I. Miller, C. Schafer, and H. Stiller. 2022. Application Guide for the 2022 Sea Level Rise Technical Report. https://aambpublicoceanservice.blob.core.windows.net/oceanserviceprod/hazards/sealevelrise/noaa-nos-techrpt02-global-regional-slr-scenarios-us-application-guide.pdf Date Accessed: September 10, 2022

Conner, K. L. C., D. R. Kerper, L. R. Winter, C. L. May, and K. Schaefer. 2011. Coastal Flood Hazards in San Francisco Bay-A Detailed Look at Variable Local Flood Responses. Solutions to Coastal Disasters 2011 - Proceedings of the 2011 Solutions to Coastal Disasters Conference:448–460. DOI:10.1061/41185(417)40 https://ascelibrary.org/doi/10.1061/41185%28417%2940 Date Accessed: September 4, 2022

Conomos, T. J. 1979. Properties and Circulation of San Francisco Bay Waters. Page San Francisco Bay: The Urbanized Estuary

CPC. 2020. Guidance for Incorporating Sea Level Rise Into Capital Planning, Assessing Vulnerability and Risk to Support Adaptation. City and County of San Francisco, Capital Planning Committee, adopted September 22,

2014, revised and adopted December 14, 2015, San Francisco, CA. https://onesanfrancisco.org/sea-level-rise-guidance/

Dacre, H. F. 2020. A review of extratropical cyclones: observations and conceptual models over the past 100 years. Weather 75:4–7. DOI:10.1002/wea.3653

Dacre, H. F., and J. G. Pinto. 2020, December 1. Serial clustering of extratropical cyclones: a review of where, when and why it occurs. Nature Research. DOI:10.1038/s41612-020-00152-9

Danard, M. B., S. K. Dube, G. Gönnert, A. Munroe, T. S. Murty, P. Chittibabu, A. D. Rao, and P. C. Sinha. 2004. Storm surges from extra-tropical cyclones. Natural Hazards 32. DOI:10.1023/B:NHAZ.0000031312.98231.81

DeFlorio, M. J., D. W. Pierce, D. R. Cayan, and A. J. Miller. 2013. Western U.S. extreme precipitation events and their relation to ENSO and PDO in CCSM4. Journal of Climate 26:4231–4243. DOI:10.1175/JCLI-D-12-00257.1

DHI. 2011. Regional Coastal Hazard Modeling Study for North and Central San Francisco Bay. Prepared for the Federal Emergency Management Agency Region IX in support of the San Francisco Bay Area Coastal Study

DHI. 2013. Regional Coastal Hazard Modeling Study for South San Francisco Bay. Prepared for the Federal Emergency Management Agency in support of the San Francisco Bay Area Coastal Study

Drobyshevski, Y., J. R. Whelan, H. Wadhwa, and V. Anokhin. 2014. Determination of design metocean conditions by response based analysis. Proceedings of the International Conference on Offshore Mechanics and Arctic Engineering - OMAE 1B. DOI:10.1115/OMAE2014-24657 Date Accessed: September 4, 2022

Fasullo, J. T., B. L. Otto-Bliesner, and S. Stevenson. 2018. ENSO's Changing Influence on Temperature, Precipitation, and Wildfire in a Warming Climate. Geophysical Research Letters 45:9216–9225. DOI:10.1029/2018GL079022

FEMA. 2005. Guidelines for Coastal Flood Hazard Analysis and Mapping for the Pacific Coast of the United States. Washington, DC, USA. https://www.fema.gov/guidelines-coastal-flood-hazard-analysis-and-mapping-pacific-coast-united-states

FEMA. 2008. Guidance of Coastal Flood Hazard Analyses and Mapping in Sheltered Waters Technical Memorandum. Prepared by the Federal Emergency Management Agency, Washington, DC, USA

FEMA. 2015. Mapping Repetitive Loss Areas. Federal Emergency Management Agency, Washington, DC, USA

FEMA. 2016. Guidance for Flood Risk Analysis and Mapping: Coastal Flood Frequency and Extreme Value Analysis. Federal Emergency Management Agency, Washington, DC, USA. www.fema.gov/guidelines-and-standards-flood-risk-analysis-and-

Ghanbari, M., M. Arabi, J. Obeysekera, and W. Sweet. 2019. A Coherent Statistical Model for Coastal Flood Frequency Analysis Under Nonstationary Sea Level Conditions. Earth's Future 7:162–177. DOI:10.1029/2018EF001089

Goddard, L., and A. Gershunov. 2020. Impact of El Niño on Weather and Climate Extremes. Geophysical Monograph Series 253:361–375. DOI:10.1002/9781119548164.CH16 https://onlinelibrary.wiley.com/doi/full/10.1002/9781119548164.ch16 Date Accessed: September 4, 2022

Goring, D. G., S. A. Stephens, R. G. Bell, and C. P. Pearson. 2011. Estimation of Extreme Sea Levels in a Tide-Dominated Environment Using Short Data Records. Journal of Waterway, Port, Coastal, and Ocean Engineering 137:150–159. DOI:10.1061/(asce)ww.1943-5460.0000071

Gratiot, N., E. J. Anthony, A. Gardel, C. Gaucherel, C. Proisy, and J. T. Wells. 2008. Significant contribution of the 18.6 year tidal cycle to regional coastal changes. Nature Geoscience 1:169–172. DOI:10.1038/ngeo127

Griggs, G., K. Patsch, and L. Savoy. 2005. Living with the Changing California Coast. University of California Press

Gubareva, T. S., and B. I. Gartsman. 2010. Estimating distribution parameters of extreme hydrometeorological characteristics by L-moments method. Water Resources 37:437–445. DOI:10.1134/S0097807810040020

Gumbel, E. J. 2004. Statistics of extremes:375. https://books.google.com/books/about/statistics_of_extremes.html?id=kxcg8b5xsuwc Date Accessed: September 4, 2022

Hamlington, B. D., T. Frederikse, P. R. Thompson, J. K. Willis, R. S. Nerem, and J. T. Fasullo. 2021. Past, Present, and Future Pacific Sea-Level Change. Earth's Future 9. DOI:10.1029/2020EF001839

Hayhoe, K., D. J. Wuebbles, D. R. Easterling, D. W. Fahey, S. Doherty, J. Kossin, W. Sweet, R. Vose, and M. Wehner. 2018. Our Changing Climate. Pages 72–144 in D. R. Reidmiller, C. W. Avery, D. R. Easterling, K. E. Kunkel, K. L. M. Lewis, T. K. Maycock, and B. C. Stewart, editors. Impacts, Risks, and Adaptation in the United States: Fourth National Climate Assessment, Volume II. U.S. Global Research Program, Washington D.C. DOI:10.7930/NCA4.2018.CH2

Hosking, J., and J. Wallis. 1997. Regional Frequency Analysis: An Approach Based on L-Moments. Cambridge: Cambridge University Press. DOI:10.1017/CBO9780511529443

Hosseini, S. R., M. Scaioni, and M. Marani. 2018. On the influence of global warming on Atlantic hurricane frequency. Pages 527–532 International Archives of the Photogrammetry, Remote Sensing and Spatial Information Sciences - ISPRS Archives. International Society for Photogrammetry and Remote Sensing. DOI:10.5194/isprs-archives-XLII-3-527-2018

IPCC. 2021. Summary for Policymakers. In: Climate Change 2021: The Physical Science Basis. Contribution of Working Group I to the Sixth Assessment Report of the Intergovernmental Panel on Climate Change [Masson-Delmotte, V., P. Zhai, A. Pirani, S. L. Connors, C. Péan. https://www.ipcc.ch/report/ar6/wg1/

James Barnts, Mary Beth Broeren, Lesley Ewing, Laurie Johnson, Ray Lenaburg, Robert Olson, Ricardo Pineta, Charles Real, Rune Storesund, Patti Sutch, Ken Topping, and Brian Tucker. 2014. California's Tsunami Risk: A Call for Action. A Report from the California Tsunami Policy Working Group

Kim, S. T., W. Cai, F. F. Jin, A. Santoso, L. Wu, E. Guilyardi, and S. il An. 2014. Response of El Niño sea surface temperature variability to greenhouse warming. Nat Clim Change 4:786–790. DOI:10.1038/nclimate2326 Date Accessed: September 4, 2022

Koohi Kheili, A. G., Y. Drobyshevski, M. Kimiaei, and M. Efthymiou. 2021. Iterative methodology for response based analysis of an FPSO mooring system. Marine Structures 78:102973. DOI:10.1016/J.MARSTRUC.2021.102973 Date Accessed: September 4, 2022

Marjani, S., O. Alizadeh-Choobari, and P. Irannejad. 2019. Frequency of extreme El Niño and La Niña events under global warming. Climate Dynamics 2019 53:9 53:5799–5813. DOI:10.1007/S00382-019-04902-1 https://link.springer.com/article/10.1007/s00382-019-04902-1 Date Accessed: September 4, 2022

May, C., M. Mak, E. Harris, M. Lightner, J. Guyenet, J. Vandever, S. Kassem, and L. Adleman. 2016a. Extreme Storms in San Francisco Bay – Past to Present. Federal Emergency Management Agency

May, C., M. Mak, E. Harris, M. Lightner, and J. Vandever. 2016b. San Francisco Bay Tidal Datums and Extreme Tides Study. Prepared by AECOM for the Federal Emergency Management Agency Region IX and the San Francisco Bay Conservation and Development Commission

May, C., M. Mak, O. Hoang, C. Patricola, and M. Wehner. 2019. San Francisco Bay Storm Events. Prepared by Silvestrum Climate Associates and Lawrence Berkeley National Laboratory for the San Francisco Public Utilities Commission, Port of San Francisco, San Francisco International Airport, and the Office of Resilience and Capital Planning, San Francisco, CA

McPhaden, M. J., A. Santoso, and W. Cai, editors. 2020. El Niño Southern Oscillation in a Changing Climate. DOI:10.1002/9781119548164 https://agupubs.onlinelibrary.wiley.com/doi/book/10.1002/9781119548164 Date Accessed: September 4, 2022

NASA. 2021. Rising Waters: How NASA is monitoring sea level rise. https://www.nasa.gov/specials/sea-level-rise-2020/

NCDC. 1998. The El Nino Winter of '97-98. Technicap Report 98-02. April 1998. National Climatic Data Center

NRC. 2012. Sea-Level Rise for the Coasts of California, Oregon, and Washington: Past, Present, and Future. National Academies Press

OPC, and CNRA. 2018. State of California Sea Level Rise Guidance. Prepared by the California Ocean Protection Council and the California National Resources Agency. http://www.opc.ca.gov/webmaster/ftp/pdf/agenda_items/20180314/item3_exhibit-a_opc_slr_guidance-rd3.pdf

Park, T. W., Y. Deng, and M. Cai. 2012. Feedback attribution of the El Nio-Southern Oscillation-related atmospheric and surface temperature anomalies. Journal of Geophysical Research Atmospheres 117. DOI:10.1029/2012JD018468

Patricola, C. M., J. P. O'Brien, M. D. Risser, A. M. Rhoades, T. A. O'Brien, P. A. Ullrich, D. A. Stone, and W. D. Collins. 2019. Maximizing ENSO as a Source of Western US Hydroclimate Predictability. Climate Dynamics. DOI:10.1007/s00382-019-05004-8 https://doi.org/10.1007/s00382-019-05004-8

Patricola, C. M., and M. F. Wehner. 2018. Anthropogenic influences on major tropical cyclone events. Nature 563:339–346. DOI:10.1038/s41586-018-0673-2

Patricola, C. M., M. F. Wehner, E. Bercos-Hickey, F. V. Maciel, C. May, M. Mak, O. Yip, A. Roche, and S. Leal. 2022. Future Changes in Extreme Precipitation over the San Francisco Bay Area: Dependence on Atmospheric River and Extratropical Cyclone Events. Weather and Climate Extremes 36. DOI:10.1016/j.wace.2022.100440

Port of San Francisco. 2021a. Shoreline Elevation Explorer. Pathways Climate Institute, San Francisco, CA

Port of San Francisco. 2021b. Draft Coastal Storms Report. San Francisco, CA

Sanderson, D. R., M. B. Gravens, and R. L. Permenter. 2019. Methodology for Identifying a Subset of Representative Storm Surge Hydrographs from a Coastal Storm Modeling Database. Journal of Coastal Research 35:1095–1105. DOI:10.2112/JCOASTRES-D-18-00052.1

Serafin, K. A., P. Ruggiero, P. L. Barnard, and H. F. Stockdon. 2019. The influence of shelf bathymetry and beach topography on extreme total water levels: Linking large-scale changes of the wave climate to local coastal hazards. Coastal Engineering 150:1–17. DOI:10.1016/j.coastaleng.2019.03.012

SF Planning. 2019. Zoning Map, Zoning Districts. Page DataSF Open Data Portal, City and County of San Francisco Planning Department. https://data.sfgov.org/geographic-locations-and-boundaries/zoning-map-zoning-districts/3i4a-hu95

SFEI. 1998. Historical and Modern Baylands (EcoAtlas Version 1.50b4). Page San Francisco Estuary Istitute & the Aquatic Science Center

Sidder, A. 2019. As Sea Levels Rise, Expect More Floods. Eos 100:8–11. DOI:10.1029/2019eo122097

Sievanen, L., J. Phillips, C. Colgan, G. Griggs, J. F. Hart, E. Hartge, T. Hill, R. Kudela, N. Mantua, and L. W. Karina Nielsen. 2018. California's Coast and Ocean Summary Report, In: California's Fourth Climate Change Assessment. Publication number: SUM-CCCA4-2018-011

Stanley, S. 2016. In the Eastern Pacific Ocean, the "Blob" Overshadows El Niño. Eos, Geophysical Research Letters 97. DOI:10.1029/2016EO056237

Sweet, W., G. Dusek, J. Obeysekera, and J. Marra. 2018. Patterns and Projections of High Tide Flooding Along the U.S. Coastline Using a Common Impact Threshold. National Oceanic and Atmospheric Administration, U.S. Department of Commerce, National Ocean Service, and the Center for Operational Oceanographic Products and Services., Silver Spring, Maryland

Sweet, W. V., R. Horton, R. E. Kopp, A. N. LeGrande, and A. Romanou. 2017a. Ch. 12: Sea Level Rise. Climate Science Special Report: Fourth National Climate Assessment, Volume I. Page (D. J. Wuebbles, D. W. Fahey, K. A. Hibbard, D. J. Dokken, B. C. Stewart, and T. K. Maycock, Eds.). U.S. Global Change Research Program, Washington, DC. DOI:10.7930/J0VM49F2 https://science2017.globalchange.gov/chapter/12/

Sweet, W. V., B. D. Hamlington, R. E. Kopp, C. P. Weaver, P. L. Barnard, D. Bekaert, W. Brooks, M. Craghan, G. Dusek, T. Frederikse, G. Garner, A. S. Genz, J. P. Krasting, E. Larour, D. Marcy, J. J. Marra, J. Obeysekera, M. Osler, M. Pendleton, D. Roman, L. Schmied, W. Veatch, K. D. White, and C. Zuzak. 2022b. Global and Regional Sea Level Rise Scenarios for the United States: Updated Mean Projections and Extreme Water Level Probabilities Along U.S. Coastlines. NOAA Technical Report NOS 01. National Oceanic and Atmospheric Administration, National Ocean Service., Silver Spring, Maryland. https://oceanservice.noaa.gov/hazards/sealevelrise/noaa-nos-techrpt01-global-regional-slr-scenarios-us.pdf

Sweet, W. V., M. Menendez, A. Genz, J. Obeysekera, J. Park, and J. J. Marra. 2016. In tide's way: Southeast Florida's September 2015 sunny-day flood. Bulletin of the American Meteorological Society 97:S25–S30. DOI:10.1175/BAMS-D-16-0117.1

Taherkhani, M., S. Vitousek, P. L. Barnard, N. Frazer, T. R. Anderson, and C. H. Fletcher. 2020. Sea-level rise exponentially increases coastal flood frequency. Scientific Reports 10:1–17. DOI:10.1038/s41598-020-62188-4

Teegavarapu, R. S. V., and A. R. Schmidt. 2019. Variations and Trends in Global and Regional Sea Levels. Pages 361–401 in R. Teegavarapu, editor. Trends and Changes in Hydrodynamic Variables: Links to Climate Variability and Change. Elsevier. DOI:10.1016/B978-0-12-810985-4.00007-4

University of Hawaii. 2021. Flooding Days Projection Tool. Page NASA Sea Level Change, University of Hawaii Sea Level Center. https://sealevel.nasa.gov/flooding-days-projection

USACE. 1984. San Francisco Bay Tidal Stage vs. Frequency Study. United States Army Corps of Engineers, Washington, DC, USA

USACE. 2019a. ER 1100-2-8162, Incorporating Sea Level Change in Civil Works Programs. United States Army Corps of Engineers, Washington, DC, USA

USACE. 2019b. EP 1100-2-1, Procedures to Evaluate Sea Level Change: Impacts, Responses, and Adaptation. United States Army Corps of Engineers, Washington, DC, USA

USACE. 2020. USACE Sea-Level Change Curve Calculator (Version 2019.21). Page United States Army Corps of Engineers. http//corpsmapu.usace.army.mil/rccinfo/slc/slcc_calc.html Date Accessed: August 22, 2020

USGS. 1999. El Nino sea-level rise wreaks havoc on California's San Francisco Bay region. Spring:175–99

Vandever, J., M. Lightner, S. Kassem, J. Guyenet, M. Mak, and C. Bonham-Carter. 2017. Adapting to Rising Tides Bay Area Sea Level Rise Analysis and Mapping Project. Prepared by AECOM for the San Francisco Bay Conservation and Development Commission, the Metropolitan Transportation Commission, and the Bay Area Toll Authority, San Francisco, CA

Vecchi, G. A., C. Landsea, W. Zhang, G. Villarini, and T. Knutson. 2021. Changes in Atlantic major hurricane frequency since the late-19th century. Nature Communications 12. DOI:10.1038/s41467-021-24268-5

Zervas, C. 2009. Sea Level Variations of the United States 1854-2006. Technical Report NOS CO-OPS 053 53

Zervas, C. 2013. Extreme Water Levels of the United States 1893–2010:200

Zhang, Z., F. M. Ralph, and M. Zheng. 2019. The Relationship Between Extratropical Cyclone Strength and Atmospheric River Intensity and Position. Geophysical Research Letters:10. DOI:10.1029/2018GL079071

Appendix A
Threshold Selection Plots

USACE, 1992 Baseline
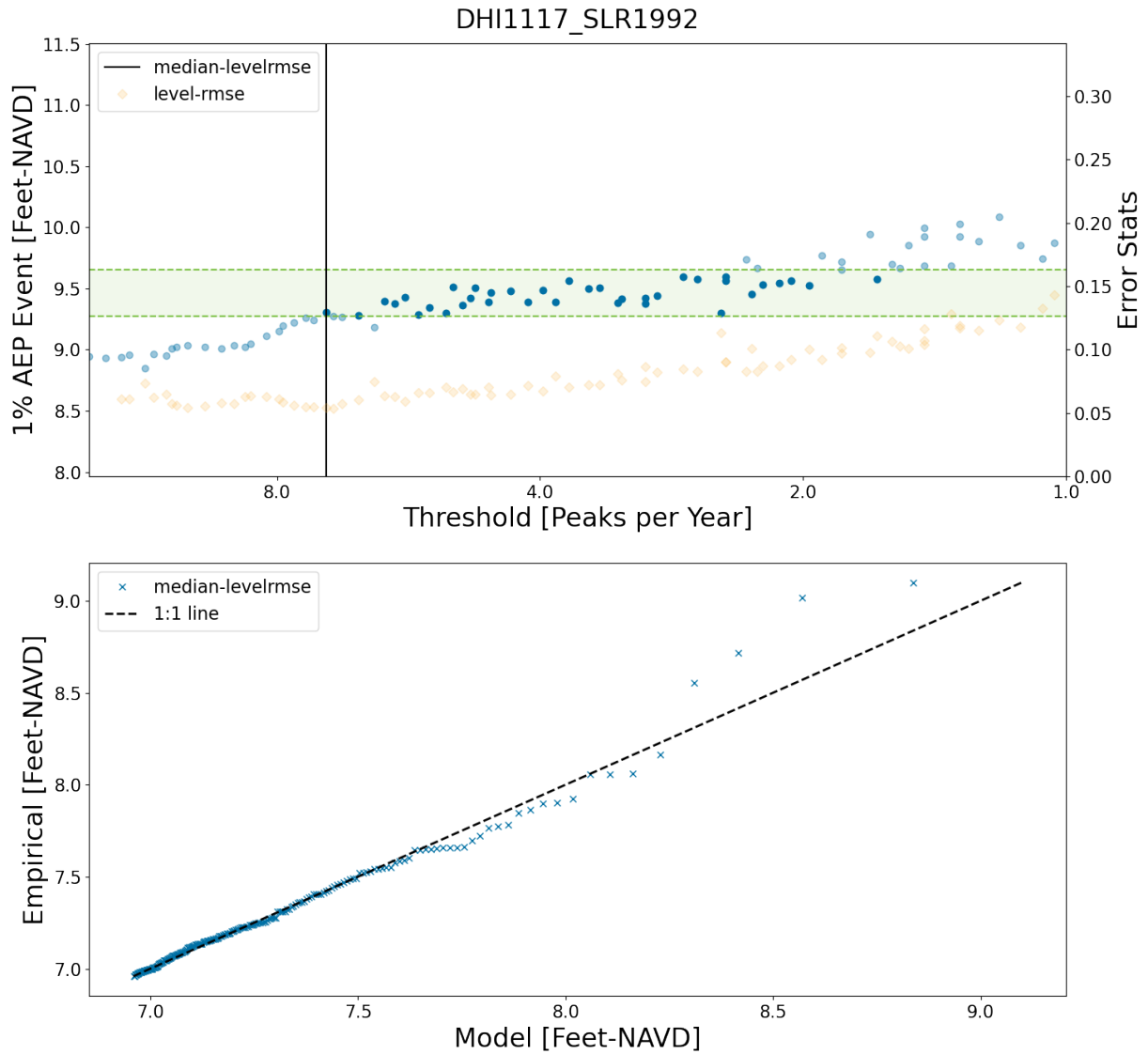
Figure A-1 Quantile Threshold Selection (top) and Q-Q Plot (bottom) – 1992 Baseline (MA1; DHI ID 1117)
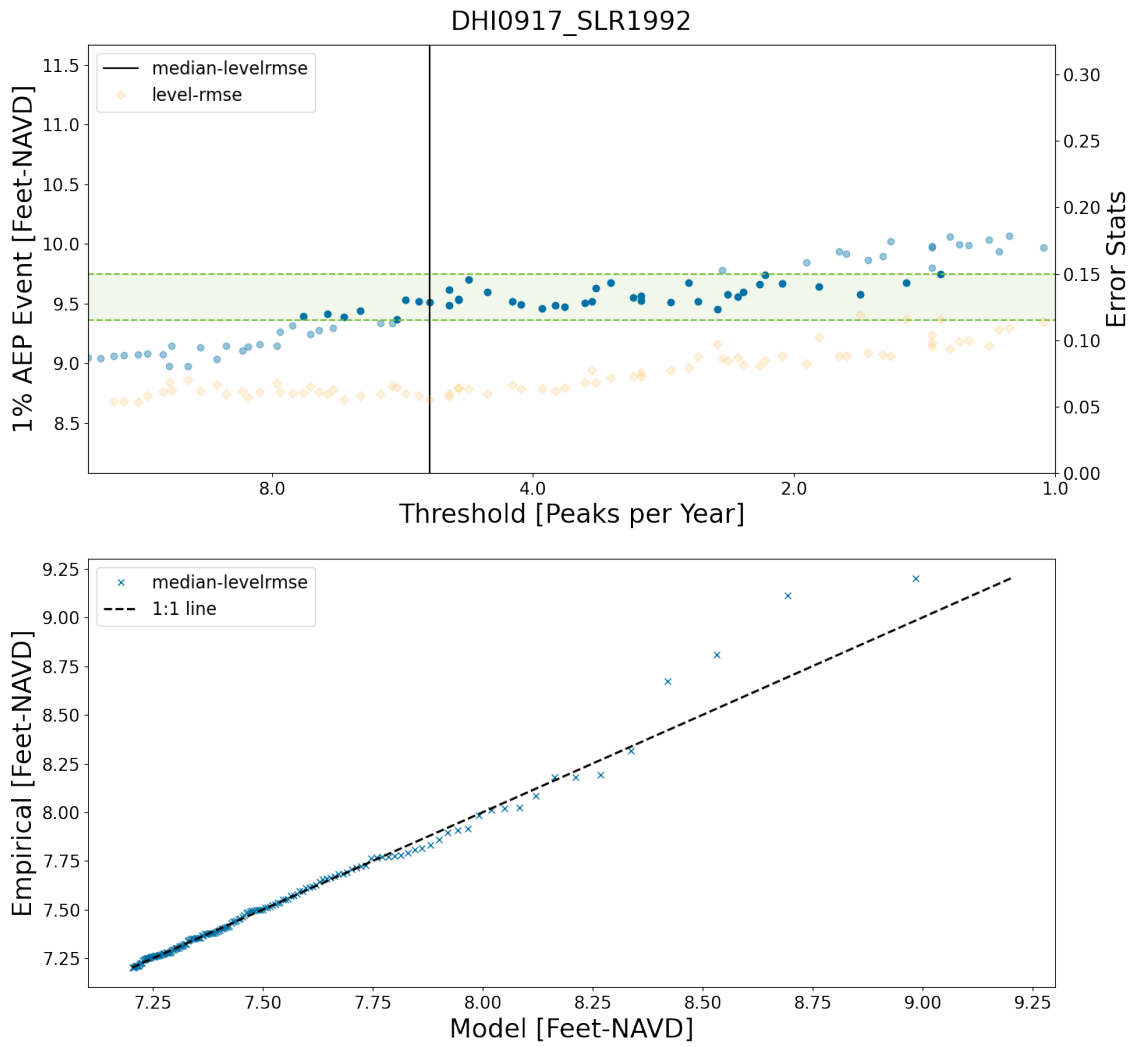
Figure A-2 Quantile Threshold Selection (top) and Q-Q Plot (bottom) – 1992 Baseline (MA2; DHI ID 917)
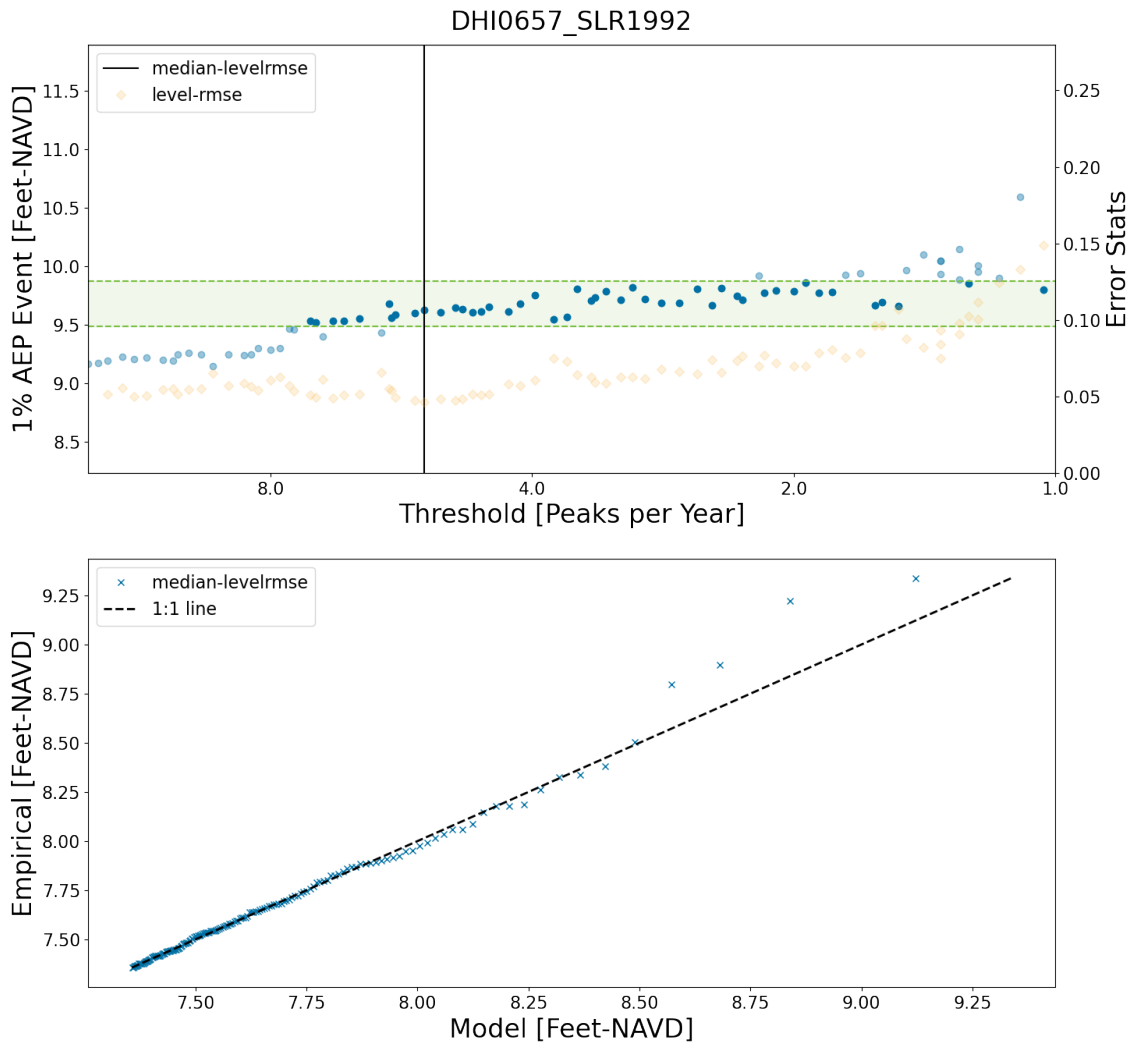
Figure A-3 Quantile Threshold Selection (top) and Q-Q Plot (bottom) – 1992 Baseline (MA3; DHI ID 657)
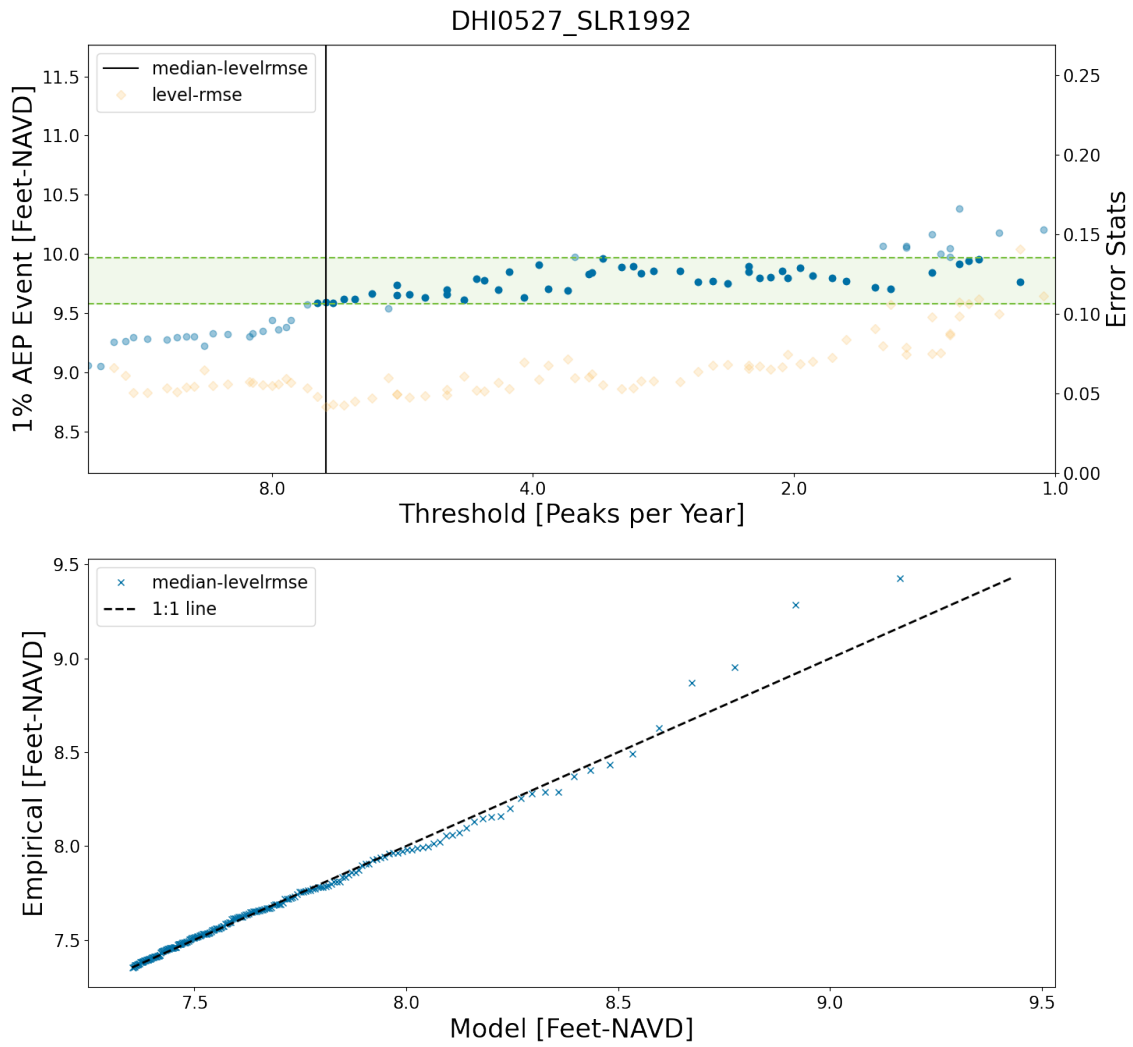
Figure A-4 Quantile Threshold Selection (top) and Q-Q Plot (bottom) – 1992 Baseline (MA4; DHI ID 527)

California OPC, 2000 Baseline
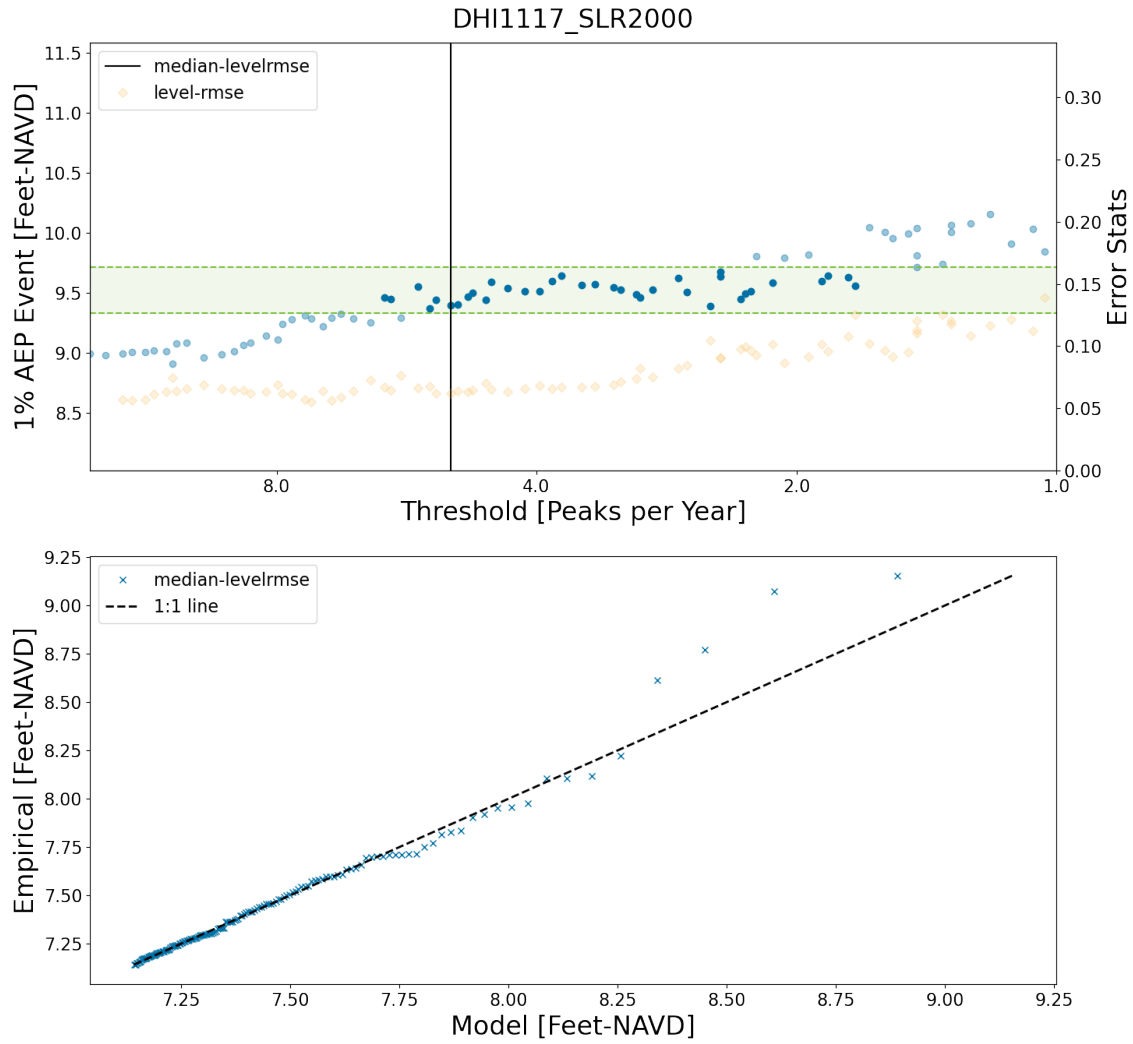
Figure A-5 Quantile Threshold Selection (top) and Q-Q Plot (bottom) – 2000 Baseline (MA1; DHI ID 1117)
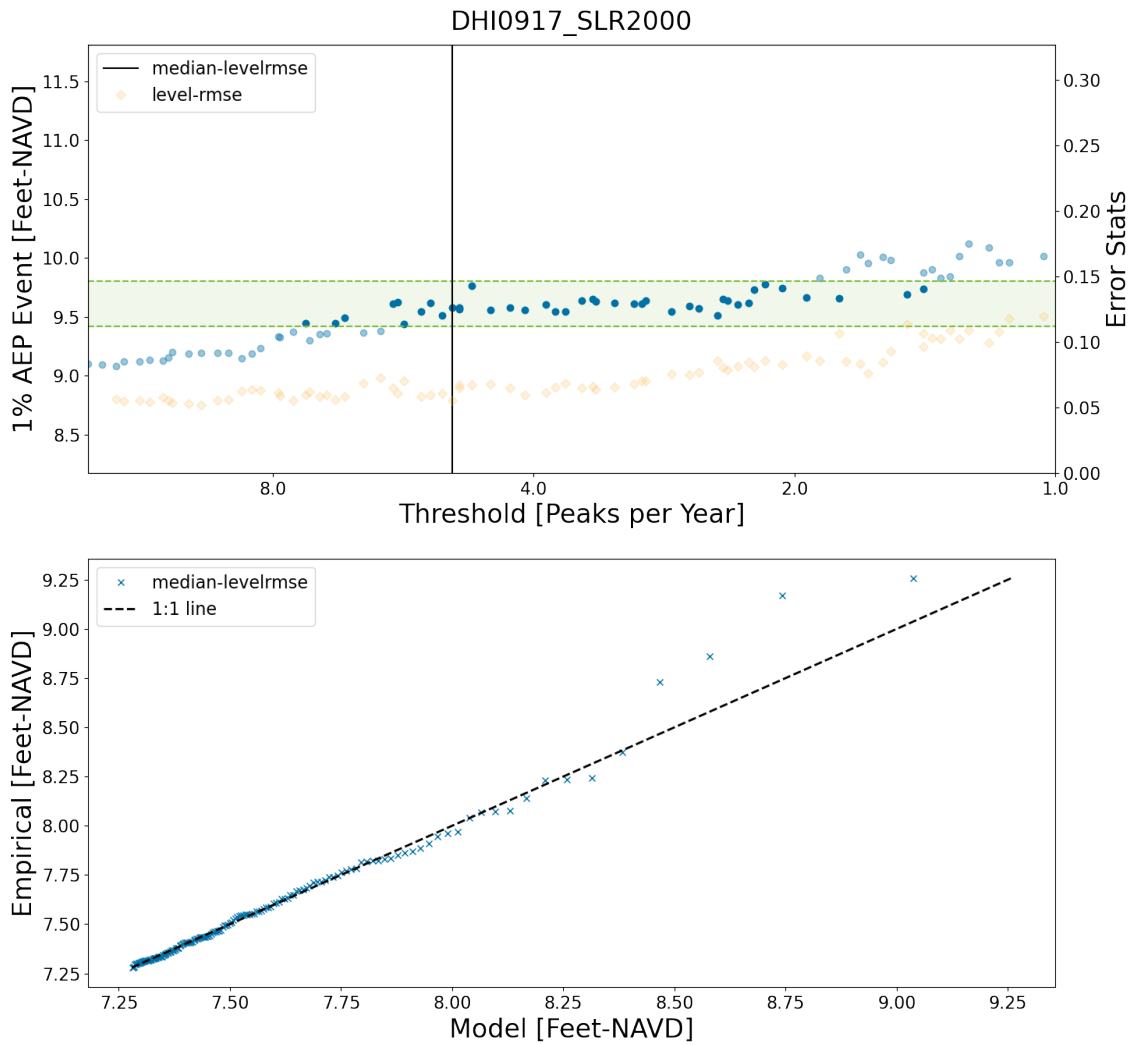
Figure A-6 Quantile Threshold Selection (top) and Q-Q Plot (bottom) – 2000 Baseline (MA2; DHI ID 917)
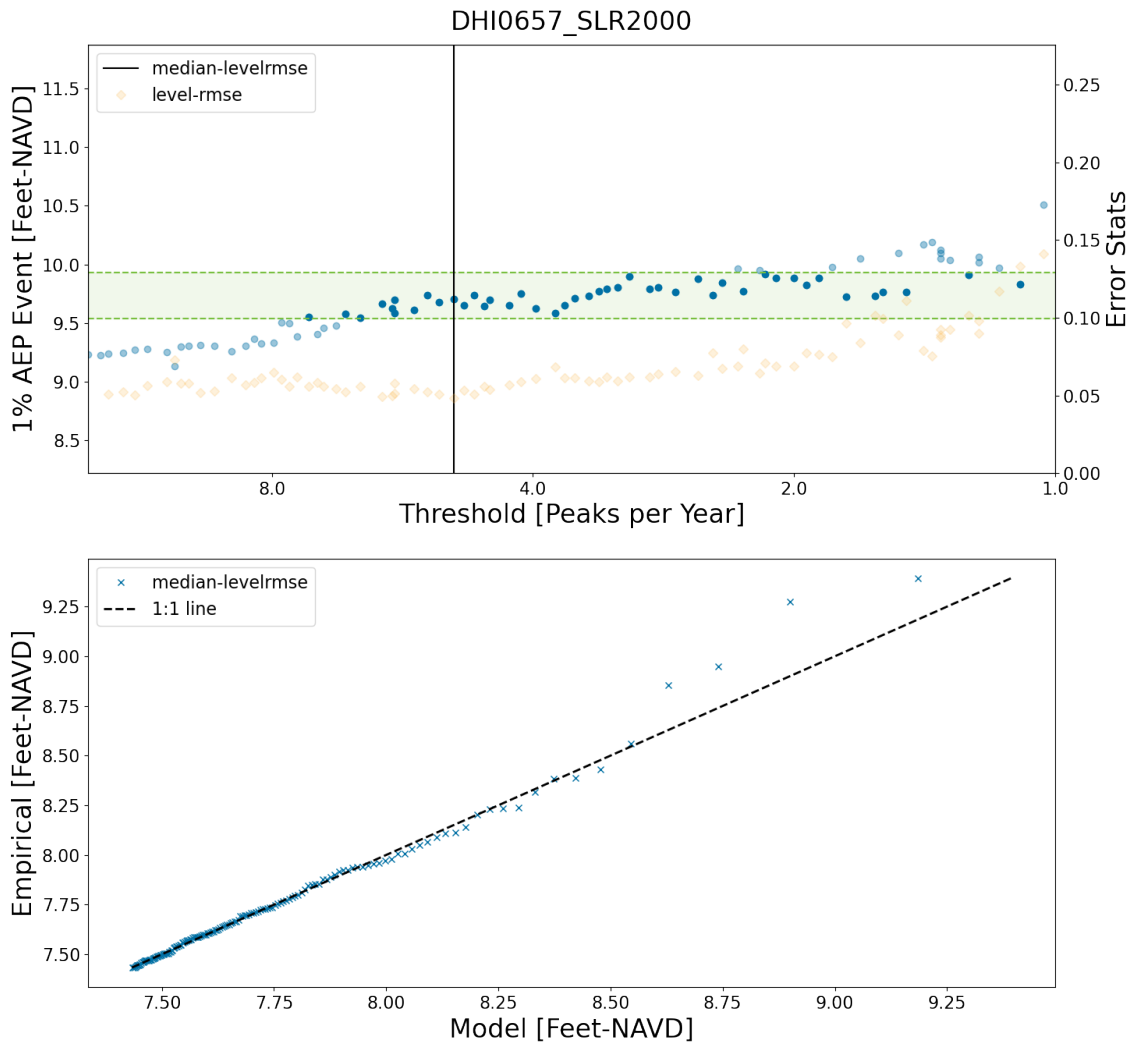
Figure A-7 Quantile Threshold Selection (top) and Q-Q Plot (bottom) – 2000 Baseline (MA3; DHI ID 657)
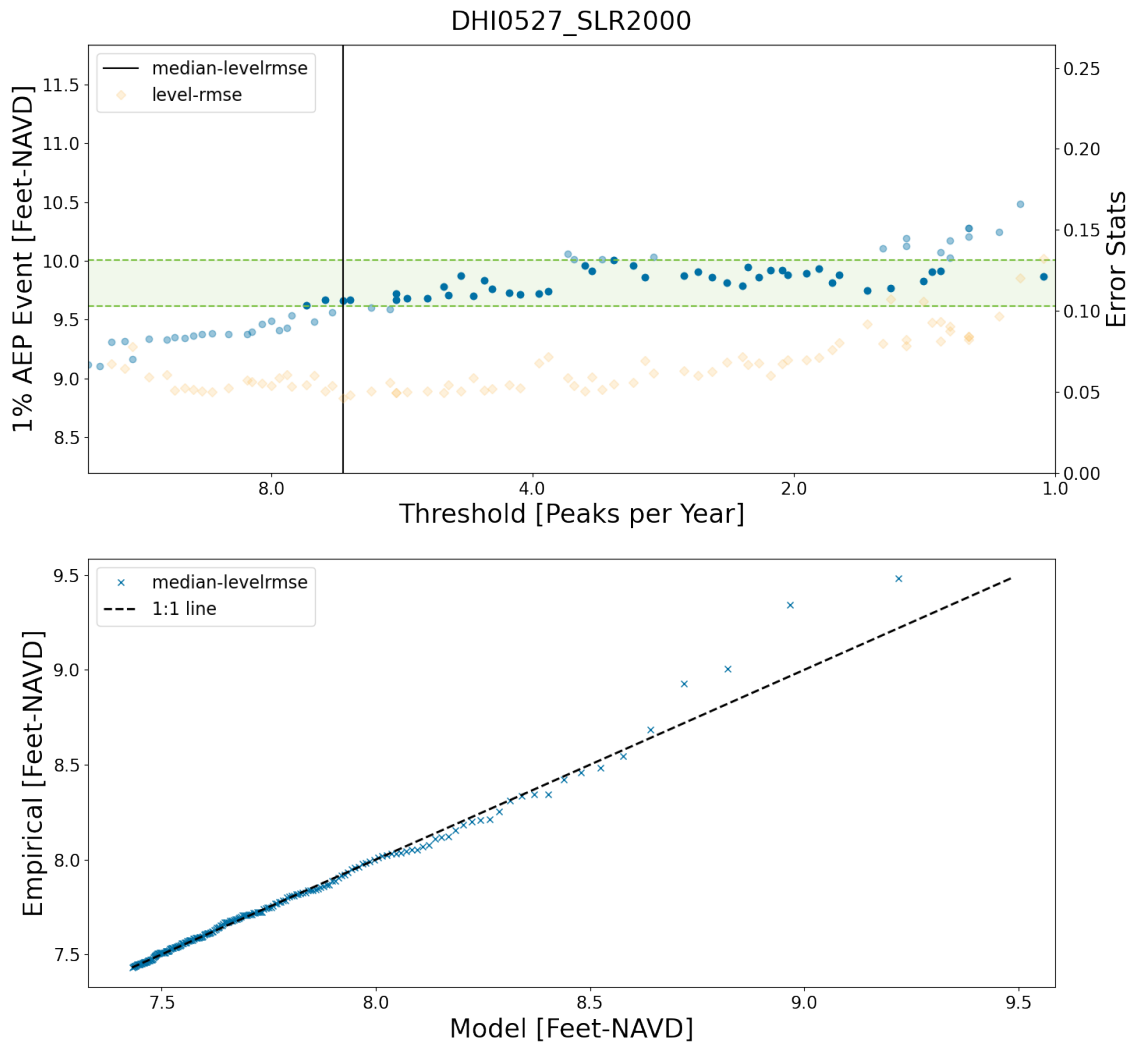
Figure A-8 Quantile Threshold Selection (top) and Q-Q Plot (bottom) – 2000 Baseline (MA4; DHI ID 527)

THIS PAGE IS INTENTIONALLY BLANK.

Appendix B
Storm Event Hydrographs

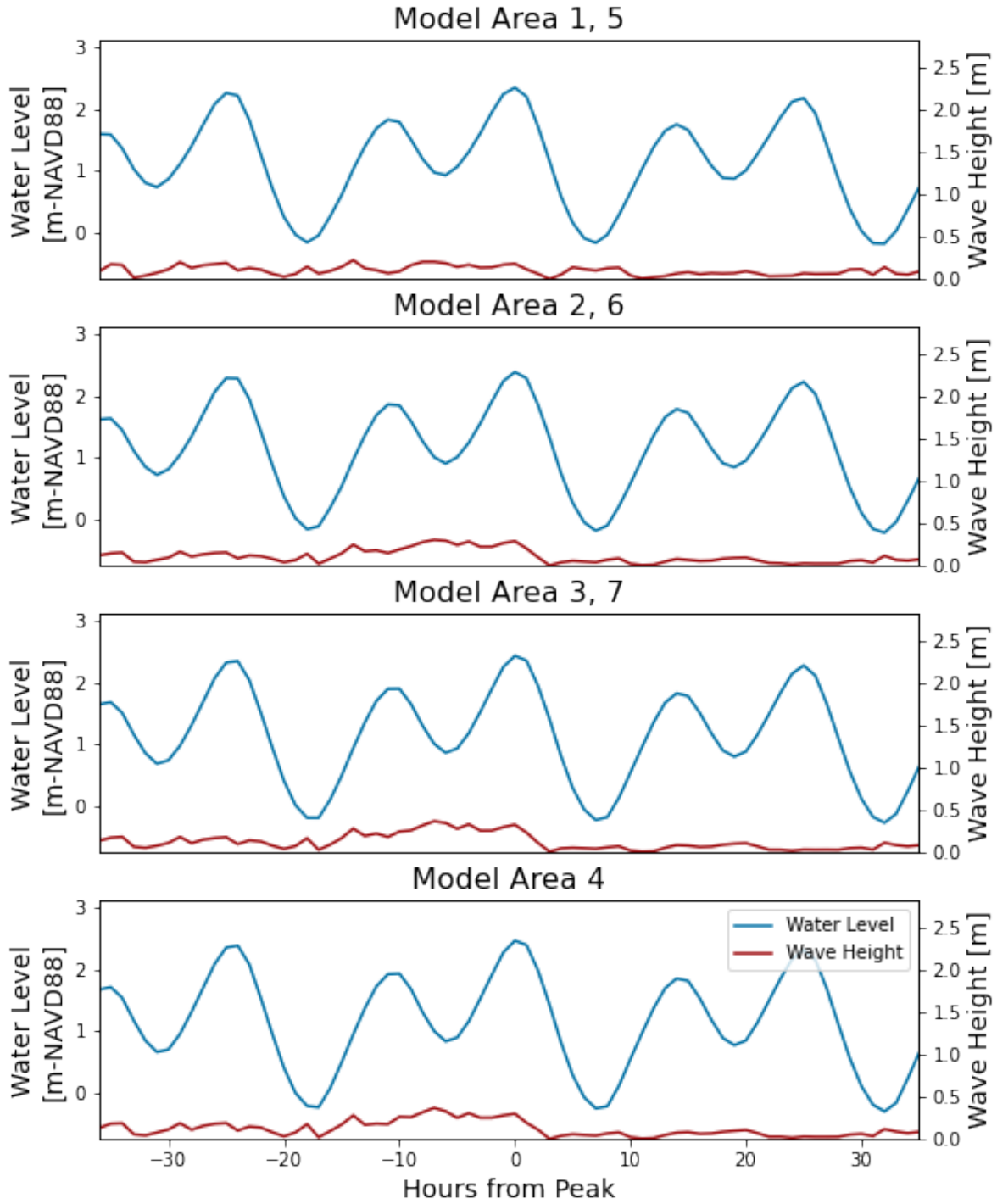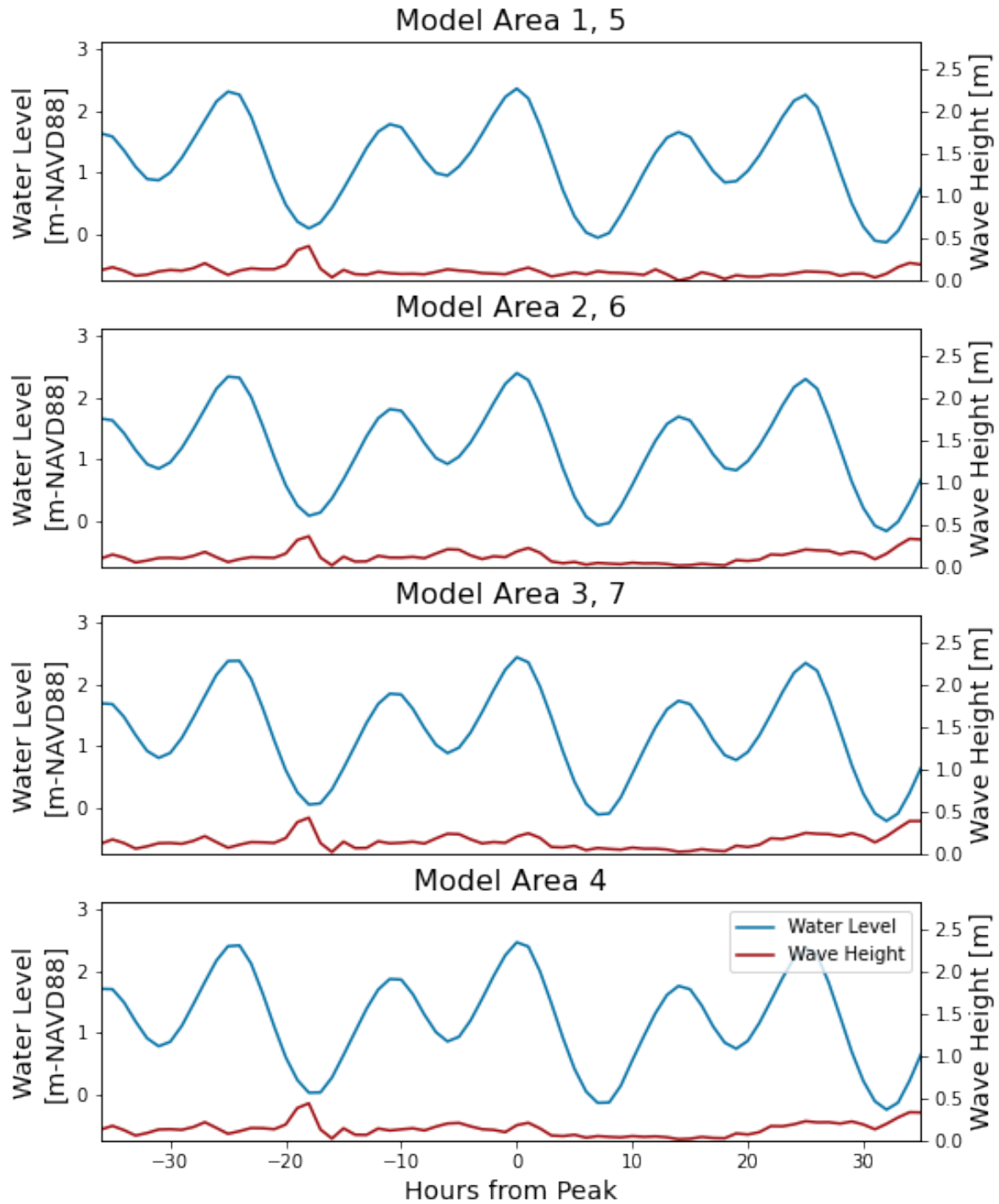Storm 1, 1992, SLR1992_R1_1.0yr_001
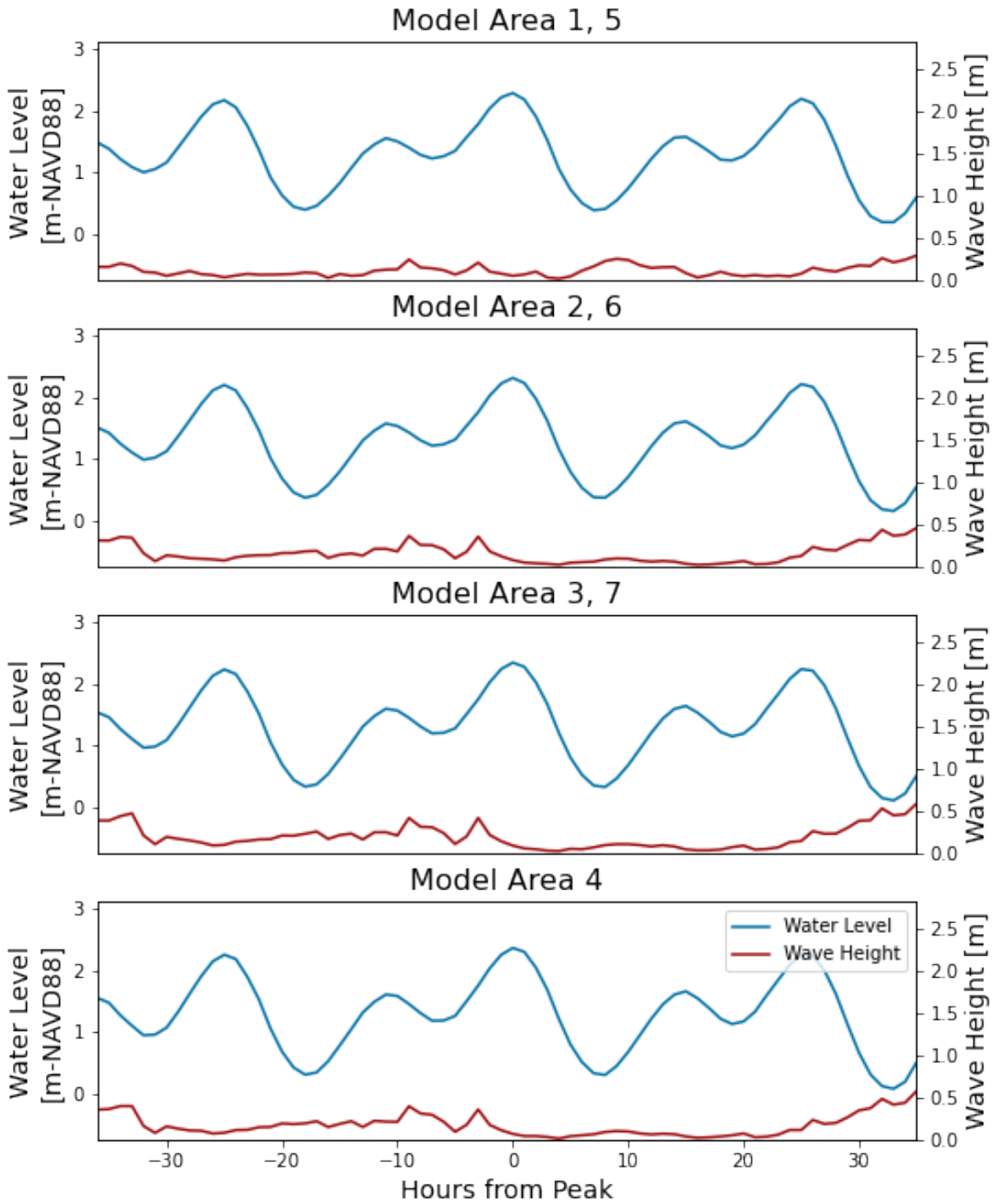
Storm 2, 1992, SLR1992_R1_1.0yr_002
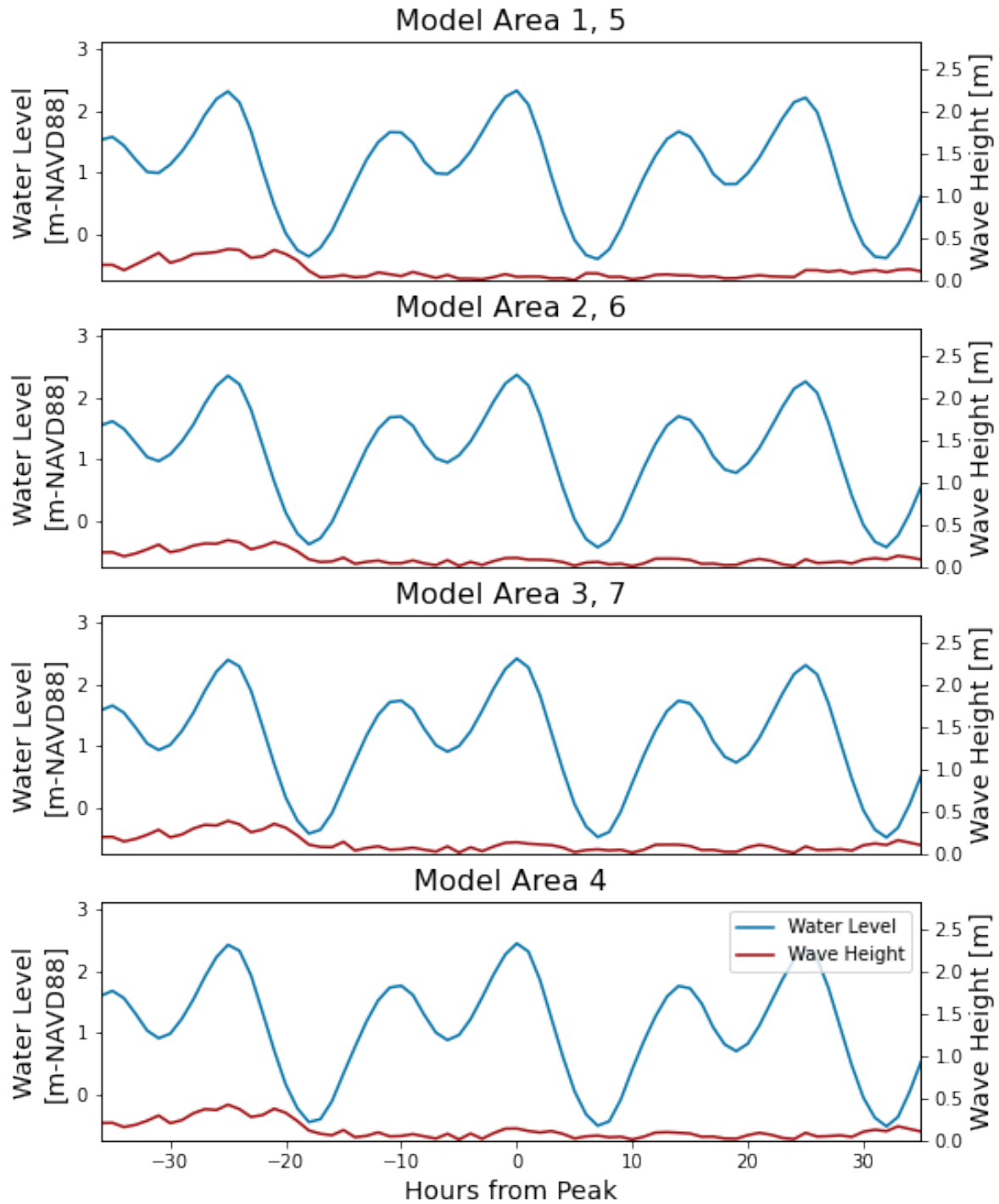
Storm 3, 1992, SLR1992_R1_1.0yr_003
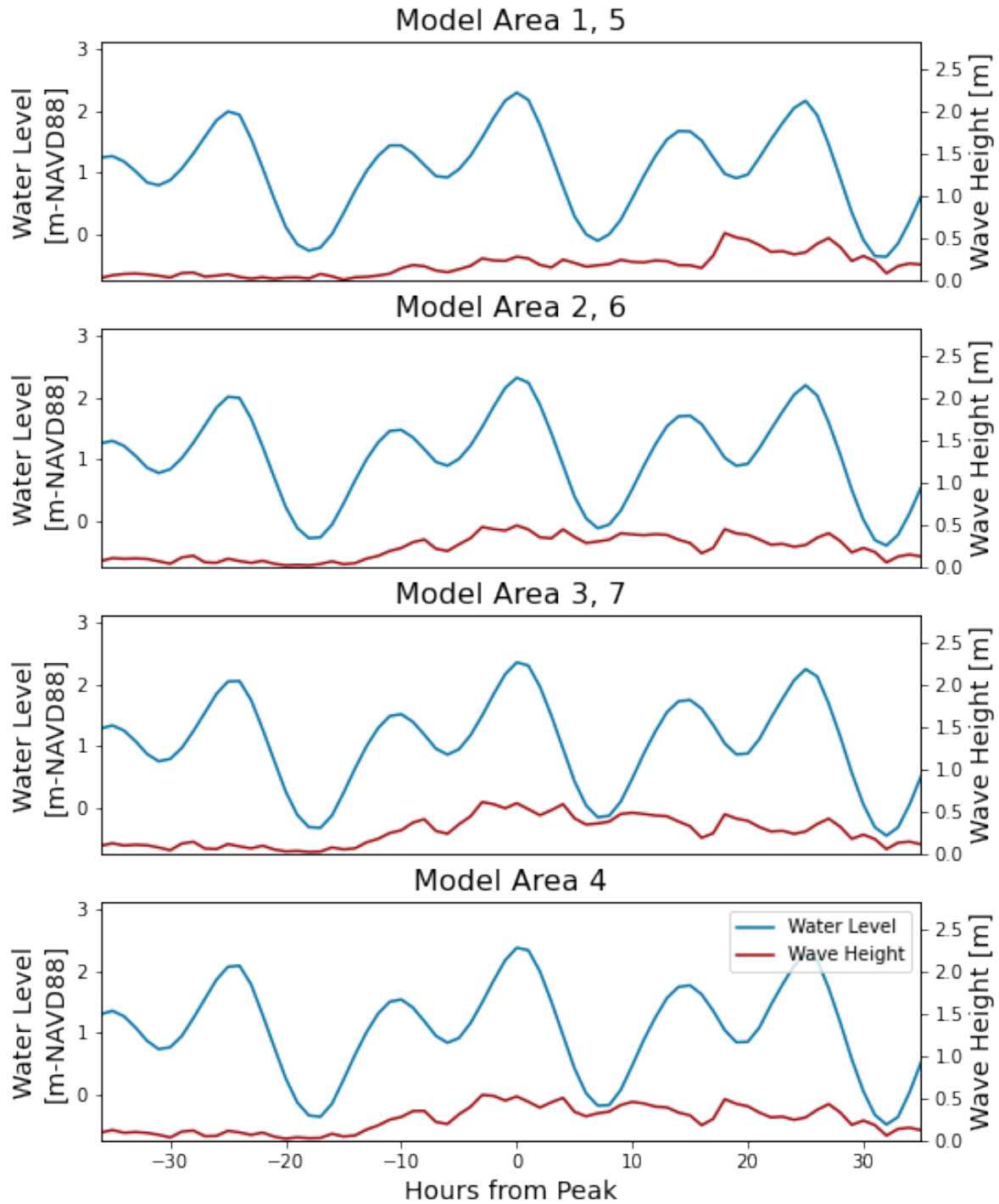
Storm 4, 1992, SLR1992_R1_1.0yr_004
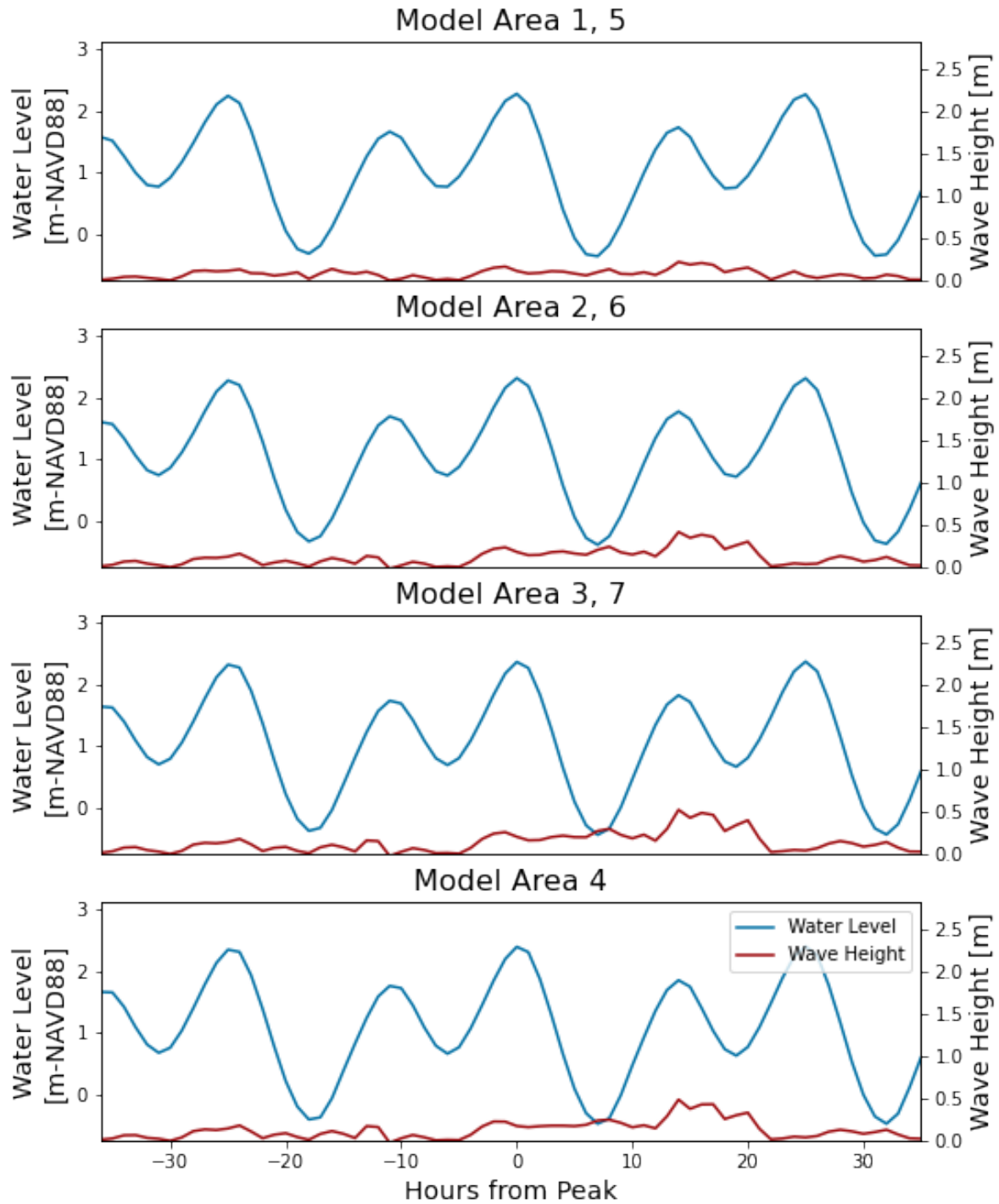
Storm 5, 1992, SLR1992_R1_1.0yr_005
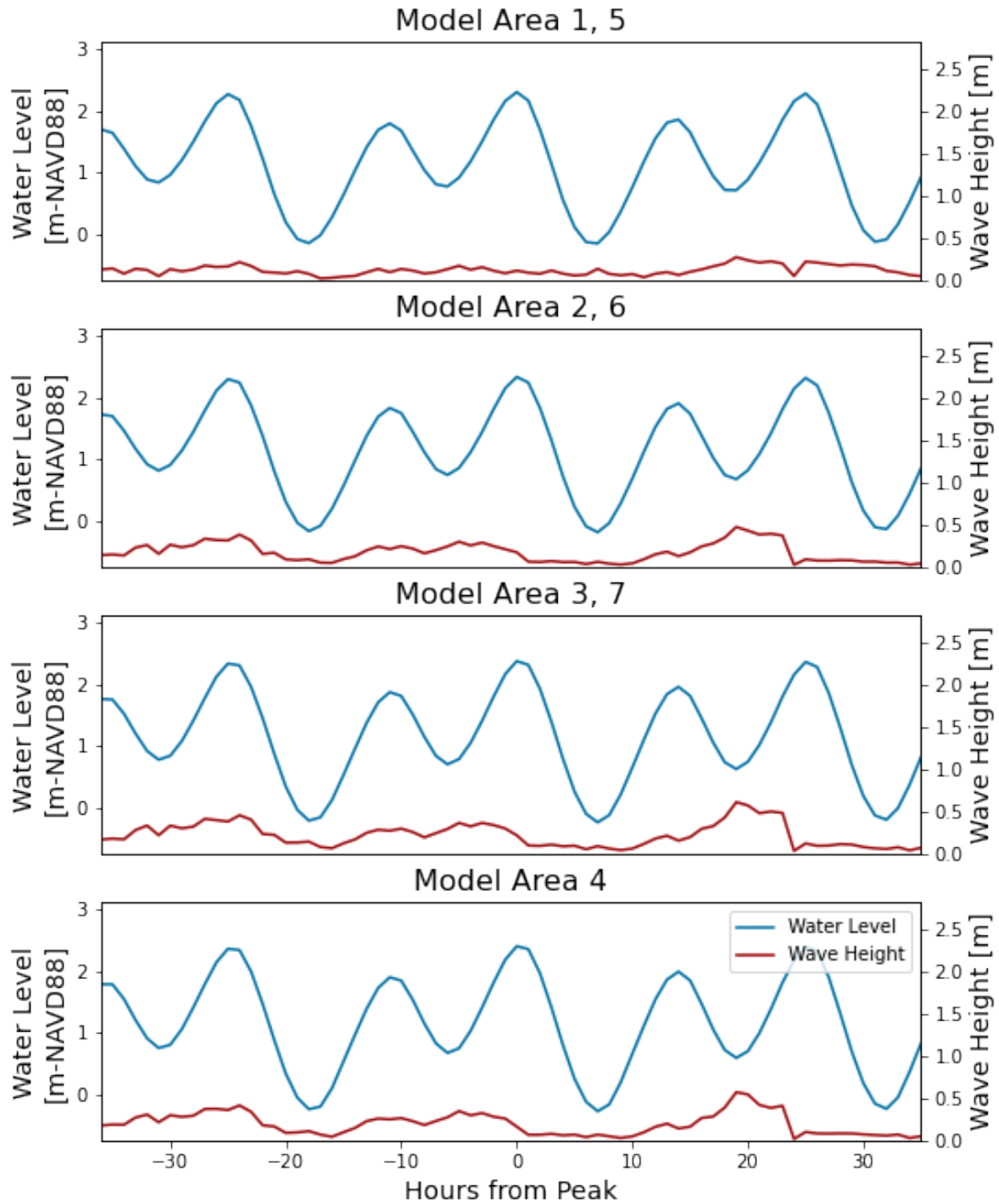
Storm 6, 1992, SLR1992_R1_1.0yr_006

Model Area 1, 5

Model Area 2, 6

Model Area 3, 7

Model Area 4
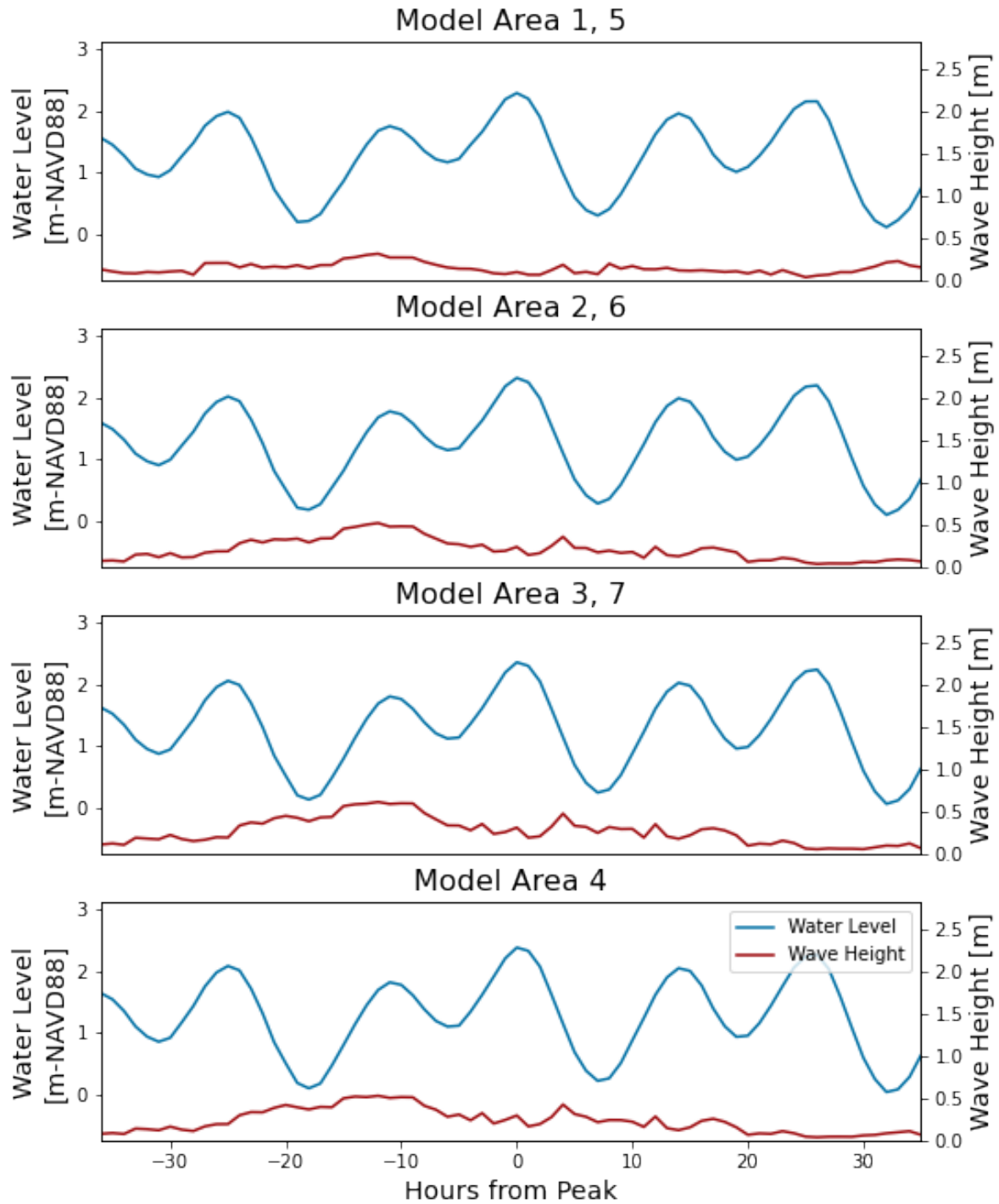
Storm 7, 1992, SLR1992_R1_1.0yr_007
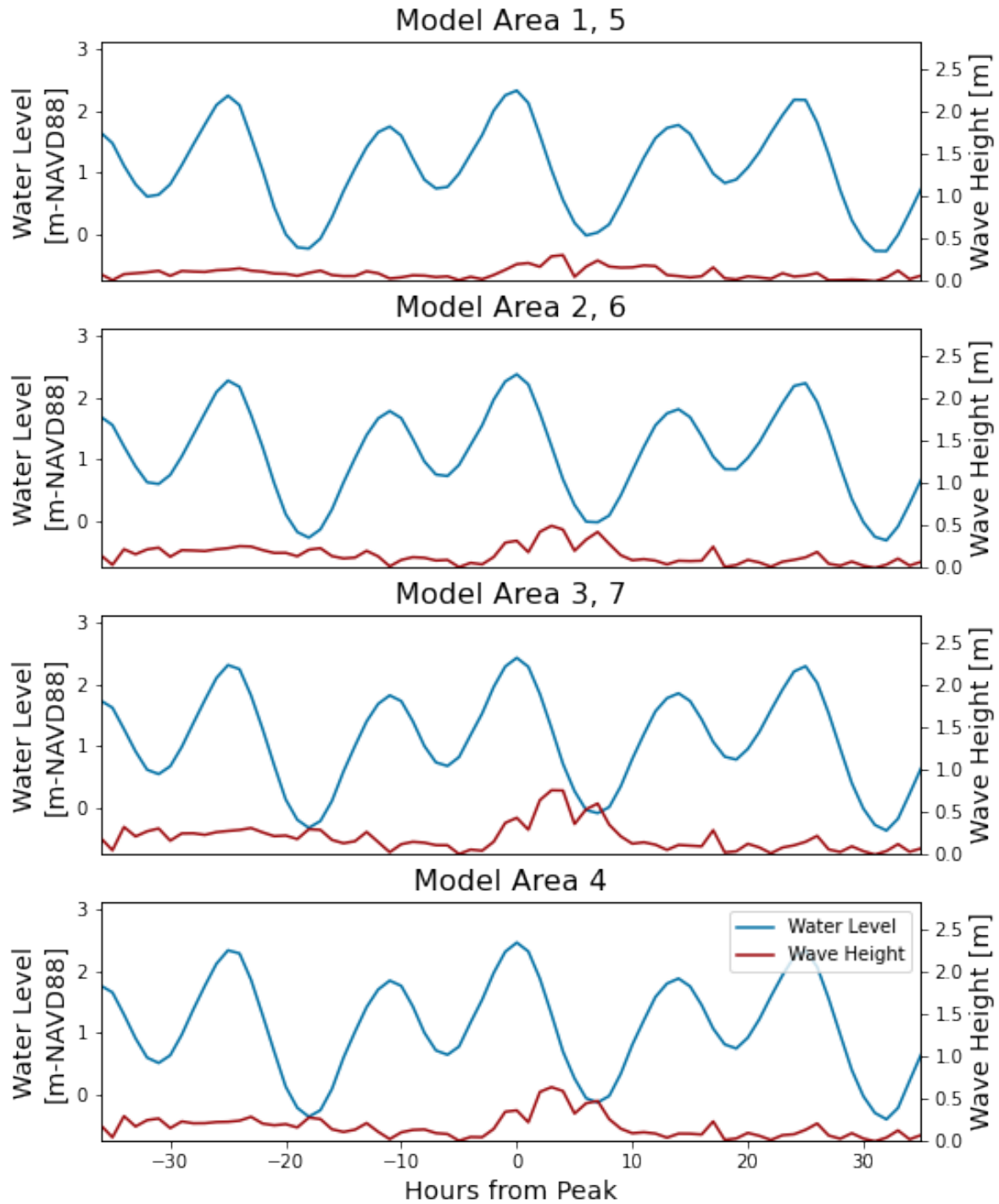
Storm 8, 1992, SLR1992_R1_1.0yr_008
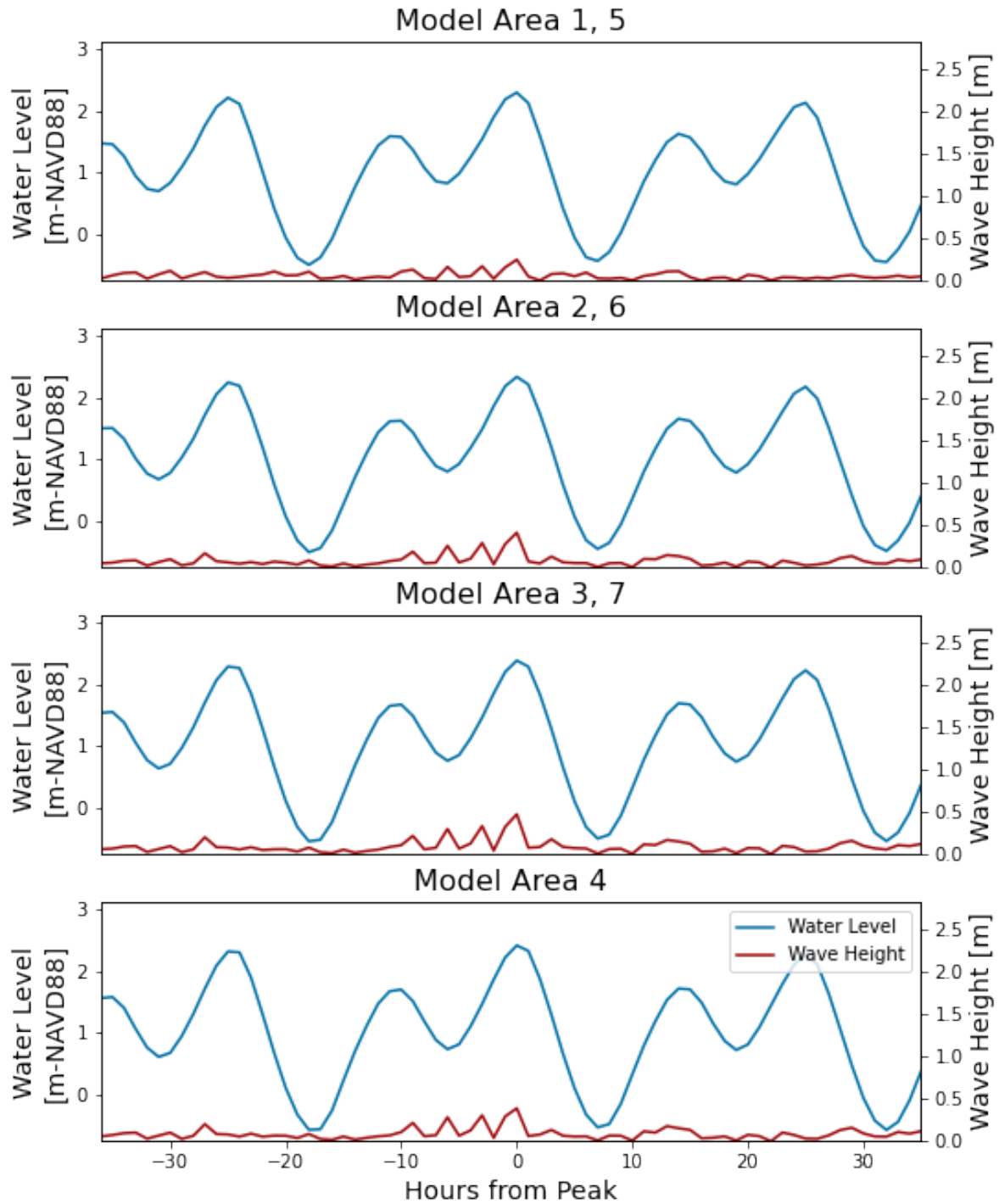
Storm 9, 1992, SLR1992_R1_1.0yr_009
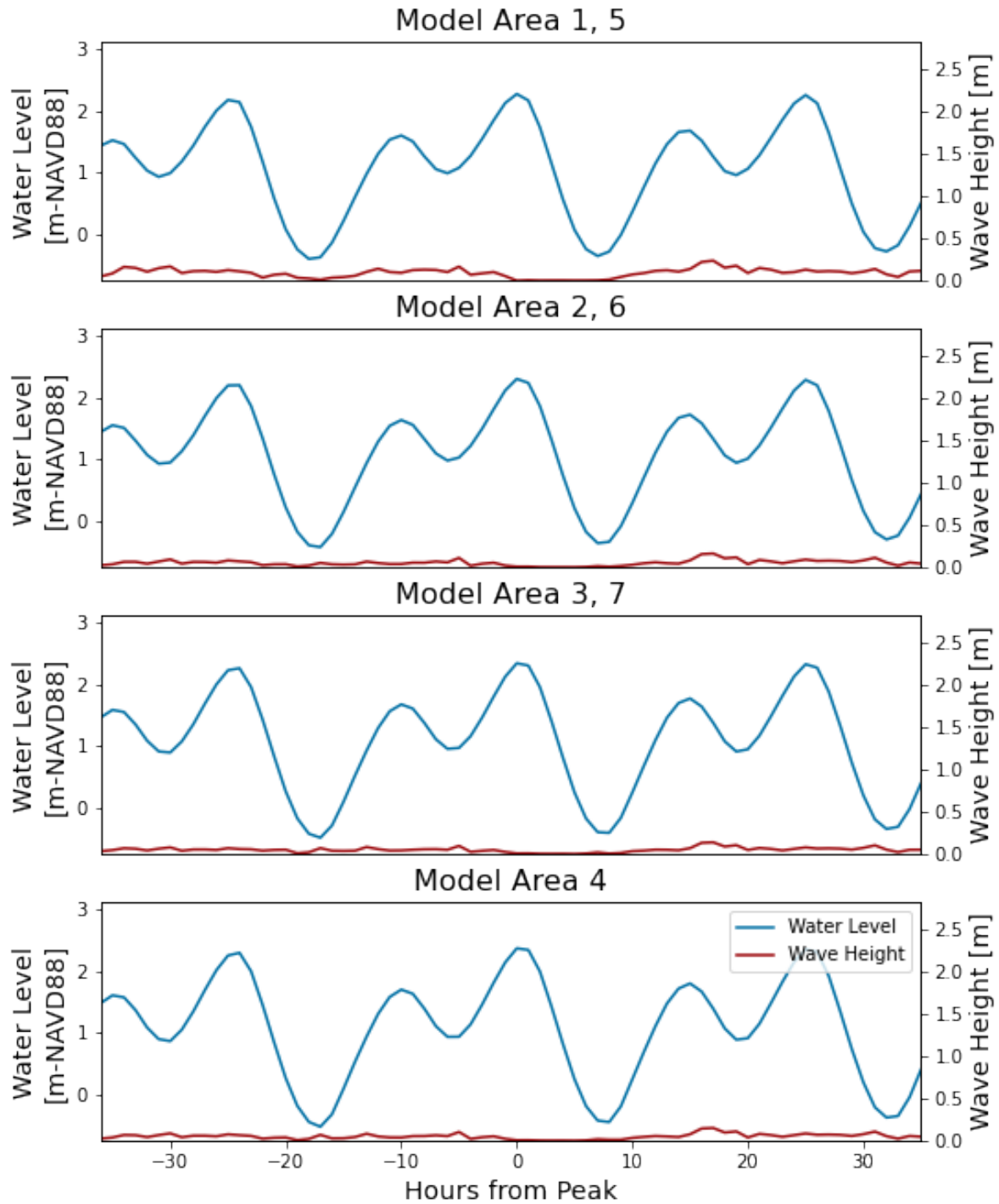
Storm 10, 1992, SLR1992_R1_1.0yr_010
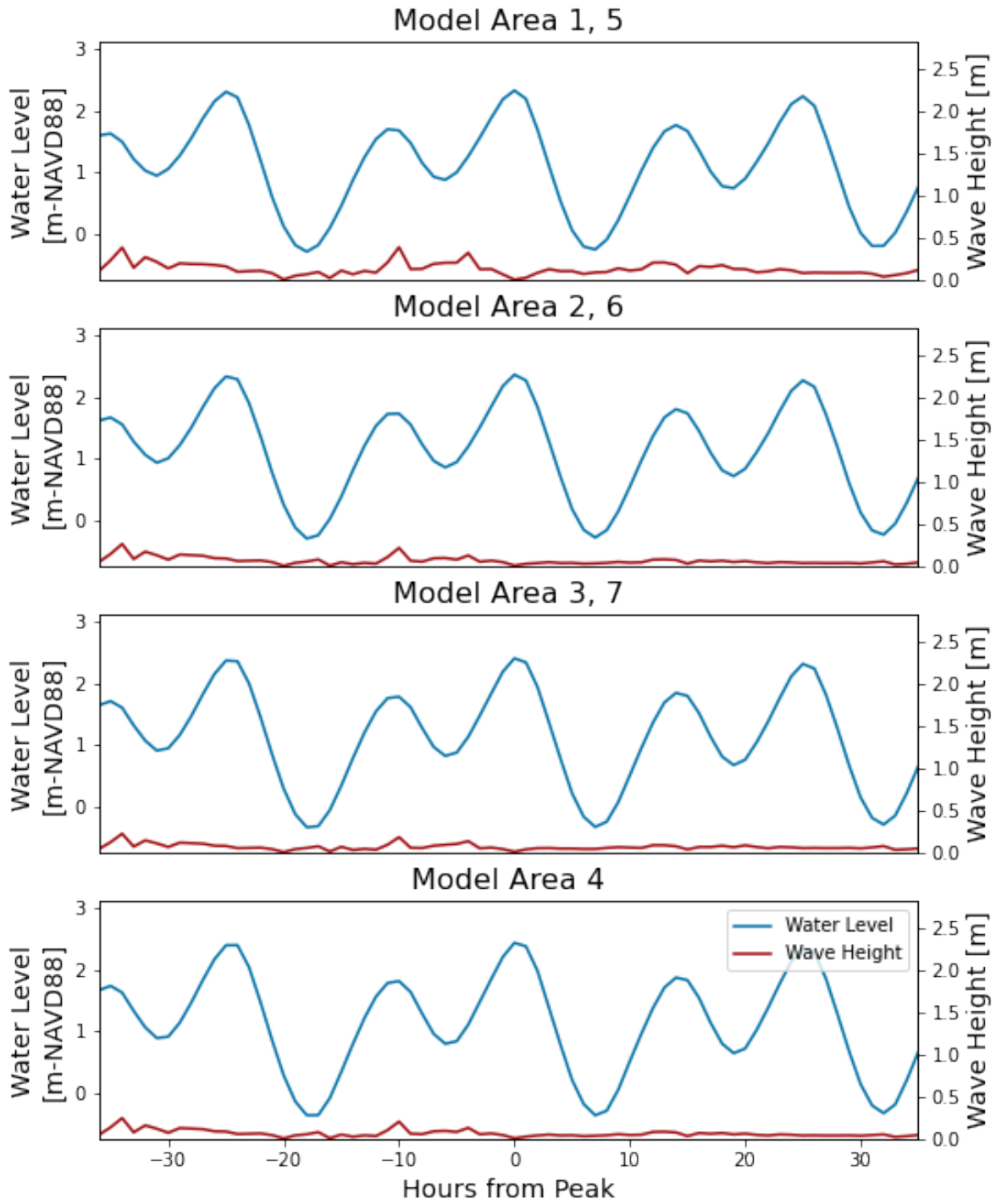
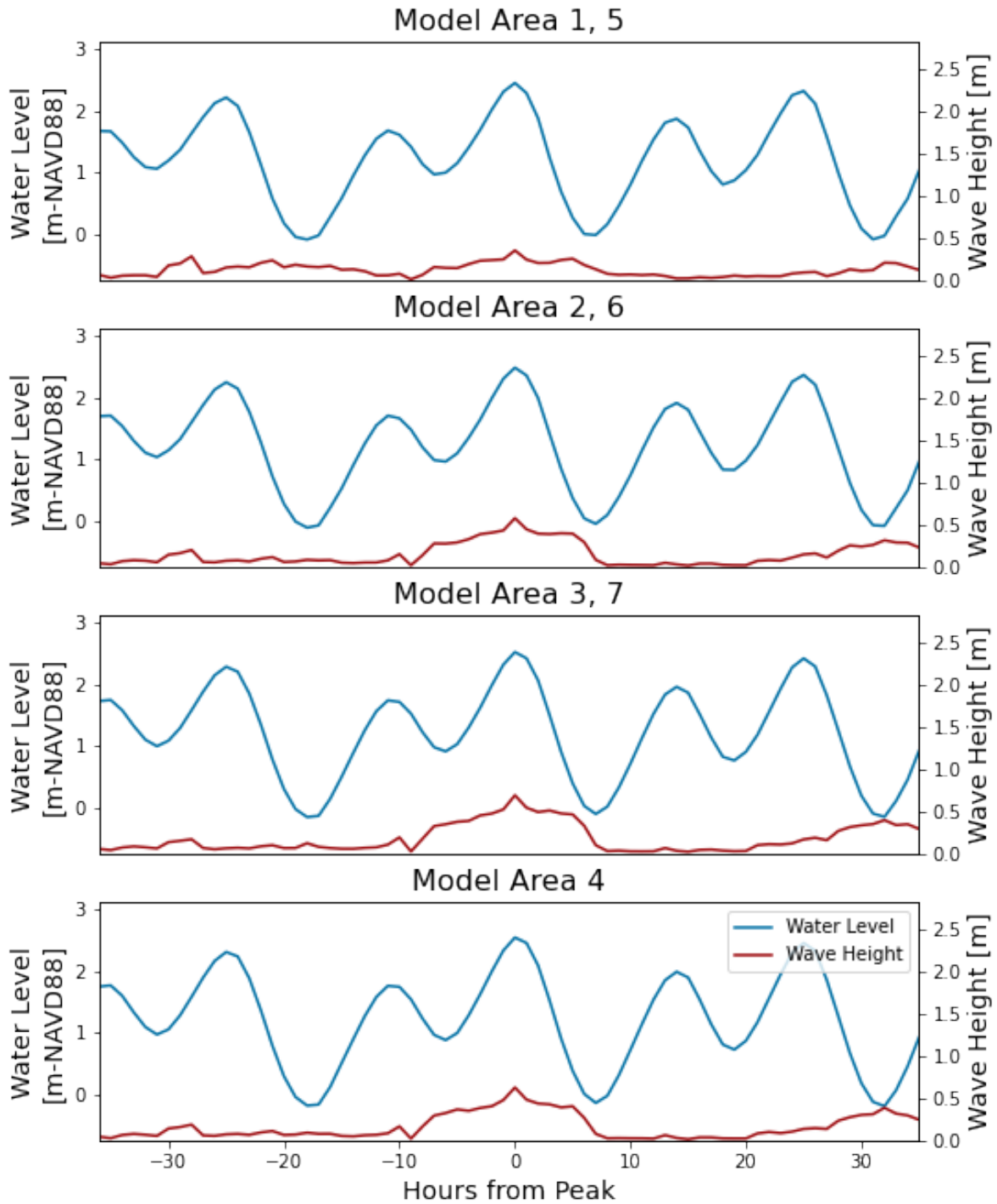Storm 11, 1992, SLR1992_R1_1.0yr_011
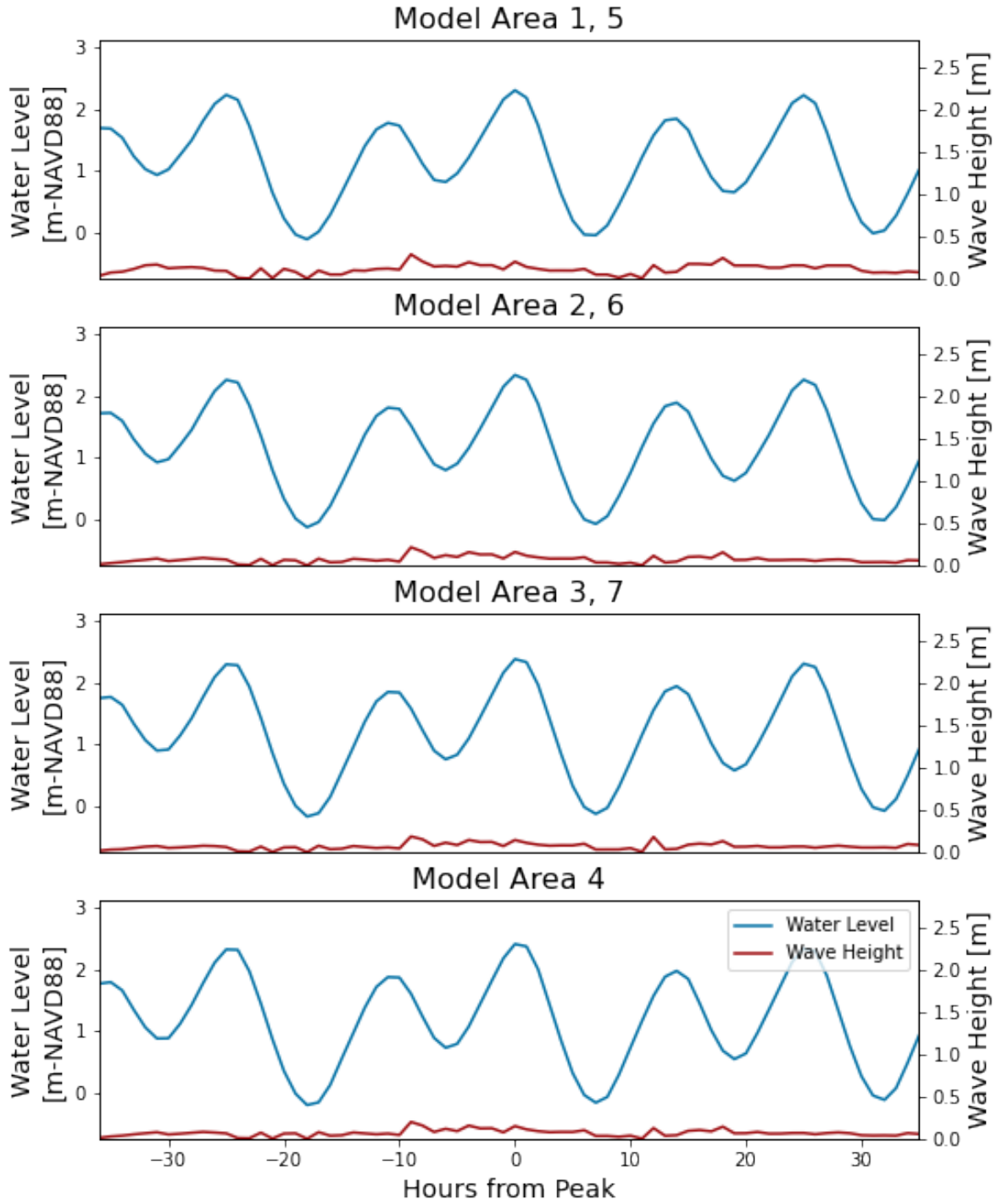
Storm 12, 1992, SLR1992_R1_1.0yr_012
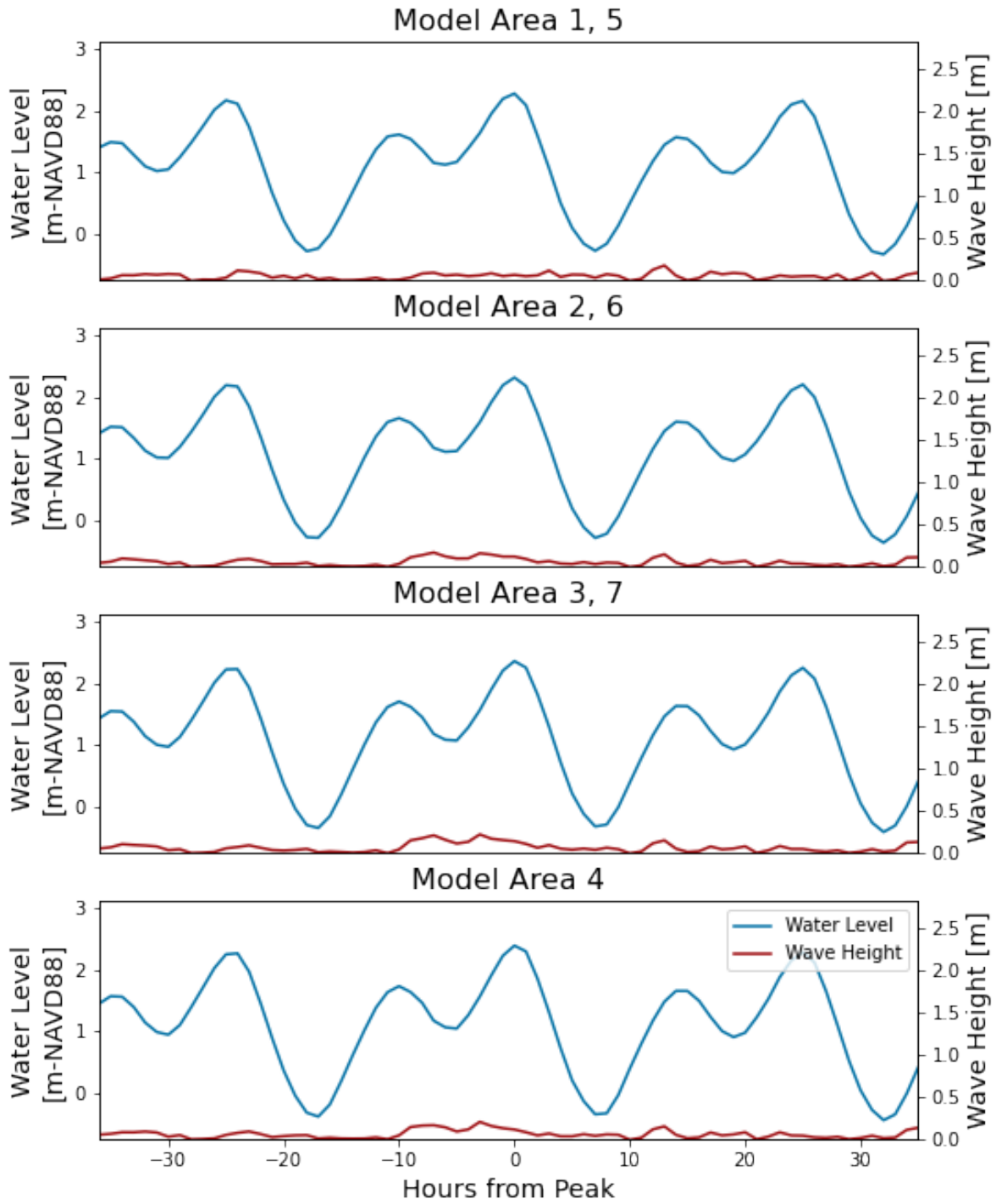
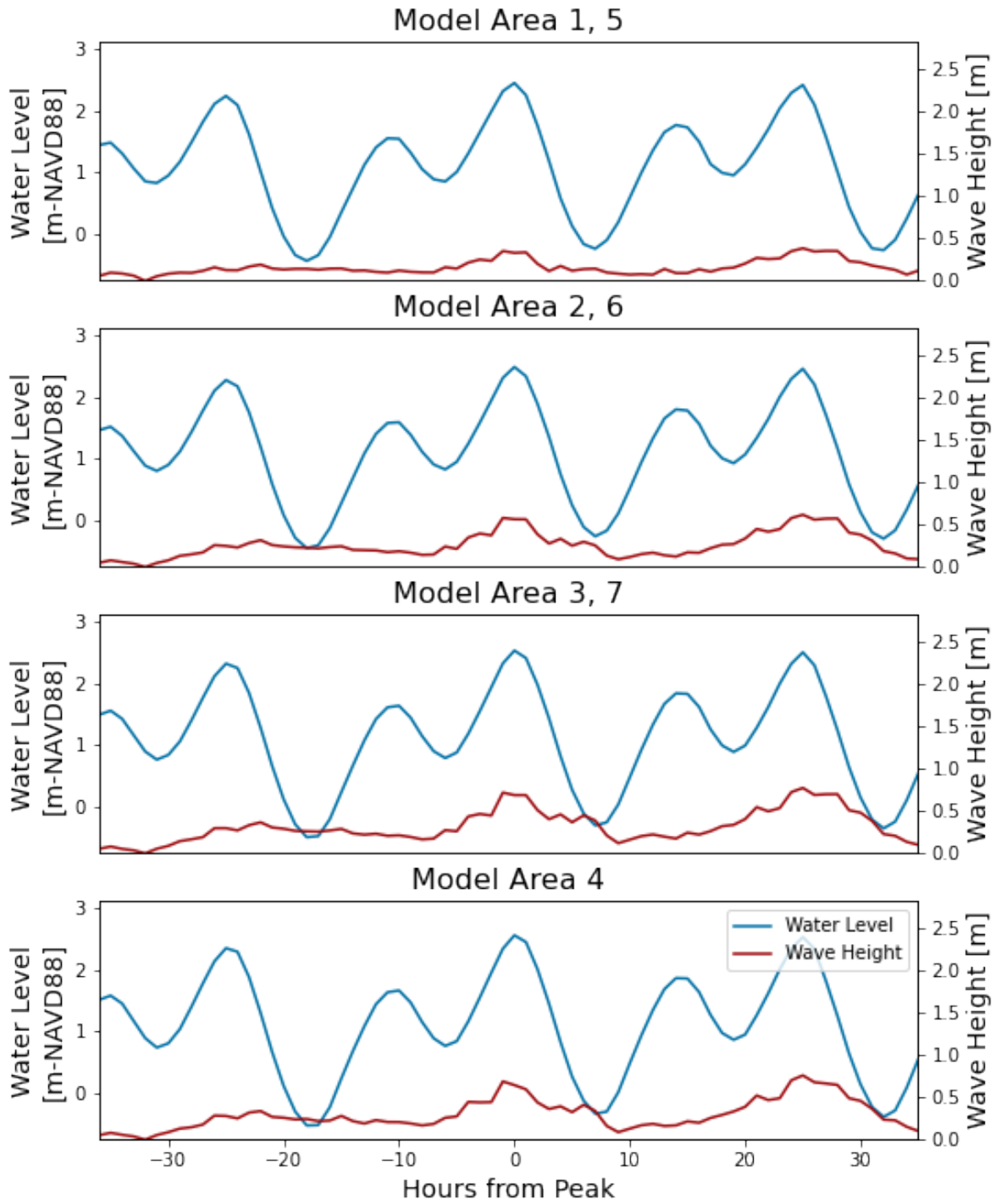# Storm 13, 1992, SLR1992_R1_1.0yr_013
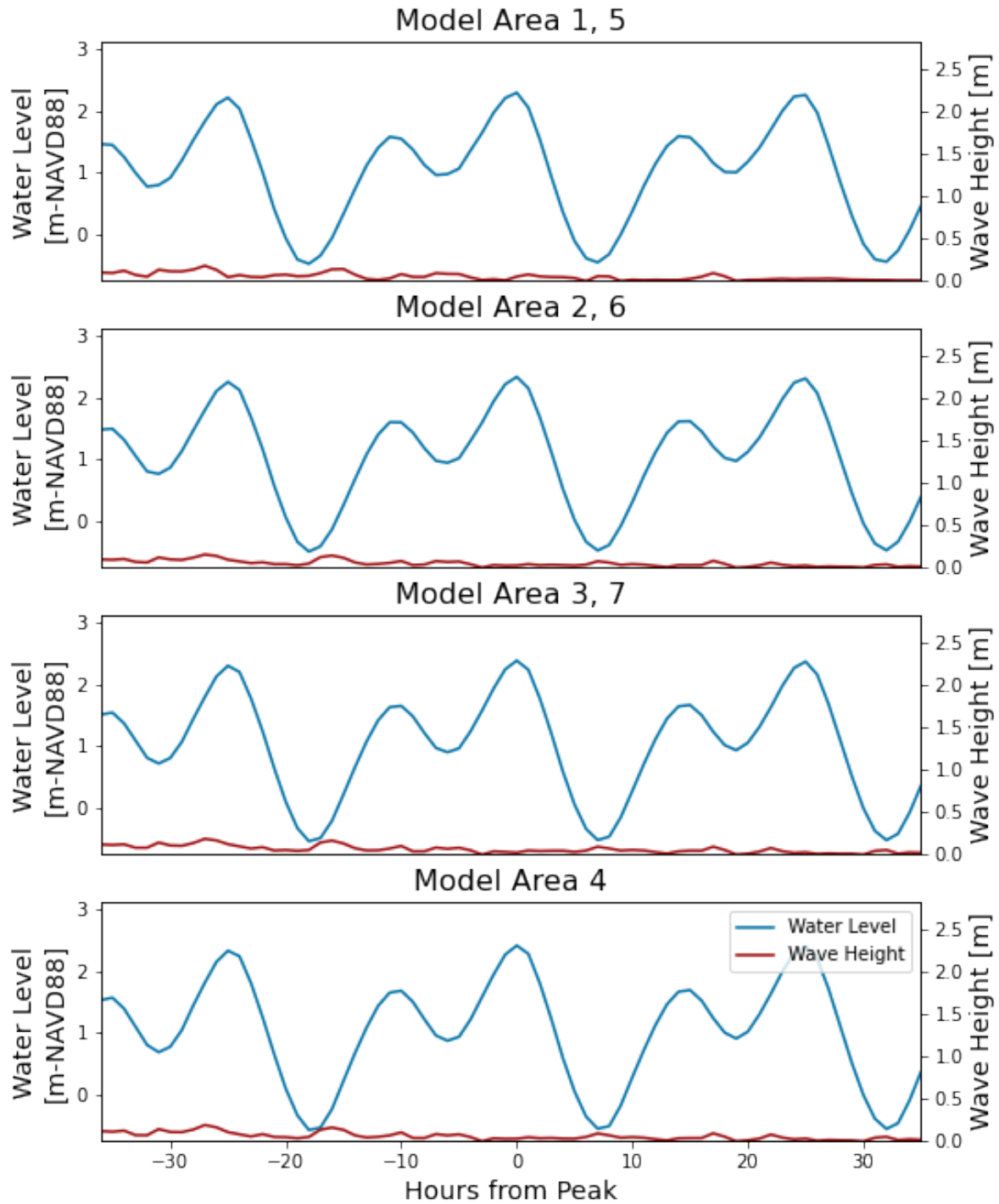
Storm 14, 1992, SLR1992_R1_1.0yr_014
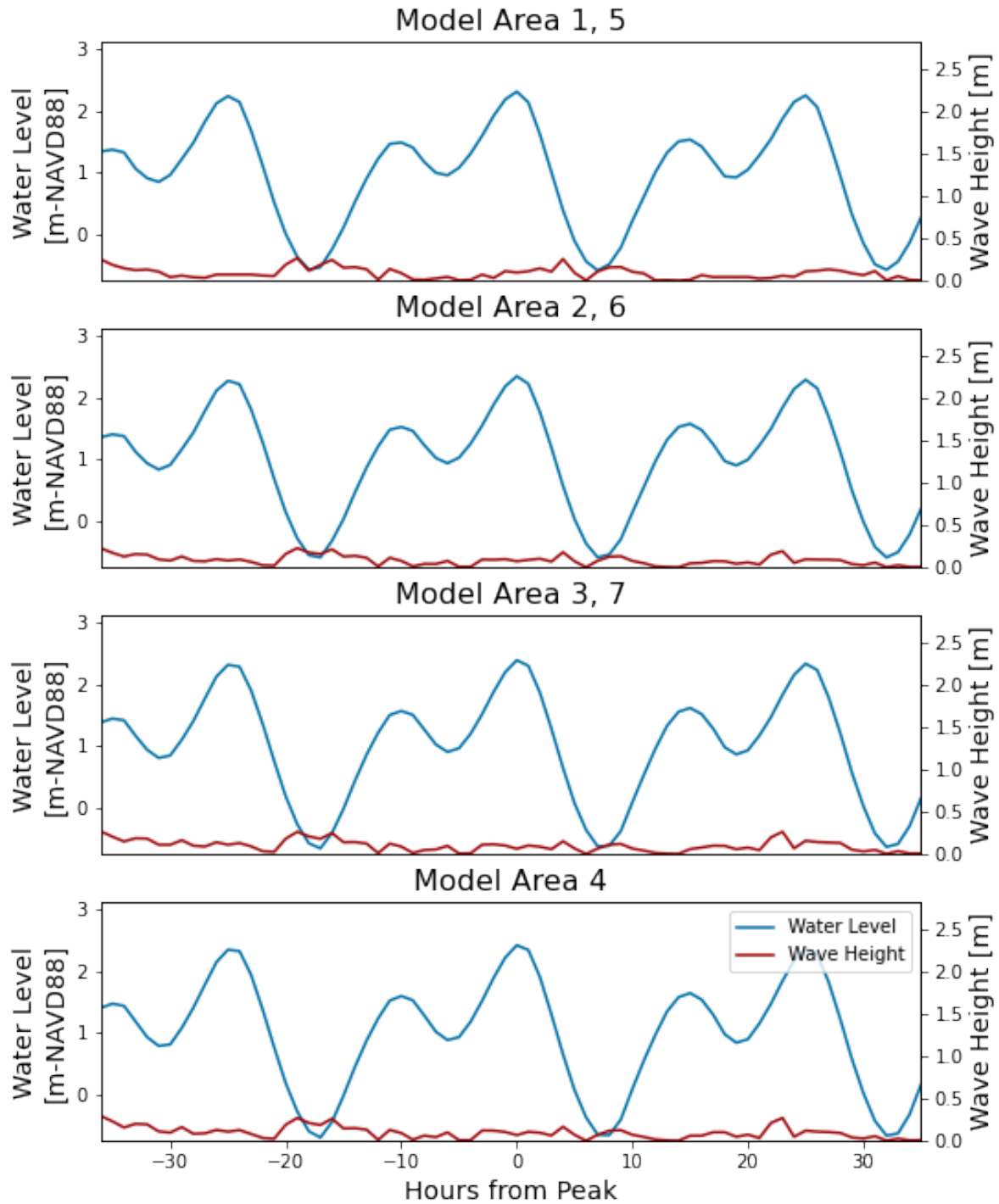
Storm 15, 1992, SLR1992_R1_1.0yr_015
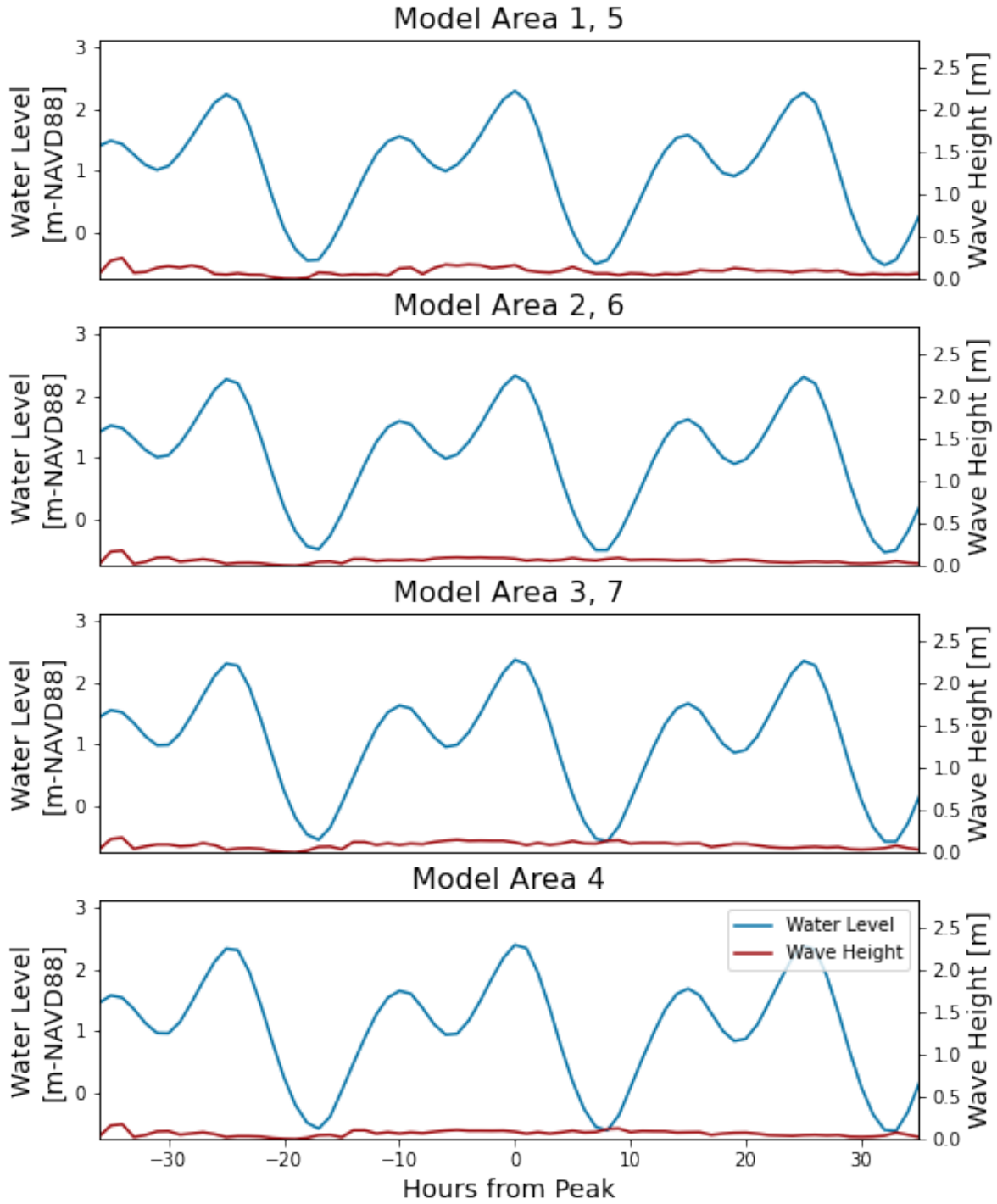
Storm 16, 1992, SLR1992_R1_1.0yr_016
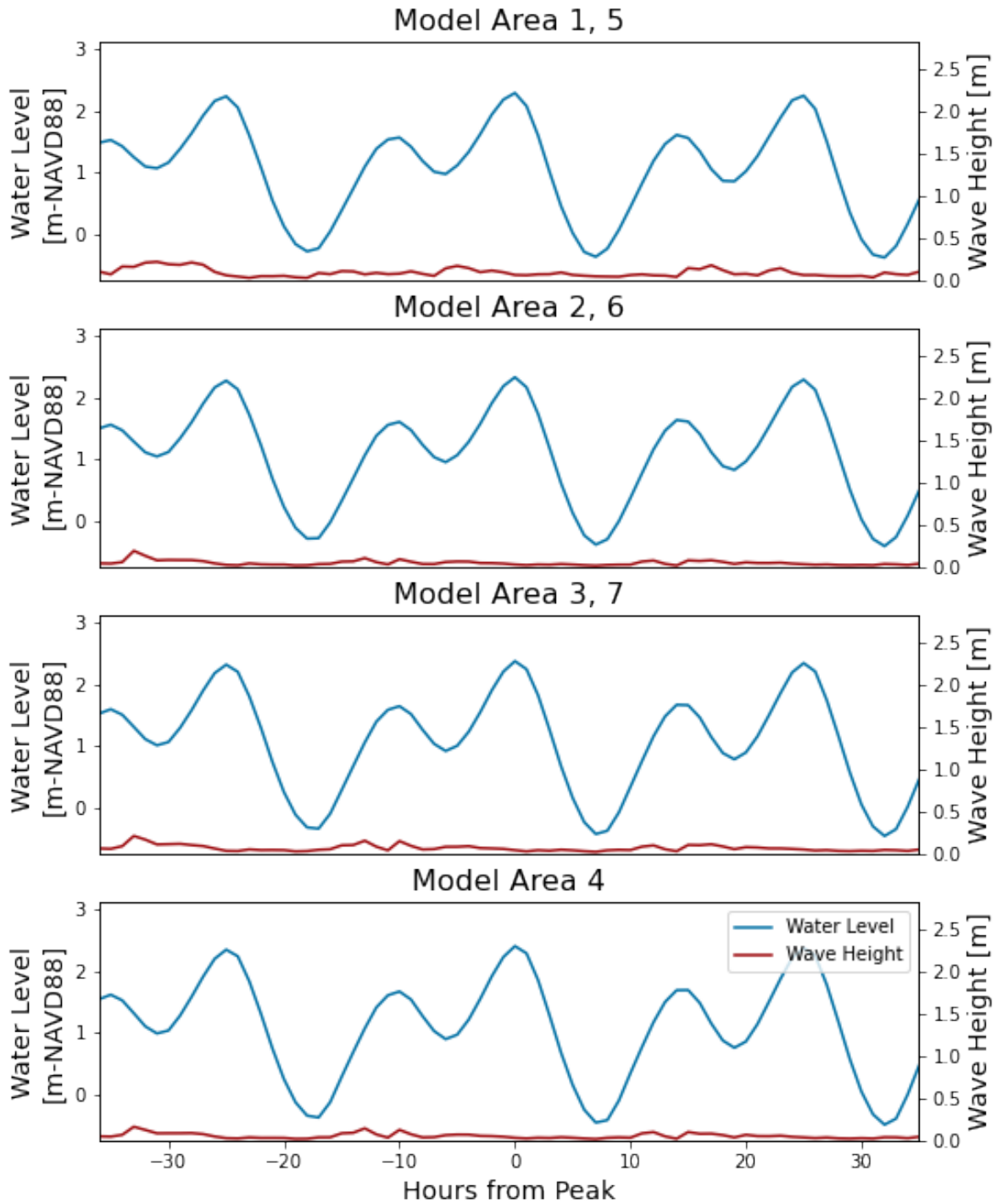
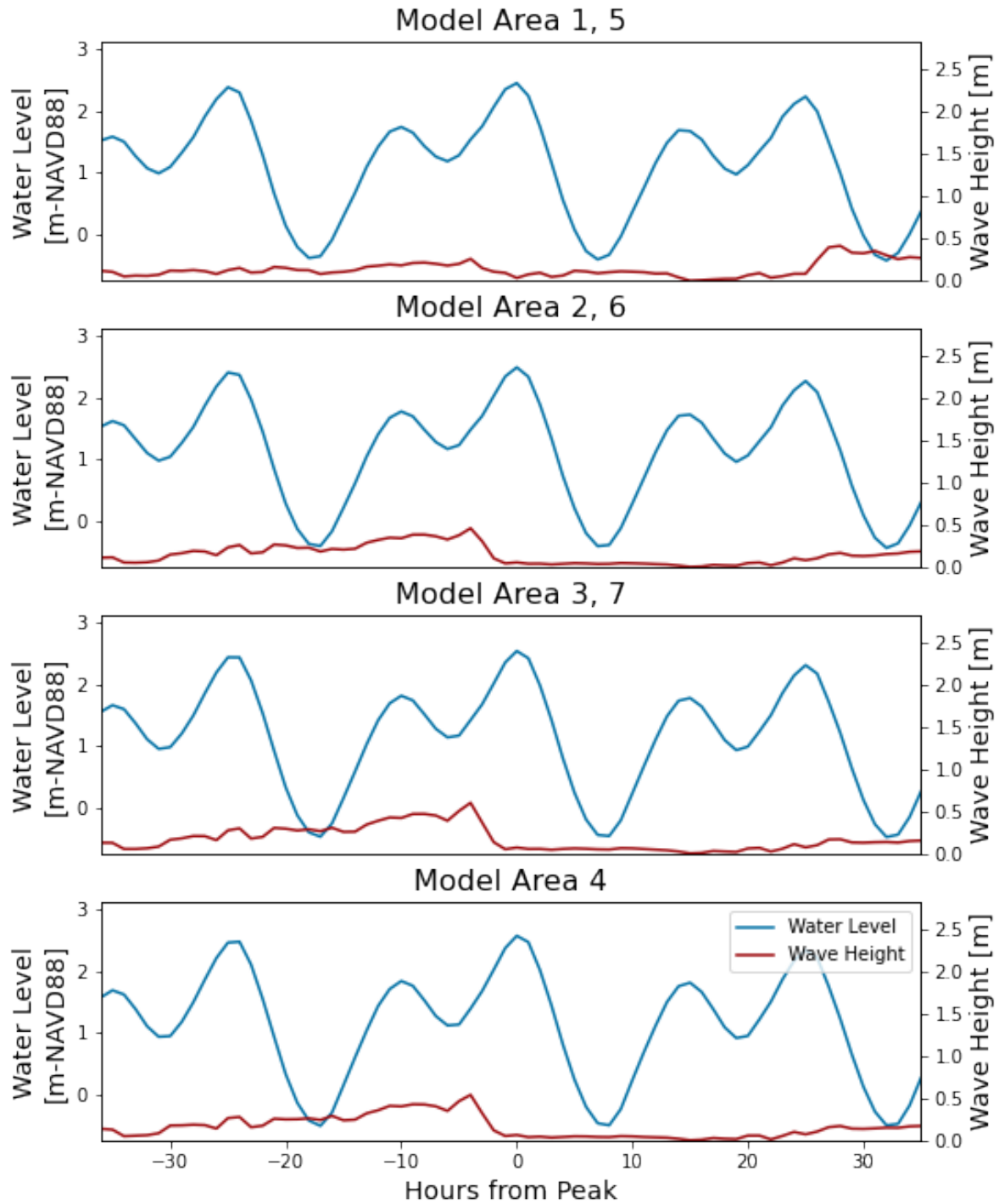# Storm 17, 1992, SLR1992_R1_1.0yr_017
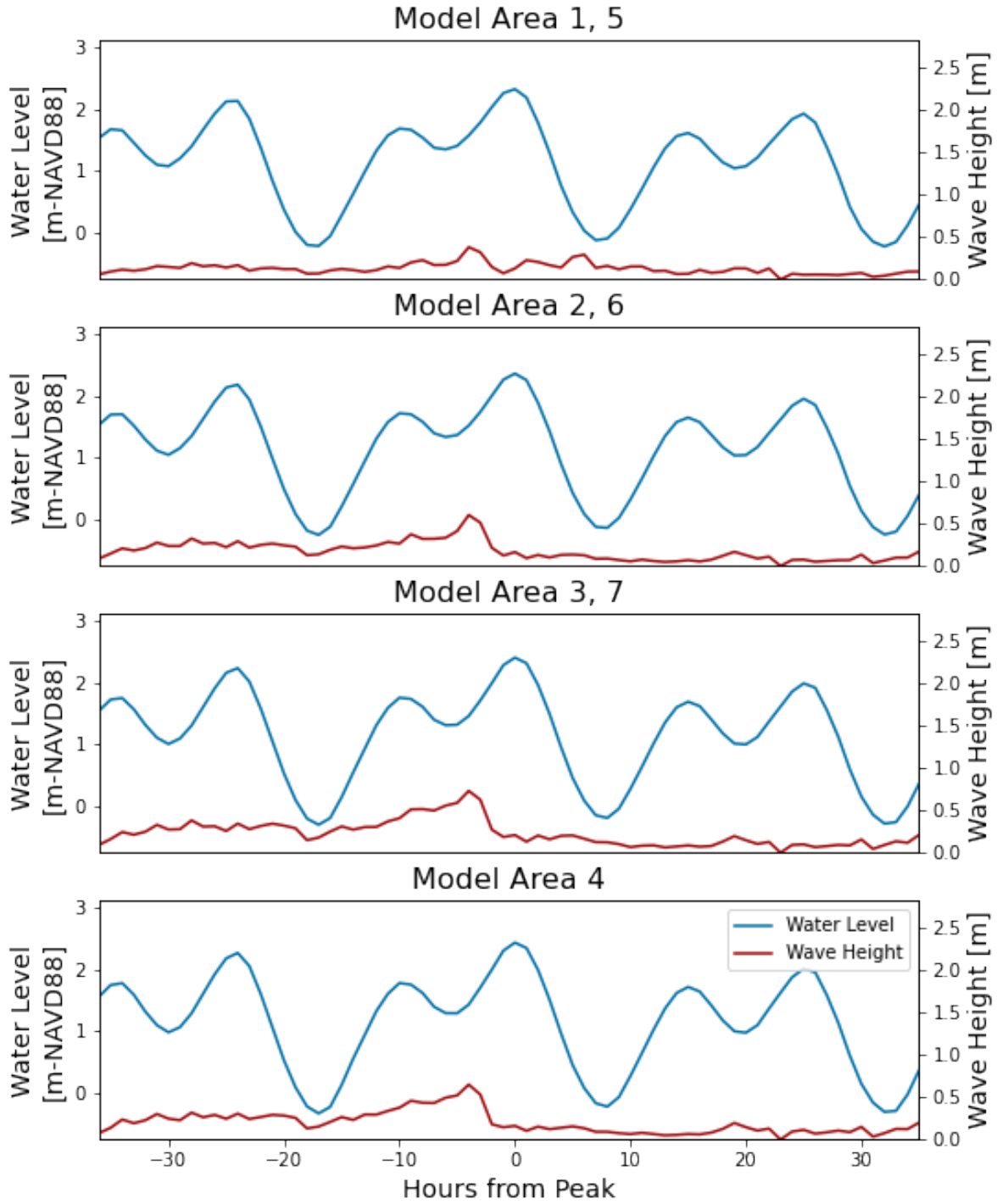
Storm 18, 1992, SLR1992_R1_1.0yr_018
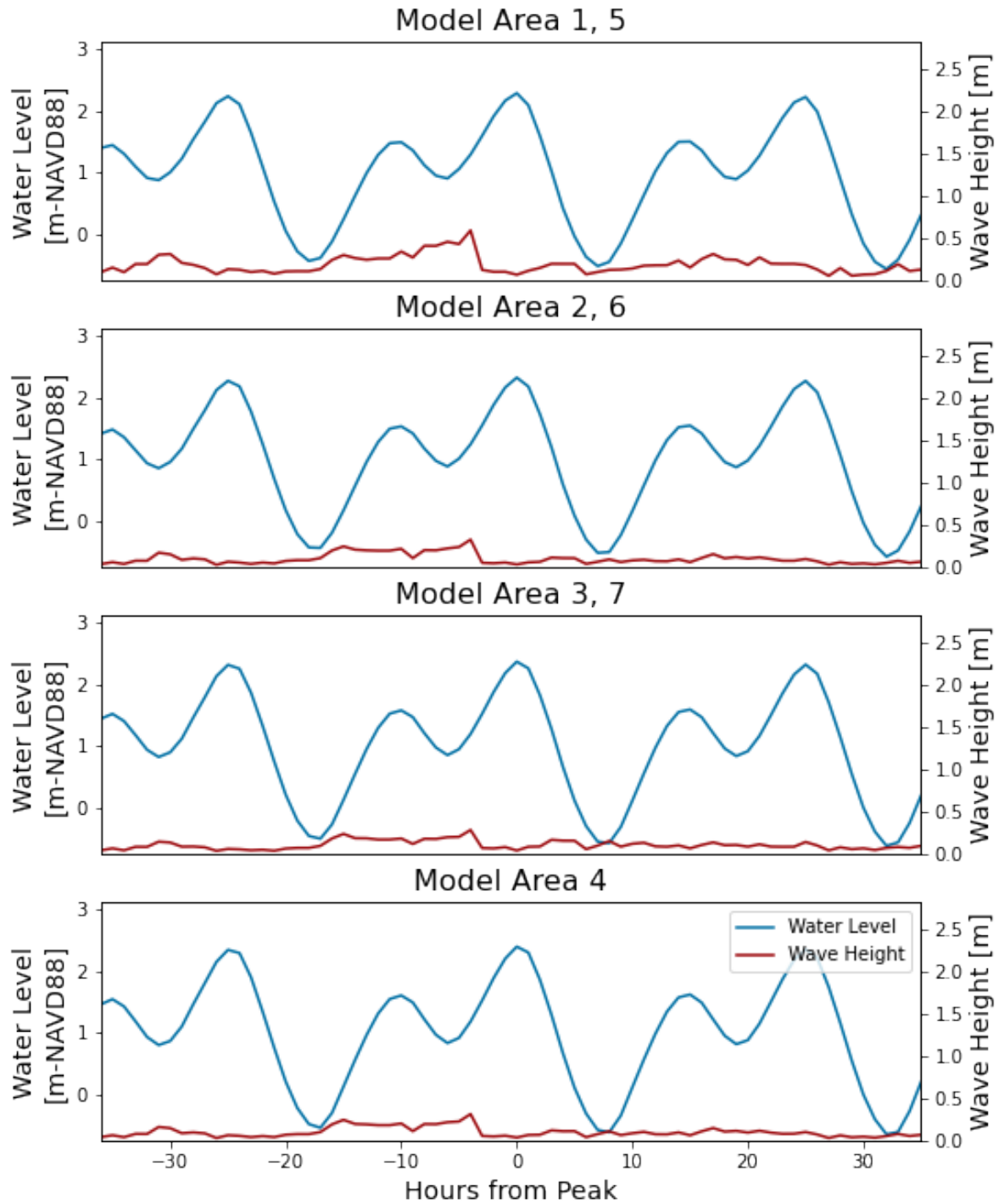
Storm 19, 1992, SLR1992_R1_1.0yr_019
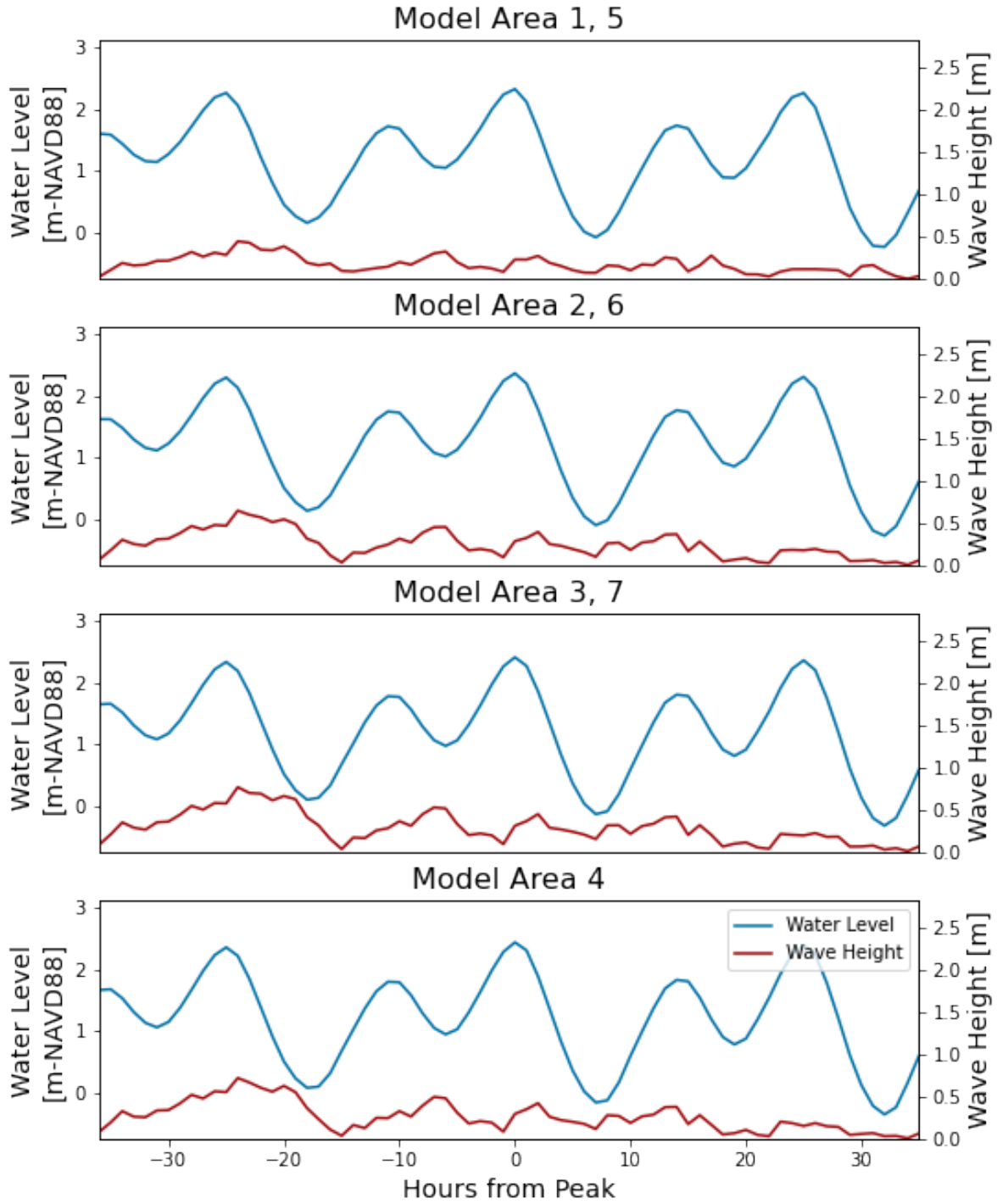
Storm 20, 1992, SLR1992_R1_1.0yr_020
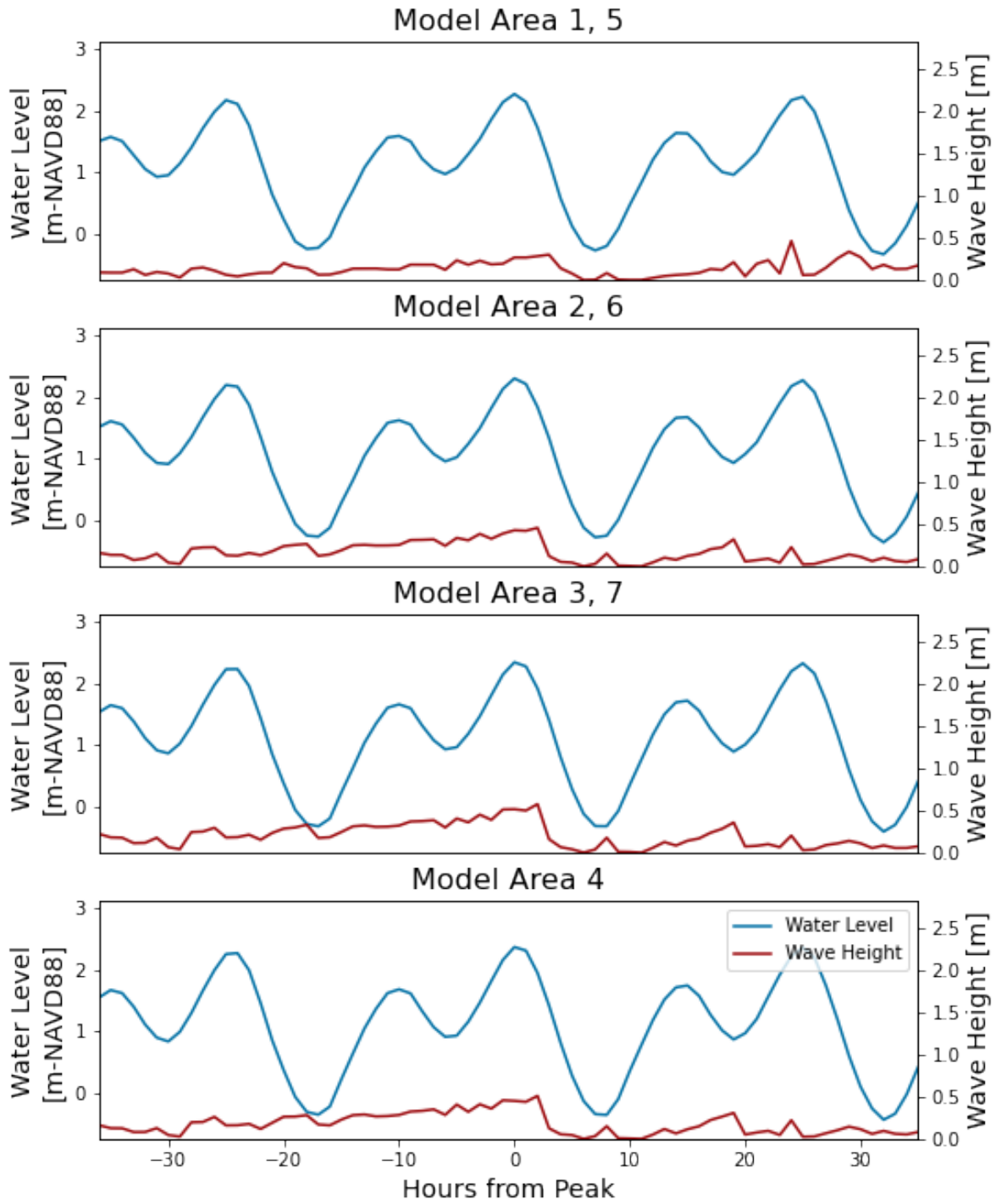
Storm 21, 1992, SLR1992_R1_1.0yr_021
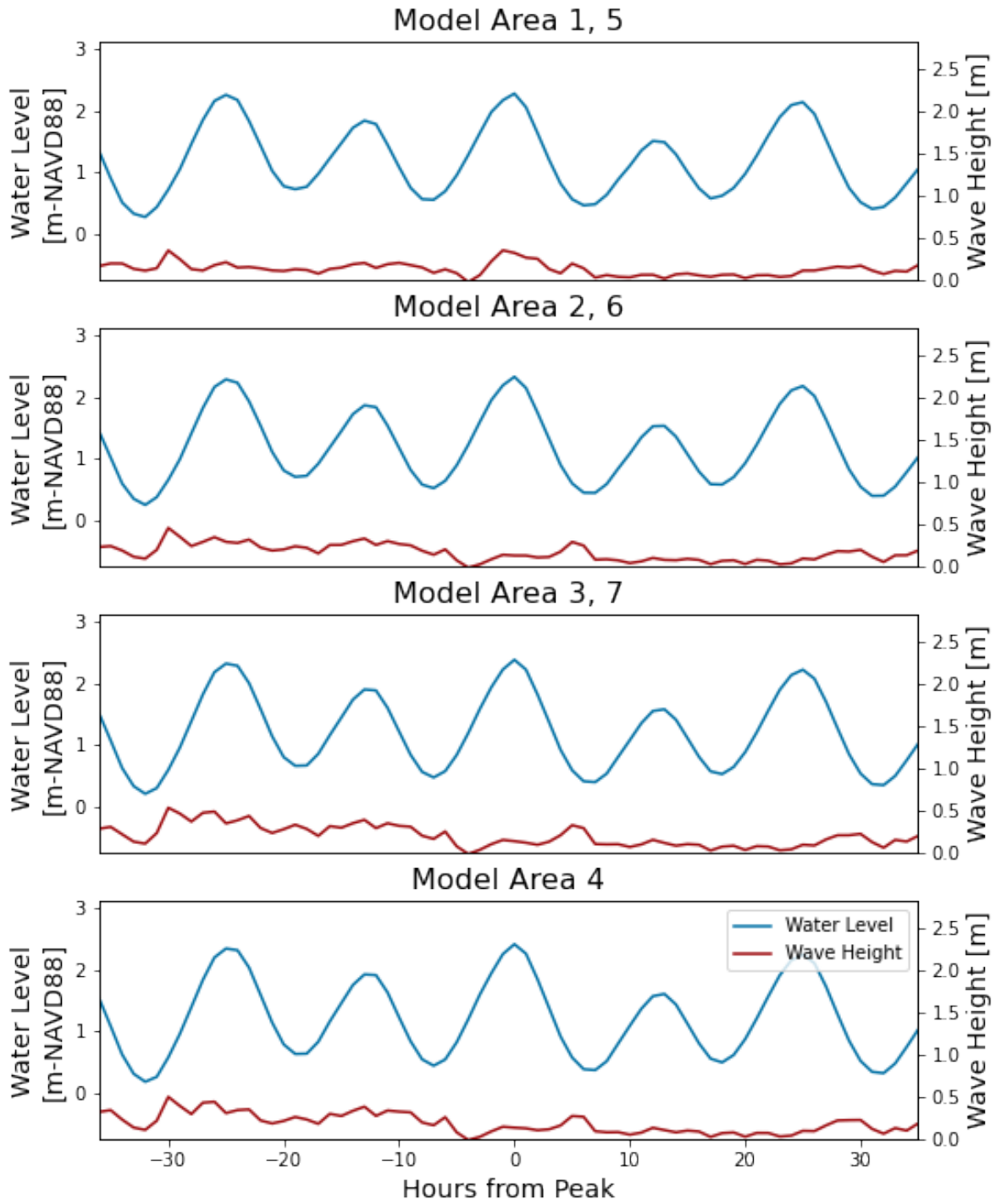
Storm 22, 1992, SLR1992_R1_1.0yr_022
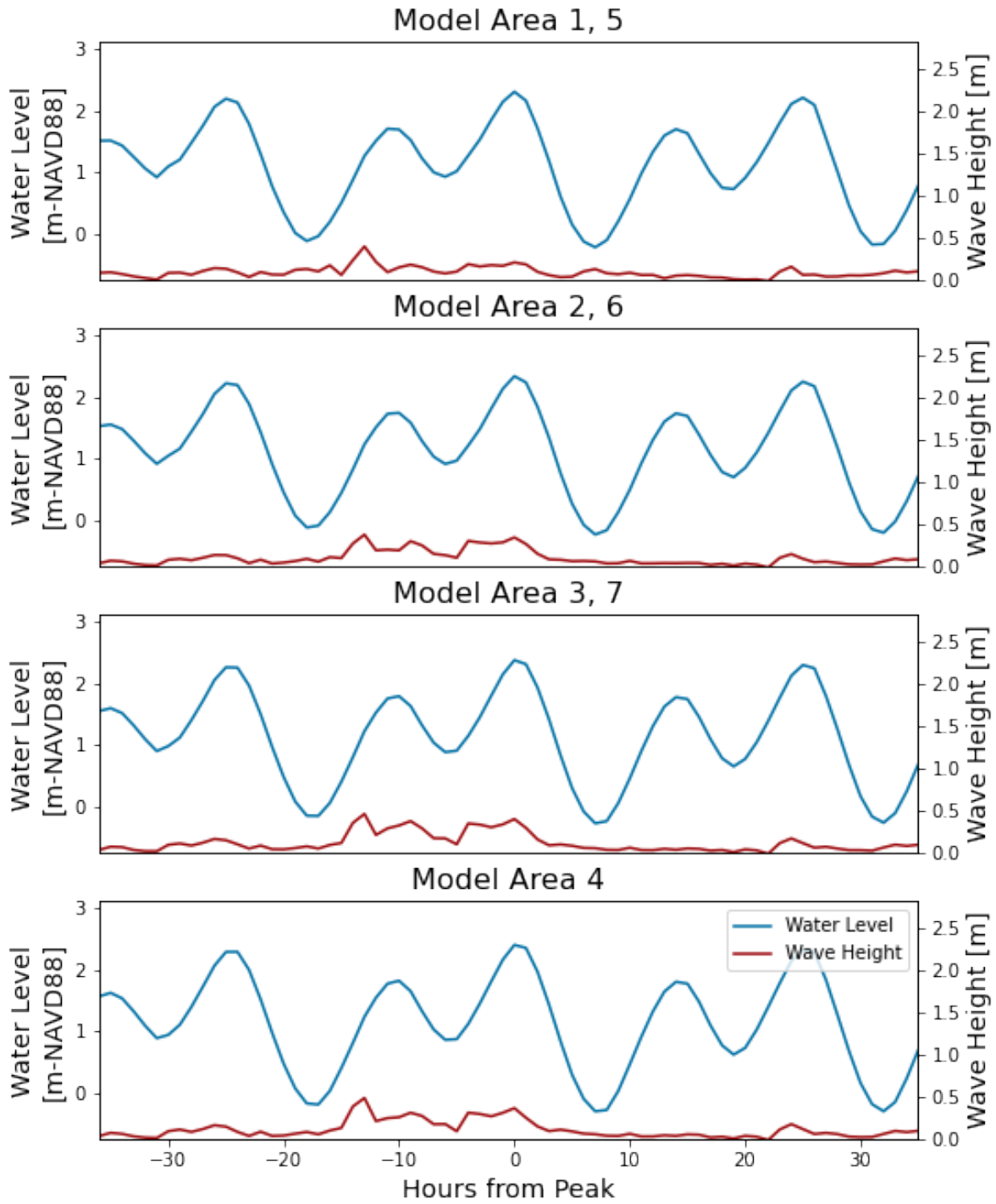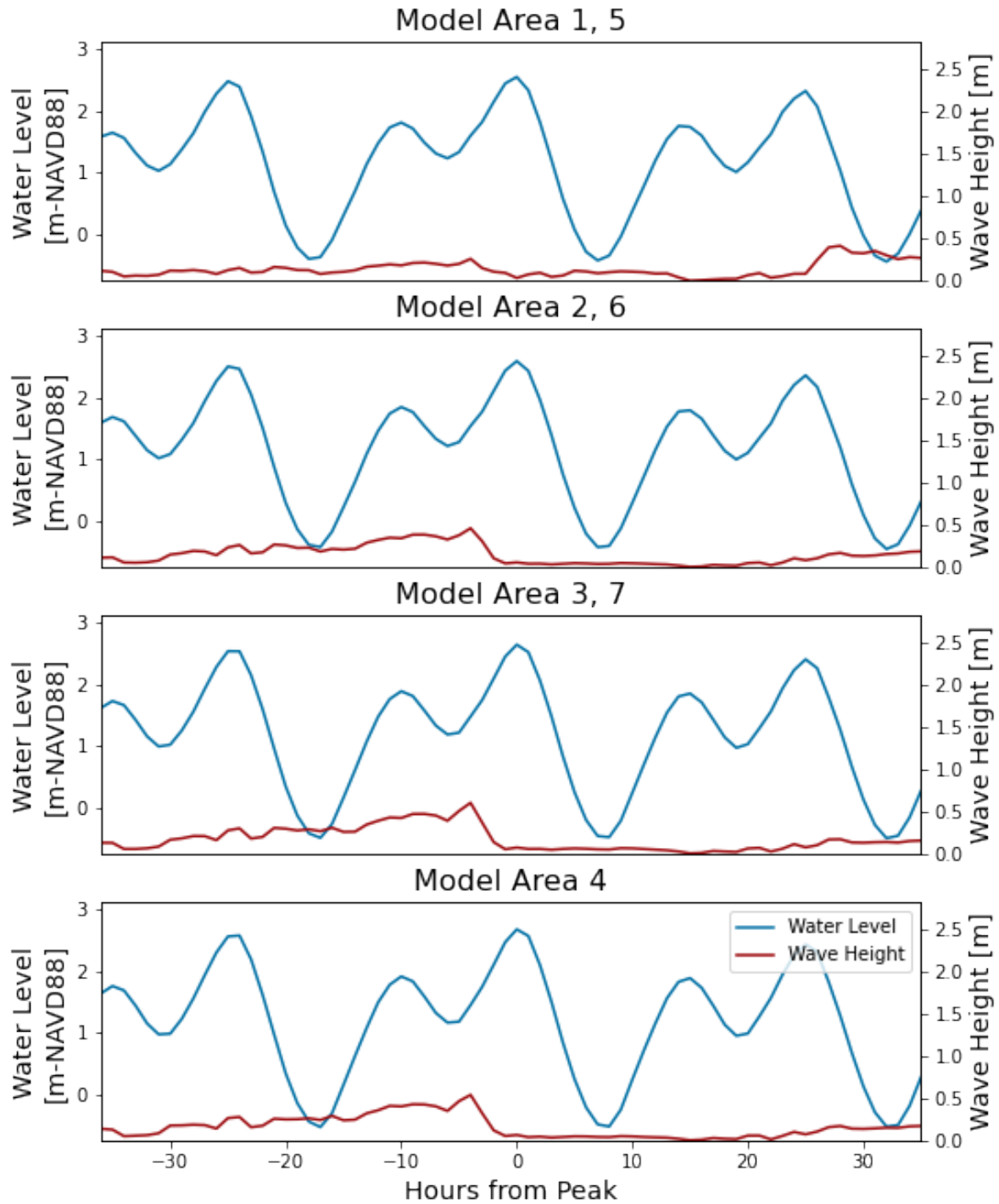
Storm 23, 1992, SLR1992_R1_1.0yr_023
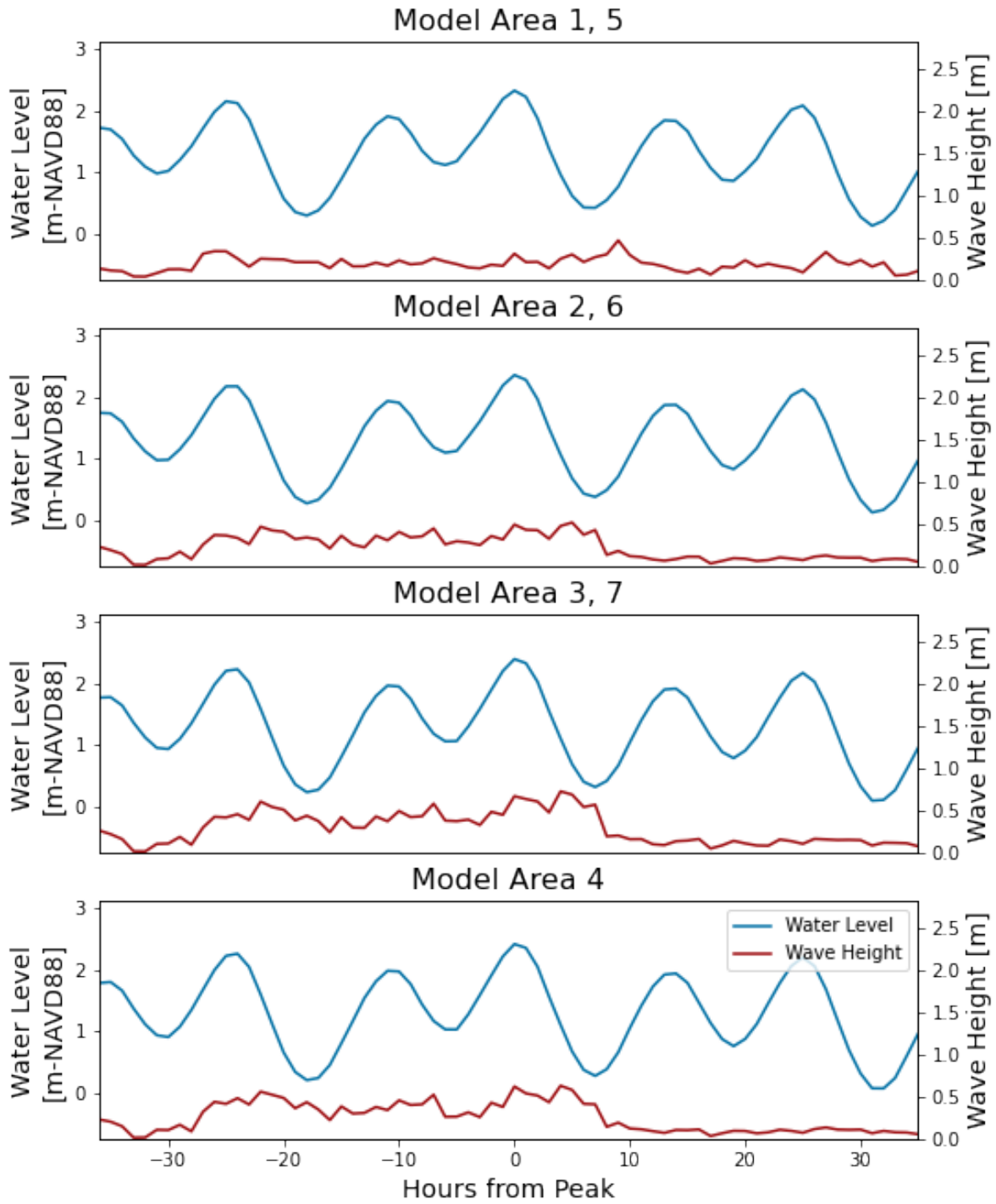
Storm 24, 1992, SLR1992_R1_1.0yr_024
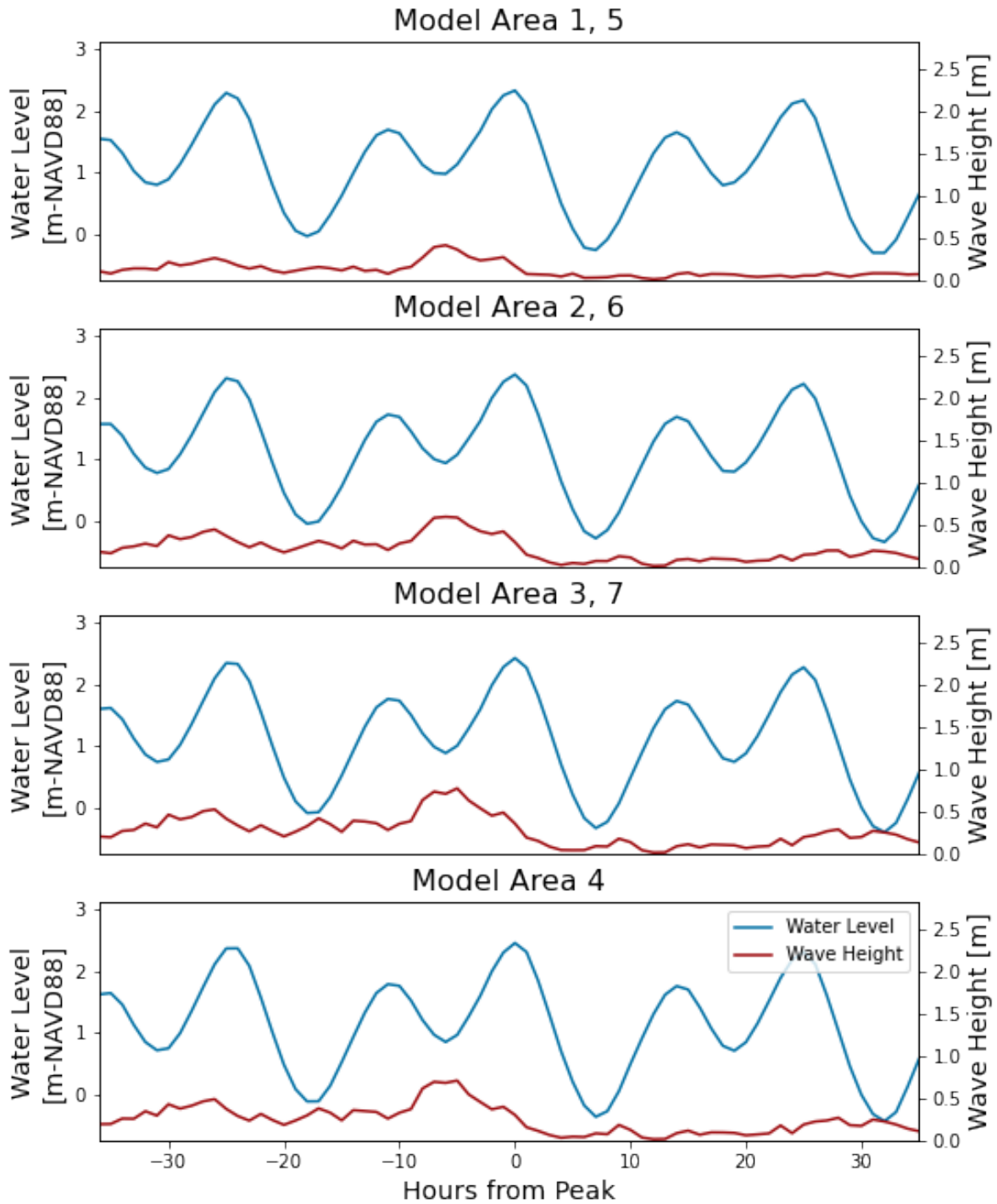
Storm 25, 1992, SLR1992_R1_1.0yr_025
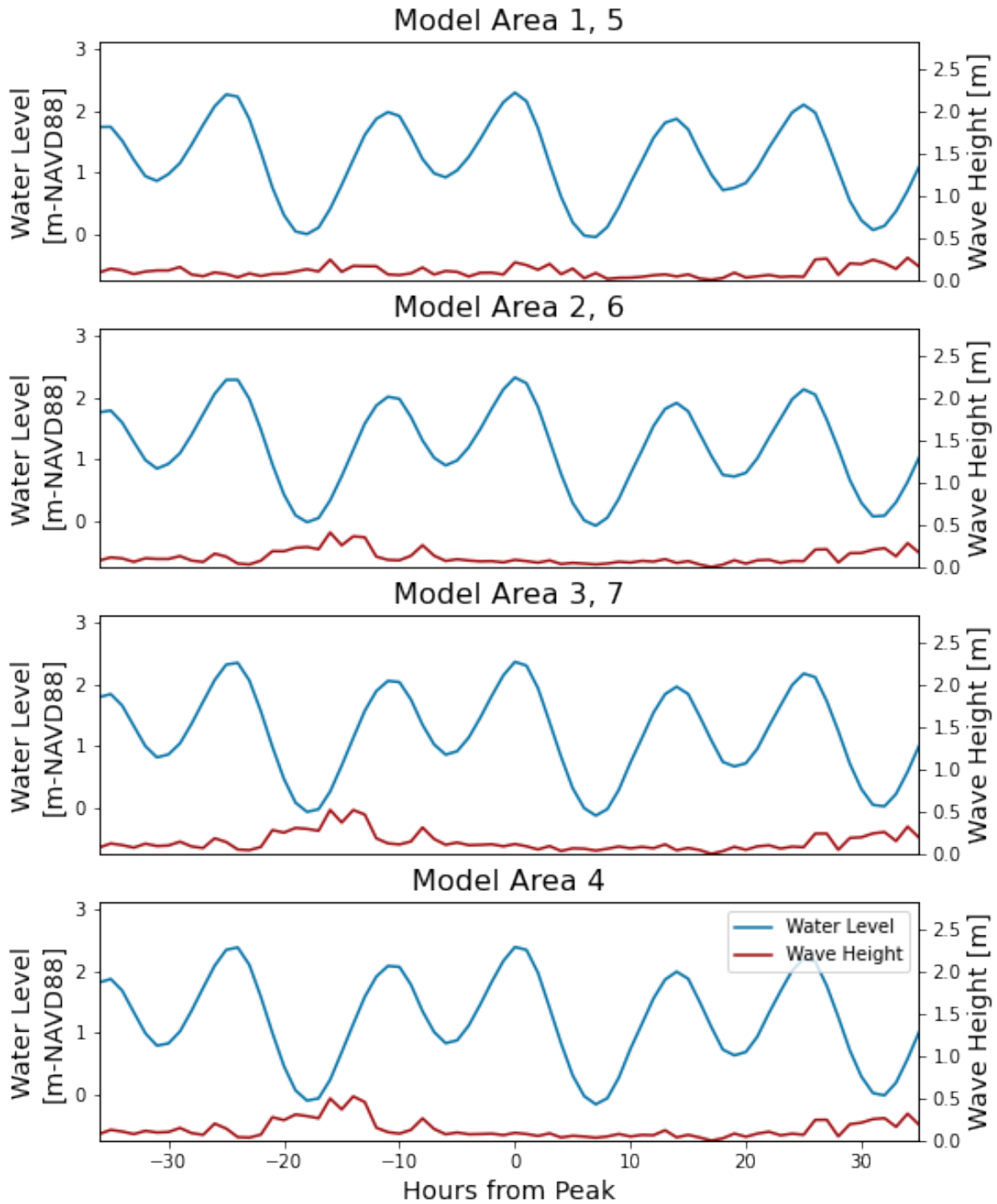
Storm 26, 1992, SLR1992_R1_1.0yr_026
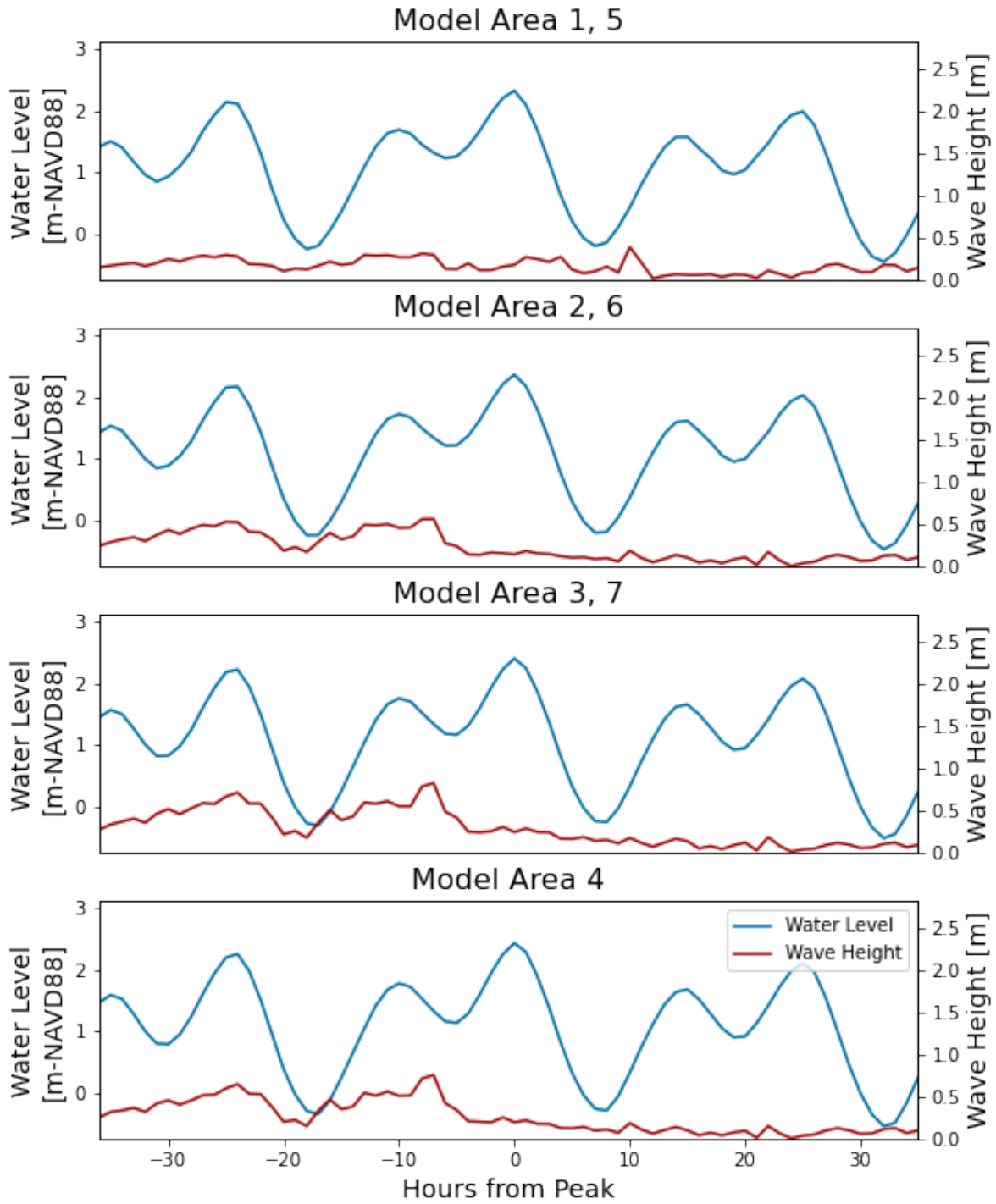
Storm 27, 1992, SLR1992_R1_1.0yr_027
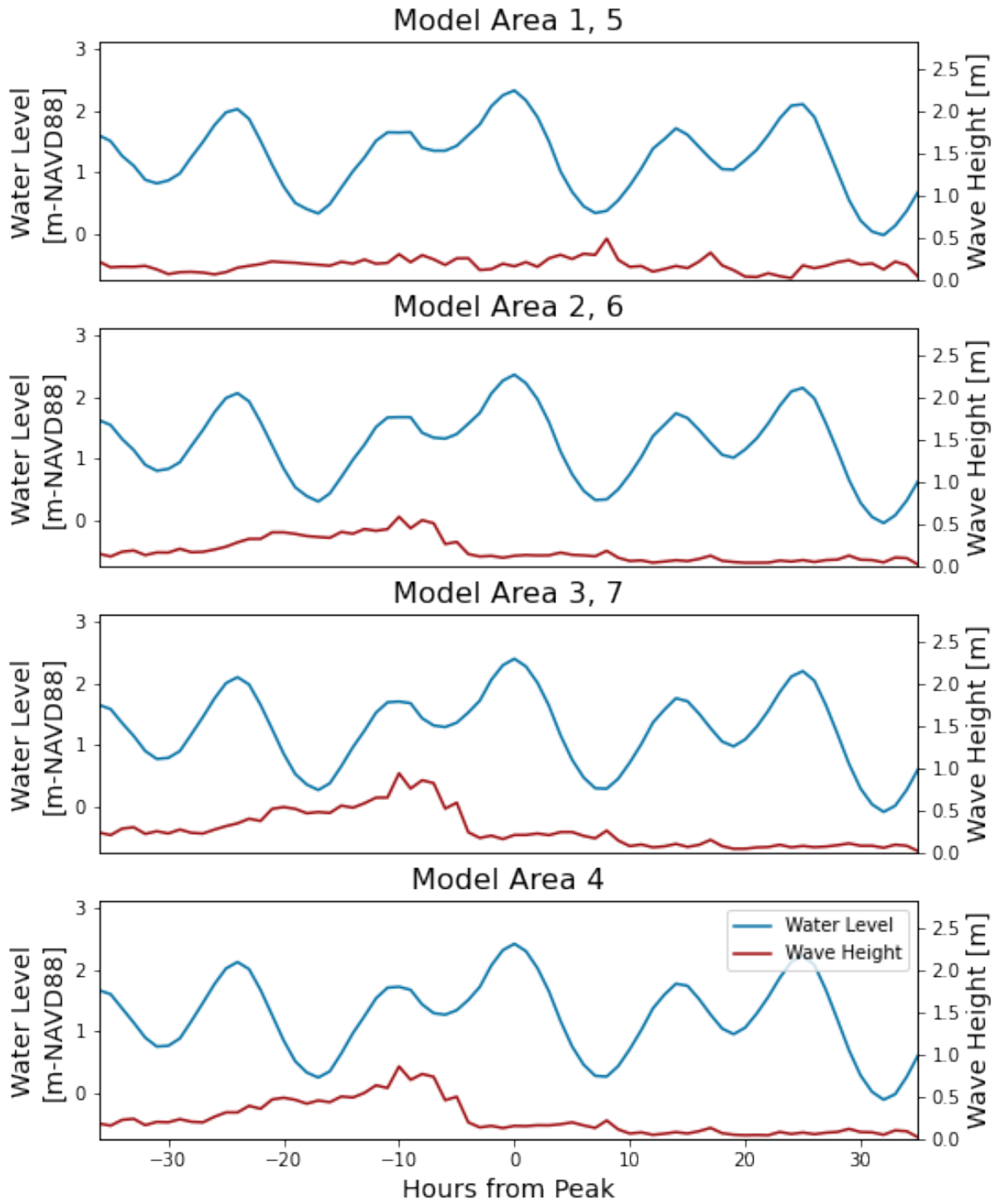
Storm 28, 1992, SLR1992_R1_2.0yr_001
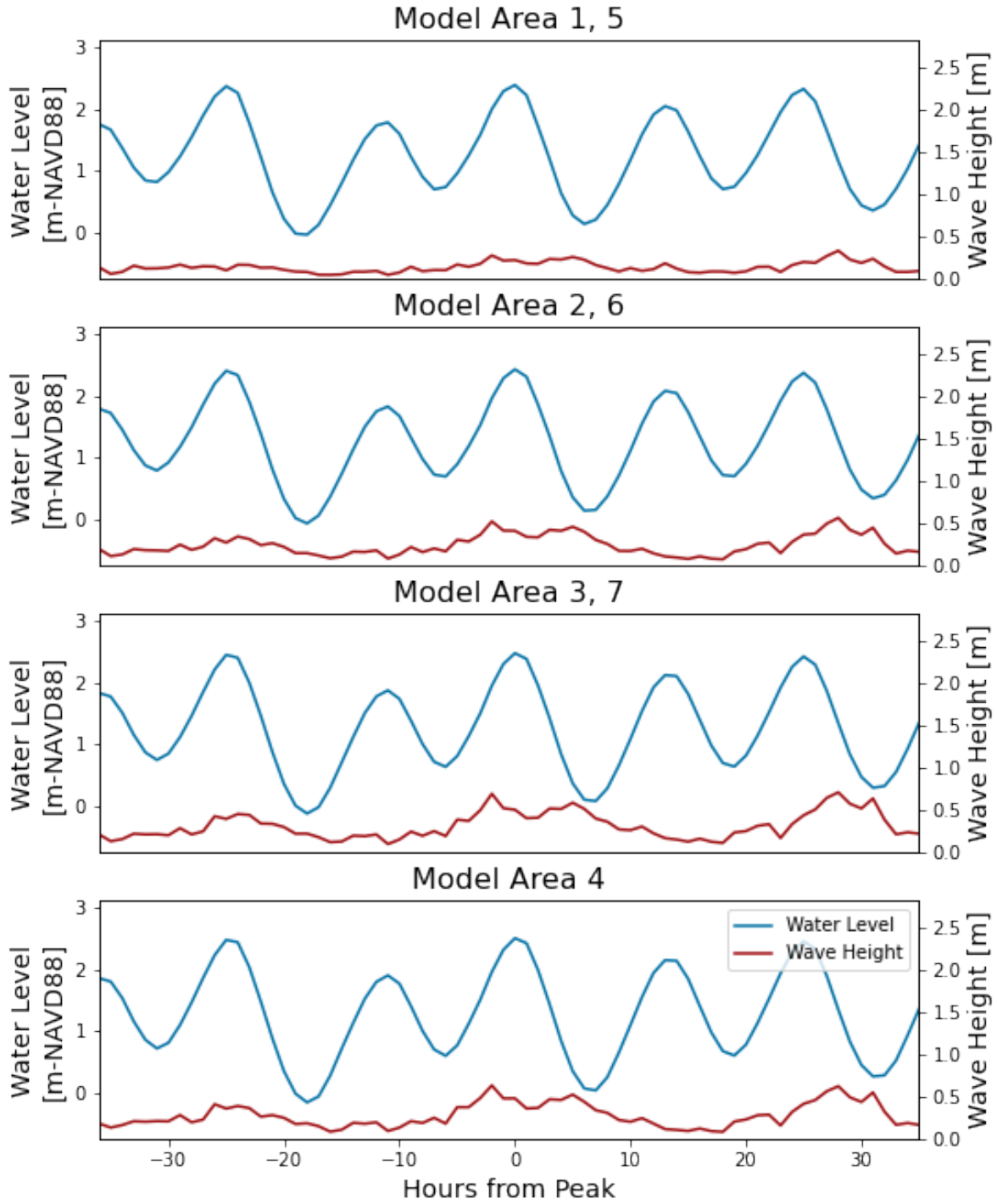
Storm 29, 1992, SLR1992_R1_2.0yr_002
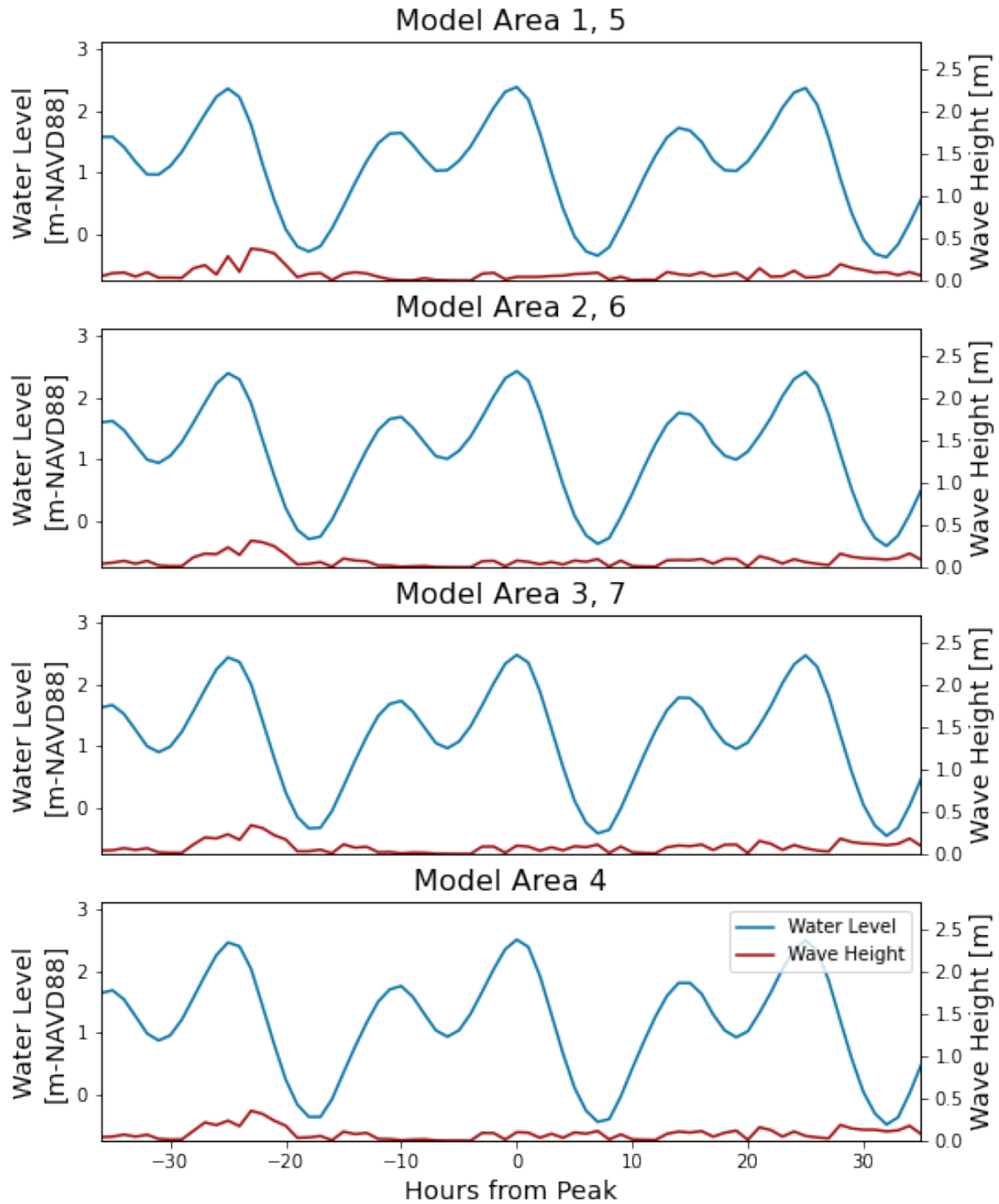
Storm 30, 1992, SLR1992_R1_2.0yr_003
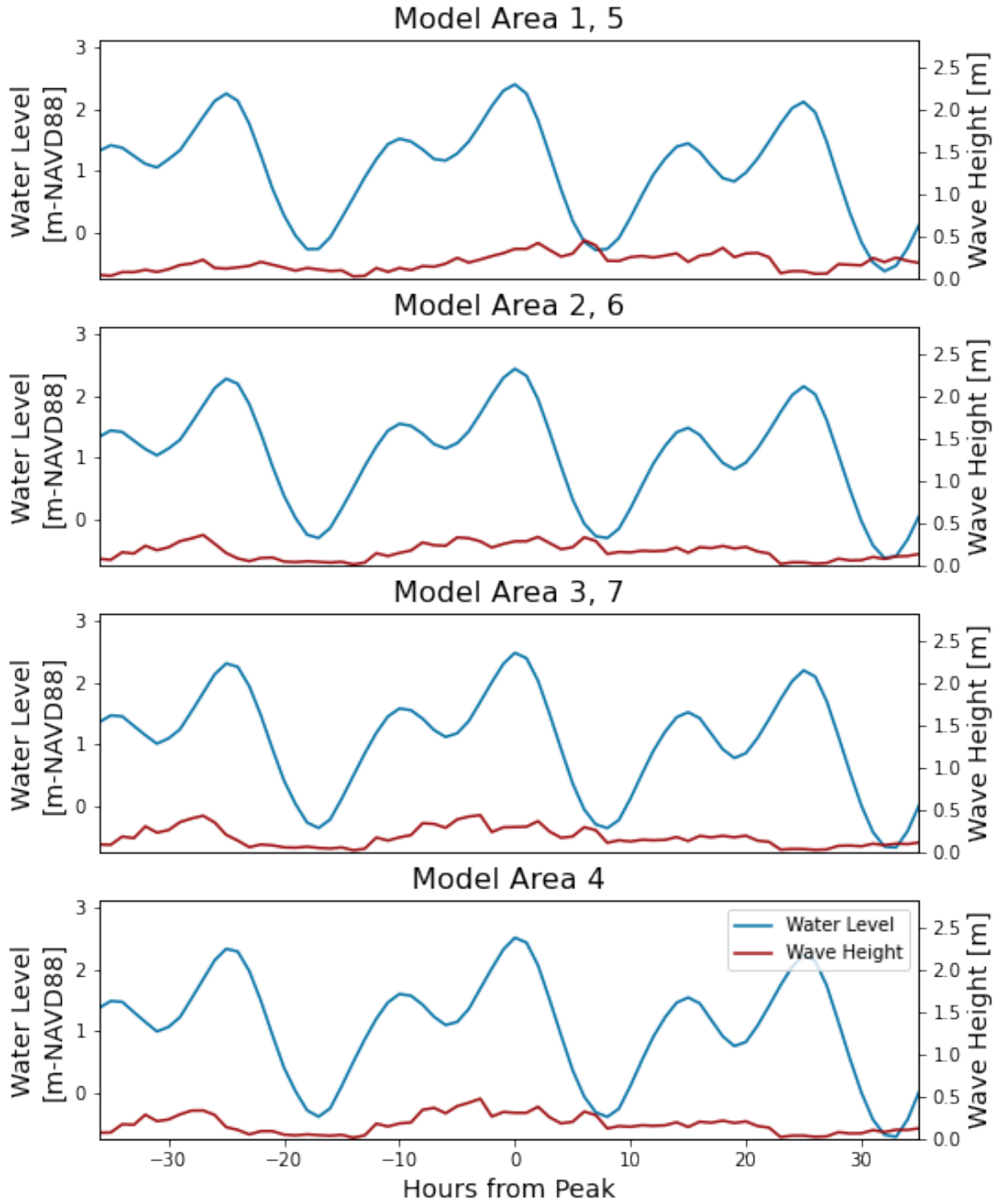
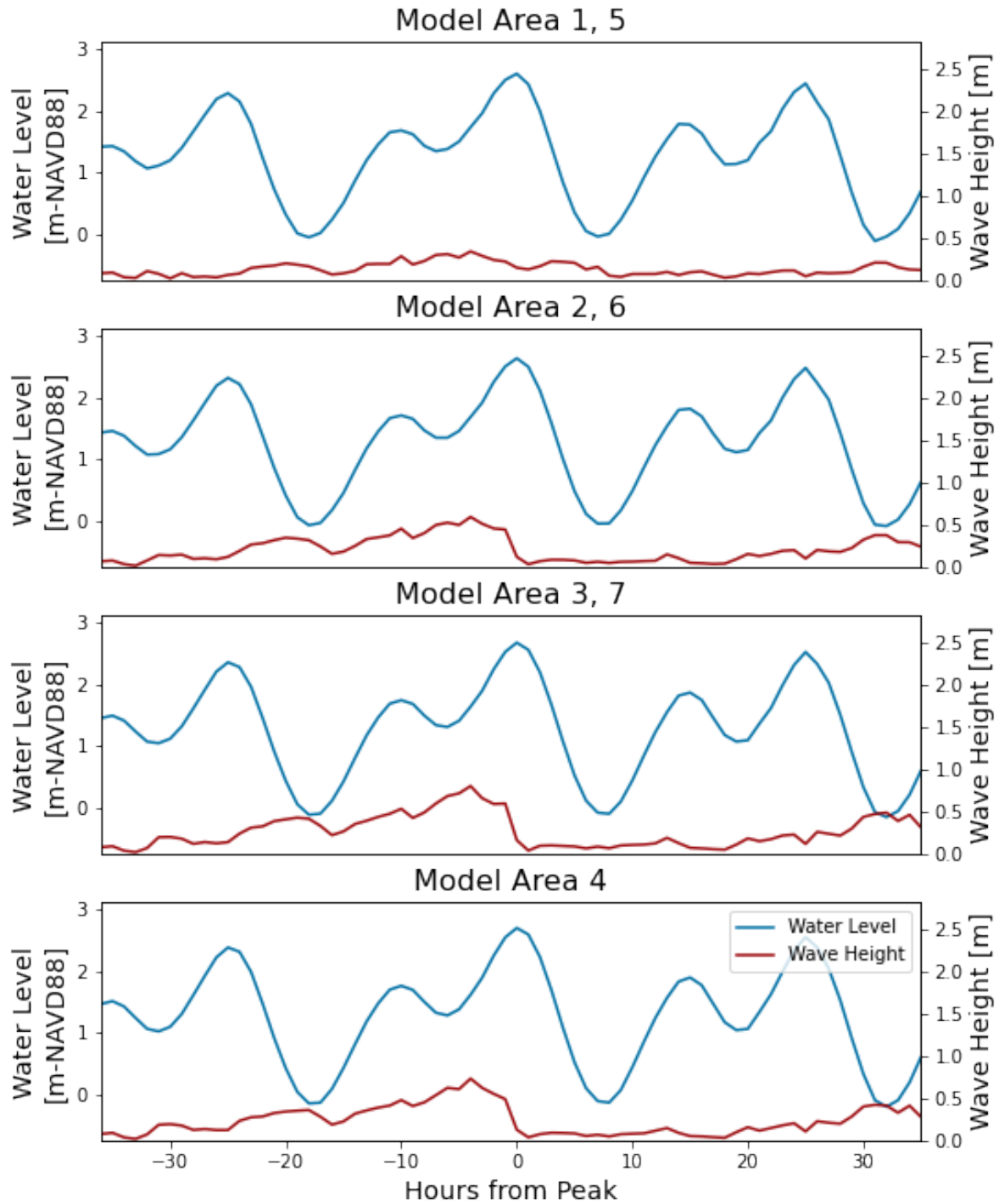# Storm 31, 1992, SLR1992_R1_2.0yr_004
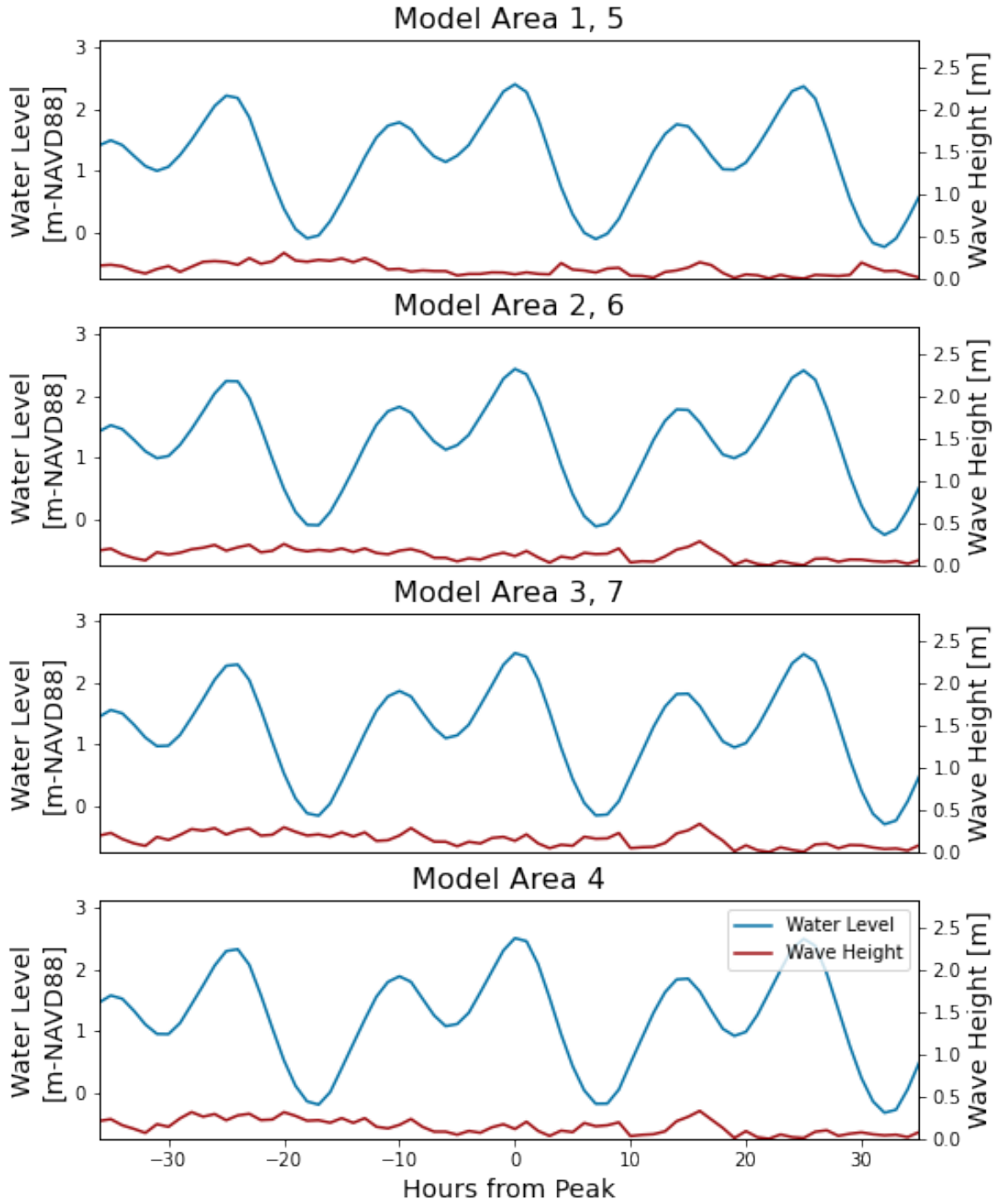
Storm 32, 1992, SLR1992_R1_2.0yr_005
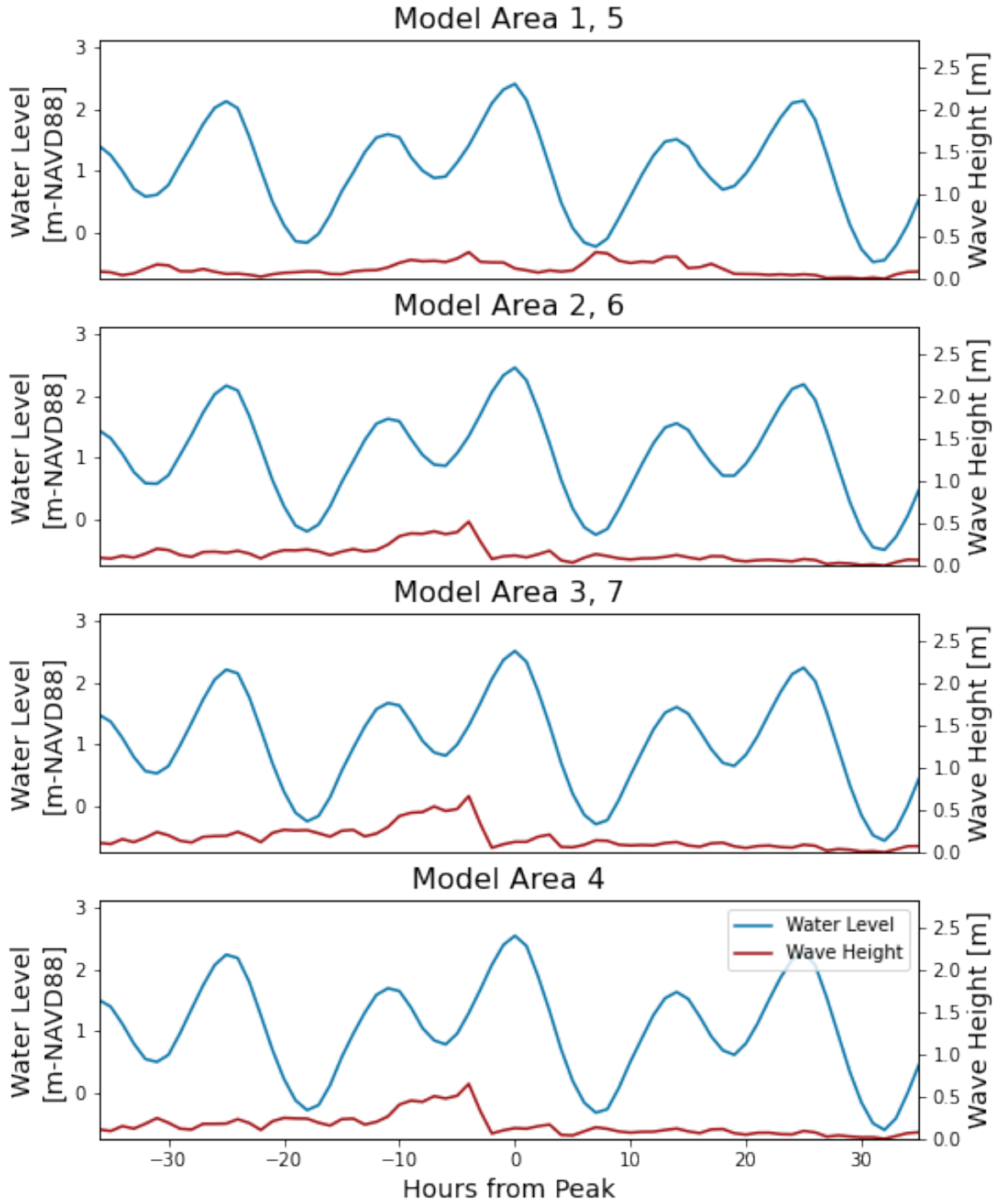
Storm 33, 1992, SLR1992_R1_2.0yr_006
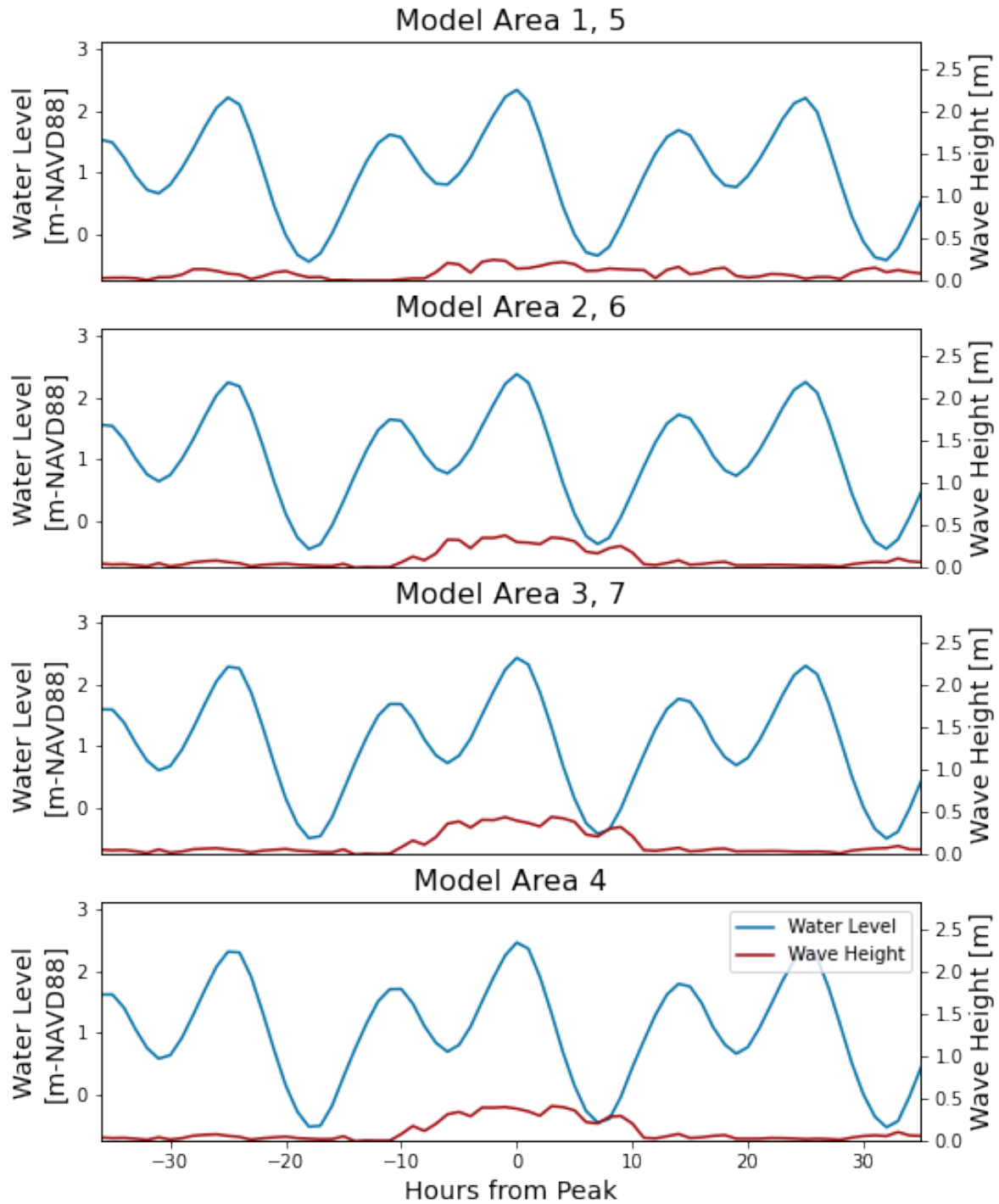
Storm 34, 1992, SLR1992_R1_2.0yr_007


Model Area 1, 5

Model Area 2, 6

Model Area 3, 7

Model Area 4
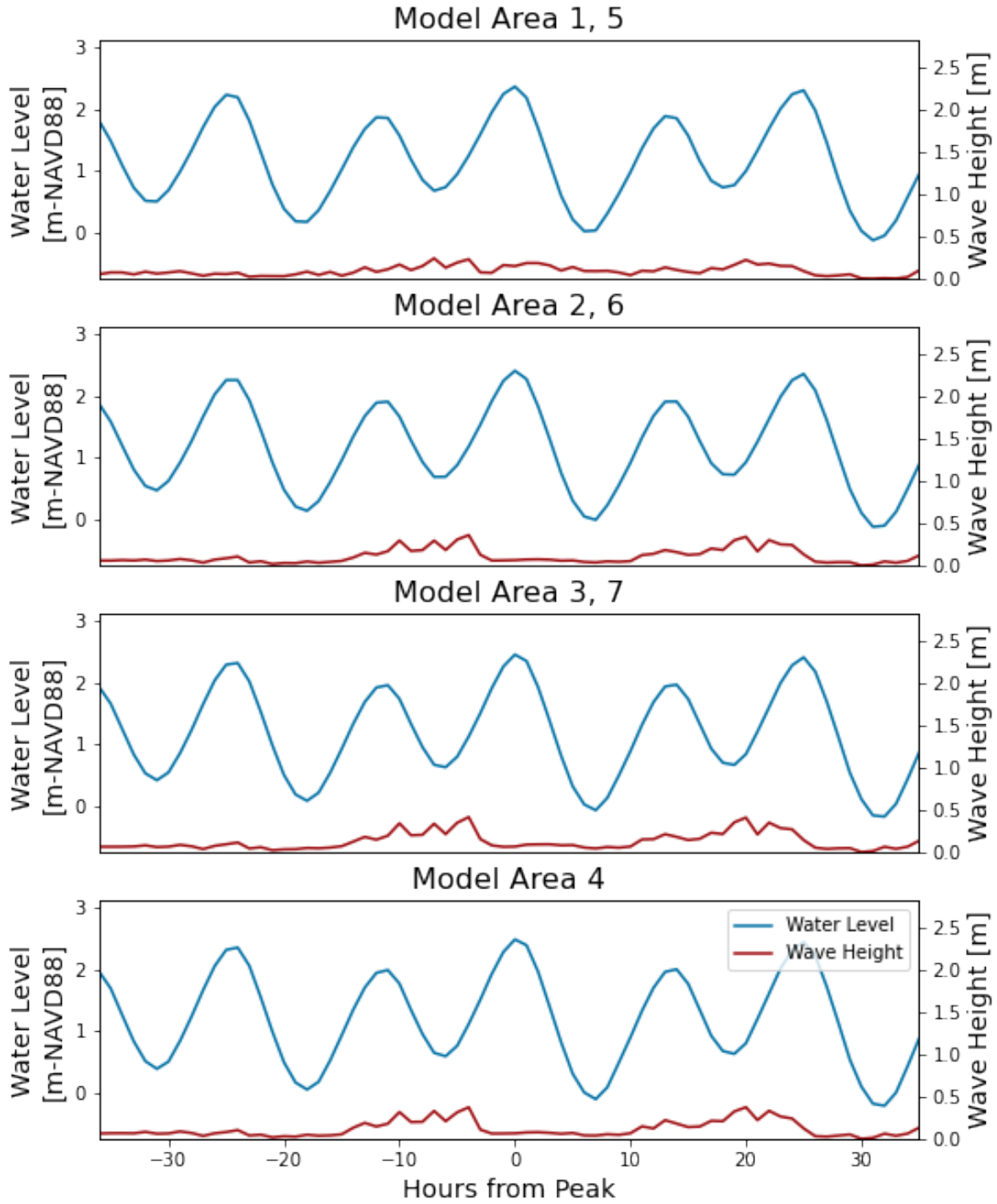
Storm 35, 1992, SLR1992_R1_2.0yr_008
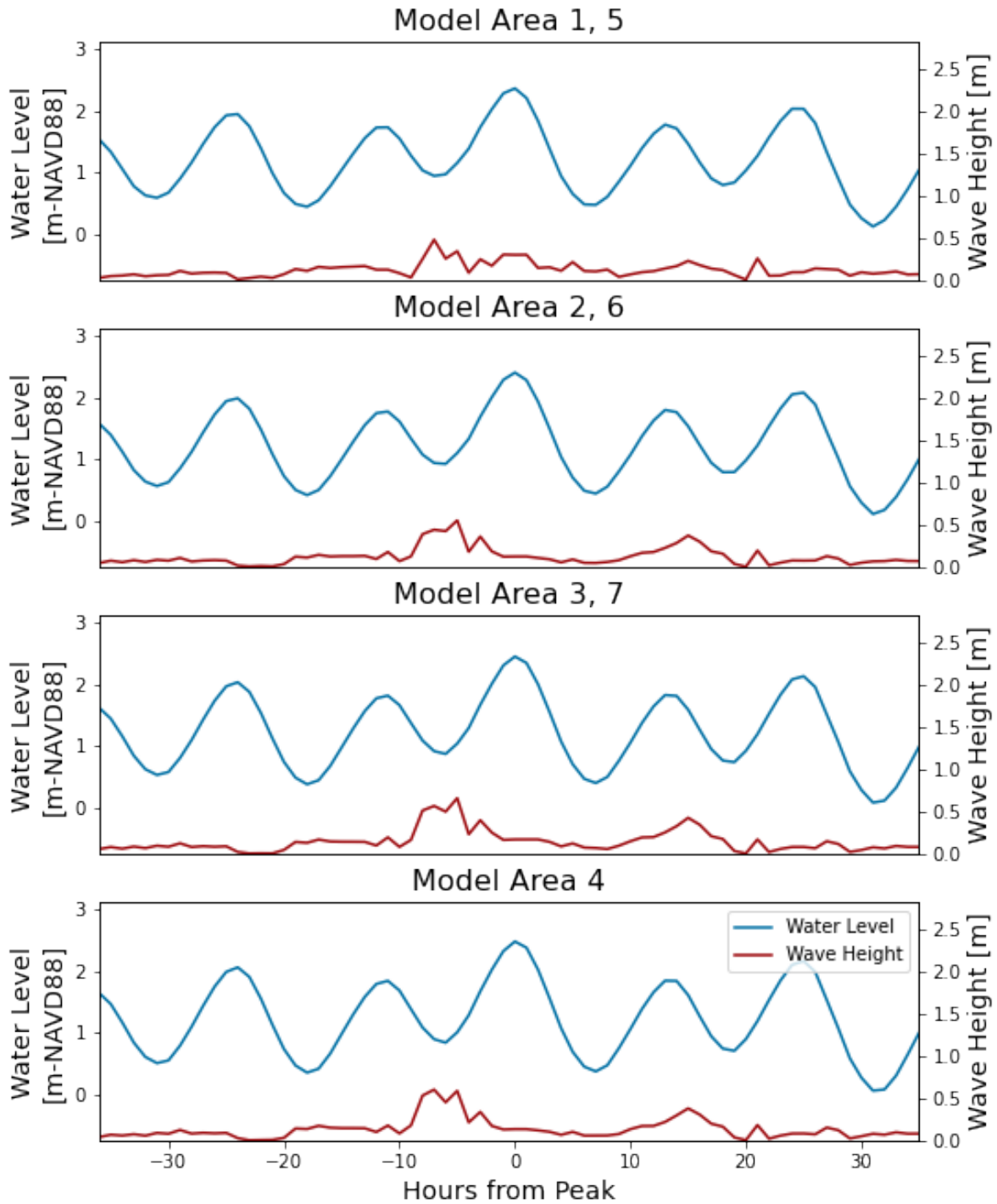
Storm 36, 1992, SLR1992_R1_2.0yr_009

Storm 37, 1992, SLR1992_R1_2.0yr_010

Storm 38, 1992, SLR1992_R1_5.0yr_001

Model Area 1, 5

Model Area 2, 6

Model Area 3, 7

Model Area 4
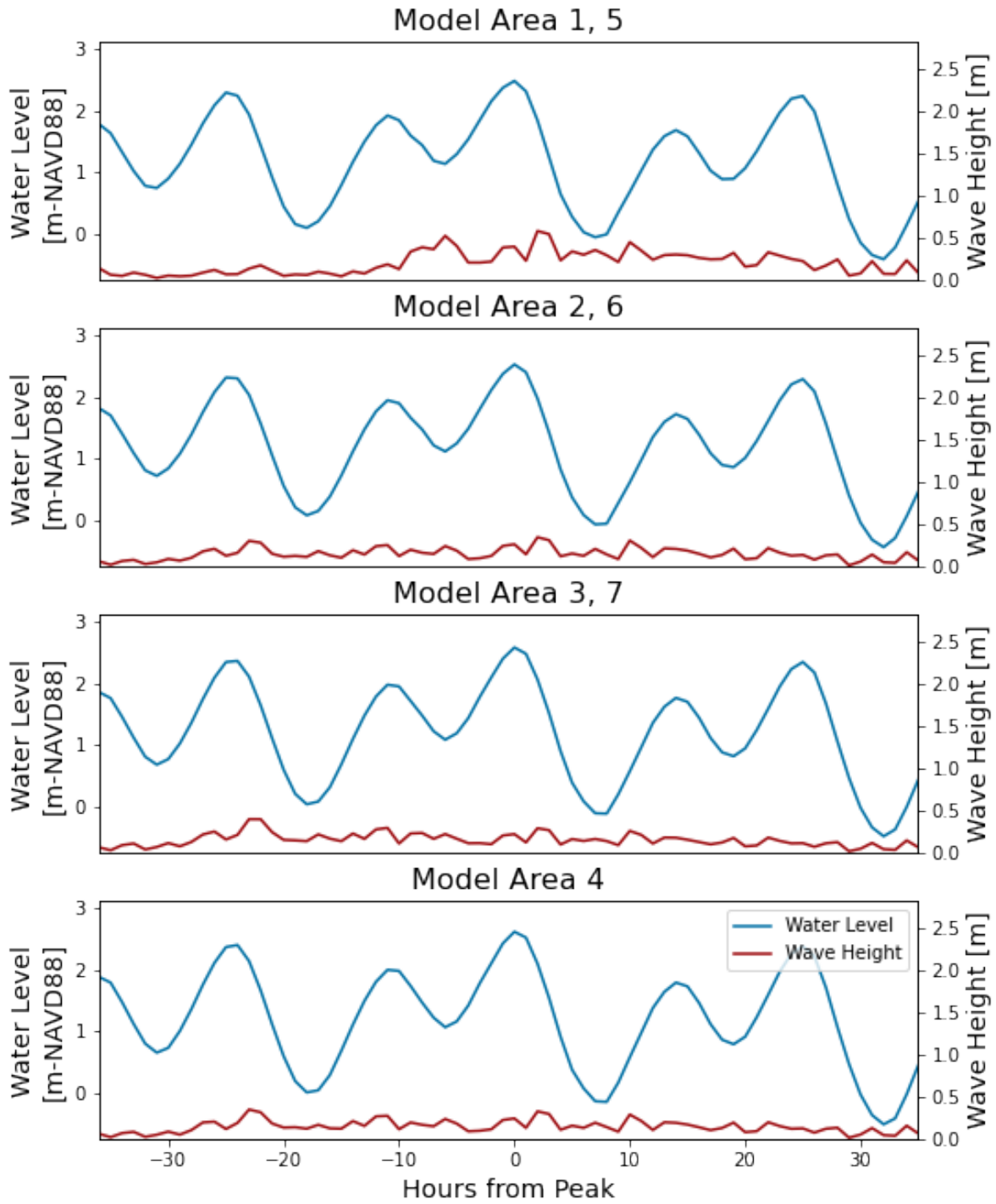
Storm 39, 1992, SLR1992_R1_5.0yr_002

Storm 40, 1992, SLR1992_R1_5.0yr_003

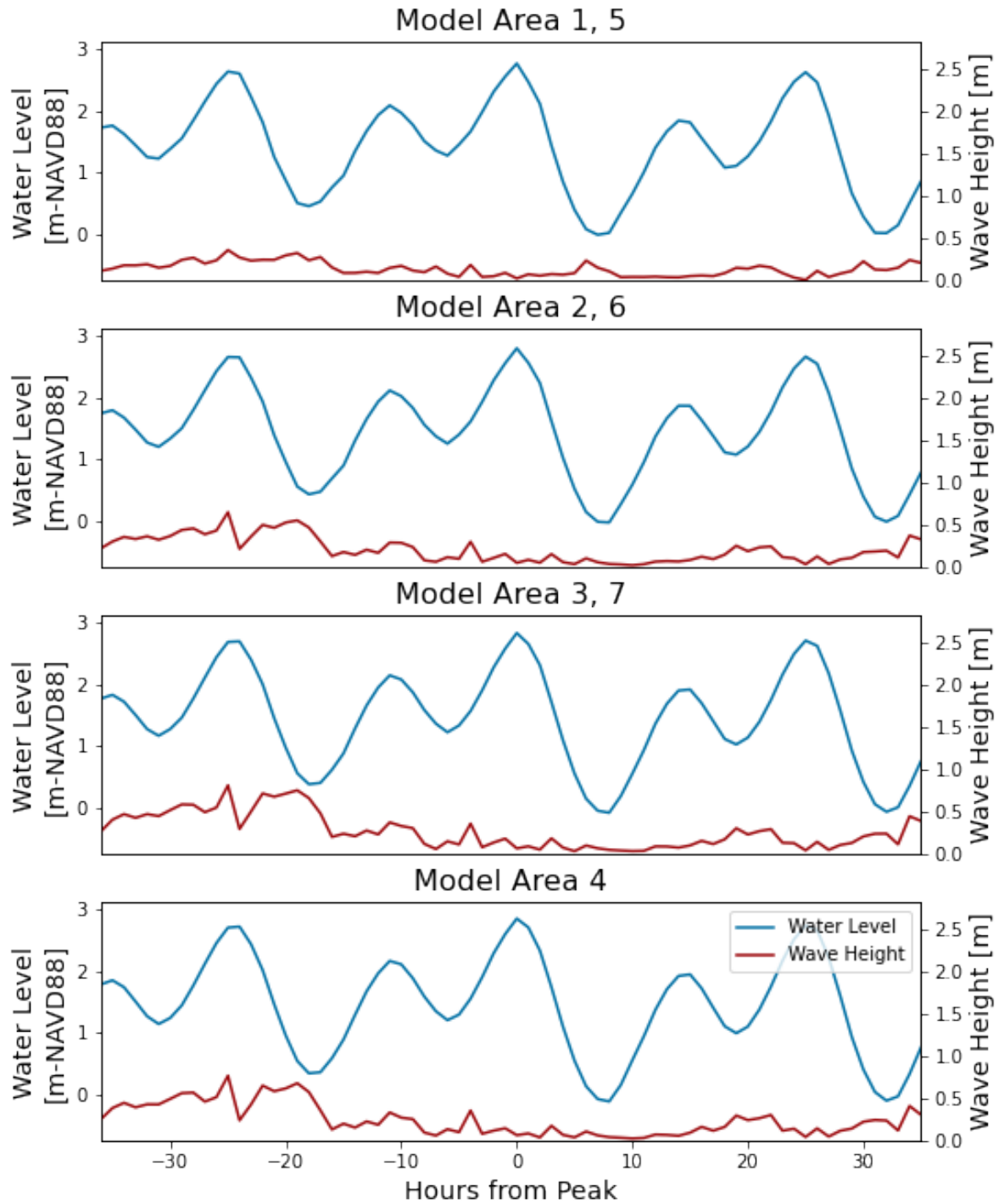# Storm 41, 1992, SLR1992_R1_5.0yr_004

Storm 42, 1992, SLR1992_R1_10.0yr_001

Storm 43, 1992, SLR1992_R1_25.0yr_001
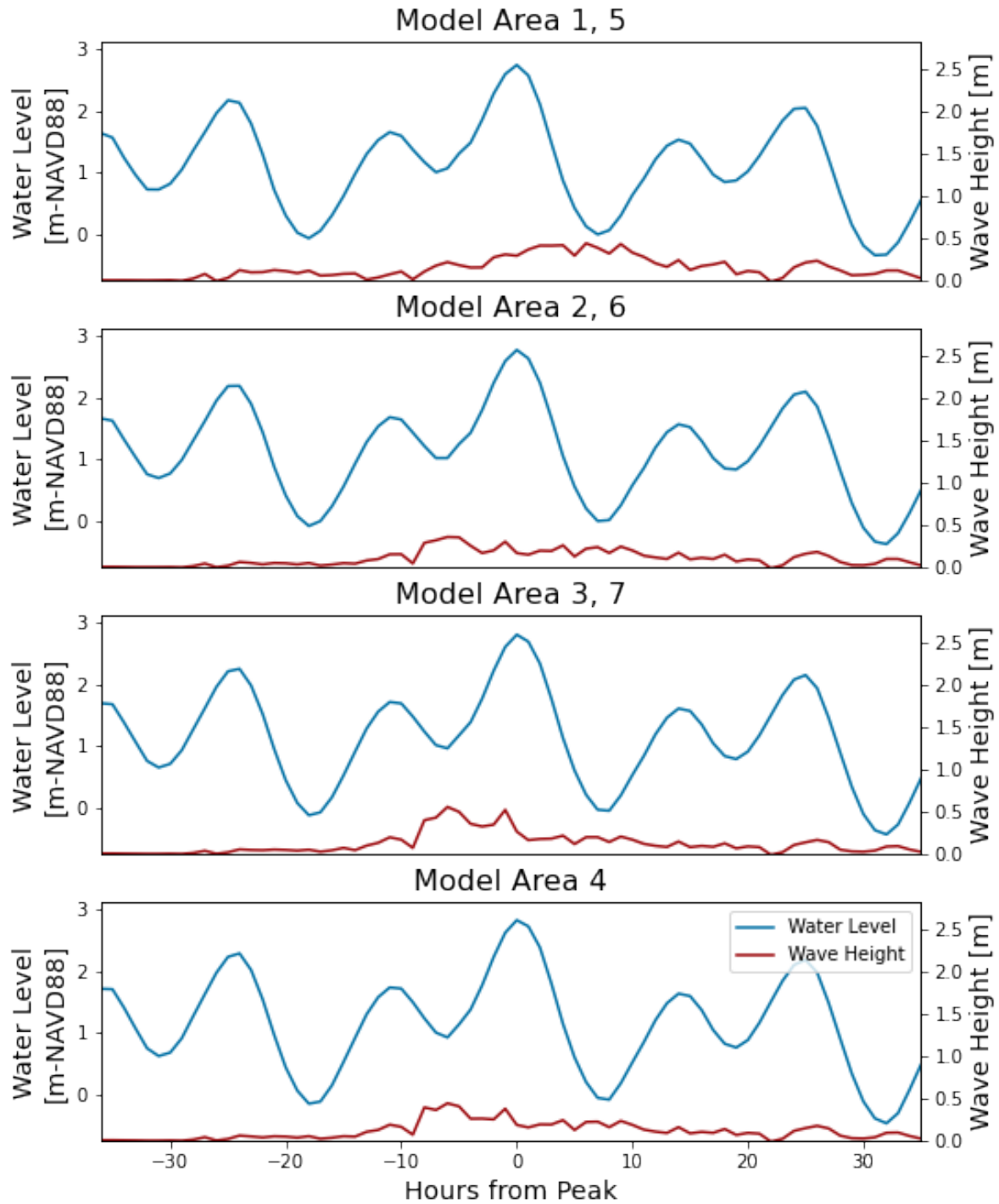
Storm 44, 1992, SLR1992_R1_25.0yr_002
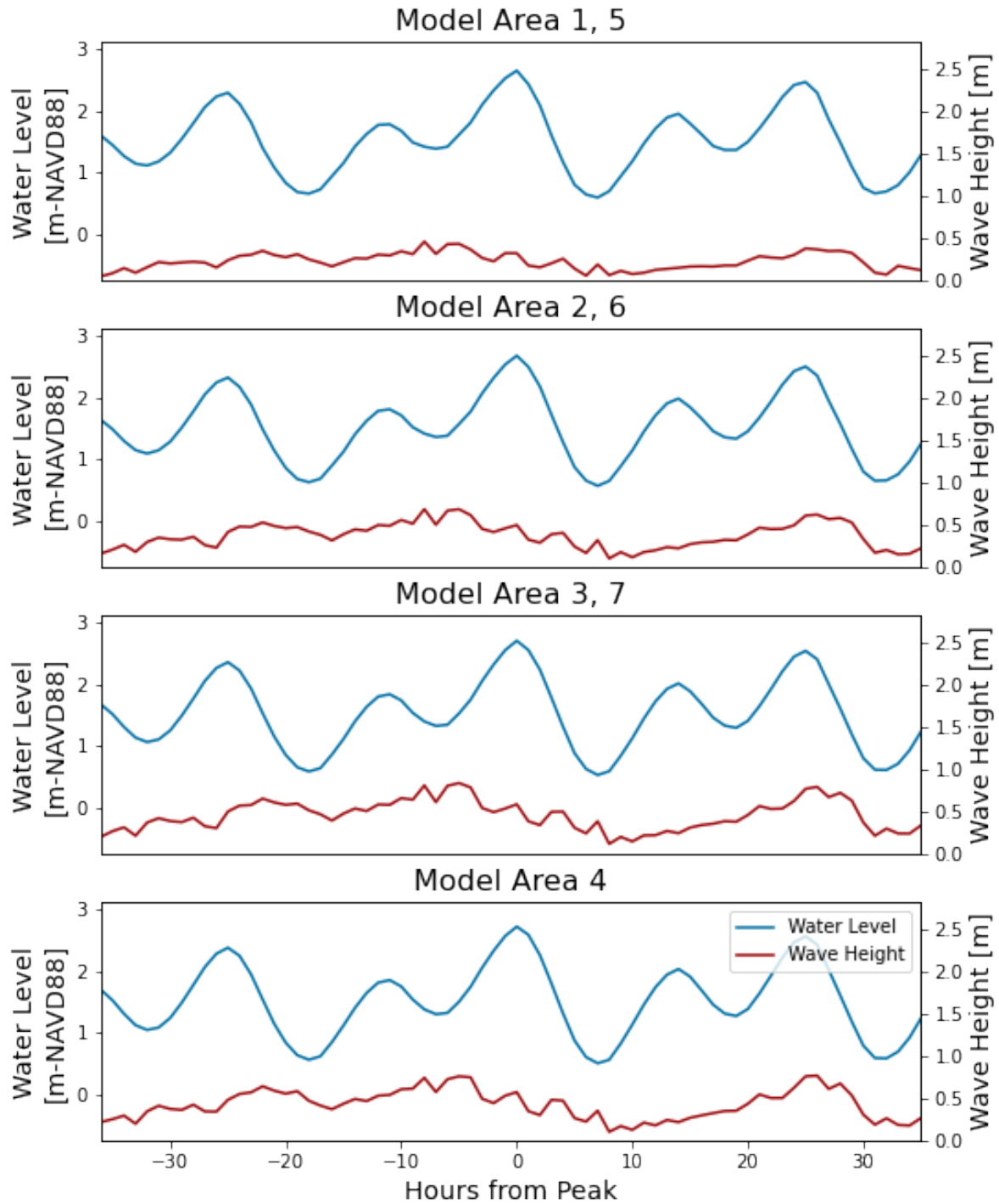
Storm 45, 1992, SLR1992_R1_50.0yr_001

Storm 46, 1992, SLR1992_R1_50.0yr_002

Storm 47, 1992, SLR1992_R1_100.0yr_001